Light Trapping in Photonic Crystal Based Thin Film Solar Cells

Doctoral Thesis

Nikhil Deep Gupta
(College ID-2012REC9530)

DEPARTMENT OF ELECTRONICS & COMMUNICATION ENGINEERING,
MALAVIYA NATIONAL INSTITUTE OF TECHNOLOGY, JAIPUR, INDIA

June 2017

Light Trapping in Photonic Crystal Based Thin Film Solar Cells

Doctoral Thesis

Submitted By

Nikhil Deep Gupta
Research Scholar
(College ID-2012REC9530)

Under Supervision of

Dr. Vijay Janyani
Associate Professor,
Dept. of ECE, MNIT, Jaipur

DEPARTMENT OF ELECTRONICS & COMMUNICATION ENGINEERING,
MALAVIYA NATIONAL INSTITUTE OF TECHNOLOGY, JAIPUR, INDIA

June 2017

Light Trapping in Photonic Crystal Based Thin Film Solar Cells

Submitted By

Nikhil Deep Gupta
Research Scholar
(College ID-2012REC9530)

Under Supervision of

Dr. Vijay Janyani
Associate Professor
Dept. of ECE, MNIT, Jaipur

Submitted in fulfillment of the requirements of the degree of Doctor of Philosophy

to the

DEPARTMENT OF ELECTRONICS & COMMUNICATION ENGINEERING,
MALAVIYA NATIONAL INSTITUTE OF TECHNOLOGY, JAIPUR, INDIA

June 2017

Certificate

This is to certify that the thesis entitled "**Light Trapping in Photonic Crystal based thin film solar cells**" being submitted by Nikhil Deep Gupta is a bonafide research work carried out under my supervision and guidance in fulfillment of the requirement for the award of the degree of Doctor of Philosophy in the Department of Electronics & Communication Engineering, Malaviya National Institute of Technology Jaipur, India. The matter embodied in this thesis is original and has not been submitted to any other University or Institute for the award of any other degree.

_____

Dr. Vijay Janyani

(Associate Professor)

(Dept. of ECE, MNIT, Jaipur)

Declaration of Authorship

I, Nikhil Deep Gupta, declare that this thesis titled, 'Light Trapping in Photonic Crystal based Thin Film Solar Cell' and the work presented in it are my own. I confirm that:

- This work was done wholly or mainly while in candidature for a research degree at this University.
- Where any part of this thesis has previously been submitted for a degree or any other qualification at this University or any other institution, this has been clearly stated.
- Where I have consulted the published work of others, this is always clearly attributed.
- Where I have quoted from the work of others, the source is always given. With the exception of such quotations, this thesis is entirely my own work.
- I have acknowledged all main sources of help.
- Where the thesis is based on work done by myself jointly with others, I have made clear exactly what was done by others and what I have contributed myself.

Signed: _____

Date: _____

"The optimism combined with the perseverance might help an average individual to achieve extremes."

-Anonymous

Acknowledgement

I am a firm believer that nobody in this world is complete without the firm support of a team. Here, I would take an opportunity to thank all those, who directly or indirectly left everlasting impressions in my soul and mind while working for my Ph.D.

Kahlil Gibran, a noted American writer, once said, “The teacher, who is indeed wise, does not bid you to enter the house of his wisdom, but rather leads you to the threshold of your mind.” Dr. Vijay Janyani, Associate Professor, Department of Electronics and Communication, who is my supervisor as well as mentor, follows the same philosophy. Indeed it is the good fortune and privilege to work and learn from such an understandable mentor. I would like to express my sincere appreciation and thanks to him, as he has been a brain behind evolving me not only as a researcher but also as a person. He has encouraged me throughout my research, advised me whenever the path was wrong. Your advices on both research as well as on my career have been priceless. For a budding researcher like me, writing thesis with high standard is not an easy task, where your expertise has helped a lot to accomplish the task. He is unarguably the most influential person during my post graduate career.

I would also like to express my sincere gratitude to Dr. Manish Mathew, Senior Scientist, Optoelectronics Devices Group at CSIR-CEERI, Pilani, Rajasthan for the continuous and unconditional support he has showered upon me. He is the first one after my guide, who took my idea seriously and took me to the realm of electronics fabrication and helped me to refine my work and translate it from theory to practice. I am really indebted to the blessings he showered upon me like an elder brother. Also, I would like to thank, Dr. Rajendra Singh, Associate Professor, Department of Physics, IIT-Delhi, to have faith in me and provide access to his lab and facilities, only due to which I have achieved the end results.

I would also like to thank my thesis committee members, whose support in my thesis work is undoubtedly invaluable. Dr. K. K. Sharma, HOD, Dr. D. Boolchandani, Convener DPGC, Dr. Vineet Sahula, former HOD, Department of Electronics and Communication Engineering at MNIT, Jaipur too always encourages me to follow ideas with passion and motivated me to achieve my goals, even at hardships. I also express my thanks to my DPGC committee members; including Dr. G. Singh, Dr. R. Sharma and Dr. R. Maddila, for their patience with which they

discussed my views and inspired me with their wisdom. Sometimes, their inquiries had burnt my mind, however ultimately they helped to polish my work.

The support that my family has poured upon during my Ph.D. work is simply beyond the limits of the words. It is simply not possible enough to put the love, efforts and sacrifices; they took to allow me to cherish my dreams. My mom, my wife, and my brothers, they are the pillars of my life. I would especially like to express appreciation to my beloved wife Neha, who tirelessly supported me for my research work and was always to my support in the moments when there was no one to answer my queries. Even, if I serve them to each day of my life, I could not equate what they did for me. Love you all.

Here, I would also like to thank all of my near and dear ones who supported me in writing, and incented me to strive towards my goal. They stood firm throughout my hard times, enjoyed together and cherished happiness. Although, it is not possible to sum up each and everyone in the few lines, but some of them are simply invaluable to my success includes Dr. Sanjeev Kumar Metya, Dr. Vipin Pal, Dr. Nagesh Janrao, Amit Kumar Garg, Shashikant Sharma, Nitesh Kumar, Mukesh Kumar Gupta and Monika Maun (IIT-Delhi). Al last, thanks to all my fellows for the stimulating discussions, and for all the fun we have had in the last four years.

I take this opportunity also to acknowledge the active support and grant provided by the Department of Science and Technology (DST), Delhi through Solar Energy Research Initiative (SERI) under the project entitled “Efficiency Enhancement in the thin film GaAs solar cell using Photonic Crystal as a back reflector” (Grant FR/203C). I am grateful to SERI-DST, Delhi for understanding the requirement of the exploration of this field and for giving this opportunity to work in this area which can one day, not only change the scenario of the modern world of alternate energy sources but may also prove to be a boon for countries like India.

In conclusion, I just wish that the readers of the thesis, to have a well understandable and enjoyable reading and ultimately would appreciate the concept and would try their hands to do something similar.

Abstract

The present world is desperately looking towards renewable energy sources to solve its problems of energy crisis and pollution. There are simultaneous efforts throughout the world to find suitable and sustainable alternative energy sources that can replace the conventional sources and at the same time fulfill our energy demands. Out of many available resources, solar photovoltaic technologies seem to be one of the best available solutions. However, their high cost to efficiency ratio restrict their much anticipated terrestrial development. Thin film solar cells (TFSC) seem to overcome the cost factor, by replacing thick active layers by micron or even nano meter scale absorption layer. However, the main problem with TFSC is their low efficiency. One of the possible ways to overcome the limitation is to use certain kind of light trapping structure (LTS), which can improve the optical path length of photons inside the active layer and thus can improve their optical absorption and results in improvement of the overall output result. However the problems associated with the commonly used LTS, which includes planar anti reflection coating at the top and metallic back reflector, the researchers have extensively discussed about the requirement of random as well as periodically patterned LTS. Advantages of periodic structures over random structures, such as easy reproducibility and scalability led to the development of periodic patterned LTS like PhC LTS.

In this context the thesis proposes the designs and examines the performance of PhC LTS for GaAs and InGaN/GaN based solar cells through numerical simulations as well as experimental demonstrations. The thesis presents the performance analysis of the PhC LTS by incorporating them at the back as a Photonic Band Gap structure, as a diffraction grating assisted by Distributed Bragg Reflector; at front surface of the cell etched above active layer and at front surface etched through active layer. The work also presents the comparison among the performance of these proposed structures and predicts the best design for the future PhC pattern based structure for GaAs and InGaN/GaN solar cells. The thesis also aims to find the Lambertian light trapping values for GaAs and InGaN/GaN active layer based cells and investigates how the performance of the proposed solar cell designs varies with thickness of active layer and to analyze how PhC based LTS effect their performance. The work also demonstrates the fabrication challenges and possible process flow for proposed structure design based on metal organic chemical vapor deposition (MOCVD) and electron beam lithography (EBL) including

others. Based on these procedures, one of the proposed designs has been fabricated and experimentally investigated.

The results have demonstrated through simulation and practical designs that the PhC LTS indeed has the ability to enhance the optical absorption of the TFSC, irrespective of the absorption material used and the position where these periodic patterns are incorporated in the solar cell structure. The performance enhancement due to PhC structures in solar cells is attributed to the improvement in the optical path length for high wavelength photons, better coupling of incident light to the active layer and also to the reduction in the reflections throughout the entire wavelength range, respective to the position of the PhC location in the geometry. It has been found that the effect of PhC LTS is more prominent for thinner active layers and diminishes with increasing active layer thickness. Although, the PhC LTS improves the performance of presented designs irrespective of their location in the device, the overall scale of effect depends upon their location. It has been shown that the effect of front LTS geometry remains constant irrespective of the active layer thickness whereas notable variations in the effect of back LTS occur with variation in active layer thickness. The thesis also presents the discussion for the practical design of the proposed structure, which is indeed a complex process, however here achieved successfully. The results obtained through practically designed structure also followed the predicted trend and confirm the PhC LTS ability to enhance the performance of proposed TFSC.

Contents

List of Figures

List of Tables

Abbreviations

a-Si	**A**morphous **Si**licon
AC	**A**lternating **C**urrent
AM	**A**ir **M**ass
ARC	**A**nti **R**eflection **C**oating
BCBJ	**B**ack **C**ontact **B**ack **J**unction
BR	**B**ack **R**eflector
CASE	**C**ommission for **A**dditional **S**ources of **E**nergy
CEERI	**C**entral **E**lectronics **E**ngineering **R**esearch **I**nstitute
CERC	**C**entral **E**lectricity **R**egulatory **C**ommission
CdTe	**C**admium **Te**lluride
CIGS	**C**opper **I**ndium **G**allium **S**elenide
COP'21	**21**st **C**onference **o**f the **P**arties
CPV	**C**oncentrated **P**hoto**v**oltaics
CSIR	**C**ouncil of **S**cientific and **I**ndustrial **R**esearch
CVD	**C**hemical **V**apor **D**eposition
CZTS	**C**opper **Z**inc **T**in **S**ulfide
DBR	**D**istributed **B**ragg **R**eflector
DC	**D**irect **C**urrent
DNES	**D**epartment of **N**on-conventional **E**nergy **S**ources
EBL	**E**lectron **B**eam **L**ithography
EQE	**E**xternal **Q**uantum **E**fficiency
FDTD	**F**inite **D**ifference **T**ime **D**omain
FF	**F**ill **F**actor
FWHM	**F**ull **W**idth at **H**alf **M**aximum
GaAs	**G**allium **A**rsenide
GaN	**G**allium **N**itride
GDP	**G**ross **D**evelopment **P**roduct
GoI	**G**overnment **o**f **I**ndia
GW	**G**iga **W**att

HIT	**H**etero-junction with **T**hin **I**nterfacial
INDC	**I**ntended **N**ationally **D**etermined **C**ontributions
InGaN	**I**ndium **G**allium **N**itride
INUP	**I**ndian **N**anotechnology **U**ser **P**rogram
IQE	**I**nternal **Q**uantum **E**fficiency
ISA	**I**nternational **S**olar **A**lliance
I_{sc}	**S**hort **C**ircuit **C**urrent
ITO	**I**ndium **T**in **O**xide
JNNSM	**J**awaharlal **N**ehru **N**ational **S**olar **M**ission
LASER	**L**ight **A**mplification by **S**timulated **E**mission of **R**adiation
LED	**L**ight **E**mitting **D**iodes
LTS	**L**ight **T**rapping **S**tructure
MBE	**M**olecular **B**eam **E**pitaxy
MNES	**M**inistry of **N**on-conventional **E**nergy **S**ources
MOCVD	**M**etal **O**rganic **C**hemical **V**apor **D**eposition
MoP	**M**inistry **o**f **P**ower
MNRE	**M**inistry of **N**ew and **R**enewable **E**nergy
MQW	**M**ultiple **Q**uantum **W**ell
MW	**M**ega **W**att
NCPRE	**N**ational **C**entre for **P**hotovoltaic **R**esearch and **E**ducation
NISE	**N**ational **I**nstitute of **S**olar **E**nergy
NREL	**N**ational **R**enewable **E**nergy **L**aboratory
NRF	**N**anoscale **R**esearch **F**acility
NTPC	**N**ational **T**hermal **P**ower **C**orporation
NVVN	**N**TPC's **V**idyut **V**yapar **N**igam **L**td
PBC	**P**eriodic **B**oundary **C**onditions
PBG	**P**hotonic **B**and **G**ap
PECVD	**P**lasma **E**nhance **C**hemical **V**apor **D**eposition
PhC	**P**hotonic **C**rystal
PL	**P**hoto**l**uminescence

PML	**P**erfectly **M**atched **L**ayer
PMMA	**P**oly **M**ethyl **M**eth**a**crylate
PPA	**P**ower **P**urchase **A**greement
PV	**P**hoto**v**oltaics
PVD	**P**hysical **V**apor **D**eposition
PWE	**P**lane **W**ave **E**xpansion
$\mathbf{R^{Auger}}$	**A**uger **R**ecombination
$\mathbf{R^{non\text{-}rad}}$	**N**on-**R**adiative **R**ecombination
$\mathbf{R^{spon}}$	**S**pontaneous **R**adiative **R**ecombination
$\mathbf{R^{SRH}}$	**S**hockley-**R**ead **H**all **R**ecombination
RCWA	**R**igorous **C**oupled **W**ave **A**nalysis
RES	**R**enewable **E**nergy **S**ources
RF	**R**adio **F**requency
RIE	**R**eactive **I**on **E**tching
RSM	**R**eciprocal **S**pace **M**apping
SEM	**S**canning **E**lectron **M**icroscopy
Si	**Si**licon
$\mathbf{SiO_2}$	**Si**licon Dioxide
SPS	**S**hort **P**eriod **S**uperlattice
SPV	**S**olar **P**hoto**v**oltaic
S-Q	**S**hockley-**Q**ueisser
SRH	**S**hockley **R**eal **H**all
SWE	**S**taebler-**W**ronski **E**ffect
TCO	**T**ransparent **C**onducting **O**xide
TFSC	**T**hin **F**ilm **S**olar **C**ells
TPV	**T**hermo **P**hoto**v**oltaics
$\mathbf{V_{oc}}$	Open Circuit Voltage
XRD	**X**-**R**ay **D**iffraction

Dedicated to the memories of my grandparents, my father and to my mother, wife and family for their endless love, support and encouragement. . .

Chapter 1

Introduction

1.1. Introduction

Today one of the main crises the world is going through is the crisis of energy, mainly electrical energy. The problem is even worse in the developing countries like India. Even after almost 70 years of independence, many parts of our country are still not connected to the electricity grid system or those which are connected to the grid are not able to get a 24 hour supply of electricity, especially the semi-urban and rural areas of our country are the major victims of this problem.

The demand for energy, on the other hand, has been continuously increasing with the development of the country. This increase is exponential due to growth of population and thus to fulfill its demands, more industrialization and technical developments are required, which in turn increase the requirement of energy. However, the problem lies in the fact that the present reserves of the conventional energy sources will not be able to sustain in the future if we continue to harness them at this increasing rate and would ultimately ruin and might create the everlasting furor in the society. Another problem with the present conventional energy sources is their adverse effect on environment due to pollution, which with each passing day is becoming demon for the mankind; therefore one has to search for some alternatives for sustainable future. Thus, in today's world one of the biggest concerns is for the affordable and sustainable energy. This worldwide requirement for future access to affordable and sustainable energy is driving the development of more efficient renewable energy programs.

Electricity from renewable energy sources (RES) is increasingly been seen as the viable solution for energy deficiency, energy security and for social environment. Among many RES and technologies, electricity produced directly from the sun using solar photovoltaic (SPV) technology is gaining interest due to impetus from the governments and investments from private

enterprises. Solar energy is especially attractive as an alternative because it does not generate any fumes or gases, inexhaustible, abundant, pollution free and distributed throughout the earth. The SPV technologies are now increasingly seen as the major electricity source for Indian scenario. The announcement of Jawaharlal Nehru National Solar Mission (JNNSM) confirms this, which target to install about 20,000 MW of solar PV modules in India by 2022, having record solar power capacity addition of over 3000 MW during the financial year 2015-16 [1].

The main reason for not looking at SPV technology this much seriously earlier was because of its high initial cost. The cost is still formidable but with rising diesel and electricity prices, increased concern for climate change, need to find sustainable energy solutions and with considerable government support, SPV technology is increasingly being seen as viable option for our current and future energy supply [2].

One of the most incredible things about photovoltaic power is its simplicity. It is almost completely solid state, from the solar cell to the electricity delivered to the consumer. Whether the application is a solar calculator with a PV array of less than 1 W, or a 100 MW grid-connected PV power generation plant, all that is required between the solar array and load are electronic and electrical components. Compared to other sources of energy humankind has harnessed to make electricity, PV is the most scalable and modular form. A PV system consists of integrated assembly of PV modules designed to convert solar energy into electrical energy to provide a particular service in conjunction with grid or in off grid situations.

The solar cells are considered as the major building block for the SPV system, which are responsible for the efficient conversion of the solar spectrum photons into useful charge carriers, which ultimately convert sunlight energy into electricity. The working of the solar cells is based upon the well-known principle of photovoltaic effect, first recognized in 1839 by French physicist A. E. Becquerel [3]. However, it took almost 45 years for the first solar cell to be realized by Charles Fritts in the year 1883 [4]. Slowly, though steadily, technological progress has been taking place since then, resulting in increasing efficiency of the solar cells and PV systems and reducing per unit cost. Still, the cost per unit of electricity production is higher for the SPV systems as compared to electricity generated through conventional sources like coal or gas. Thus, in order to take this per unit generation cost down, one of the major solutions, is to either increase the efficiency of solar cells or reduce the amount of active material required for a

solar cell to achieve particular efficiency values, which ultimately reduces the per watt cost of a solar cell.

The requirement to reduce this cost has motivated a trend of thinning down the semiconductor wafers for photovoltaic cells, during the so called second generation of solar cell research and development era, in order to obtain more wafers and the larger total surface area from a bulk raw material. Thin film technology is of much commercial interests because it offers lower costs and possibilities for mass production and deployment and can prove to be the boon for the terrestrial application publicity of solar cells. The main problem with the thin film solar cell (TFSC) is its low efficiency, compared to the thick active layer cell design, leading to the limited absorption of solar spectrum photons in the active layer. During the past several years, various research and development activities have been proposed to overcome this problem and provide a low cost, high efficiency TFSC. Driven by the same idea and to add some new useful insight into the concept, an attempt has been made in the thesis to demonstrate an interesting and curious subject of subwavelength periodic structures (viz. Photonic Crystal Structures) through simulations and practical experiments for TFSC using Gallium Arsenide (GaAs) and Indium Gallium Nitride (InGaN)/Gallium Nitride (GaN) as active materials.

1.2. Indian Energy Scenario

Before we proceed towards my contribution, it is necessary to look into the Indian energy scenario, so that one can appreciate the difference between the demand and supply of electricity in our country and why it is necessary to look towards the alternate sources to fulfill our energy needs. India has been the third largest consumer of primary energy in the world after China and USA since 2013 [5, 6], and this demand for energy supply continues to climb on account of the country's dynamic economic growth and modernization over the past several years owing to its high economic growth rate. The uninterrupted supply of the energy, which is both affordable as well as environment friendly, is required to sustain this growth process over the long duration.

Although, India has large coal reserves and achieved notable overall growth in coal and natural gas production over the past two decades, India is increasingly dependent on imported fossil fuels and imports nearly 45% of its total primary energy sources. India was the second top coal consumer in the year 2015 after China and ranks third in oil consumption with 195.5 million tons in 2015 after USA and China. India's energy demand has almost doubled during the last two

decades, however, the per capita energy consumption in India is still well under the world average [7] and thus its energy demand will grow exponentially in the coming years to balance with the development of the country. In terms of installed capacity India is among the top 5 major countries and contributes about 4 percent of global power generation. The total installed capacity for India has been listed in Table 1.1 (as on 31st Aug., 2016) [8].

Table 1.1: Total Installed Power (as on 31-08-2016) for India

Fuel Source	Installed Capacity (in MW)	% of Total
Total Thermal	***212,569***	***69.44 %***
Coal	186,593	60.96 %
Gas	25,057	08.19 %
Oil	919	00.29 %
Hydro	***42,968***	***14.04 %***
Nuclear	***5,780***	***1.89 %***
Renewable Energy Sources**	***44,783***	***14.63 %***
Total	***306,100***	***100 %***

***Renewable Energy Sources includes Small Hydro Power, Wind Energy, Solar Energy, Biomass Gasifier, Biomass Power, Urban and Industrial waste power* [8].

From the table, one can easily observe that most of our energy demands are fulfilled through primary energy resources like coal and gas, both of which are depleting fast and at the same time polluting the environment at an alarming rate leading the world to take a serious call through UN Climate Change Conference Paris 2015 or 21st Conference of the Parties (COP'21) [9]. Almost all of the major countries in the world including India agreed for 'Intended Nationally Determined Contributions' (INDC), during the summit and submitted their climate action plans ahead of the COP21. In the action plan they outlined how, and by how much, countries will reduce their emissions, and the actions they will undertake to strengthen climate resilience. In recognition of the growing problem of climate change, India declared a voluntary goal of reducing the emissions intensity of its Gross Development Product (GDP) by 20–25%, over 2005 levels, by 2020, despite having no binding mitigation obligations as per the convention [10]. Thus, in order to achieve these voluntary goals, India is running one of the largest renewable capacity expansion programs in the world.

During the past decade, the contribution of RES in Indian installed energy has increases from about 2% in the year 2005 to over 14% in the year 2016. The noteworthy achievement in the

previous decade is to be significantly scaled up with the aim to achieve 175 GW renewable energy capacity till 2022. Among various RES, although wind energy contribution has continuously been topping the chart, solar energy sector has done tremendous development during the past few years in India and became the second most installed RES (including both solar thermal and PV). Solar power installed capacity has increased from only 3.7 MW in 2005 to about 8000 MW in 2016. The installed RES capacity for India has been listed in Table 1.2.

Table 1.2: Installed Grid Interactive Renewable Power Capacity in India (as on 31st July, 2016) [11, 12]

Source	Total Installed Capacity (in MW)	Installation target for the year 2022 (in MW)
Wind Power	27,441.15	60,000.00
Solar Power	8,062.00	100,000.00
Biomass Power (Biomass & Gasification and Bagasse Cogeneration)	4,860.83	*10,000.00
Waste-to-Power	115.08	
Small Hydro Power	4,304.27	5,000.00
Total	44,783.33	175,000.00

* *The target is given for "bio-power" which includes biomass power and waste to power generation.*

Solar power in India is poised to grow significantly with JNNSM, which is one of a major initiatives of the Government of India (GoI) to publicize solar energy. The ambitious solar expansion program seeks to enhance the installed solar energy capacity to 100 GW by 2022, which is expected to be scaled up further thereafter. From Table 1.2, we can analyze that solar power is under 9% of its target till date and thus require dramatic expansion in the near future to achieve the target of 100 GW till 2022. To achieve this goal GoI is running a scheme for development of 25 Solar Parks, Ultra Mega Solar Power Projects, canal top solar projects and one hundred thousand solar pumps for farmers are at different stages of implementation. GoI is also promoting solarization of all the 55,000 petrol pumps across the country out of which about 3,135 petrol pumps have already been solarized [10]. India has also decided to anchor a global solar agency, International Solar Alliance (ISA), currently having Interim secretariat at National Institute of Solar Energy (NISE), Gurugram, India, for all countries located between the Tropic of Cancer and the Tropic of Capricorn to develop an international agency solely dedicated for the development and exchange of solar energy related technologies around the globe.

Thus, there are serious efforts going on for the promotion and development of solar energy across the country with the support of GoI, and thus the sun seems to be shining for the field and can solve the problem of energy scarcity for our country. However, all these efforts are needed to be supported through the active research and development in the field to provide affordable and innovative solutions which can be used as an alternatives for the existing systems.

1.2.1. Jawaharlal Nehru National Solar Mission (JNNSM)

As mention earlier, GoI is poised to make significant development in the field of solar energy through JNNSM [1, 11], which was launched in the year 2010 to encourage the development of solar energy systems in our country. The mention of the mission is important in the thesis as it is one of the basic inspiration to study the subject highlighted in the following work, which can eventually help in the energy solution for our country.

The objective of the JNNSM under the brand 'Solar India' is to establish India as a global leader in solar energy, by creating the policy conditions for its diffusion across the country as quickly as possible. The mission has initially set a target of 20,000 MW, which has been later revised to 100 GW till 2022 and stipulates implementation and achievement of the target in 3 phases (first phase upto 2012-13, second phase from 2013 to 2017 and the third phase from 2017 to 2022) for various components, including grid connected solar power.

The successful implementation of the JNNSM requires the identification of resources to overcome the financial, investment, technology, institutional and other related barriers which confront solar power development in India. The penetration of solar power, therefore, requires substantial support. The policy framework of the mission will facilitate the process of achieving grid parity by 2022.

In order to facilitate grid connected solar power generation in the first phase, a mechanism of “bundling” relatively expensive solar power with power from the unallocated quota of the GoI (Ministry of Power, MoP) generated at NTPC coal based stations, which is relatively cheaper, has been proposed by the Mission. This “bundled power” would be sold to the distribution utilities at the Central Electricity Regulatory Commission (CERC) determined prices.

The projects will be selected under this scheme in such a manner so as to provide for deployment of both SPV Technology Projects and Solar Thermal Technology projects in a ratio of 50:50, in

MW terms. The success of the mission can be evident from the fact that the installed solar energy capacity has enhanced manifold during the past few years reaching the level of more than 8 GW and compelled the policy makers to prioritize the sector and rescale the target achievable capacity to 100 GW till 2022. In the mission, special emphasis is also given towards the development for the Solar PV technologies including p-type silicon wafers and n-type silicon wafers, hetero junction with thin interfacial (HIT) module, back contact back junction (BCBJ) modules, crystalline silicon photovoltaic cells of more than 24 % cell efficiency, high efficiency Concentrating PV (CPV) and non-silicon based solar PV technologies. All and all the purpose of the scheme is to develop new solar energy systems in our country to meet the shortage of our electricity needs and to establish India as a global leader in the field of solar energy, by creating the policy conditions for its diffusion across the country as quickly as possible.

1.3. Introduction to Solar Cells

Solar energy unarguably plays an important role in sustenance of life on earth as nearly all sources of energy are directly or indirectly depends on heat and light from the sun, right from photosynthesis in plants to burning of fossil fuels. Solar radiation accounts for most of the available renewable energy on earth as sources such as wind, hydroelectricity and biomass are also dependent by one way or other over the solar energy. Thus, the energy from the sun is being utilized over the years through different ways however still there is huge potential to tap the solar radiation received on earth. The total solar energy that the earth absorbs is approximately 3,850,000 EJ/year [12]. Even the amount of energy obtained in one hour is more than the world’s energy requirement for one year. Also the amount of solar energy reaching the earth is so enormous, that in one year it is about twice as much as will ever be obtained from all of the earth's non-renewable resources combined. Hence it is important to harness this vast source of energy and forms the basis of the Solar PV and Solar Thermal based technologies.

In simplest of terms, a solar cell is a semiconductor device which converts light into electricity. It produces a voltage and current as light incidents on it. As long as there is sunlight, the solar cell will provide a direct current (DC) of electric power, which can be converted into standard alternating current (AC) supply. PV offers various advantages compared to other energy technology like its source, the sun is infinite, produces pollution free clean energy, it has no

moving parts, modular, can be installed in different sizes and places. Also, material used for making solar cells and modules can be recycled.

The three most important functions of a solar cell are classified as carrier generation, carrier separation, and carrier collection [13]. The generation of carriers occurs in the bulk active material region of the solar cell device which is solely responsible for the absorption of photons and then conversion of those photons into charge carriers. The separation of these generated carriers requires an electric field, like as provided by p-n junction, and for effective carrier collection, a proper contacting method is required. Take an example of a popular silicon (Si) solar cell. Here, generation of carriers takes place in active Si material through absorption of photons. The electron hole pairs generate across the device, and these carriers are then separated out by the p-n junction leading to the formation of a potential, and hence a current. One of the many available contact designing schemes can be used to ensure maximum current collection. Additionally light trapping geometry has also been incorporated into the designs of the solar cells like anti-reflective coatings and back reflectors, which are used to enhance the performance of the cells. The design of the light trapping structures (LTS) plays a vital role for the efficient functioning of the solar cell devices, which is also the main objective of the thesis and will be discussed in detail during the following chapters. A schematic of a basic silicon solar cell is shown in Figure 1.1.

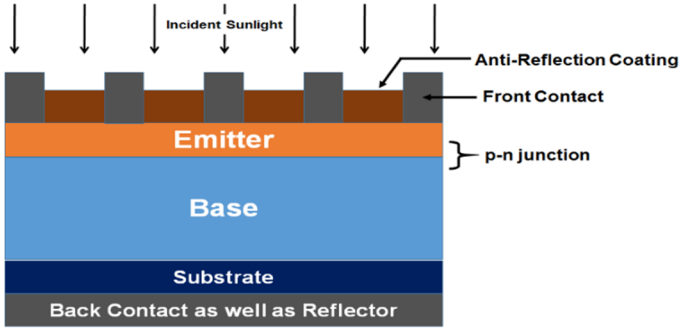

Figure 1.1: Schematic diagram of a basic silicon solar cell

A design of a solar cell starts with an unpolished wafer of required orientation. The important parameters to be kept in mind while choosing a substrate for solar cells, is its orientation, resistivity, thickness and doping [12]. Typical thickness of wafers used for Si solar cells is about 180-200 μm. The resistivity values should be small. Over the substrate there is a thick lightly doped base and thin heavily doped emitter region, which come in contact with each other to form p-n junction. The base is kept thick in order to allow most of the incident photons to be absorbed

in this region and lightly doped to improve diffusion length. The emitter layer is kept as thin as possible to allow most of the light to pass towards the base region and heavily doped in order to reduce sheet resistance. However the emitter should not be extremely thin as this would ultimately increase the series resistance of the device [13].

In order to reduce reflections from the top surface of a solar cell device usually an anti-reflection coating (ARC) is placed at the top. Similarly in order to absorb the photons in the active layer which are usually passed through the cell without getting absorbed, a back reflector (BR) is commonly employed, as shown in Figure 1.1. Both ARC and BR are considered to be part of the LTS, which however increase the design complexity and cost of the overall device, but the addition to performance capability to the cell they provide usually decreases the overall per watt cost of the cell. Designing of LTS has been an active area of research for quite sometimes, in order to obtain high efficiency solar cells and is also one of the motives of this thesis work. The contact formation is also an important step in solar cell design. Usually a grid like metal pattern running across the cell is used to collect the charge carriers. The smaller contacts are called the fingers, and these fingers terminate on a bus bar, which is thicker and wider [12]. The top contact design is an important aspect, because, a larger number of contacts would mean better collection but at the expense of larger shadowing losses, thus there is a need of a trade-off between the two in order to achieve optimal results. Thus, the overall design parameters required for a solar cell irrespective of a material system can be summed up as follows [13]:

i. The thickness of the active region should exceed the absorption depth of incident photons range for efficient light absorption. However, for TFSC where the active layer thickness is limited, it should be compensated through LTS at the back.
ii. The junction should be thin compared to both the diffusion length in the emitter and the absorption length for the active material to avoid fruitless absorption of light at the front of the cell.
iii. Emitter should be doped heavily to provide better carrier collection and support the light doping of base which improves absorption of the photons in the base region.
iv. Reflections of light from the top should be reduced using an optimized ARC. Commonly ARC is also considered as a part of a LTS.

1.3.1. Brief History of Solar Cells

The early history of the solar cells dates back to the 18th century, when Alexander Edmond Bacquerel first found the phenomenon of photovoltaic effect. The brief summary of some of the important events that remarkably take the field forward (and especially related to our subject of study), took place during all these years has been listed below [14]:

1839 - Photovoltaic effect observed by A. E. Becquerel through an electrode in a conductive solution exposed to light [3].

1877 - W.G. Adams and R.E. Day observed the photovoltaic effect in solidified selenium and published a paper on the selenium cell [15].

1883 - A modern solar cell like device developed by Charles Fritts using selenium on a thin layer of gold provided less than 1% efficiency [4].

1904 - W. Hallwachs made a semiconductor-junction solar cell (copper and copper oxide) [16].

1918 - Czochralski produced a method to grow single crystals of metal [17]. Decades later, the method was adapted to produce single-crystal silicon.

1932 - Audobert and Stora discovered the photovoltaic effect in Cadmium selenide (CdSe).

1954 - On April 25, 1954, Bell Labs announced the invention of the first practical silicon solar cell [18]. These cells had about 6% efficiency.

1957 - D. M. Chapin, C. S. Fuller and G. L. Pearson received patent US2780765 [19], "Solar Energy Converting Apparatus" and referred it as the "solar battery."

1958 - T. Mandelkorn, U.S. Signal Corps Laboratories, created n-on-p silicon solar cells. Vanguard I, the first solar powered satellite, was launched.

1959 - Hoffman Electronics creates a 10% efficient commercial solar cell.

1961 - W. Shockley and H. J. Queisser published a paper for single junction achievable efficiency limit [20].

1967 - Soyuz 1 is the first manned spacecraft to be powered by solar cells

1970 - First highly effective GaAs heterostructure solar cells were created by Z. Alferov and his team in the USSR [21].

1976 - D. Carlson and C. Wronski of RCA Laboratories created first amorphous silicon PV cells, which have an efficiency of 1.1% [22].

Late 1970s - the "Energy Crisis" gave rise to interest for photovoltaic and active and passive solar technologies.

1980 - The Institute of Energy Conversion at University of Delaware developed the first TFSC exceeding 10% efficiency using Cu_2S/CdS technology.

1981 - Commission for Additional Sources of Energy (CASE) established under GoI to promote RES [23].

1982 – E. Yablonovitch and G. D. Cody published an article for Lambertian light trapping limit for weak absorbing materials [24]. Department of Non-conventional Energy Sources (DNES), that incorporated CASE, was created in the then Ministry of Energy under GoI [23].

1985 - 20% efficient silicon cells were created by the Centre for Photovoltaic Engineering at the University of New South Wales [25].

1988 - The Dye-sensitized solar cell was created by M. Grätzel and B. O'Regan [26].

1989 - Reflective solar concentrators were first used with solar cells.

1991 - Efficient Photoelectrochemical cells were developed.

1992 - A separate ministry established in GoI under the name of Ministry of Non-Conventional Energy Sources (MNES) [23]. University of South Florida fabricates a 15.89-percent efficient thin-film cell.

1993 - The National Renewable Energy Laboratory's (earlier known as Solar Energy Research Institute) Solar Energy Research Facility was established at Colorado, US.

1994 - NREL develops a GaInP/GaAs two-terminal concentrator cell (180 suns) which became the first solar cell to exceed 30% conversion efficiency.

1996 - Graetzel, École Polytechnique Fédérale de Lausanne, Lausanne, Switzerland achieved 11% efficient energy conversion with dye-sensitized cells that use a photoelectrochemical effect.

1999 - Total worldwide installed photovoltaic power reached 1,000 megawatts.

2002 - M. A. Green modified the Lambertian limits for any type of absorbing material. J. M. Gee published a paper on Photonic Crystals based enhanced absorption [27].

2004 - C. Honsberg, O. Jani et al. published a pioneer work for InGaN/GaN based solar cell devices [28].

2006 - Ministry of Non-Conventional Energy Sources (MNES) renamed as Ministry of New and Renewable Energy (MNRE) by GoI [23].

2007 - University of Delaware claimed to achieve new world record in Solar Cell Technology without independent confirmation - 42.8% efficiency [29].
2008 - NREL had set a world record in solar cell efficiency with a PV device having efficiency of 40.8 percent under the concentrated energy of 326 suns [30].
2010 - JNNSM launched by GoI to tap the vast solar potential that India having and set the target to achieve 20 GW installed solar energy by the year 2022 [11].
2010 - The National Centre for Photovoltaic Research and Education (NCPRE) at IIT Bombay was launched in 2010 and is a part of the JNNSM of the GoI [12]. The objective of the center is to be the one of the leading PV research and education centers in the world and aims to create and execute the blueprint for human resource development for PV in India.
2012 - Alta Devices broke the single junction cell efficiency world record at 28.8% [31].
2015 - The solar energy target has been modified to 100 GW to be achieved till 2022 [1].
2016 - India achieved installed solar energy capacity of over 8 GW. University of New South Wales engineers established a new world record for unfocused sunlight conversion to electricity with an efficiency increase to 34.5% for four junction cell [32]. Alta Devices broke the dual-junction cell efficiency world record at 31.6% in 2016 [31].

Although I have tried to incorporate most of the major events that took place in the history related to the solar cell development, I also wish to gracefully acknowledge the contributions of all the events which ultimately led to the happenings of these milestones.

1.3.2. Broad Classification of Solar Cells

The solar cells are classified on the basis of various parameters depending upon the requirement. Popularly, the solar cells are classified on the basis of the active material used to design the device like Si solar cell, Gallium Arsenide (GaAs) solar cell etc. The solar cells can also be classified on the basis of number of junctions used to separate the generated charge carriers like a design having the one single layer of light-absorbing material is considered as single-junction cell or having multiple physical configurations known as multi-junction solar cells.

Solar cells are also widely classified as *first*, *second* and *third* generation cells. The first generation cells usually include conventional, traditional or wafer-based cells generally made of crystalline silicon which is a commercially leading solar cell technology. Second generation cells commonly account for TFSC primarily designed to reduce the size, weight and cost of the solar

cell devices, and include amorphous silicon, CdTe, GaAs and CIGS cells which are commercially significant in space based applications, utility-scale photovoltaic power stations, building integrated photovoltaics or in small stand-alone power system. The third generation of solar cells includes a novel thin-film technologies or emerging photovoltaics - most of them have not yet been commercially applied and are still in the research or development phase - to provide low cost high efficiency solutions like organic solar cells, nanostructures based designs, perovskite based structures etc.

One of the major classification of the solar cells is based on the substrate geometry like *crystalline*, *thin film* and *multi-crystalline* solar cells. Crystalline solar cells, one of the most prevalent solar cells, are further sub categorized as monocrystalline or polycrystalline. Mono-crystalline, also known as single crystalline, are the purest form of the material like crystalline Si where all the crystals are arranged in the same direction providing better material quality and strength which in turn provide better device output. However as the cells are made from large cylindrical ingots, the resultant product is usually expensive and results in significant amount of waste of the original ingot. Unlike monocrystalline-based solar panels, polycrystalline solar panels do not require the Czochralski process. Polycrystalline material molecules does not have the same alignment in all the directions. Raw silicon is melted and poured into a square mold, which is cooled and carefully solidified and cut into perfectly square wafers. Thus, the process is less expensive as compared to monocrystalline growth with less waste. However, the polycrystalline material based cells suffer from efficiency setback due to compromise with the quality of the active material.

The drawbacks of the crystalline solar cells such as their expensiveness and weight led to the development of a class of solar cell known as TFSC. Some authors categorized solar cells as thin film depending upon the process of the layer deposition techniques whereas some others classify them as per the thickness of the active layer. Usually the TFSC have very thin active layer having thickness in sub μm or even in nm range. They have several advantages which make them attractive for the mass production and viable option for terrestrial applications. However, their main shortcoming is small efficiency. TFSC will be further discussed in next section.

There is another class of solar cells known as multi-junction solar cells, which considered to overcome the shortcomings of both single crystal as well as TFSC. The class consists of multiple

thin films of different materials or same material having different composition having different band gaps, in order to absorb as much solar spectrum as possible. The highest efficiencies of solar cell till date has been achieved through multi-junction solar cells as can be seen from Figure 1.2. However, the main problem with the multi-junction solar cells is its complexity of design as there is a requirement to put different lattice materials over each other with band gap in specific order. In such a case, there is a need of optimized complex fabrication issues to be handled carefully to get the desired results.

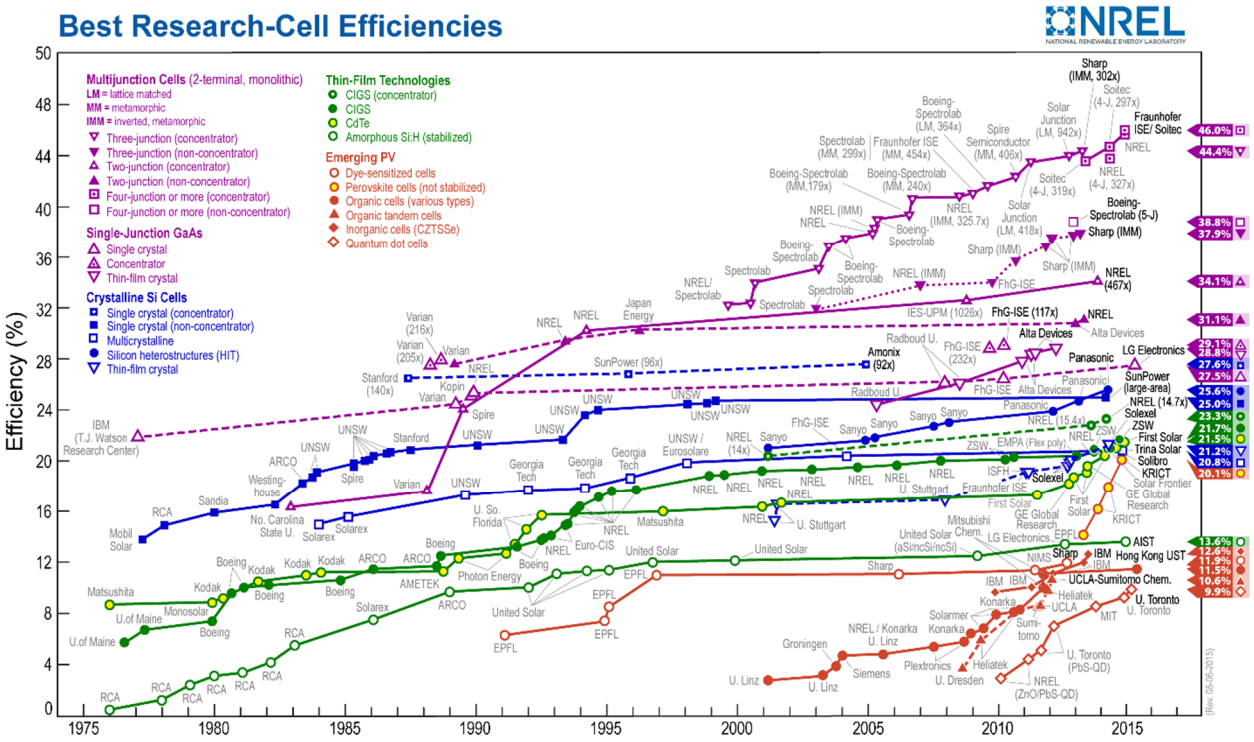

Figure 1.2: Solar cell efficiency chart [35]

There are also a class of solar cells known as concentrated solar cell, which uses a concept of concentration of sunlight, i.e., to increase the input incident light in order to improve the overall output. However, for concentrated solar cells, the basic requirement is that the absorbing material should perform well under high temperature and radiation as the concentration increases the temperature of the overall system well above the atmospheric temperature. GaAs is usually preferred for concentration solar cells. There are many other emerging classes of solar cells like perovskite solar cells, organic solar cells, quantum dot solar cells, thermo-photovoltaics, nano-structures based solar cells etc. which are more or less still in their nascent stages and thus various research studies around the world are going to get the high efficiency solar cells having

high stability with less weight and cost that would be robust over the long duration of its operation under practical conditions.

1.3.3. Thin Film Solar Cells

Thin film solar cells, as discussed above, were basically evolved in an attempt to find the low cost light weight alternative to the bulky and expensive crystalline solar cells [13]. TFSC are considered to be the part of second generation solar cells. These TFSC are basically designed by depositing the thin films of active material over the substrate of choice, having thickness varying from a few nm to tens of μm, much less than the crystalline solar cells. The layers of thin film are commonly deposited using available depositing schemes like physical vapor deposition (PVD) or chemical vapor deposition (CVD). Reduction in thickness of active layer eventually makes TFSC flexible, lower in weight and cost and have less drag or friction. Commercially available technologies for TFSC ranges from Amorphous Si (a-Si), Cadmium Telluride (CdTe), Copper Indium Gallium (Di)Selenide (CIGS) to GaAs.

Basic parameters that are required to be kept in mind while designing a TFSC include an active material with high absorption coefficient, as these materials usually have low diffusion length. Several designs use extended electric fields such as p-i-n junction to assist carrier collections. Usually in TFSC losses near the front surfaces are more thus the designs incorporate a window layer to reduce these kind of losses. TFSCs usually suffer from the problem of low efficiency, which is primarily due to the fact that absorbing material is not able to absorb the entire solar spectrum photons, due to its limited thickness. Thus, in order to improve the absorption of these otherwise un-absorbed photons, TFSC commonly employ same LTS, as discussed earlier. It is also the basic purpose of the thesis to discuss in detail the effect of periodic pattern LTS with TFSC to improve the absorption in these structures.

a-Si is considered to be one of the most matured TFSC technology and has been in commercial production since 1980 [13]. a-Si is a non-crystalline, allotropic form of silicon, that uses plasma enhanced CVD (PECVD) or sputtering type of deposition process to deposit a very thin layer of few μm over substrate, such as glass, plastic or metal. As the bandgap of a-Si is about 1.7 eV, it can absorb a large part of solar spectrum and can perform well under weak light. However, a-Si based solar cells suffers from problem like high inherent disorder and dangling bonds in the materials, responsible for its bad conductivity. The cell also suffers from the Staebler-Wronski

effect (SWE), a typical loss in electrical output due to changes in photo and dark current conductivity caused by prolonged exposure to sunlight. These problems ultimately degrade the output efficiency of the device and need to be addressed carefully to achieve high efficiency out of the device.

CdTe is one of the predominant TFSC technology that accounts for more than half of the thin film market. The lab efficiency of these cells has improved all through these years reaching almost the level of multi-crystalline Si cells [33] as can be visualize from Figure 1.2. However the major drawback for the wide commercialization of the technology is the toxicity of Cadmium and the use of rare earth material like tellurium and that too in the anionic form. Another type of thin film technology, CIGS is also considered as an important TFSC class having already achieved lab efficiency of over 20% [34]. CIGS is the direct band gap material having high absorption coefficient making it an attractive choice for the TFSC. The addition of Gallium in CIS improves the performance of the device through improvement in its band gap as well as electrical properties of back contact. However, the design problem in the device like limitation of photon absorption at high wavelength due to poor carrier collection and high recombination at heterojunction and at grain boundaries due to high defect densities seriously restricts the further development of the technology.

There is another class of TFSC termed as GaAs solar cells, which has been here and studied for more than 50 years due to its variety of peculiarities. The most high efficiency single junction solar cell belongs to the class of III-V compound semiconductors, specifically Gallium Arsenide (GaAs), due to its direct band gap and near to ideal band gap value [20] for solar cells as can be seen from Figure 1.2. However the main limitation with GaAs material is its expensiveness that ultimately hampers its use for terrestrial applications, thus its use is basically restricted to the space and for concentrated solar cell applications. Although, various unique qualities of GaAs such as it has high absorption coefficient with high radiation and temperature resistivity provide it an edge over Si and make it an exceptional material for solar cell applications. However, to make the material acceptable for terrestrial solar cell applications, it is required to achieve high efficiency with extremely thin films of GaAs active material which could ultimately reduce the requirement of GaAs material and eventually cut down the cost [35].

The efficiency of thin-film single-junction GaAs solar cells has improved substantially over the

past several years [34], however they are still under the Shockley limit [20]. There are several factors which are responsible for this efficiency limitation, including the absorbing material limited thickness, various recombination factors which become dominant with increasing active layer thickness [13], [36]. Thus, it is required to improve the design for these cells to achieve high efficiency out of the device with extremely thin films, which is also one of the aims of the thesis. In the succeeding literature, we will discuss in details, about the reasons responsible for the efficiency limitations and how one can improve the performance of the thin film GaAs solar cells using periodic patterned LTS to get notably high absorption in the device with ultra-thin GaAs layers that will ultimately be helpful in the increase of the terrestrial popularity of the device.

The National Renewable Energy Laboratory (NREL) also classifies several other thin film processes as emerging solar cells technologies, which are still in the research and development phase and mostly yet to be commercialized [37]. These technologies usually considered as third generation solar cells include Copper Zinc Tin Sulfide (CZTS) solar cell, dye sensitized solar cell (also known as "Grätzel cell"), organic solar cell, perovskite solar cells, polymer solar cells, InGaN/GaN based solar cell etc. Out of these, perovskite solar cell has done tremendous development during the past few year, reaching almost 20% efficiency [38, 39].

During the last few years, interest has also grown towards the design and development of InGaN/GaN based solar cells. InGaN material has shown the potential for full solar spectrum applications after it has been established that it is possible to tune the bandgap of $In_xGa_{1-x}N$ compounds from 0.7 (for InN) to 3.4eV (for GaN) [40, 41]. Moreover, other unique properties of $In_xGa_{1-x}N$ alloys like direct band gap, high absorption coefficient (~10^5 cm^{-1}) near the band edge, good thermal stability, irradiation resistance, excellent chemical tolerance (i.e. not easily corroded by chemical solutions) and high carrier mobilities also add to the advantages that it could offer to the design and fabrication of high efficiency thin film cells [42, 43]. The comparison of material properties of Si, GaAs and InGaN/GaN has been discussed in Table 1.3.

Due to all these qualities of $In_xGa_{1-x}N$ alloys, InGaN/GaN hetero-structures have gained much attention for solar cell applications [44, 45]. However, the problem with the InGaN solar cell is the unavailability of the lattice matched substrate, which limits the thickness of the epitaxial InGaN layer that can be grown and also due to the limited miscibility of the Indium in GaN

hampers development of high indium content layer, which limits the band gap of the active layer and thus restricts the output efficiency of the device. During the thesis I will also discuss about the effect of periodic structures in the absorption enhancement of the InGaN/GaN solar cells, the details of which will be discussed in further sections.

Table 1.3: Material Comparison between Gallium Arsenide (GaAs), Indium Gallium Nitride (InGaN) and Silicon (Si) at Room Temperature

Parameter compared	**Gallium Arsenide (GaAs)**	**Indium Gallium Nitride (InGaN)**	**Silicon (Si)**
Band Gap	1.42 eV	Tunable band gap given by the Equation $E_{gInGaN} = xE_{gInN} + (1-x)E_{gGaN} - b.x.(1-x)$ where x is the Indium content, E_{gInN} = 0.7 eV, E_{gGaN} = 3.42 eV and b is the bowing parameter considered as 1.43	1.11 eV
Gap: Direct or Indirect	Direct	Direct	Indirect
Electron Mobility	$\leq$8500 $cm^2/(V.s)$	$\leq$4400 $cm^2/(V.s)$ (for InN)	$\leq$1500 $cm^2/(V.s)$
Hole Mobility	$\leq$450 $cm^2/(V.s)$	$\leq$39 $cm^2/(V.s)$ (for InN)	$\leq$400 $cm^2/(V.s)$
Electron Diffusion Coefficient	$\leq$200 cm^2/s	$\leq$115 cm^2/s (for InN)	$\leq$36 cm^2/s
Hole Diffusion Coefficient	$\leq$10 cm^2/s	$\leq$2 cm^2/s (for InN)	$\leq$12 cm^2/s
Absorption Coefficient near band edge (accounts for absorption of the photons near band edge)	10^4 cm^{-1}	10^5 cm^{-1}	10^3 cm^{-1}
Thermal Stability	High	High	Low
Minority Carrier Lifetime	10^{-8} s	10^{-8} s	10^{-6} s
Temperature coefficient (accounts for performance degradation with temperature)	0% (almost no performance loss with respect to temperature)	0% to positive (performance might enhance with temp rise for certain range)	Negative (means performance reduces with temp. rise)
Crystal Structure	Zincblende	Wurtzite	Diamond (other structures are also possible)
Cost of material and manufacturing	Very High	High	Low
Growth or Deposition Process Used	Usually Molecular Beam Epitaxy (MBE) or Metal Oxide Chemical Vapor Deposition (MOCVD) process is used	Molecular Beam Epitaxy (MBE) or Metal Organic Chemical Vapor Deposition (MOCVD) process is used	Deposition of Si could be done through variety of methods ranging from sputtering to atomic layer deposition (ALD) to Plasma-enhanced chemical vapor

			deposition (PECVD) etc.
Substrate Used for growth	GaAs (lattice matched). Other substrates are also used to reduce the overall cost but due to lattice mismatch results in inferior results as compared to GaAs substrate.	No lattice matched substrate available. Usually grown over the sapphire substrate. Due to the lattice mismatch between the substrate and grown layer the efficiency achieved is usually smaller than the theoretical predictions.	Si (lattice matched). As Si is not expensive and easily available there is no problem to grow Si over the lattice match substrate. However as the absorption coefficient is small and it is a indirect band gap material, the limiting efficiencies predicted are always less than the GaAs value,
Performance under high heat and low light	High with less degradation	High but less than GaAs	Low and degrades early
World Record Efficiency	28.8±0.9% (GaAs thin film, Alta Devices)	Less than 5% (the efficiency is basically limited to problems arises in the growth of InGaN layer over lattice mismatch substrate system)	25.6±0.5 (Si Crystalline, Panasonic HIT)
Electron Diffusion Length	≤15 μm	≤11 μm (for InN)	≤60 μm
Holes Diffusion Length	≤3 μm	≤1 μm (for InN)	≤35 μm

1.3.4. Characteristics of the Solar Cell: Summary

There are various parameters which are used to characterize and evaluate the performance of a solar cell. There are basically five parameters which are used to describe the performance of the solar cells, which include current-voltage (I-V) curve, short circuit current (I_{sc}), open circuit voltage (V_{oc}), Fill Factor (FF), and Efficiency (η) together with incident spectrum (air mass). All these terms are related to each other through some mathematical formulation.

I-V curve of a solar cell is the superposition of the I-V curve of the solar cell ideal diode in the dark with the light-generated current [46]. Whenever the light is incident over the cell, the I-V curve get shifted down to the fourth quadrant where power can be extracted from the diode. The IV curve is derived using the diode law and given as [13, 20]:

$$I = I_0\left[exp\left(\frac{qV}{nkT}\right)-1\right]-I_L \tag{1.1}$$

where I_L is the light generated current, q is the charge of an electron, V is the applied voltage, k is the Boltzmann constant, T is the temperature in degree Kelvin, I_0 is the dark saturation current in

the absence of light and *I* is the net current flowing through the diode. Here, n is an ideality factor, is a measure of a junction quality and the type of recombination in the cell. It is a number lies between 1 and 2 which typically increases as the current decreases.

The short-circuit current is the current through the solar cell when the voltage across the solar cell is zero [47]. I_{sc} is due to the generation and collection of light-generated carriers. For an ideal solar cell having no loss, I_{sc} and I_L are identical, which can be found after putting V=0 in Equation (1.1). Therefore, the short-circuit current is the largest current which can be drawn from a cell. However, practically I_{sc} is always less than the light generated current. I_{sc} depends upon number of factors including area of the cell, incident light source intensity, the spectrum of the incident light, the optical properties of the cell material as well as the collection probability of the carriers inside the cell, depends upon the surface passivation and diffusion length.

The open-circuit voltage, V_{oc}, is the maximum voltage available from a solar cell when there is no current out of the device at open circuit condition. V_{oc} corresponds to the amount of forward bias on a cell due to the bias of the solar cell junction with the light-generated current [13]. V_{oc} can be derived using the Equation (1.1) by putting $I=0$. The modified equation becomes:

$$V_{oc} = \frac{nkT}{qV} ln\left(\frac{I_L}{I_0} + 1\right) \tag{1.2}$$

From the Equation (1.2), it is clear that V_{oc} depends upon the light generated current and reverse saturation current. I_0 causes the main effect in determining the value of V_{oc}, since this may vary by orders of magnitude, as it depends on recombination in the solar cell. In an ideal condition, the V_{oc} increases with increasing electronic band gap of the material, however, this increase in the band gap restricts the amount of incident spectrum that an active material could absorb and thus eventually reduces the value of I_{sc}. Thus, to find the optimal value of both the factors simultaneously and to extract maximum power output, there is a need to have a trade-off between the values of these two factors and for this, one should have the value of the material band gap near to 1.4 (near to the band gap of GaAs) for single junction solar cell [20].

Fill Factor (FF) is an important parameter for the characterization of a solar cell, which determines the highest possible power output from the device. At both I_{sc} and V_{oc}, the power output from the solar cell is zero. FF is defined as the ratio of the maximum power, P_m out of a

solar cell to the product of I_{sc} and V_{oc}, i.e., to the ideal power, P_0=Isc.Voc. In other words it defines the squareness of the I-V curve. Mathematically, FF is given as:

$$FF = \frac{P_m}{P_0} = \frac{V_m \times I_m}{V_{oc} \times I_{sc}} \tag{1.3}$$

where V_m and I_m are the voltage and current at maximum power point respectively. A solar cell with a higher voltage has a larger possible FF since the rounded portion of the I-V curve takes less area. Ideally for a loss less cell, FF can take maximum value of unity, however, practically there is no such device and thus FF is always less than unity. Typical values of FF for Si and GaAs solar cell is around 0.82 and 0.89 respectively, and thus the value of FF ultimately depends upon the active material type and quality.

The efficiency is the most frequently used parameter to compare the solar cells performances. Efficiency is defined as the fraction of the incident light that is converted into useful output. Efficiency term is again divided into two different terms, one is internal quantum efficiency (IQE), which defines the conversion ratio of incident photons into charge carriers and second is external quantum efficiency (EQE), which defines the ratio of incident photons actually reached the collection terminals to provide useful output. The efficiency not only depends upon the device quality but also on the spectrum and intensity of the incident sunlight and the temperature of a solar cell, i.e., it also depends upon the test conditions and thus need to be carefully controlled as per the standard specified conditions. Terrestrial solar cells are measured under AM1.5 conditions and at a temperature of 25°C [48]. Usually, efficiency, η, has been defined as:

$$\eta = \frac{V_m \times I_m}{P_s} \tag{1.4}$$

where P_s is the incident light power density, considered as 1000 W/m^2 for terrestrial solar cell test conditions. The Equation (1.4) can be relate to *FF*, I_{sc} and V_{oc} using Equation (1.3) as

$$\eta = \frac{V_{oc} \times I_{sc} \times FF}{P_s} \tag{1.5}$$

The above mention quantities are important parameters as they defines the actual performance of a solar cell and thus during the thesis will be considered to compare the outputs of the designed structures with the reference values.

Together with all the above defined parameters, the output efficiency of the solar cells depends primarily upon the incident spectrum. The solar spectrum varies throughout the day as well as with location. Thus there is a need to define a standard reference spectra to allow the performance comparison of different photovoltaic devices from different labs. Thus, the standard spectra were refined in the early 2000's to standardize the cell test conditions internationally [49]. The air mass (AM) coefficient, which defines the direct optical path length through the Earth's atmosphere and expressed as a ratio relative to the path length vertically upwards, i.e. at the zenith, is usually used to characterize the performance of solar cells under standard conditions [50]. For a path length *L* through the atmosphere, for solar radiation incident at angle z relative to the normal to the Earth's surface, the AM coefficient is given as [13]:

$$AM = L/L_0 \approx 1/\cos z \tag{1.6}$$

where L_0 is the zenith path length at sea level and z is in degrees. The AM number is thus dependent on the sun's elevation path through the sky. The spectrum above the atmosphere, approximated by the black body at temperature 5,800 K, is referred to as "AM0. Solar cells used for space power applications are generally characterized using AM0 [49]. Average power of AM0 is considered as 1366.1 W/m^2 for characterization. The spectrum at sea level with the sun directly overhead (after entering in atmosphere) is referred to as "AM1". AM1 (z=0°) to AM1.1 (z=25°) is considered to characterize performance of solar cells in equatorial and tropical regions. Solar cells for terrestrial purposes, as already mentioned previously, are tested at AM 1.5, which corresponds to the sun at a 48.2° angle from the zenith point, with a temperature of 25 °C [48].

Two different standards are basically defined for terrestrial use. The AM1.5 Global spectrum is designed for flat plate modules and has an integrated power of 1000 W/m^2. The AM1.5 Direct (+circumsolar) spectrum is defined for solar concentrator work. It includes the direct beam from the sun plus the circumsolar component in a disk 2.5 degrees around the sun. The direct plus circumsolar spectrum has an integrated power density of 900 W/m^2 [48]. The different solar spectra are represented in Figure 1.3. Although, the AM1.5 solar spectrum has a range of 100 nm to 1 mm, however most of the irradiance occurs between 250 and 2500 nm [48], as shown in Figure 1.3, having maximum irradiance in the visible region of light (400 to 700 nm), thus it is required that a solar cell should strive to absorb as much in the visible region of the solar

spectrum as possible, which is also the primary motive of the thesis. The presented work has made an attempt to efficiently utilize the spectrum for the active materials used for the designs through incorporation of periodically patterned sub-wavelength structures for light trapping.

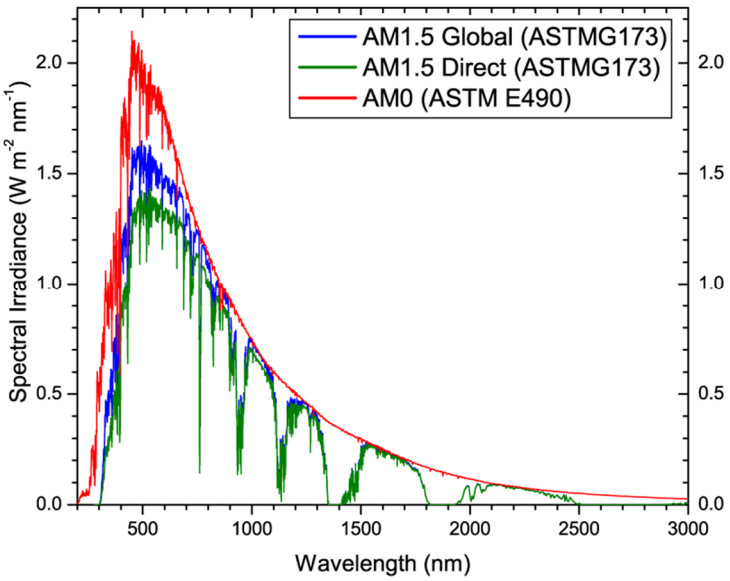

Figure 1.3 Standard Solar Spectra [48].

1.3.5. Need of Light Trapping in Thin Film Solar Cells

As discussed before, during past decades, thin film technologies have shown that they have the capability to provide the solution to the problem of low efficiency to cost ratio [13]. TFSC technology has been attracting a lot of attention especially due to its ability to provide light weight flexible solar cells using small amount of active absorbing material. Reducing device thicknesses, not only reduces the cost of the device, but also helps in higher production throughput and better device stability [51].

Although, thin film technologies, superficially, seems to have all the solution of the bulk solar cells, but basically they suffers from the problem of low efficiencies. The low efficiency achieved in case of TFSC is usually due to thinning of the active layer material, having thickness less than the absorption depth required to absorb entire solar spectrum wavelength photons. Thus, the large fraction of available spectrum lost due to incomplete absorption. Ideally, the incomplete absorption occurs only due to the absorption depth limitations in TFSC, but practically there are losses also due to reflections from the top surface as well as electrical losses, like interface and non-radiative recombination, including others.

Now, in order to improve the absorption and hence efficiency of these TFSC, certain kind of light trapping technique must be introduced. Light trapping is the process in which the optical mean path length of the incident photons in the active layer virtually becomes more than the absorption depth required to absorb those photons. Thus, eventually the cell could absorb the photon before it could leave the device, and that too without really increasing its thickness.

Usually single layer planar ARC at the top and planar metallic layer at the bottom as a back reflector (BR) has been used for light trapping in the solar cells [13]. ARC at the top is basically used to reduce the reflection from the top surface of cell due to the sudden index variation from the incident medium to absorbing medium. Therefore, ARC will provide help in index matching for the incident light and thus maximize absorption. However, to design an ARC which could provide high incident light coupling through minimizing reflections over the entire solar spectrum range and also reducing outward movement of photons from the top surface by increasing the oblique escape angle for the coupled photons, is really difficult to design. BR are basically placed at the bottom of a cell in order to increase the optical path length for those photons for which absorbing layer and ARC combination is not enough to absorb. Designing of an ideal low loss back reflector has also been an active layer of research in recent times. Theoretically, a typical loss less LTS could enhance absorption by $4n^2$ (where n is refractive index of the absorbing material) [24].

However, till date, the above mentioned structure [52], could not achieve even half of the value suggested in [24] through LTS due to shortcomings such as intrinsic losses from surface plasmon modes generated at the granular metal-dielectric interface [53]. Due to the reason, during the past several years, several new light trapping schemes have been proposed for the efficiency enhancement of the TFSC. It is also the basic purpose of the thesis to design highly efficient LTS for the TFSC using periodic patterning and will be discussed in subsequent sections in detail.

Thus, light trapping could prove to be a boon for the development of the high efficiency low cost LTS structures. LTS could help in their terrestrial application promotion as only few nm of active material cell might provide the efficiency comparable to hundreds of micron thick cell, thus decreasing the cost without compromising with the efficiency. Thus, a design of low loss, near-to-ideal LTS is very much a requirement for the development of high efficiency TFSC, through which it might achieve the efficiency near to Shockley-Queisser (S-Q) limit [20].

1.4. Introduction to Photonic Crystal

Photonic Crystals (PhC) are considered analogous to the semiconductors, as they allow the control of photons as semiconductors do for the electrons. PhC are the artificial structures having periodic variations in the refractive index of the materials arranged in a manner to give the structure a shape of a crystal [54]. Basically, the term PhC is the study of two important terms 'Photonics + Crystals'. Photonics denotes the term light whereas the term crystal is included as the PhC structure has the geometry of a crystal. PhC are particularly important in the field of the nano-photonics as they have the important property of scaling down the size of the structure according to the frequencies in use. Thus, they can be designed efficiently for both microwaves as well as for the visible range region. Some of the most promising applications based on PhC are waveguides, solar cells, LEDs, power splitter, direction couplers, bends etc.

When PhC structures are placed perpendicular to the direction of incident light, the strong contrast in the refractive index induces a gap in the spectra of the propagating photonic modes. Because of this strong contrast in the refractive index between the background material and rods (or holes) incorporated in that background, forbidden band gaps in frequency occur. These frequency band gaps are almost analogous to forbidden energy band gaps in the semiconductors, where no electrons can reside. These band gaps are commonly known as Photonic Band Gaps (PBG). In PBG region, no mode is allowed to propagate through the PhC structure. Utilizing and manipulating these band gaps make the possibility of light matter interaction enhanced. Thus, the PhC can be tuned as per our requirement. This provides an efficient method for the confinement and manipulation of light.

The simplest form of the photonic crystal is a one-dimensional periodic structure such as a multilayer film like Bragg Grating. The propagation of the electromagnetic wave in such structures was first studied by Rayleigh in 1887 [55] and it was shown that such a system has a forbidden band gap. The possibility to create two- and three-dimensional photonic crystal with two and three-dimensional forbidden band gaps was suggested independently by Yablonovich and John in 1987 [56, 57].

In order to illustrate the possible configurations of PhC structures, Figure 1.4 shows schematically the one, two and three-dimensional PhC structures. One-dimensional (1-D) PhCs shown in Figure 1.4 (a) are simple multilayer films consisting of alternating layers with high and

low refractive index repeated periodically, in single direction only. Figure 1.4 (b) shows a two-dimensional (2-D) PhC (top view), which is a system of air holes drilled in a high refractive index background material (basically known as hole type PhC structure). This structure is periodic in two dimensions and considered infinite in the third one. Also, a 2-D PhC structure having high refractive index rods etched in the low refractive index background are successfully patterned (commonly referred as rod type PhC structure). A membrane of finite height shown in Figure 1.4 (c) with the same hole pattern is also classified as a 2-D PhC structure. This structure is frequently referred to as PhC slab. Figure 1.4(d) shows a three-dimensional (3-D) PhC, which is an arrangement of dielectric bulks of high refractive index situated in air. This is so called "woodpile" structure [54]. It is periodic in all dimensions and it demonstrates a complete forbidden band gap that means that the light concentrated within has no way to escape.

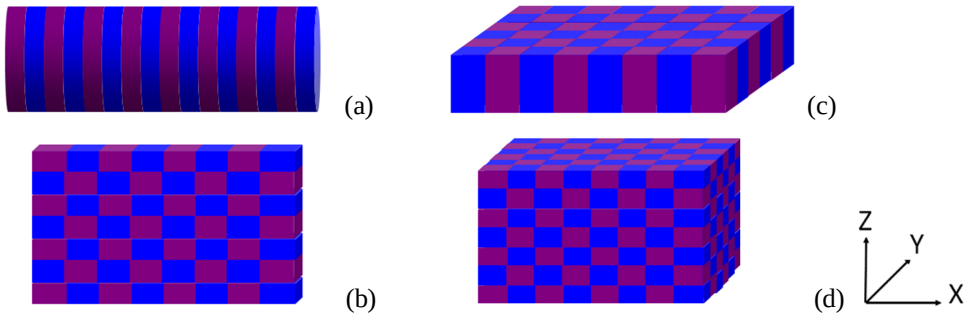

Figure 1.4: Possible configurations of the PhC Structures (a) 1-D, (b) 2-D, (c) 2-D slab, (d) 3-D structures. Here blue color represent one refractive index (n1) and violet represent different refractive material (n2).

Usually, fabrication of the 3D structure is more complex as compared to 2D PhCs structure and thus 2D structures have attracted a great deal of attention in recent years. The condition when incident waves are normal to the 2D PhC structure and in general out of the plane of periodicity of the structure at an angle to the normal direction of incidence, the 2D PhCs act as diffracting grating structures due to the periodic arrangement of the holes or rods in a background [58]. During the last decade or so, the interest in the PhC based solar cell has been immensely increased, as they can allow to control the propagation and confinement of light and thus one could manipulate the light matter interaction as per requirement. Both theoretical and experimental studies have been done on the subject including combining PhC as a single low loss dielectric back reflector [59], PhC as a diffraction grating [60, 61] or designing PhC within the absorbing material itself [62, 63]. The results obtained through all these years of research for PhC structures based solar cell have indeed been exciting. However still the research is its

nascent stage and thus lot of research is still required to prove the effectiveness of PhC structure irrespective of the solar cell material used, which is also one of the motives of the thesis work.

1.4.1. Brief History of Photonic Crystal

The initial concept that led to the development of the field of complex PhC structures, was initially proposed by Lord Rayleigh in the year 1887. However, it almost took a century to first conceptualize or reinvent the concept to be used for modern day applications through higher dimension complex periodic structures to control and manipulate the propagation of electromagnetic waves. The brief summary of some of the important events that remarkably take the field forward (and especially related to our subject of study), took place during all these years has been listed below [64]:

1887 - The English physicist Lord Rayleigh experimented with periodic multi-layer dielectric stacks, showing they had a photonic band-gap in one dimension [55].

1972 - A detailed theoretical study of one-dimensional optical structures was performed by Vladimir P. Bykov. He was the first to investigate the effect of a photonic band-gap on the spontaneous emission from atoms and molecules embedded within the photonic structure [65].

1987 - Prediction of photonic crystals, coincidentally, simultaneously by E. Yablonovitch [56] and S. John [57].

1990 - Computational demonstration of PhC by K. M. Ho et al. [66].

1991 - Experimental demonstration of microwave PhC by E. Yablonovitch et al. [67]

1991 - Yablonovitch produced first PhC by mechanically drilling holes known as Yablonovite.

1992 – E. Ozbay and G. Tuttle, Ames Lab - Iowa State Univ., manufactured a PhC in a layer-by-layer fashion.

1994 – J. Wijnhoven and W. Vos, Amsterdam University, created an almost true 3D photonic band-gap by using sub-micron sized silica spheres [68].

1995 - Demonstration of large scale 2D PhC in infrared range by U. Gruning et al. [69]. John D. Joannopoulos et al. first published an organized book on PhC structures [54].

1996 – T. Krauss made the first demonstration of a 2D PhC at optical wavelengths [70].

1998 - S.Y. Lin, Sandia National laboratories, designed a 3D PhC operating at infrared wavelengths.

1999 – P. St. J. Russell et al. demonstrated photonic band-gap fibers [71].

2000 - The first demonstration of "inverse opal" structures [72].

2002 –J. M. Gee published a paper on PhC based enhanced absorption for Si material [27].

2006 - Supercontinuum generation in PhC fiber is first reported [73].

2007 - A naturally-occurring PhC was discovered in scales of a Brazilian beetle [74]. N.N. Feng et al. [61] and P. Bermel [59] published detailed work for PhC structures based solar cells.

2008 – T. Baba introduced the concept of slow light in PhC [75].

2010 – Zannoto et al. described for light trapping regimes in solar cells using PhC [63].

2012 - J. N. Munday derived the effect of photonic bandgap materials on the Shockley limit [76].

2013 - Light trapping and near-unity solar absorption in a 3-D PhC structure [77].

2014 - Solar thermos-photovoltaic energy conversion systems with 2-D tantalum PhC absorbers and emitters were proposed [78].

2015 – Proposal by Al-Rashid et al. [79] for optical biosensing of multiple disease markers in a photonic-band-gap lab-on-a-chip.

Although I have tried to incorporate most of the major events that took place in the history related to the PhC structure development with special emphasis on PhC based solar cell, I also wish to gracefully acknowledge the contributions of all the events which ultimately led to the happenings of these milestones.

1.4.2. Electromagnetic Approach to Photonic Crystal

The theory of PhC can be adopted using the book written by Skoda [80]. Relation between the frequency *f*, the velocity *c* and the wavelength λ_0, of the radiation field in free space is given as $c=f.\lambda_0$. When the wave number is defined as $k = 2\pi/\lambda_0$, the relation between the angular frequency ω and *k* is obtained as

$$\omega = ck \tag{1.7}$$

This equation is commonly known as the dispersion relation and is the basic foundation on which the theory of PhC is based. There is another term which defines the forbidden frequency band for the PhC, that is, the Density of States. The density of states of the radiation field in the volume *V* of free space is denoted as $D(\omega)$ and proportional to ω^2 . It can be written as

$$D(\omega) = \left(\omega^2 V \Big/ \pi^2 c^3 \right) \tag{1.8}$$

The density of states in the uniform material is obtained by replacing *c* by *v* in this equation

where *v* is the velocity of light in medium. This gives the dispersion relation for uniform material which results into a straight line without any discontinuities. The optical properties of atoms and molecules strongly depend on *D(ω)* and it is possible to design and modify *D(ω)* by changing the optical properties of atoms and molecules. This is the key idea of PhC and it is schematically illustrated in Figure 1.5.

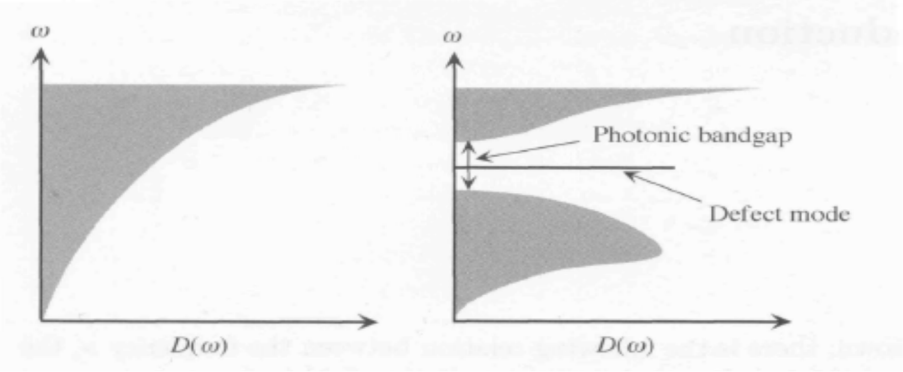

Figure 1.5: Schematic illustration of the density of states of the radiation field (left) in free space and (right) in a PhC [78].

Unlike the density of state of the radiation field in free space, the PhC density of states has a forbidden band gap for a range of angular frequency. In order to demonstrate the generation of PBG, here the author will demonstrate and analyze the performance of the 1-D PhC structure and the same can be applied to analyze the performance of higher dimensions crystal structures.

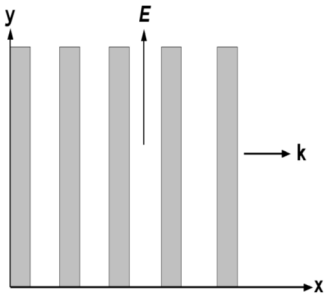

Figure 1.6: Geometry for the calculation of the dispersion relation of a 1-D PhC structure.

The figure shown above is used to demonstrate the forbidden frequency band gap calculations for one dimensional PhC structure. Only the electromagnetic wave propagated in the *x* direction and polarized linearly is considered. The *y* axis is taken in the direction of the polarization. The electric field of the propagated wave is denoted by a complex function *E(x,t)*. The wave equation for *E(x,t)* is given by

$$\left[c^2 / \varepsilon(x)\right]\left[\partial^2 E / \partial x^2\right] = \left[\partial^2 E / \partial t^2\right] \tag{1.9}$$

where $\varepsilon(x)$ denotes the relative dielectric constant of the PhC. It is assumed that the magnetic permeability of the PhC is equal to unity. Because $\varepsilon(x)$ is a periodic function of x, the dielectric constant can be written as

$$\varepsilon(x+a)=\varepsilon(a) \tag{1.10}$$

where a is the period or lattice constant of the periodic structure. The function $\varepsilon^{-1}(x)$ is also periodic and can be expanded in a Fourier series. It is known from the solid-state theory [81] that the Bloch's theorem holds for the electronic Eigen states in ordinary crystals because of the spatial periodicity of the potential energy that an electron feels due to the regular array of atomic nuclei. The same theorem holds for electromagnetic waves in PhC. Any Eigen mode in the 1-D crystal is thus characterized by a wave number k and expressed as follows

$$E(x,t)\equiv E_k(x,t)=u_k(x)\exp\{i(kx-\omega_k t)\} \tag{1.11}$$

where ω_k denotes the eigen-angular frequency and $u_k(x)$ is a periodic function expressed in the same manner as Equation (1.10). Thus, it can also be represented using the Fourier series. Using this, Equation (1.11), can now be expressed as

$$E_k(x,t)=\sum_{m=-\infty}^{\infty} E_m \exp\{i(k+2\pi m/a)x-i\omega_k t\} \tag{1.12}$$

where $\{E_m\}$ are the Fourier coefficients. For simplicity, it is being observed that only components with m = 0 and ±1 are dominant in the expansion $\varepsilon^{-1}(x)$. Therefore equation for $\varepsilon^{-1}(x)$ can be represented as

$$\varepsilon^{-1}(x)\approx k_0+k_1\exp\{i(2\pi/a)x\}+k_{-1}\exp\{-i(2\pi/a)x\} \tag{1.13}$$

Now, Equation (1.12) and (1.13) are substituted into the Equation (1.9), which gives

$$k_1\{k+2(m-1)\pi/a\}^2E_{m-1}+k_{-1}\{k+2(m+1)\pi/a\}^2E_{m+1}\approx\{(\omega_k/c)^2-k_0(k+2m\pi/a)^2\}E_m \tag{1.14}$$

Sakoda showed that E_0 and E_{-1} are dominant and all other terms can be neglected. Using this assumption, Equation (1.14) can be rearranged as

$$\left\{\left(\omega_k/c\right)^2-k_0k^2\right\}E_0-k_1\left\{k-2\pi/a\right\}^2E_{-1}=0 \tag{1.15}$$

$$k_{-1}k^2E_0-\left\{\left(\omega_k/c\right)^2-k_0\left(k-2\pi/a\right)^2\right\}E_{-1}=0 \tag{1.16}$$

The above two linear equations have non trivial solution only when the determinant of coefficients vanishes, therefore

$$\begin{vmatrix} \left(\omega_k/c\right)^2 - k_0 k^2 & k_1\left\{k - 2\pi/a\right\}^2 \\ k_{-1}k^2 & \left\{\left(\omega_k/c\right)^2 - k_0\left(k - 2\pi/a\right)^2\right\} \end{vmatrix} = 0 \tag{1.17}$$

If one introduces $h = k - \pi/a$, the solutions are then given by [80]

$$\omega_{\pm} \approx \frac{\pi c}{a\sqrt{k_0 \pm |k_1|}} \pm \frac{ac}{\pi |k_1| \sqrt{k_0}} \left(k_0^2 - |k_1|^2/4\right) h^2 \sqrt{3} \tag{1.18}$$

as far as $h << \pi/a$. So, there is no mode in the interval

$$\frac{\pi c}{a\sqrt{k_0 - |k_1|}} \le \omega \le \frac{\pi c}{a\sqrt{k_0 + |k_1|}} \tag{1.19}$$

This gap disappears when $k_1=0$. This result can be interpreted that the modes with $k \approx \pi/a$ and $k \approx -\pi/a$ were mixed with each other when the refractive index of the ingredient materials are repeated periodically and this mixing led to a frequency splitting.

In general, those wave vectors which differ from each other by a multiple of $2\pi/a$ should be regarded as the same because periodic repetition of the dielectric constant of the PhC material. When the spatial modulation is small enough the dispersion relation is close enough to the $\omega = vk$ (i.e. a straight line), but it should thus be expected with the wave vector in the first Brillouin zone $[-\pi/a, \pi/a]$, thus for forbidden frequency band to appear the foremost requirement is the periodic variation in the refractive index of the material used to design PhC devices.

In addition, if two dispersion lines cross each other, a frequency gap appears. All these facts are schematically illustrated in Figure 1.7. There are an infinite number of frequency gaps in the spectrum. However, it should be noted that this is true only as far one deals with electromagnetic waves travelling along the *x* direction, or in the direction in special modulation of dielectric constant variation takes place and that there is no gap when one takes into consideration the modes travelling in other directions.

The dispersion relation of a 2-D PhC is quite different because of the fact that all wave vectors are not parallel to each other in 2-D [54, 80]. For example, Figure 1.8(a) shows the reciprocal

lattice space of a 2-D square lattice. Dashed line boundary represents the first Brilloun zone. There are three highly symmetric points in the first Brilloun zone, that is, the Γ point (0,0), the X point (π/a, 0) and the M point (π/a, π/a). The second example, the reciprocal lattice space of a 2-D hexagonal lattice, is presented in Figure 1.8(b). The three highly symmetric points are the Γ point (0,0), the K point ($4\pi/3a$, 0) and the M point (π/a, $-\pi/a\sqrt{3}$).

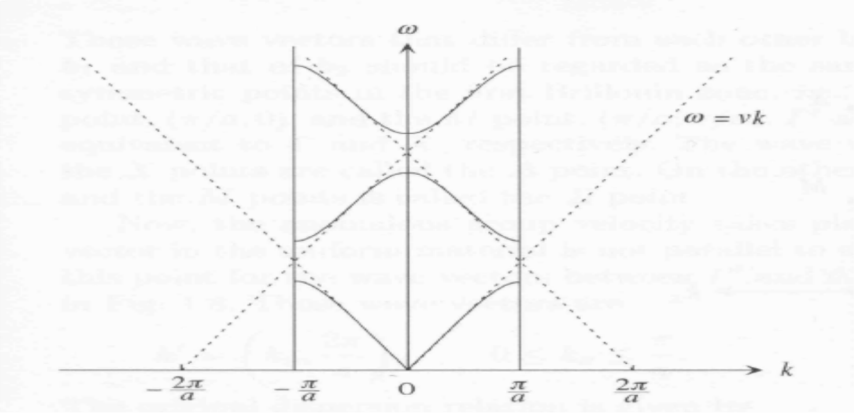

Figure 1.7: Dispersion characteristic of a one-dimensional photonic crystals (solid lines). The boundary of the first Brillouin zone is denoted by two vertical lines. The dispersion lines in the uniform material are denoted by the dashed lines [80].

The configuration of the first Brilloin zone of 3-D PhC depends on the type of the lattice: it can be the simple cubic or the fcc lattice. Although, the shape of the dispersion relation may vary as per the dimensions of periodicity for PhC structures, the basic phenomenon responsible for the creation of the PBG remains same as described above and gives opportunity to control and manipulate photons and thus light to explore this magical world of photonics through solution of Maxwell equations.

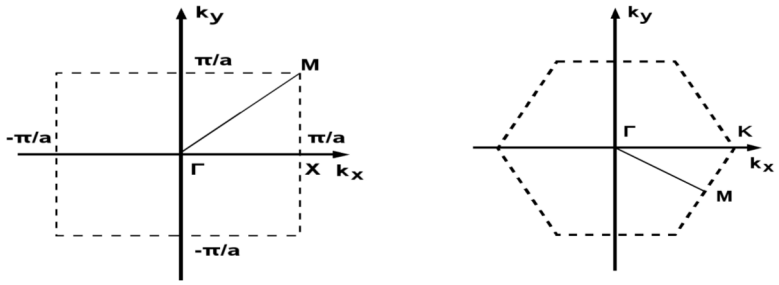

(a) (b)

Figure 1.8: First Brillouin zones of 2-D (a) square lattice and (b) hexagonal lattice

Thus, when PhC structures are used as a PBG material we can say that light is not allowed to travel through the structure unless there is a defect in the otherwise perfect crystal, this property

of PhC could be used to design near to ideal reflectors. As discussed earlier, BR is one of the important requirements to design high efficiency TFSC and thus it can be used to design efficient BR for TFSC.

However, if PhC structures plane of periodicity is perpendicular to the direction of incident light, the structures act as a diffraction grating as described in detail by Biswas et al. [58], provided that the period of the PhC structure is more than the incident wavelength in the medium. The detailed theory of the working of the PhC structure as a diffracting structure will be discussed in the subsequent chapters whenever they would be used in the proposed designs. Using this property of the PhC structures, one can select the light modes allowed to transmit or reflect or to maximize the path length of photons and thus it allows the regulation of propagation of required range of light as per desire and thus this kind of PhC configuration can be used to design both the BR as well the ARC for a solar cell and contribute in its performance enhancement.

1.5. Motivation of this Thesis and Problem Definition

The thesis aims at improving the overall efficiency of the TFSC by designing, optimizing, simulating and fabricating structures based upon 2D PhC LTS, especially to demonstrate their effect for performance enhancement of GaAs and InGaN/GaN active layer based cells. The importance of the study of this field increases manifolds because of the fact that in the world going through energy and pollution crises (especially counties like India), is looking for sustainable alternatives of the energy and thus looking towards cost effective and energy efficient solar photovoltaic technologies with much hope.

As discussed during previous sections, the main limitation with the crystalline or first generation solar cells is their expensiveness, which led to the development of the field of TFSC. However, these so called second generation cells theoretically seem to overcome many of the problems of thick cells, suffer set back due to their limited output efficiency as discussed in previous sections. Thus, the researchers set their target to find the high efficiency TFSC devices, which led the world towards the so called third generation cells.

To improve the output of TFSC, one of the best technique is the use of LTS. However, the normally used planar layers for LTS have their limitations as discussed earlier [13, 53]. Thus, to overcome the shortcomings of the above mentioned structure, novel structural schemes including

either random or ordered dielectric LTS designs [60, 82] have been studied. Although in case of random LTS, enhancement could be achieved over broad spectrum, these structures are difficult to be engineered, rescale and reproduce. The second LTS including ordered periodic pattern (like PhC LTS), has the advantage that in this geometrical parameters could be easily varied and the whole structure could be fully engineered using modern lithography techniques, which is the one of the key motivation for this work.

There are several ways by which PhC can be used with the solar cells, depending on the particular requirement. Several scientists and researchers have used them in their designs for different purposes. Taking inspiration from these studies and motivated by the diversity of advantages that PhC structures could provide to the design of TFSC performance, the thesis attempts to outline the effectiveness of these sub-wavelength periodic structures for GaAs and InGaN/GaN active layer based cell through different device configurations. The principal aims and goals to study the subject are summarized as follows:

- The thesis aims to improve the overall efficiency of the TFSC through the innovative design of incorporating PhC structures with absorbing material to increase the optical path length and hence the absorption of the photons, which would otherwise pass through the TFSC unabsorbed.
- To design various periodic photonic LTS for GaAs and InGaN/GaN TFSC and to check their effectiveness with these active layer material cells and to demonstrate how PhC structures effect varies with the choice of active material.
- To design and to perform the simulation and experimental analysis of the TFSC using PhC structure (a) as a PBG structure at the back, (b) as a diffraction grating at the back assisted by distributes bragg reflector, (c) at front surface of the cell etched above active layer, and (d) at front surface etched through active layer.
- To compare the performance of the various PhC based LTS and predict the best design for the future PhC pattern based structure for GaAs and InGaN/GaN solar cells.
- To find the Lambertian light trapping values for GaAs and InGaN/GaN active material cells and compare the results with PhC based proposed designs.
- To predict and demonstrate how the performance of the proposed solar cell designs varies with thickness of active layer and to analyze how PhC based LTS effect their performance.

- To study the possible fabrication procedure of the proposed structures design and to carry out their fabrication followed by experimental analysis.
- The result may prove to be very useful for the fabrication of the future nano-sized PhC structures and lead to the further development in this area in our country.

The results may prove to be the boon for the TFSC studies and market and may mobilize the industry to look towards PhC designs to enhance efficiency of solar cells devices especially from Indian perspective as such kind of studies have not been performed and thus can prove to be a boost for further development of high efficiency TFSC in the region.

1.6. Outline of this work

The thesis, written especially to describe light trapping in thin film solar cell using Photonic crystals, is organized as follows – Chapter 2 discusses the concept of PhC based thin film solar cell and describes the basic details of the subject. In general, the chapter presents the idea of light trapping in thin film solar cell through PhC structures and deals with the motivation behind studying the subject. The chapter also discusses the current research scenario in the comprehensive manner and also proposes the possible modifications from these already presented works, and provides the brief idea about the structures that would be discussed in the later parts of the thesis. The chapter also provides the motivation behind studying the light trapping in GaAs and InGaN/GaN solar cell structures using PhC structures. In the later section of the chapter, we will discuss about the simulation strategy adopted to find out the results about the proposed structures. Next, the chapter discusses in brief about the growth and fabrication technologies adopted to get the final practical device.

The chapter 3 presents and analyzes the study by optical and electrical simulations and numerical modelling, the impact of introducing a 2D PhC made of a GaAs rods embedded within a silica matrix and placed on the backside of a GaAs TFSC as a PBG structure. The goal is to create a broadband reflector inducing a weak parasitic absorption and that could also serve for light-trapping purposes. A solar cell based on a planar Aluminum reflector is used as a reference. The optical and electrical properties of the resulting cells are numerically investigated in order to discuss the potential of this approach. Those factors that reduce the efficiency of a GaAs cell are

also considered in the presence of PhC back reflector. The results show that the 2D PhC configuration proposed could have a real potential for enhancing the efficiency of such cells.

The chapter 4 presents a design optimization for an efficient LTS which includes single planar ARC layer at the top assisted by 2D PhC diffraction grating and Distributed Bragg Reflector (DBR) at the back. As a representative example, the LTS geometry for 500 nm GaAs active layer is optimized to obtain maximum absorption and the physics behind absoption is described in details. Two material combinations possible for the back trapping structure will be discussed. The chapter also discusses in details how the effect of proposed LTS changes with variation in active layer thickness. It has been observed that the overall cell efficiency can be enhanced 3.5 times for a 100 nm-thick cell with proposed LTS and this enhancement becomes only 1.5 times for 1500 nm-thick cell. It is found that for thin cells the improvement is mainly contributed by the optimized back trapping structure and ceases for thick cells whereas the contribution from the ARC remains almost constant irrespective of cell thickness. The chapter also deals with the performance analysis of the proposed design with GaAs Lambertian limits.

The chapter 5 presents a design using 2D PhC structure GaAs solar cell with a periodic pattern extending from top Transparent Conducting Oxide (TCO) to inside the p-AlGaAs window layer placed just above the active layer of GaAs material. The chapter presents the theoretical optical study and optimization of all the required parameters. The performance of the proposed structure is also compared with Lambertian limits and the planar cell, taken as reference. The chapter also presents the analysis of the PhC structure effect on the performance of the design with the thickness variation of absorption layer.

The chapter 6 proposes the structure of p-i-n InGaN/GaN based solar cell having PhC based LTS at the top assisted by the planar metallic (Aluminum) BR. The chapter demonstrates two different designs, in one the PhC structure etching depth extends from the top ARC up to the p-GaN layer, whereas in the other design the PhC LTS etching depth has been extended up to the $In_xGa_{1-x}N$ absorbing layer. The chapter presents the theoretical optical simulation studies and optimization of the required parameters of the structure. The work also demonstrates the Lambertian light trapping limits for the practical Indium concentrations in $In_xGa_{1-x}N$ active layer cell and presents the comparison between the proposed designs and a planar reference cell. The studies are carried out for various Indium concentrations.

The chapter 7 demonstrates the design, simulation, fabrication and analysis of InGaN/GaN superlattice solar cell with PhC structure at the top surface. The chapter discusses the light trapping phenomenon in superlattice (ten pairs of $In_{0.18}Ga_{0.82}N$/GaN structure) which is experimentally grown by metal organic chemical vapor deposition whereas the PhC structure has been realized through electron beam lithography. Both simulation and experimental results are demonstrated.

Chapter 8 provides the conclusion for the thesis work with a brief discussion about the noticeable contributions originating from this work. The chapter also proposes some recommendations for future research in the subject, in context of recent interest in TFSC described in literature.

Chapter 2

Photonic Crystal based Thin Film Solar Cell: a Review

2.1. Introduction

The last chapter presented the glimpse about the requirement of light trapping in TFSC and the basic need to incorporate these LTS in the solar cell devices. It has been said that, LTS can prove to be crucial for wider acceptance of TFSC, as only few nm of active material inside a solar cell might provide the performance comparable to hundreds of micron thick active layer cell, which ultimately can reduce the cost of the final device and that too without effecting efficiency. Thus, a design of low loss near-to-ideal LTS is very much a requirement for the development of high efficiency TFSC.

In the previous chapter, the discussions about the commonly used LTS like planar ARC at the top and metallic reflector at the back has also been carried out. However, the problems associated with these kind of a structure propelled the research community to look towards more efficient designs that could be used with active solar cell materials to improve the absorption of incident solar photons. This chapter presents the exciting field of PhC structures as an alternative, to be used these structures with TFSC as an efficient low loss LTS.

The chapter deals with the definition of the problem, which describes the need of a PhC LTS and its advantages when they are used inside the solar cell device. The chapter also discusses about the current research scenario of the subject and where the further work can be done with proposed modifications. The chapter also provides the summary behind the motivation of using GaAs as an active material in solar cell device for light trapping studies and also discusses the reason behind choosing another alternative active material, InGaN for light trapping studies. The

chapter also discusses in brief about the modelling and simulation approach followed in the later parts of the thesis, together with brief summary of the growth and fabrication processes that would be adopted to fabricate the proposed structures.

2.2. Definition of the Problem: Light Trapping in Thin Film Solar Cell Using Photonic Crystal Structures

With the commonly used ARC and metallic BR based structures, it is not possible to even achieve half of the possible Lambertian light trapping values [24]. Thus, one has to look towards the more efficient alternatives, like randomly patterned or periodically patterned LTS for TFSC. However, as it is also complex to reproduce and rescale the randomly patterned structures, it is better to look towards the periodically patterned structures for light trapping.

This took us to the attractive world of PhC structures, as it gives us the opportunity to modify the light and light-matter interaction as per our requirement. As discussed in the last chapter (section 1.4), this peculiarity opens up wide range of possibilities for the field of photonics and optics, including the field of solar photovoltaics. PhC structures could be incorporated within the solar cell in the number of ways, depending on the particular requirement. Researchers examined the use of PhC with solar cells for different applications extending from PhC as a diffracting element to the PhC as an absorbing structure. But, the technology still is in its early days and several studies are required to be done before it could be commercialized. This has motivated us to look at the wide dimensions of possibilities, which PhC could offer to the field of TFSC.

Various studies have been done on the subject in the past including PhC as a single low loss dielectric BR [59], PhC as a diffraction grating [60, 61], designing PhC within the absorbing material itself [62, 63]. These studies are basically performed either using 1D or 2D PhC structure [54, 83, 84, 85], as designing and fabrication of 3D PhC is still a difficult task. In the succeeding section, brief discussion about the current status will be presented, to highlight the critical review of the subject which will help in identifying the possible gaps to fill.

2.3. Current Research Scenario of the Subject and Proposed Modifications

During the past decade or so, several research articles and journal papers have come up the proposed area of research, but the research is still its early days and there is a lot of scope to further modify the design and achieve results than those already proposed. In the following

paragraphs, we will discuss about some of the works that can be considered as important to the proposed research area and also present the possible modifications that can further provide the improvement in performance of the cell.

Wang et al. in [86], illustrated that the back-side mirror plays an important role in TFSC having based their studies on the GaAs active material. Traditionally, a metallic backside contact is used to reflect incident sunlight back toward the front of the cell to enhance overall absorption and increase I_{sc}. Specially, in GaAs TFSC where radiative recombination dominates, BR serves critical role of reflecting radiatively emitted photons and contributing to photon recycling. Although, they demonstrated that the BR plays an important role for a TFSC and a near-to-ideal BR is one of the most essential requirements to achieve solar cell devices having efficiency near to Shockley limit, they did not present any practical BR that can achieve these high values. Figure 2.1 presents the modified version of the schematic structure presented in [86], proposing one of the possible ways where PhC structure can be used as a LTS. It is also one of the basic structures analyzed in this thesis and the results will present the benefit that PhC LTS at the back could provide for TFSC.

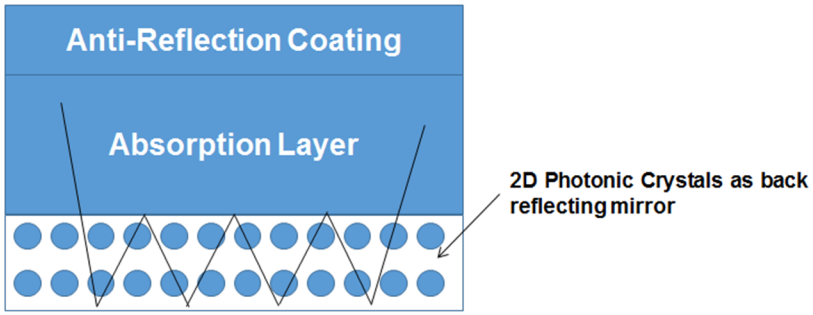

Figure 2.1: Prototype of Thin film solar cell using PhC as back mirror

A. Chutinan et al. in [87], theoretically demonstrated significant enhancement in efficiency of thin crystalline Si solar cells by using PhC structures as the light absorbing layer. In particular, a relative increase of 11.15% and 3.87% in the energy conversion efficiency compared to the optimized conventional design were achieved for 2μm and 10μm thicknesses, respectively. The article presented a good physical insight into the behaviour of PhC structures as an absorbing layer. Figure 2.2 presents the schematic diagram of the presented structure in a simplistic way. Still, the design can be modified to study the effect of different kind of periodic structures on the

performance of the TFSC and to predict which type of a structure is more feasible from theoretical and practical point of view.

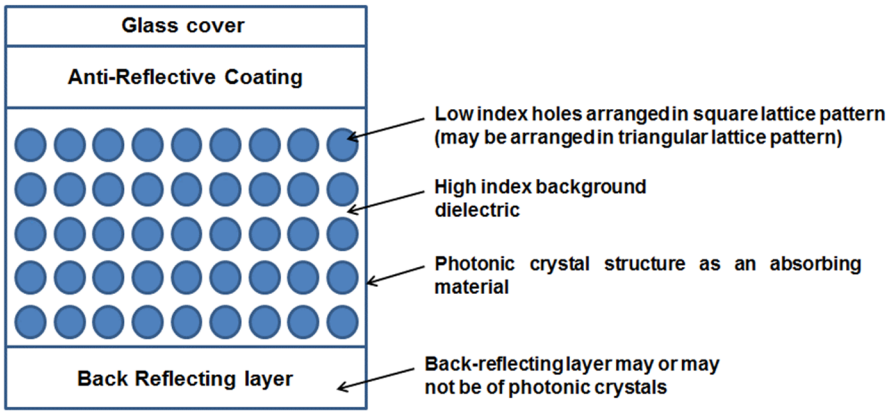

Figure 2.2: Solar cells using PhC structure as an absorbing material

J. N. Munday in [76] demonstrated PhC at the top of the solar cell as PBG structure to block the absorption of particular wavelength photons but at the same time to disallow the emission of the same range of photons. This although, as he suggested, might reduce the spectrum available for absorption, at the same time also reduce the emission from the cell, and thus increases V_{oc} of the structure without reducing I_{sc} to the same amount. This increases the overall efficiency of the cell as the density of the minority carriers available for absorption increases. The effect might be more prominent for those materials for which radiative recombination is the dominant process, like in the case of GaAs, because a photon could be recycled through radiative recombination and thus would be available again to be absorbed by the solar cell material.

Bozzola et al. in [62] and Zannoto et al. in [63] also proposed PhC at the top for Si active material, however, they used PhC design as a diffraction structure at the front to control the coupling of light from the top, having their plane of periodicity perpendicular to the incident light. Thus, the PhC structure has been used to increase the index matching between the incident medium and the absorbing layer. The design can be modified to use PhC at the top to work both as a ARC as well as a coupling structure for both high and low wavelength photons and assited by BR (which may or may not be patterned), and the effectiveness of the periodic nano-structures for active materials other than Si can also be investigated Schematic diagram of the proposed structure based on the PhC design at the top is shown in Figure 2.3.

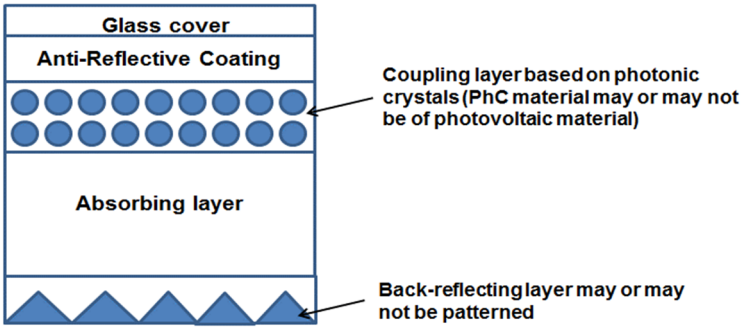

Figure 2.3: Solar cells using PhC structure at the top

D. Zhou and R. Biswas in [60] illustrated LTS for hydrated a-Si:H TFSC, utilizing low loss 1-D PhC as Distributed Bragg reflectors (DBR) at the backside of the solar cells. Between the DBR and the absorber layer, there is a layer of 2-D PhC composed of a-Si and SiO_2. The 2D PhC layer will diffract light at oblique angles, so that total internal reflections are formed inside the absorber layer. The design can be modified (Figure 2.4) for other more efficient solar cell materials like GaAs, CIGS and CdTe to check how their performance changes with incorporation of PhC structures and to show whether the findings are equally applicable to these strong aborbing materials or not.

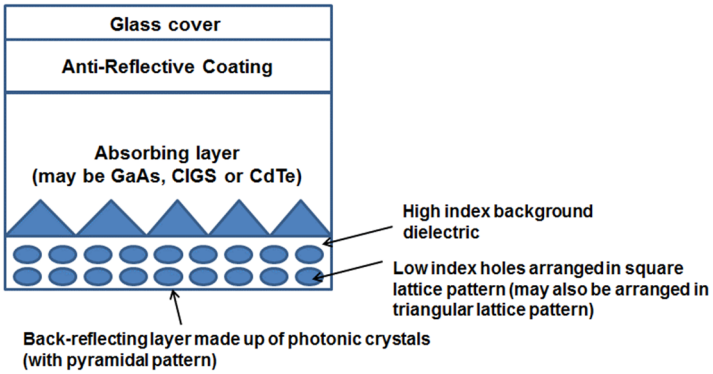

Figure 2.4: Solar cell structure having PhC at the back assisted by pyramidal symmetry.

G. Demesy et al. in the aticle [88], suggested that using only a µm of Si, sculpted in the form of a modulated nanowire PhC, solar power conversion efficiency in the range of 15%–20% can be achieved and choosing a specific modulation profile provides antireflection, light trapping, and back-reflection over broad angles in targeted spectral regions for high efficiency power conversion, and illustrated efficiency improvement over their straight counterparts made of an equivalent amount of Si. Using their analysis, one may study and research in this trend to look at what happens if PhC are added together with nanowires as a back reflecting material as shown in Figure 2.5, having combinations of different materials and configurations.

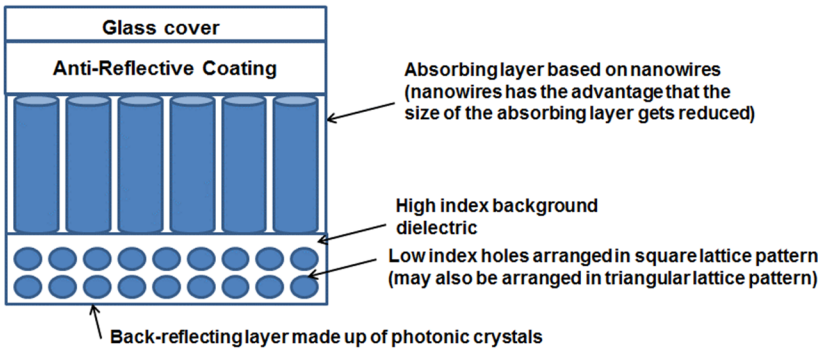

Figure 2.5: Solar cell using nanowires as an absorbing material and PhC as back reflector.

S. B. Mallick et al. in [89] referred that the indirect band gap of Si requires a light trapping approach to be used to maximize optical absorption for solar cells. Thus they used PhC based approach to maximize light harvesting in a 400 nm-thick Si layer by tuning the coupling strength of incident radiation to quasi-guided modes over a broad spectral range. The structure consists of a double layer PhC with the upper layer having holes which have a smaller radius compared to the holes in the lower layer. They showed that the spectrally averaged fraction of photons absorbed was increased 8-fold compared to a planar cell with equivalent volume of active material, which results in an enhancement of maximum achievable photocurrent density. However, no discussion on possibility of fabrication or any experimental results have been presented.

Eyderman et al. in [90] demonstrated a significant increase of solar absorption in ultra-thin layers of GaAs. They articulated that depending upon a PhC structure and the nature of its packaging, almost over 90% solar absorption can be achieved in the wavelength range from 400–860 nm. They also demonstrated the effect of PhC structure in the performance of GaAs solar cell for 100-300 nm thin GaAs active layer cell, and concluded that it is possible to achieve over 26.3 mA cm^{-2} maximum achievable photocurrent density with a slanted conical-pore PhC packaged with SiO_2 and deposited on a silver back-reflector. However, they have shown the effect of the PhC structures on the performance of the GaAs cell only in the limited thickness range and also did not provide much details about the effect of other structures included in LTS.

Mutitu et al. in [91], have presented LTS that could be applied to stand alone and multiple junction TFSC. The designs incorporate 1-D PhC structures as band pass filters that reflect high energy photons (400 – 1100 nm) and transmit small energy ones (1100 -1800 nm) at the interface between two adjacent cells. In addition, nano structured diffractive gratings that cut into the PhC

layers were incorporated to redirect incoming waves and hence increase the optical path length of light within the solar cells. They also showed preliminary fabrication results of the proposed light trapping grating structures (Figure 2.6), although the work did not discuss anything about the complete cell design with 2D PhC LTS.

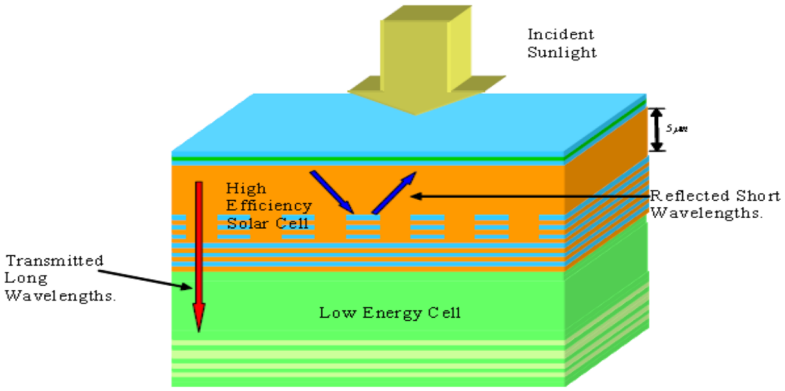

Figure 2.6: Schematic diagram showing a multiple junction solar cell with the short wavelengths being reflected back into the first cell and long wavelengths are being transmitted to the lower energy solar cells [89].

Florescu et al. in [92] shown that the ability to control the thermal emission and absorption of radiation in a PhC, enables the realization of high-efficiency solar cells. They combined predictive modeling, fabrication, and measurements to provide a basis for understanding and controlling the thermal emission and absorption of radiation in complex PhC structures and to use them for solar cell applications. They demonstrated that the thermal emission in PhC is characterized by spectral- and angular selectivity. They concluded that the spectral selectivity eliminates wavelength-band mismatch between the semiconductor energy gap and blackbody emission, on the other hand, the use of angle-selective absorbers based on suitably designed PhC structures can opens new avenues for realizing high-efficiency Thermo-Photovolativs (TPV) systems (Figure 2.7).

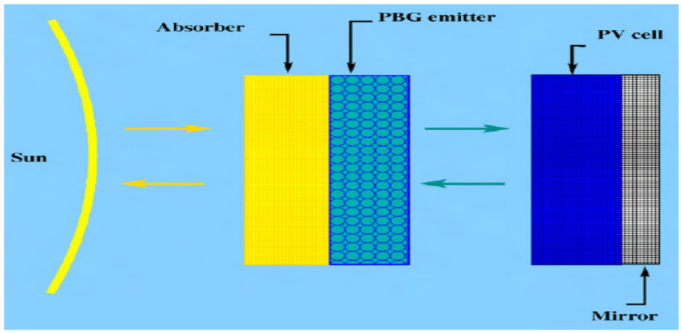

Figure 2.7: Schematic of the PhC based TPV conversion. An intermediate absorber is heated by absorbing thermal radiation. The PV cell is illuminated by radiation from emitter transmitted by a filter [90].

All of the above mentioned works have helped in exploring the insights of PhC structures usability for solar cell applications by one way or the other. Many other researchers have also put their efforts to demonstrate the utility of the PhC structures with solar cells, however due to the restriction of space, it is not possible to re-summarize all of them all together. Here, the author wish to acknowledge all their efforts to highlight what PhC structures are capable of doing from solar cell perspective and inspiring budding researchers. Although, all of the research work done during the past decade or so, demonstrated the effectiveness of PhC structures, most of these articles were concentrated to show the effect of PhC structures for Si or amorphous Si solar cell, which are usually weakly absorbing materials and did not demonstrate the effect using practical designs and materials. Thus, it is also important to predict and demonstrate the effectiveness of PhC structures for other active materials from practical design aspects.

Also, most of the research work done during the past, concentrate either using PhC at the back or at the front, whereas it is rare to find the studies simultaneously comparing the performance of the PhC structure based solar cell altogether. Thus, it is also one of the key motivation of the thesis to demonstrate the performance of the TFSC having PhC LTS at the front as well as the back and to compare their performance and predict the best theoretical and practical structures.

Most of the scientific works (except few and that too in limited range) presented in the above articles demonstrate the effect of the PhC structures for a particular thickness active material, providing very limited information about the variation in performance of the cell with active layer thickness and how the effectiveness of the PhC LTS varies with the active layer thickness. Through the thesis, the work will also try to demonstrate the variation in the effectiveness of the PhC LTS with changes in active layer thickness for both top and back PhC structures.

Although some of the previous studies have shown the practical device performance for PhC LTS based TFSC through fabrication, most of these articles did not provide the complete solar cell designs with ARC and BR geometry (having PhC incorporated) in the final device form. Thus, through the thesis, together with simulation and modelling, the work will also try to exhibit the final device having PhC configuration incorporated with active material, to compare and analyze the performance of the PhC structure based design with planar structure and simulation results to ascertain the role of PhC structures in the efficiency enhancement of TFSC. Thus, at last I could sum up that after analyzing the work and outcomes previously demonstrated through

great scientific efforts, I am hopeful that, I may further put some useful contribution into the field, which may enhance the results further and ultimately help the solar cells industry and the environment and society especially from Indian perspective.

2.4. Motivation for Light Trapping Studies in GaAs Solar Cell using Photonic Crystal Structures

As discussed in the previous sections, it is also important to predict and demonstrate the effectiveness of PhC structures for active materials other than Si. Relative to Si, III-V compound have several advantages (kindly refer to Table 1.3), such as having a direct band gap which makes them a better optical absorber, also their composition could easily be altered to replace III type compound with another III group material to make ternary and quaternary compounds having different band gaps. The best understood and most widely used III-V compound is GaAs [13] and also most suitable for solar energy conversion [20, 93], yet the use of the material for terrestrial solar cell applications is still restricted, basically due to the cost of the material as well as due to the poisonous nature of Arsenic.

Over visible spectrum, i.e. in the wavelength range of interest the absorption of GaAs is about 10 times more than that of Si. GaAs has also much better temperature coefficient and radiation resistance than Si, thus its performance is less affected by temperature and radiations than Si [35]. In pure GaAs material, radiative recombination predominates over other type of recombination, so the transition of carriers from conduction to valence band is more probable as compared to Si. Moreover, Auger recombination is much slower in GaAs than in Si, because of much less intrinsic carrier concentration. In GaAs devices, Shockley Read Hall (SRH) recombination dominates in the space charge region due to the high carrier density in the junction region due to high absorption coefficient of GaAs materials [13]. Also, surface recombination is higher in GaAs than in Si, thus usually it is used with a window layer of higher electrical band gap in solar cell devices to deflect generated carriers away from front surface.

Due to all these peculiarities, GaAs is an undisputed choice for the space solar cells, however in order to make them attractive for terrestrial applications one needs to look towards the techniques that could reduce the overall cost of the solar cell device, the main portion of which is due to the cost of GaAs material itself. Thus, in order to reduce the cost of the cell, we have to

reduce the use of GaAs material in the device, which can be achieve through reducing the active layer thickness. However, with decrease in the active layer thicknesses, there would be a decrease in the output efficiency, since to absorb a particular energy photon, the absorption layer is required to be of particular minimum thickness [13]. The relationship between absorption coefficient of a material, α, and wavelength of incident photon, λ is given as:

$$\alpha = 4\pi k / \lambda \tag{2.1}$$

where k is the imaginary part of the refractive index. The relation demonstrates that as the wavelength of incident photons increases, the value of α decreases, thus the comparatively thicker active layers are required to absorb these high wavelength photons. The fact points out that although GaAs has high absorption coefficient, still if we reduce its thickness to get inexpensive cell out of it, it is not possible to absorb all the spectrum photons and thus in that case one has to compromise with efficiency. On the basis of the relationship given in Equation (2.1) and the GaAs material parameters [94], the graph shown in Figure 2.8 demonstrates the relationship between absorption depth (inverse of α) and incident photon wavelength.

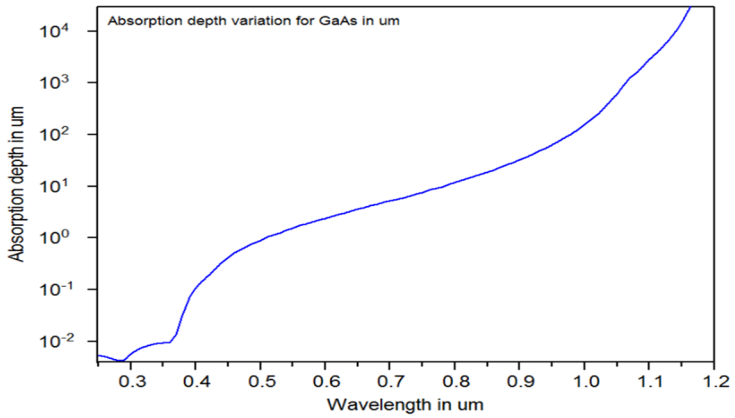

Figure 2.8: Variation in the absorption depth with incident photon wavelength for GaAs material

From the figure, one can analyze that for very thin layers of about 1 μm or less, large part of the spectrum AM1.5 shown in Figure 1.3, especially in the higher wavelength range cannot be absorbed in the active layer. Thus, a large part of the incident spectrum will be lost for the thinner GaAs active layer cell, unless certain kind of efficient light trapping mechanism has been applied with the device. Also, there is considerable reflections from the top surface throughout the incident spectrum due to abrupt change in the refractive index from incident to absorbing medium. So, the primary objectives for optimization of a thin GaAs solar cell structure are [13]:

i. To design a suitable light trapping mechanism, by which efficient harvesting of high wavelength photons could be possible, in case of very thin active region.
ii. To design efficient anti reflective coating which could help in reducing reflections from the top of the device.
iii. Design structure which could minimize front and back surface recombination.

Here, through the thesis, the motivation is to present the enhanced incident photon absorption inside a thin GaAs active layer for solar cell device through the incorporation of PhC LTS. During the thesis, the author will demonstrate and discuss about the performance evaluation (especially optical performance) for PhC LTS added as a back reflector (having PBG structure as well as a diffraction grating) and also as a front surface for efficient light harvesting to absorb these otherwise unabsorbed photons. The goal is to create an ultra-thin GaAs active layer cell which should be of high efficiency with PhC LTS and to show how the effectiveness of PhC LTS for the GaAs active layer based cell varies with the thickness of active layer itself.

2.5. Looking for Alternative: Light Trapping in InGaN/GaN based Solar Cell using Photonic Crystal Structures

In India, although we have made fast paced growth in recent years, there are constraints for nanofabrication and still very few facilities are available for growth of GaAs devices and thus, even after making every possible efforts to grow and fabricate the structure through contacting India's best labs, unfortunately none of them replied positively due to their limitations. We have made attempts to collaborate with INUP at IIT-Bombay as well as at IISc-Bangalore, together with other prestigious labs including RRCAT-Indore, SSPL-Delhi, TIFR-Mumbai, CEERI-Pilani etc. but regrettably they do not have all the possible facilities required for the growth of GaAs structure and fabrication of the device, as they all have some constraints basically related to the growth of the GaAs heterojunction structure.

Meanwhile, while discussing with various scientists and experts, the idea emerged to rather show the effectiveness of the PhC LTS with InGaN/GaN based device, which has fair chances of being grown and fabricated and thus could help us to demonstrate experimentally the performance improvement in the solar cell device due to these periodic patterns. As a result, with the help and motivation of Dr. Manish Mathew at CEERI-Pilani and Dr. Rajendra Singh at IIT-Delhi, we

went ahead with the research studies of design, growth and fabrication of superlattice based InGaN/GaN solar cell, and fortunately were able to fabricate the proposed structure and can claim based on the experimentally verified results that the PhC LTS enhance the performance of the solar cell device irrespective of the active layer material.

Thus, I have tried to explore the effect of PhC LTS for InGaN/GaN based solar cell structure, as some Indian labs including CSIR-CEERI, Pilani are currently working for the growth and fabrication of InGaN/GaN based devices and also the growth technologies used for the InGaN/GaN material systems are almost similar as used for the GaAs based devices. Recent developments in the Group III-Nitride material growth and fabrication progress, have enabled their demonstration in the design of Light Emitting Diodes (LED) [95, 96], photodetectors, LASER diode etc. both for specialized as well as commercial applications.

Group III-Nitride material has also shown the potential for full solar spectrum applications after it has been established that it is possible to tune the bandgap of $In_xGa_{1-x}N$ compounds from 0.7 (for InN) to 3.4eV (for GaN) [40, 41]. Moreover, other unique properties of $In_xGa_{1-x}N$ alloys like good thermal stability, irradiation resistance, excellent chemical tolerance (i.e. not easily corroded by chemical solutions) and high carrier mobilities also add to the advantages that it could offer to the design and fabrication of high efficiency thin film cells [42, 43]. Due to all these qualities of $In_xGa_{1-x}N$ alloys, InGaN/GaN hetero-structures have gained much attention for solar cell applications [44]. Many research groups have reported their efforts in the investigation of the $In_xGa_{1-x}N$/GaN sapphire-based PV devices, mainly including multiple quantum well (MQW) [97], p-i-n junction [45, 98], and short-period superlattice (SPS) designs [99].

However, the main problem with the $In_xGa_{1-x}N$ alloys is its epitaxial growth over lattice mismatch GaN/sapphire substrate. Thus, there is a limit to the thickness of high-quality $In_xGa_{1-x}N$ epitaxial layers that could be grown on GaN/sapphire substrate, which is only few nanometers due to the large lattice mismatch between $In_xGa_{1-x}N$ and GaN, particularly for high-Indium-containing layers [100]. Therefore, it is still a challenge to achieve $In_xGa_{1-x}N$ absorption layers with low band gap (< 2.0 eV) and large thickness at the same time. Thus, critical thickness, Indium concentration and threading dislocations (TDs) limit the conversion efficiency of solar cells [101].

However, thinning down the active $In_xGa_{1-x}N$ layer to few nm, in order to keep the grown structure epitaxy, will ultimately hamper its efficiency, no matter how good the absorption coefficient of the $In_xGa_{1-x}N$ material. The low efficiency achieved, is basically due to two reasons, first the band-gap of the active $In_xGa_{1-x}N$ layer, which limits the available solar spectrum for absorption and second, due to thinning of the active layer material, having thickness less than the absorption depth required to absorb entire available solar spectrum wavelength photons. Together with this, there are also losses due to reflections from the top surface as well as electrical losses, like interface and non-radiative recombination, including others. In order to solve the first problem, it is necessary to increase the concentration of Indium content in $In_xGa_{1-x}N$ material, which is not feasible practically till date, due to large lattice mismatch between the available substrate and $In_xGa_{1-x}N$ material which gets enhanced with increasing Indium concentration [100]. To solve the second limitation, certain kind of light trapping technique must be introduced in the cell design, which is also the basic objective of the thesis.

Chapter 6 and 7 will discuss about the effectiveness of PhC structures for p-i-n InGaN/GaN solar cells having single InGaN active layer as well as superlattice InGaN/GaN active layer structure. The design and analysis of the proposed structures have been done through simulation and experimental processes for practical Indium concentration values varies from 5% Indium concentration to 20% and the results obtained will demonstrate the effectiveness of PhC LTS for ultra-thin InGaN/GaN active layer cells and show that the effect of PhC structures is independent of the active material used to design solar cell device.

2.6. Solar Cell Modelling and Simulation Approach

One of the most important aspect of the thesis is the simulation study of the proposed designs having periodic patterns, configured to have periodicity in and out of the plane of incident light. In order to study the designed structures' optical characteristics, the author has basically used two electromagnetic simulation approaches, first is Finite Difference Time Domain (FDTD) method and other is the Rigorous Coupled Wave Analysis (RCWA) method. Although there are many computational methods available to find a solution for propagation of electromagnetic waves within a periodic structure, FDTD and RCWA are considered as two of the most stable and preferred techniques. Both these techniques provide a rigorous solution to Maxwell's equations, however both the techniques have some pros and cons. Also, there is another method

called Plane Wave Expansion (PWE) method, which is used for PBG structures frequency stop band in the thesis. Here in the succeeding paragraphs we will discuss their brief technical background and properties, which will demonstrate, why the techniques are preferred over other available methods.

The ***FDTD method***, first proposed by Yee [102] and later modified by Taflove [103], does not have any approximations or theoretical restrictions and is widely used as a propagation solution technique in integrated optics. It is easy to understand and has an exceptionally simple implementation for a full wave solver. FDTD method is based on time-domain solutions, and hence it can cover a wide range of frequency within a single simulation run, having time step small enough to satisfy the Nyquist-Shannon sampling theorem for the desired highest frequency [104]. The technique is extremely versatile because it is inherently full-vectorial without limitations on optical effects such as direction of propagation, index contrast, or backward reflections. FDTD method is a grid-based differential time-domain numerical modeling method, having Maxwell's equations (in partial differential form) modified to central-difference equations, discretized both in time and space domain, and implemented in software. The equations are solved in a cyclic manner: the electric field is solved at a given instant in time, then the magnetic field is solved at the next instant in time, and the process is repeated over and over again, until the desired transient or steady-state electromagnetic field behavior is fully evolved.

The basic FDTD algorithm can be stated as follows. Imagine a region of space which contains no flowing currents or isolated charges. Maxwell's curl equations can be written in Cartesian coordinates as six simple scalar equations. Two such equations are:

$$\frac{\partial H_x}{\partial t} = -\frac{1}{\mu}\left(\frac{\partial E_y}{\partial z} - \frac{\partial E_z}{\partial y}\right) \tag{2.2}$$

$$\frac{\partial E_y}{\partial t} = -\frac{1}{\varepsilon}\left(\frac{\partial H_z}{\partial z} - \frac{\partial H_x}{\partial x}\right) \tag{2.3}$$

The other four are symmetric equivalents of the above and are obtained by cyclically exchanging the *x*, *y*, and *z* subscripts and derivatives. Maxwell's equations defines a condition in which the *E* field temporal change is dependent upon the spatial variation of the *H* field, and vice versa. The FDTD method solves these Maxwell's equations by discretizing the equations via central differences in time and space, and then numerically solving these equations in software.

FDTD method algorithm is basically based on Yee's mesh [102] and computes the *E* and *H* field components at points on a grid with grid points spaced *Δx*, *Δy*, and *Δz* apart. The *E* and *H* field components are then interlaced in all three spatial dimensions as shown in Figure 2.9. Then, time is broken up into discrete steps (*Δt*). The *E* field components are then computed at times $t = n\Delta t$ and the *H* fields at times $t = (n+1/2)\Delta t$, where *n* is an integer representing the compute step. For example, the *E* field at a time *t* = *nt* is equal to the *E* field at t = (*n*-1) Δ*t* plus an additional term computed from the spatial variation, or curl, of the *H* field at time t [104].

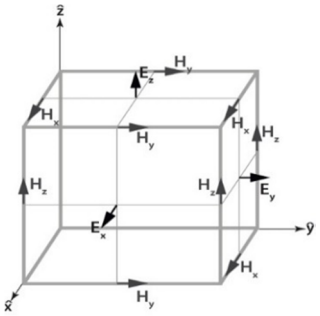

Figure 2.9: Schematic diagram of Yee cell. The H field is computed at points shifted one-half grid spacing from the E field grid points [99].

This method results in six equations that can be used to compute the field at a given mesh point, denoted by integers *i*, *j*, *k*. For example, two of the six are:

$$H_{x(i,j,k)}^{n+1/2} = H_{x(i,j,k)}^{n-1/2} + \frac{\Delta t}{\mu \Delta z}\left(E_{y(i,j,k)}^{n} - E_{y(i,j,k-1)}^{n}\right) - \frac{\Delta t}{\mu \Delta y}\left(E_{z(i,j,k)}^{n} - E_{z(i,j-1,k-1)}^{n}\right) \qquad (2.4)$$

$$E_{x(i,j,k)}^{n+1} = E_{x(i,j,k)}^{n} + \frac{\Delta t}{\varepsilon \Delta y}\left(H_{z(i,j,k)}^{n+1/2} - H_{z(i,j,k-1)}^{n+1/2}\right) - \frac{\Delta t}{\mu \Delta z}\left(H_{y(i,j,k)}^{n+1/2} - H_{y(i,j-1,k-1)}^{n+1/2}\right) \qquad (2.5)$$

These equations, including the other four cyclic equations are iteratively solved in a leapfrog manner, alternating between computing the *E* and *H* fields at subsequent Δ*t*/2 intervals. Thus, we can sum that, each field component during FDTD method solution depends on the field of the previous time step itself and the surrounding component in Yee's algorithm. One of the most important parameters for the FDTD algorithm is the use of appropriate boundary conditions. One of the most effective is the perfectly matched layer (PML), in which both electric and magnetic conductivities are introduced in such a way that the wave impedance remains constant, absorbing the energy without inducing reflections. Periodic boundary conditions (PBC) are also important because of their applicability to periodic structures such as PhC structures. There are a number of variations on the PBC, but they all share the same common idea: the boundary condition is

chosen such that the simulation is equivalent to an infinite structure composed of the basic computational domain repeated endlessly in all dimensions.

The accuracy of the FDTD results depends upon the space and time step size used. The smaller the step size, more accurate the result is. In order to produce an accurate simulation, the spatial grid must be small enough to resolve the smallest feature of the field to be simulated. Usually this is dictated by the wavelength in the material(s) to be simulated. Typically, the grid spacing must be able to resolve the wavelength in time, and therefore usually be less than $\lambda/10$ where λ is the wavelength in the material(s). Also, since the FDTD algorithm is based in the time domain, to obtain a stable simulation, one must adhere to the Courant condition which relates the spatial and temporal step size, given as,

$$c * \Delta t < 1 \Big/ \sqrt{\left\{\left(1/\Delta x^2\right) + \left(1/\Delta y^2\right) + \left(1/\Delta z^2\right)\right\}} \tag{2.6}$$

where c is the velocity of light and, for the case of a non-uniform grid, the grid sizes represent the smallest grid size in the simulation. Thus, all and all, the FDTD method is a popular numerical method, having arbitrary structure applicability, broadband calculation ability and its applicability to the nonlinearity and dispersion problems, however, the process is computationally demanding and usually time consuming due to the iterative calculation process. Thus, it is not always easy to solve the complex structures with high precision through limited memory computational devices and as, RCWA has proved again and again their ability to accurately solve periodic grating structures, thus during the thesis RCWA method has also been used to solve PhC based designs, especially where they are used as diffracting structures.

RCWA method is a rigorous computational electromagnetics semi-analytical method which is typically applied to solve scattering from periodic dielectric structures. RCWA represents the electromagnetic fields as a sum over coupled waves [105]. A periodic permittivity function is represented using Fourier harmonics. Each coupled wave is related to a Fourier harmonic, allowing the full vectorial Maxwell's equations to be solved in the Fourier domain. The diffraction efficiencies are then calculated at the end of simulation. RCWA gives diffraction results in terms of the diffraction efficiency of each order, which is the standard form of analytical theory. The spatial field distributions are derived from the Fourier harmonics. RCWA

method has an additional advantage that it eliminates possible stability problems, which may be encountered in other numerical schemes, such as the transfer matrix method [106].

Here, the number of harmonics (which determines the truncation of Fourier expansion) play an important part in determining the accuracy of the result. The number of harmonics, M are used to expand the refractive index and field in Fourier space. The greater the value of M used, the more accurate the simulation will be. However, the greater the value of M used, more simulation time and memory are required. Thus, a convergence study on the value of M needs to be performed, where several simulations are required to be done with different harmonics to analyze the behavior of simulation results.

In order to solve the Maxwell equations, a structure has been considered as multilayer periodic structure which is decomposed into stacks of layers with a vertically homogenous region considering staircase approximation with regard to the lattice cross section shape. This approach facilitates physical insights into the problem and also provides important numerical advantages [62]. The algorithm considers the structure to have horizontal PBC. The multilayer structure has been designed in the vertical direction, having periodic structure in horizontal direction.

For an example of mathematical solution of Maxwell equation through RCWA, consider a case of 2D diffraction properties calculation of a 1D grating with an arbitrarily-oriented sinusoidal permittivity function that is below a superstrate and above a substrate as shown in [107, 108]. The configuration used for the simulation is shown is Figure 2.10. RCWA begins with describing the electric fields in the superstrate (region 1, represents the region of incident light, which contain both incident and reflected waves), grating region (region 2, represents the transmission grating, which contain transmitted and reflected waves), and substrate (region 3, represents the substrate, which contain only forward diffracted (transmitted) waves) as described in Figure 2.10 by the summation of their reflected and transmitted waves of all orders, i:

$$E_1 = exp\left[-j\left(\beta_0 x + \xi_{10} z\right)\right] + \sum_i R_i \, exp\left[-j\left(\beta_i x + \xi_{li} z\right)\right] \tag{2.7}$$

where the first and the second term represents the incident wave and the sum of all reflected diffraction orders in the superstrate region, respectively. In this equation, $\beta_i = k_1 sin\theta - iKsin\Phi$ for any integer i (the wave order); $\xi_{li}^2 = k_l^2 - \beta_i^2$ for l = 1, 2, or 3 (the region index); $k_l = (2\pi\square_l)^{1/2}/\lambda$ for l = 1, 2, or 3; here k is the wave vector, β is the propagation constant, λ is the free-space wavelength; j is the imaginary number, θ is the angle of incidence of the light, Φ is the angle of

tilt of the sinusoidal permittivity of the grating, R_i is *i*th reflected wave normalized amplitude, which are to be calculated through RCWA method.

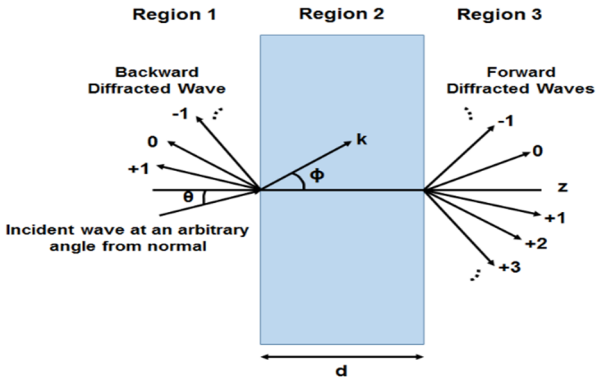

Figure 2.10: Planar diffraction grating structure with a sinusoidal permittivity used to demonstrate the RCWA algorithm.

Inside the diffraction grating one must consider all forward and backward diffracted waves from both bounding interfaces, which can be described by:

$$E_2 = \sum_i S_i(z) exp\left[-j\left(\beta_i x + \xi_{2i} z\right)\right] \tag{2.8}$$

where $\xi_{2i} = k_2 cos\theta' - iKcos\Phi$, θ' is the angle of refraction inside the modulated region, and $S_i(z)$ is the normalized amplitude of the *i*th wave field at any point within the modulated region. The transmitted waves into the substrate can be described by:

$$E_3 = \sum_i T_i \, exp\left[-j\left(\beta_i x + \xi_{3i}\left(z - d\right)\right)\right] \tag{2.9}$$

where T_i is the normalized amplitude of the *i*th transmitted wave. The term coupled-wave, discussed above comes from the expression of each *i*th wave (each diffraction order in each region) as a superposition of an infinite number of plane waves, which completely describes the forward and backward traveling waves of that order. The permittivity of the grating region is described by an equation, either a Fourier expansion that describes the permittivity of one layer in a staircase approximation of a more complicated geometry, or, as in the example shown here, a simple equation that spatially describes the permittivity in the grating layer. The grating follows the equation:

$$\varepsilon\left(x,z\right) = \varepsilon_2 + \Delta\varepsilon \, cos\left[K\left(x \, sin\phi + z \, cos\phi\right)\right] \tag{2.10}$$

where ε_2 is the average dielectric constant of region 2, $\Delta\varepsilon$ is the amplitude of the sinusoidal relative permittivity, □ is the grating slant angle, and $K = 2\pi/\Lambda$, where Λ is the grating period.

This equation will change to match the specifics of the grating of interest, of course, but this sinusoidal index grating can describe the basic RCWA mechanism. The amplitudes of the superimposed infinite sum of waves for each diffraction order are determined after considering the modulated-region wave equation (Eigen function), given as

$$\nabla^2 E_2 + \left(2\pi/\lambda\right)^2 \varepsilon(x,z) E_2 = 0 \tag{2.11}$$

Once the permittivity and fields are appropriately described, the Eigen function is solved using scattering matrices for the field strength of each diffracted wave.

RCWA is a highly accurate method for determining the reflectivity of a periodic grating. In RCWA, numerical error basically comes from the error in describing a grating by a stair-step approximation In order to neutralize these effects, Fourier terms and diffraction orders should be calculated accordingly. Due to the Fourier and Flouquet expansions used in the derivation of this method, it is necessary to truncate the expansions appropriately in order to enable fast and efficient solution with a computer. However, the method has some limitations that include convergence problems for TM polarized light, especially for metallic grating, limitations to solve non-periodic structures, incorporation of non-linear effects and does a poor job of modeling structures with very shallow slopes. Still, as we are dealing with periodic dielectric structures during the thesis considering them as a diffraction structures, the RCWA method can be an accurate, fast and reliable tool which can predict the absorption in the structures with precision.

PWE method is also among many computational methods which are used to solve the Maxwell's equations through formulation of an eigenvalue problems from these equations. The method is widely used for the calculation of photonic band gap for the PhC structure, and thus the same has also been used in the thesis for the PBG calculations. PBG has been calculated through solution of the dispersion relation (as discussed in detail in section 1.4.2) of specific PhC configurations [80]. PWE method is highly efficient for calculating modes in periodic dielectric structures. Equations can be solved through iterative techniques, and just few band index plots in the band diagrams are required lying on the brillouin zone edges to find the value of the frequency band.

In order to find the photonic band structure, one has to find the solution of the eigenvalue problems (as discussed in section 1.4.2), for the frequency ω_k and mode function, for each required value of wavevector, *k*. The method uses the variational statement of Maxwell's

equations. It has been the case that, the function which minimizes the electric field eigenmode is the eigenvector of the operator of minimum frequency ω_k. The next lowest mode is the function which minimizes the electric field eigenmode and is simultaneously orthogonal to the lowest mode. Thus, any requires number of modes can be found by successively minimizing the electric field eigenmodes and orthogonalizing each mode to all the earlier found modes. To implement this minimization, the unknown mode function is represented as a Fourier series over plane waves from the reciprocal lattice. In the numerical implementation, the sum is truncated at a reasonable resolution and the calculation of electric field eigenmode becomes a matrix problem solved using iterative techniques, specifically known as PWE method [109].

The PWE has the main advantages of accuracy and efficiency. However, its inability to model loss and refractive index variation in the material with wavelength limited its use in some cases. Being a Fourier space method, it also suffers due to Gibbs phenomenon that affects the method's accuracy. Even, with these drawbacks, the method is widely popular in PhC structure community for calculating its PBG due to its easy implementation and accuracy for periodic dielectric structures.

2.7. Experimental Growth and Fabrication Process: Brief Discussion

One of the key works presented in the thesis is the demonstration of growth and fabrication of TFSC structure with PhC LTS. Thus, it is requisite to discuss about the required growth and fabrication technologies for practically realising the proposed structure. Hence, through the section, we will discuss in brief about these growth and fabrication processes, which will throw light on the basic techniques used during these processes. During the latter part of the thesis we will discuss about the growth and fabrication of p-i-n superlattice based InGaN/GaN solar cells having PhC LTS designed at the top. The process of designing the practical structure involves three important processes including others, which are metal organic chemical vapor deposition (MOCVD) (for the growth of InGaN/GaN epitaxial structure), RF sputtering (to deposit Indium Tin Oxide, ITO layer) and electron beam lithography (EBL) (to incorporate PhC LTS pattern).

MOCVD (also known as MOVPE (metal organic vapor phase epitaxy), OMVPE (organo-metallic vapor phase epitaxy) and OMCVD (organo-metallic chemical vapor deposition)) is a process of depositing thin epitaxial atomic layers over a semiconductor wafer with incredible precision [110]. Its ability to be scaled up to industrial-scale production with relative ease makes

it a preferred choice for industrial applications. Also, for MOCVD, the overhead costs tend to scale with production volume, which is opposite for its nearest competitor molecular beam epitaxy (MBE) method [111].

The principle of MOCVD follows that the desired atoms (that are required to be in the crystal) are combined with complex organic gas molecules and passed over a hot wafer. The molecules are broken up due to the heat and the desired atoms are deposited on to the surface, layer by layer. The properties of a crystal can be changed at an atomic scale just by varying the composition of the gas. It can grow high quality semiconductor layers (even of a nm thickness) and the crystal structure of these layers is generally perfectly aligned with that of the substrate.

MOCVD is commonly used in process for III-V compound semiconductors growth over the same crystalline substrate, especially for those based on Gallium Arsenide (GaAs) and Gallium Nitride (GaN). There are mainly two different technologies for MOCVD deposition processes: first one is the Planetary Reactor and second one is the Close Coupled Showerhead technology to deposit very thin layers of atoms onto a semiconductor wafer.

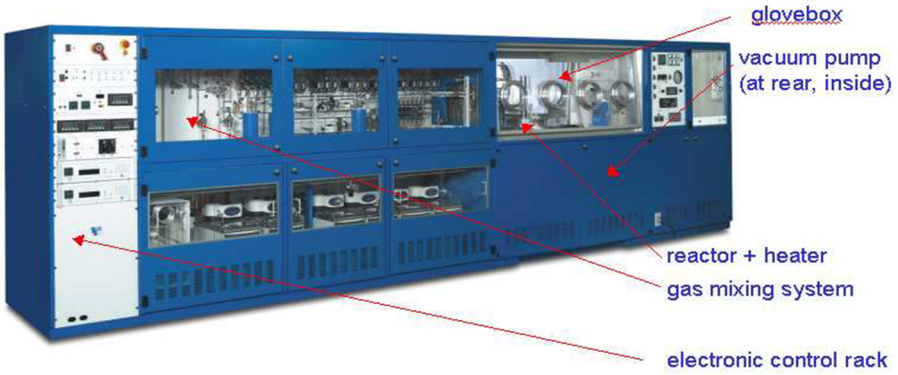

Figure 2.11: MOCVD reactor at CSIR-CEERI Pilani (Rajasthan, India)

In contrast to Molecular Beam Epitaxy (MBE) the growth of crystals in MOCVD, is by chemical reaction and not physical deposition. This takes place not in a vacuum, but from the gas phase at moderate pressures (100 to 760 Torr). As such, this technique is preferred for the formation of devices incorporating thermodynamically metastable alloys, and it has become a major process of manufacturing in optoelectronics. In MOCVD ultra-pure gases are injected into a reactor and finely dosed to deposit a very thin layer of atoms onto a semiconductor wafer. Surface reaction of organic compounds or metal-organics and hydrides containing the required chemical elements creates conditions for crystalline growth-epitaxy of materials and compound semiconductors.

In our case, GaN layer has been grown in a reactor (shown in Figure 2.11) on a substrate by introducing tri-methylgallium ($(CH_3)_3Ga$) and ammonia (NH_3). The metal-organic precursors are placed in steel cylinders called bubblers, which are kept in temperature controlled baths. Accurate temperature control of bubblers is required, since the vapor pressures of precursors are extremely sensitive to temperature. When carrier gas is passed through a bubbler, it is saturated with gaseous metalorganic material. In this system tri-methylgallium (TMGa) and tri-ethylgallium (TEGa) are use as gallium source for bulk GaN and multi quantum well respectively. Tri-methylindium (TMIn), tri-methylaluminum (TMAl) and bis-cyclopentadienylmagnesium (Cp_2Mg) are used as Gallium, Indium, Aluminum and Magnesium sources, respectively.

The gas flows are regulated with valves and mass flow controllers into the reactor. Gaseous Ammonia (NH_3) and Silane (SiH_4) are used as Nitrogen and Silicon sources respectively. Most common substrates used for growth of GaN are Sapphire (Al_2O_3), Silicon Carbide (SiC) and Silicon (Si). However, commercially as well as for laboratory purposes, Sapphire is most widely used substrate due to its wide availability. The other benefits of sapphire include its ease of handling toughness and stability at high temperature.

Another important process used, which should be discussed (due to its important role in the presented design process) is the ***sputtering*** [112]. Sputtering is basically a physical vapor deposition process used to deposit large variety of materials' thin films with high precision. Sputtering, also known as "cathodic sputtering", uses the erosive action of accelerated ions at the surface of a target material. The ions are accelerated at enough energy to remove (sputter) particles at the target surface. Usually, an electrical field is generated at high vacuum between an anode and a cathode plate (target) that is to be sputtered.

A working gas, generally Argon (Ar), is ionized on application of electrical voltage generating a glow discharge [113]. The positive Ar^+ ions accelerate towards the target (kept at –ve voltage) and sputter the atoms on its surface. In sputtering the particles of the target are displaced by means of direct "momentum transfer" (inelastic collision) between the ions and the atoms of the material to be deposited. In order to accomplish sputtering, a certain threshold energy is needed to remove atoms from the target surface and bring them into the vacuum. This is indicated by the sputtering efficiency *S*, which is the ratio of the sputtered material per Ar^+ ion. Atoms from

the target are ejected after being struck by Ar^+ ions. The atoms from the target then travel through the plasma and form a layer on the substrate.

The most common sputtering technology is magnetron sputtering in which magnets are placed near to the target to keep the density of the sputtering ions very high which enhances sputtering efficiency [113, 114]. This makes it possible to have a higher and more stable sputtering rate and ultimately a faster deposition. In magnetron sputtering coating process thickness control can be performed by sputtering time only, i.e. the coating deposition rate (thickness coated per second given as nm/s) depends on the magnetic field, the electric accelerating field and the gas pressure. If these parameters are precisely controlled, the deposition rate would be stable and reproducible under identical settings of the defined parameters.

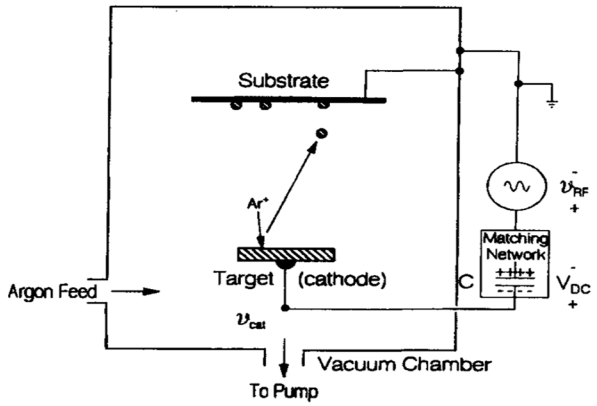

Figure 2.12: Schematic diagram for a RF sputtering process [112].

Radio Frequency (RF) sputtering is a special case of magnetron sputtering, where RF source is used to generate heat. In RF sputtering there is a blocking capacitor (C) in series with a cathode (the target) and an anode [115, 116]. The capacitor is part of an impedance-matching network that facilitates the power transfer from the RF source to the plasma discharge. The power supply is a high voltage RF source (usually fixed at 13.56 MHz). The blocking capacitor is placed in the circuit to develop the DC self-bias, and a matching network is utilized to optimize power transfer from the RF source to the plasma (Figure 2.12).

RF sputtering works well to produce highly insulating oxide films (like ITO) but here the expense is more than DC sputtering due to RF power supplies and impedance matching networks [114, 115]. Another problem is stray magnetic fields leaking for ferromagnetic targets, which also disturb the sputtering process, compensated through specially designed sputter guns with unusually strong permanent magnets.

Another important fabrication process, which need a special mention in context of the thesis work, is ***electron beam lithography (EBL)***, which is used to obtain 2-D PhC structure in nm range with high precision. Lithography (process of creating patterns) is considered as cornerstone for micro and nano fabrications. Lithography usually is a combination of several steps which includes patterning, deposition and etching. The number of levels of lithography, basically quantifies the complexity of the whole process of designing a particular device [117].

Lithography processes are usually classified on the basis of the interface that is used to define the patterns (however, many other ways of classification also exists). One of the most popular pattern creation method is based on the exposition of a deposited thin film to a beam. There are several lithographic processes which use different beam sources (like photolithography, electron beam lithography (EBL), etc.) [118]. Traditionally, photolithography, which uses light to transfer patterns, is preferred in micro fabrication techniques due to its easy processing, parallel writing over the substrate and material compatibility for most of the industrial processed materials. However, the technique is not suitable for nanofabrication, due to its resolution limitations since it is limited by the wavelength of light and optical diffraction phenomenon. Mask fabrication and its alignment also add to its limitations. Thus, in order to overcome the problem, development of UV and X-ray lithography like processes has been done, but they also have restrictions such as light sources are expensive and sometimes X-rays tends to penetrate conventional metal masks [118].

Thus, requirement to create precise nm patterns led to the development of EBL. The basics are derived from the early scanning electron microscopes, consists of scanning a beam of electrons across a surface covered with a resist film sensitive to those electrons, thus depositing energy in the desired pattern in the resist film [119]. Some of the peculiarities of the technology include its capability of creating very high resolution patterns, flexibility to work with a variety of materials; a mask less process that can write precisely in nm without diffraction problems.

The basic idea behind EBL is identical to any other lithography process, where the substrate is first coated with a thin layer of photo resist (also called as e-resist in EBL), which is a chemically active material and changed under exposure to the electron beam, where the exposed (non-exposed) areas can be dissolved in a specific solvent (positive (negative) lithography), and thus allow image transfer onto a substrate. Photoresist is usually applied to the surface of the wafer by

high-speed centrifugal spinning, known as "Spin Coating," produces a thin uniform layer of photoresist on the wafer surface. In this process a liquid solution of photoresist is give out from the wafer by rapid spin and produce uniform thin layer (0.5µm to 2.5µm). Chemicals commonly use as photoresist include Poly Methyl Methacrylate (PMMA), Poly Methyl Glutarimide (PMGI), Phenol Formaldehyde Resin (DNQ/Novolac) etc (Figure 2.13 (c)).

Development of the photoresist is also an important step for EBL. Most commonly used developer is tetra methyl ammonium hydroxide (usually used in concentrations of 0.2 - 0.26). Developer is important in controlling the development uniformity. Two methods are mainly used for the process, one is spin development and other is spray development. During spin development wafers are spun and developer is poured onto the rotating wafer whereas in spray development, the developer is sprayed rather than poured, on the wafer by using a nozzle that produces a fine spray over the wafer.

Then hard bake is used to harden the final resist image at a controlled temperature (120°C - 150°C), so that it will hold out the harsh environments of etching. Next, etching is performed using either wet chemicals such as acids, or more commonly a dry etching process (such as reactive ion etching). The photoresist will resist the etching and protect the material covered by the resist. Alternately, lift off process can also be used to selectively remove the unwanted layer area. When the etching is complete, the resist is stripped leaving the desired pattern. There are mainly two classes of stripping techniques; wet stripping and dry stripping. A simple example of stripper is acetone. Acetone tends to leave residues on the wafer.

Although the above discussion, has provided a rather simplistic view of the EBL, the process has realistic potential to design complex nm range pattern with relative ease and precision, as compared to other lithography processes. One of the most important application of EBL is in the designing of periodic PhC patterns and that is the reason, the thesis work also demonstrate the fabrication of proposed PhC pattern through EBL process. However, the EBL process also has its inherited problems like any other complex process. As it is a sequential writing process, it usually takes a long time to design a small area pattern and thus has a limitations for industrial applications where bulk processing is usually required with precision. Also, EBL is comparatively expensive than its counterparts. Thus, there are also various alternatives that have been tried such as soft lithography, nanosphere lithography etc, but these techniques are still in

the stage of development and to create reproducible devices through them is very difficult. Hence, even with all its cons, from present perspective, EBL is the most suitable technique for PhC patterning and here in our thesis, the author has used e-line plus-ultra high resolution EBL system for imaging provided by Raith available at IIT-Delhi (India).

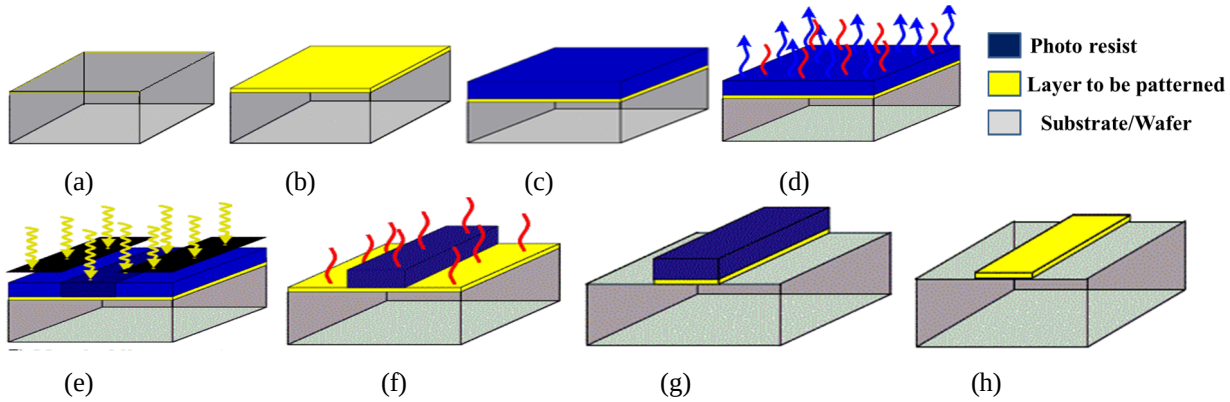

Figure 2.13: Schematic diagram for electron beam lithography process: (a) cleaned substrate, (b) deposition of layer to be deposited over substrate, (c) deposition of photoresist, (d) pre baking before electron beam exposure, (e) patterning of resist through e-beam (-ve resist), (f) development to dissolve photoresist and hard baking before etching, (g) etching to remove the unwanted area of the layer required to be patterned, (h) final pattened structure after etching and stripping.

2.8. Conclusion

The chapter presented the brief overview of the subject, which the thesis is going to demonstrate in details in the coming chapters. The chapter also discussed about the current research scenario of the subject from both national and international perspective and tried to present the research gaps and proposed modifications that may fill those gaps. The chapter also discussed about the requirement of light trapping studies for GaAs and InGaN/GaN solar cells and what are the benefits of using PhC LTS with the above mentioned absorbing materials. The chapter also presented a brief summary of the simulation approach that the thesis will use in the coming chapters to demonstrate the effectiveness of the proposed PhC LTS for the TFSC structures. The last section of the chapter discussed in brief about the important growth and fabrication process that has been used to fabricate the proposed structures and presented in the 7^{th} chapter. The discussion presented in the chapter is useful to recognize the requirement of the study of the subject and make it suitable for the readers to make basic understanding.

Chapter 3

Light Trapping in GaAs Thin Film Solar Cells Using 2D Photonic Band Gap Structure as a Single Back Reflector

3.1. Introduction

The previous chapters summarize the need for the study of the GaAs active material based TFSC and also the need to study light trapping in GaAs active material. It has been said that although the highest efficiency single junction solar cell belongs to GaAs active material [20], its use is mainly restricted to the space applications only due to its high cost and hampers its use for terrestrial applications. Thus, to make the material acceptable for terrestrial applications, it is required to achieve high efficiency with extremely thin films of GaAs active material which reduces the requirement of GaAs material and eventually cut down the cost [35].

It has also been discussed that, in order to achieve high efficiency with these cells, one has to look for ideal light trapping that could improve the photon path length within the absorbing layer without actually increasing its thickness [120]. These photons travel several passes within the device before they can be reabsorbed, giving rise to the process of photon recycling, unless they are emitted within the escape cone or absorbed by a non-perfect backside mirror [36].

As discussed in previous chapters, in order to overcome the problems associated with planar LTS, in the last decade or so, several researchers have demonstrated the potential of the PhC structures as LTS especially with thick Si and a-Si:H cells, but not reported the detailed electrical behavior for TFSC having 2-D PhC as a PBG structure at the back especially for GaAs solar

cells. Thus designing of the broadband reflector using PhC structures for GaAs solar cells needs to be explored and studied.

In this chapter, the behavior and efficiency of the thin film GaAs solar cell having PhC LTS as the broadband BR has been examined. Here, PhC structure is arranged to work as a PBG structure. The design has an added advantage that the single structure performs the task for both specular and oblique angle reflections. We have also compared the performance of the proposed structure having PhC BR with that of Al BR. The effect of non-radiative recombination, interface recombination effects and incomplete ionization have also been inspected. The simulation has been done using the Plane Wave Expansion (PWE) method, FDTD method [102] and Minilase-II program [121] through Synopsys' RSoft CAD software package.

3.2. Numerical Modelling and Simulation Approach

Numerical modelling has been performed to incorporate most of physical phenomena which limit the efficiency of the GaAs thin film cell [20], [86], in order to demonstrate the effectiveness of the PhC BR under ideal and practical conditions and the results are then compared with that of Al BR based design. Absorption spectra have been computed by well-known FDTD method, which marks for photo-generation [122]. Then the modeling of the minority carrier transport has been done through solution of the Poisson's and carrier continuity equations. The solution of these equations has been found through using the Synopsys' LaserMOD software [106] which is based on Minilase-II program. Semiconductor material parameters considered for the following equations are taken from [123], [124] unless otherwise stated. The solution of these equations using appropriate boundary conditions gives us details about how the device works electrically. The electric potential Φ is determined by Poisson's equation:

$$\nabla \varepsilon \nabla \Phi = q(n_e + n_h - N_D^+ + N_A^-) \tag{3.1}$$

where the charges are given by the densities of electrons n_e, holes n_h, and ionized donors N_D^+ and acceptors N_A^-. q is the elementary charge. These equations are then solved for each layer. Then continuity equations are solved for carrier concentration within each layer as well as at interfaces. Continuity equations are solved for direct and indirect recombination, given as following:

$$q\frac{\partial n_{e/h}}{\partial t} = \pm\nabla J_{e/h} - qR^{non-rad} - qR^{spon} + qG_{e/h} \tag{3.2}$$

Here, $G_{e/h}$ are the carrier generation rates determined through FDTD optical simulations, $R^{non\text{-}rad}$

is the non-radiative recombination rate and R^{spon} is the spontaneous radiative recombination rate whereas $J_{e/h}$ denotes current. The photo-generation is calculated at each node during simulation on the basis of absorption coefficient α of a particular material. In the numerical modeling, the author has considered absorption at each layer, but considered only the absorption in the active region towards generation of electron-hole pairs, and at other layers as loss. The non-radiative recombination $R^{non\text{-}rad}$ is the sum of contributions due to R^{dark} and $R^{interface\text{-}SRH}$ which represents dark and interface non-radiative recombination. R^{dark} comprises of Auger (R^{Auger}) and Shockley-Read-Hall (SRH) (R^{SRH}) processes. R^{Auger} recombination is modeled as:

$$R^{Auger} = \left(C_e^{Auger} n_e + C_h^{Auger} n_h\right)\left(n_e n_h - n_i^2\right) \tag{3.3}$$

Here, n_i is the intrinsic carrier density and C_e^{Auger} and C_h^{Auger} are temperature dependent Auger coefficients. The room temperature Auger coefficients C_e^{Auger} and C_h^{Auger} values as 1×10^{-42} and 2×10^{-41} m^6/s respectively are used [123]. The SRH process describes recombination via trap levels and modeled through the following equation:

$$R^{SRH} = \frac{\left(n_e n_h - n_i^2\right)}{\tau_h^{SRH}\left(n_e + n_e^{trap}\right) + \tau_e^{SRH}\left(n_h + n_h^{trap}\right)} \tag{3.4}$$

The SRH lifetimes τ_n^{SRH} and τ_p^{SRH} for electrons and holes are taken as $5*10^{-7}$ sec. [86], whereas $n_{e/h}^{trap}$, gives the trap carrier occupation, is a material dependent parameter that depends on trap energy of the material. Next, the analysis of the effect of interface recombination has been done, which is also a form of non-radiative recombination. The interface recombination rate (per surface area) is given as:

$$R^{interface-SRH} = \frac{n_e n_h - n_i^2}{\frac{1}{v_h^{interface-SRH}}\left(n_e - n_e^{trap}\right) + \frac{1}{v_e^{interface-SRH}}\left(n_h - n_h^{trap}\right)} \tag{3.5}$$

Here $v_{e/h}^{interface\text{-}SRH}$ are the interface recombination velocities, taken as 40 m/s for both holes and electrons [123]. Now, combining the results obtained through R^{dark} and $R^{interface-SRH}$ gives us the value of $R^{non\text{-}rad}$ in Equation (3.2). Next, the modeling of the radiative recombination term has been done, which is represented by R^{spon}. In bulk regions and for continuum states, an approximate expression for spontaneous recombination is given as [125] :

$$R^{spon} = B\left(n_e n_h - n_i^2\right) \tag{3.6}$$

Einstein coefficient B is a material parameter, the value for which has been taken as 2×10^{-16} m^3/s.

Next, the current densities $J_{e/h}$ in the carrier continuity equations are calculated within the framework of drift-diffusion theory, given as:

$$J_{e/h} = \pm qD_{e/h}\nabla n_{e/h} + q\mu_{e/h}n_{e/h}\nabla E_{C/V} \pm q\mu_{e/h}n_{e/h}P_{e/h}\nabla T \tag{3.7}$$

Here, $D_{e/h}$ is the diffusivity, $\mu_{e/h}$ is the mobility and $P_{e/h}$ is the thermoelectric power of electrons and holes, respectively. For Fermi statistics, the diffusivity is related to the carrier mobility via a generalized Einstein relation. The number of absorbed photons at a wavelength λ within each layer (which marks for the generation term, $G_{e/h}$) is found out as:

$$n_i(\lambda) = \frac{S(\lambda)A_i(\lambda)}{E(\lambda)} = \frac{\lambda}{hc}S(\lambda)A_i(\lambda) \tag{3.8}$$

where, $S(\lambda)$ is the specific incident spectrum [$W/m^2 \cdot nm$] which we have taken as AM1.5G [48] (as discussed in section 1.3.4), $A(\lambda)$ is the Absorption Spectra for each layer computed using FDTD and $E(\lambda)$ is the energy of a particular wavelength photon. Now, the shadowing effect of electrodes has been taken into account via efficiency term η_s multiplied to the carrier generation term obtained through continuity equation. Thus, the total number of electron-hole pairs collected by the electrodes is therefore given as:

$$N_{e-h} = \int_{\lambda} n_{e-h}(\lambda)d\lambda \tag{3.9}$$

Next, modelling of the short-circuit current density (J_{sc}) and open-circuit voltage (V_{oc}) together with the general voltage-current relationship under dark and illumination conditions to find the J-V curve of the solar cell has been carried out. The resultant equations are as follows [13] :

$$J_{sc} = eN_{e-h} \quad [A/m^2] \tag{3.10}$$

$$V_{oc} = \frac{kT}{e}\ln\left(\frac{J_{sc}}{J_0} + 1\right)[V] \tag{3.11}$$

where k is Boltzmann's constant, T [K] is the absolute temperature, and J_0 is the reverse bias saturation (or dark) current density, which is computed by an active device simulation or empirically. On the basis of the parameters defined above, the various important eventual solar cell outputs including quantum efficiencies, fill factor, efficiency etc. could be computed using the standard equations [13], and then the results obtained have been analyzed.

3.3. Design of the Structure

The basic design of the solar cell structure has been adopted from previously designed structure [86] and then the modifications have been done in the structure to incorporate 2D PBG structure

to arrive at the final proposed design. Development in the design has been accounted for considering practical materials for various layers (ARC, PhC LTS and Al BR) as opposed to ideal approach provided in the above mentioned article, and their effect on the performance of the cell studied. The cell consists of a heavily doped p-type GaAs base region in contact with the n-type GaAs emitter region. The GaAs material base and emitter are in contact with high band gap, heavily doped thin AlGaAs window layers. These layers, forming hetero-junctions with GaAs layers serve an important purpose to deflect minority carriers away from the contacts to reduce front and back surface recombination. At the top of the structure, single layer, planar ARC is integrated, which controls reflection losses from the front surface. A planar ARC layer has been considered to keep the design simple and to be more focused on the performance of PhC BR. It is well known that reflections are minimized if the refractive index of the ARC is the geometric mean of that of the materials on either side [13], as

$$n_1 = \sqrt{n_0 * n_2} \tag{3.12}$$

where n_1 is the refractive index of the ARC material, n_0 is the index of surrounding material (air) and n_2 is the refractive index of the layer beneath the ARC (which is $Al_{0.8}Ga_{0.2}As$ in our case). As per these calculations, Indium Tin Oxide (ITO), a popular transparent conducting oxide (TCO), has been considered as an ARC [126].

In order to minimize reflections, the thickness of the ARC is required to be the quarter wavelength thick for the incoming wave [13]. However, while dealing with incident solar spectrum, it is required that reflections should be minimized from the top for the entire spectrum range of interest (kindly refer to section 1.3.4 for spectrum). As it is not possible to design such an ideal ARC, having zero reflections throughout the spectrum, one has to design an ARC layer to be having minimum average reflection from the top, having zero reflection for some centralized wavelength, which is usually considered around 500-600 nm wavelength value, where incident spectrum photons are more as evident from Figure 1.3. On the basis of this, we have optimized the thickness of ARC, which for our case returns the value to 72.38 nm through optimizations, which corresponds to around 543 nm wavelength as per the material parameters used during simulations [126].

Other layers are also optimized in the similar way in order to get maximum efficiency out of the device. The parameters of the overall structure are given in the Table 3.1. Figure 3.1 (a) gives

the basic schematic diagram of the proposed structure. The PhC LTS that placed at the back of the structure is designed to have 2D hexagonal lattice, having GaAs rods in the SiO_2 background as shown in Figure 3.1 (b). The combination of the two materials has been taken keeping their availability, fabrication and electrical and optical parameters in mind, as the dielectric contrast of the two materials should provide enough Photonic Band Gap (PBG) for the desired wavelength range and at the same time should have minimum absorption. Then the PhC structure has been optimized using the PWE method, to allow the reflection of the photons for the desired range.

Table 3.1: List of various parameters used for designing the structure

S.No. (in order the layer present in the structure)	Name of the layer/parameter	Type of material	Doping (/cm^3)	Thickness of the layers (nm)
1.	ITO (Anti reflective Coating)	Dielectric	-----	72.38
2.	p- $Al_{0.8}Ga_{0.2}As$	Bulk Semiconductor (window layer)	$3*10^{+18}$ (Acceptor type)	18.00
3.	p-GaAs	Active semiconductor (emitter layer)	$1*10^{+18}$ (Acceptor type)	90.00
4.	n-GaAs	Active semiconductor (base layer)	$2*10^{+17}$(Donor type)	1500
5.	n- $Al_{0.3}Ga_{0.7}As$	Bulk Semiconductor (back surface window layer)	$4*10^{+18}$ (Donor type)	20.00
6.	Radius of the GaAs rods used for hexagonal PhC structure having SiO_2 background	Intrinsic GaAs material and dielectric SiO_2 background material	Intrinsic	42.64
7.	Period or lattice constant (*a*)	-----	-----	220.00

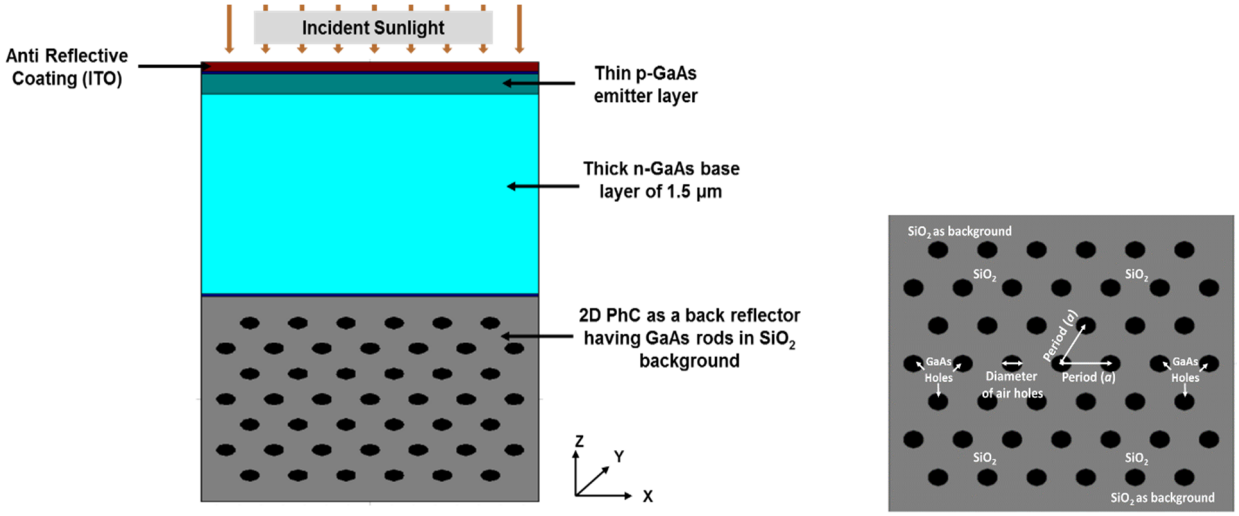

(a) (b)

Figure 3.1: (a) Structure of the proposed GaAs solar cell having 2D PhC as a BR; (b) 2D hexagonal lattice PhC structure having GaAs rods periodically arranged in SiO_2 background

The PBG appears due the index modulation of the structure. The modes of propagation and prohibition which give rise to PBG for the PhC structure can be found by solving the master equation developed from the Maxwell equation (for details please refer to section 1.4.2.), as given in Equation (3.12) [54].

$$\nabla \times \frac{1}{\varepsilon(r)} \nabla \times H(r) = \left(\frac{\omega}{c}\right)^2 H(r) \tag{3.12}$$

Here, ε is the permittivity of the PhC structure, ω is the frequency of operation, c is the velocity of light in free space and H denotes the magnetic field of the region. We have used PWE method for the solution of the Equation (3.12) (kindly refer to section 2.6 for details). We have then optimized the PhC structure to find optimal rods radius and the lattice constant, so that its PBG lies in the range of interest.

Here, as the single PBG structure is required to perform the task of both specular as well as oblique angle reflections from the back. Thus, the structure is also required to provide sufficient photon diffraction reaching BR at oblique angles. Thus, for sufficient diffraction of photons from the PhC BR, it is necessary for its period to be larger than the wavelength of light in the active layer, i.e. $a > \lambda/n(\lambda)$. This condition is satisfied for $a > 200$ nm, as per material parameters used. As per [60], for a particular active layer thickness in a solar cell structure using PhC structure, there are several diffraction resonances from the diffraction grating whose peaks overlap and leads to overall absorption enhancement. There should be several such resonances in the entire wavelength range where the active layer thickness is not enough to absorb high wavelength photons. Thus, let for an active layer thickness, t_{ACT}, all resonances should pick up the round trip phase change of $2m\pi$, so that $k_{\perp} = m\pi/t_{ACT}$, where k represents the photon momentum. The wavelength of diffracted resonant mode is given by [59]:

$$\lambda = \frac{2\pi n(\lambda)}{\sqrt{G_x^2 + G_y^2 + (m\pi / t_{ACT})}} \tag{3.13}$$

where m is an integer, n is the refractive index of GaAs and G_x, G_y are the components of reciprocal lattice vectors $(G_x = i(2\pi/a);\ G_y = j(2\pi/a))$. The diffraction resonances occur for integer values of i, j and m and exhibit peaks in the absorption for wavelengths near the band edge for values of period larger than ~ 200 nm. The gap map results after optimization of the

structure with respect to rods radius and wavelength range of interest are shown in Figure 3.2. The results are then analyzed and implemented using the Equation given below:

$$\text{Band gap value} = - \tag{3.14}$$

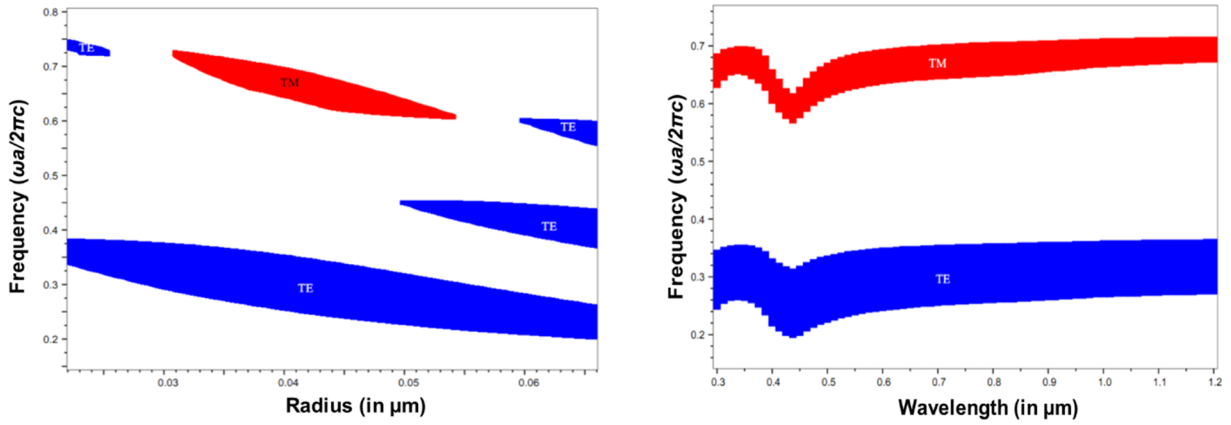

(a) (b)

Figure 3.2: Gap map diagrams for the optimization of the proposed structure with (a) variation in rods radius taking optimized period = 220 nm, (b) variation in wavelength taking optimized period =220 nm and rods radius = 42.64 nm

Here, a is the lattice constant (period) of the PhC structure and λ is the wavelength of operation. We have used period of the structure as 220 nm and rods radius to be 42.64 nm, which has given us the TE band gap range of 633.02 nm to 898.47 nm at 300 nm wavelength of photon. The PBG values are also optimized with the wavelength of incident spectrum, as shown in Figure 3.2(b), as the permittivity of the PhC structure changes with wavelength, but the starting and ending values for the PBG almost remain within the desired wavelength range.

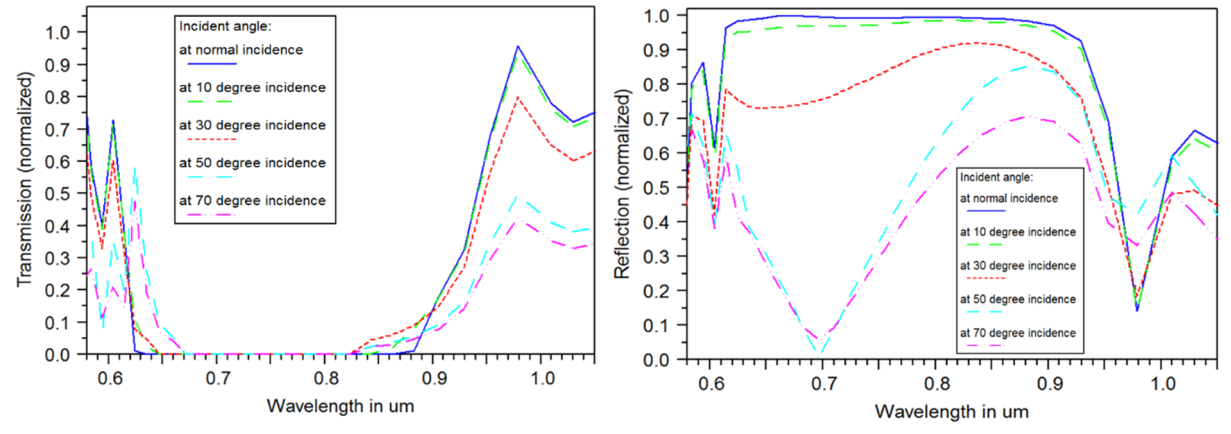

(a) (b)

Figure 3.3: (a) Transmission; (b) Reflection graph for the designed PhC structure with variation in wavelength (for normal incidence) indicates that the reflections are maximized in the desired wavelength range. The source is normalized to the value unity

The transmission and reflection graphs shown in Figure 3.3 (a) and (b) clearly indicate that the transmission through the designed PhC structure is almost zero in the desired range, i.e. from 600 nm to 875 nm. The graphs also show how the reflections and transmission varies with the incident angle for the particular wavelength of light. Although the results indicate the degradation in the performance of the proposed PhC structure with increasing incident angle, which are basically due to losses at interface and absorption in the structure due to evanescent fields, still the reflections and transmissions are much better than the metallic BR and indicates the superiority of the PhC structure in case of oblique angle reflections.

Figure 3.4 shows how the escape cone or critical angle for Al BR varies especially in the wavelength range of interest, due to which we could consider that although for higher energy photons Al BR can also perform well, for high wavelength low energy photons (for which BR is basically required), this metallic BR allows most of the photons to escape and thus does not contribute in omni-directional light trapping. The fact proves the PhC LTS superiority over Al BR and how these periodic structures can help proposed structure to enhance efficiency.

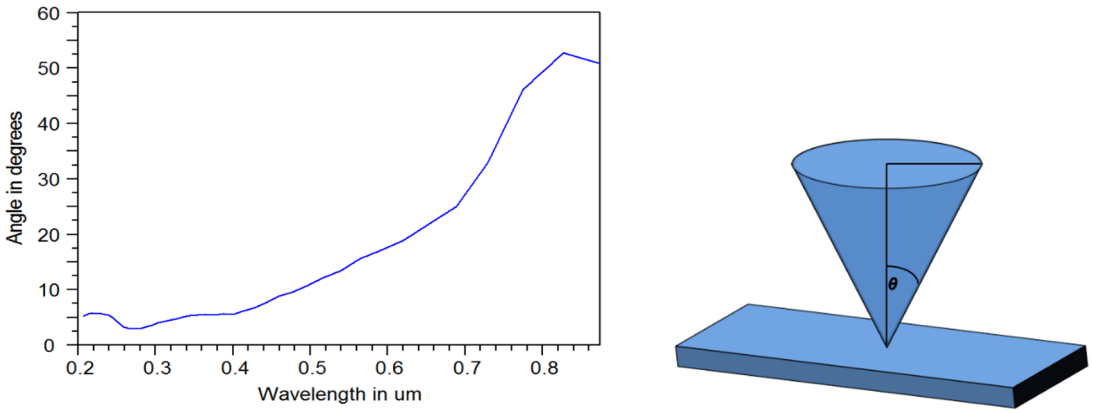

(a) (b)

Figure 3.4: (a) Escape cone or critical angle (θ) graph for Aluminum BR at different wavelengths considering Al and $Al_{0.3}Ga_{0.7}As$ interface at the back; (b) Schematic to explain escape cone

3.4. Results and Discussions

Initially, the results have been obtained for ideal case, i.e. without considering any loss, and then comparison has been made between 2D PhC and Aluminum (Al) BR designs. In the simulation studies, the author has considered cumulative 6% shadowing losses and considered that each absorbed photon in active GaAs layer produces an electron-hole pair. The perfectly matched layer (PML) boundary conditions are used in the z- direction (vertical) whereas symmetric and

anti-symmetric boundary conditions are used in the other two directions. Table 3.2 lists the summary of the various results obtained.

The results obtained show that the use of a suitable designed PhC BR notably improves the performance of GaAs solar cells as compared to Al BR. Thus, it might pave the path for next generation low cost high efficiency thin film cells. Under ideal conditions, without considering any recombination effects, the efficiency of the cell improved by the margin of about 6%. Figure 3.5 shows the comparison between efficiencies of the cell with PhC and Al BRs, under ideal and practical conditions (including various losses).

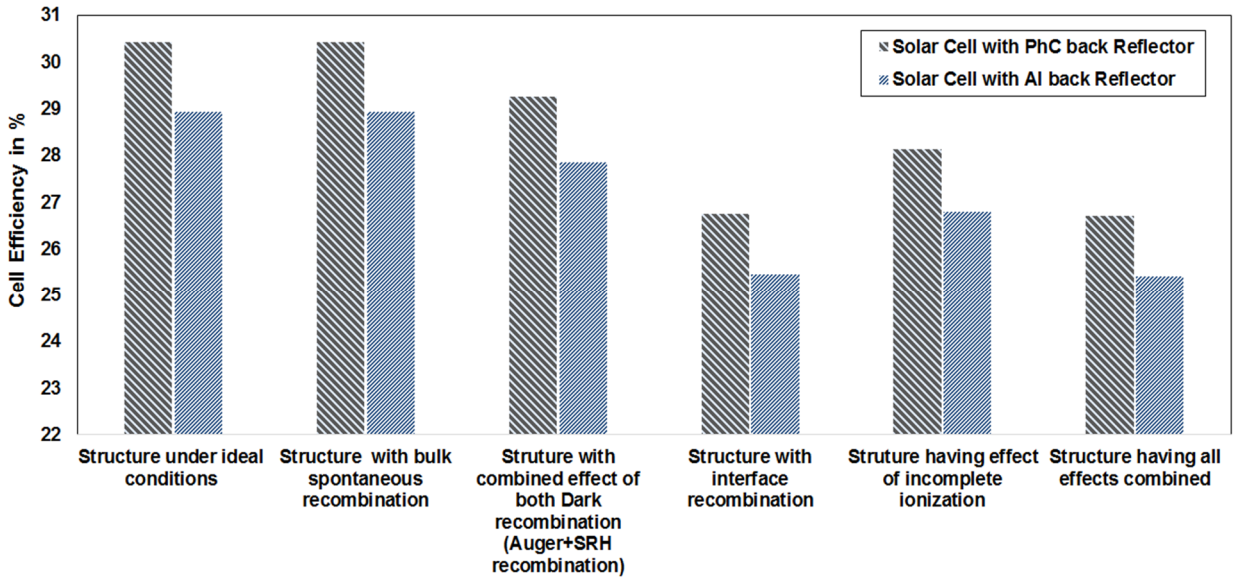

Figure 3.5: Graph showing the performance enhancement with PhC BR as compared to the Al BR

Figure 3.6 and 3.7 show the comparison between Al and PhC BRs absorption and quantum efficiencies, in the ideal case. For the low wavelength photons both the structures perform in the similar manner since in that case BR do not play any major role, as active layer thickness in itself is enough to absorb those high energy photons. But, for the high wavelength photons, BR plays an important part and results clearly indicate the major improvement in performance in case of PhC LTS, which is basically due to the reduction in losses associated with metallic reflector. The results obtained in the simulation studies show high value of the FF as compared to the previous studies, which is basically the reason for efficiency enhancement, clearly indicating the potential of the design.

The proposed structure has also been simulated considering several important practical aspects related to the GaAs solar cell to study in detail about the performance of the proposed cell and to

compare its performance with metallic reflector based cell. First, photon recycling effect has been considered and studied in both our structures (neglecting all other effects). As expected, it has been found that in PhC BR based structure, the radiative recombination effect improves the results. This improvement in efficiency is due to the reduction in losses associated with the Al BR (as mentioned in the previous sections); such as plasmonic effects, highly direction dependent reflectivity, which ultimately hampers the structure's efficiency [52]. PhC BR promises to overcome these problems as demonstrated by the results and thus could really have the potential for efficiency enhancement of TFSC.

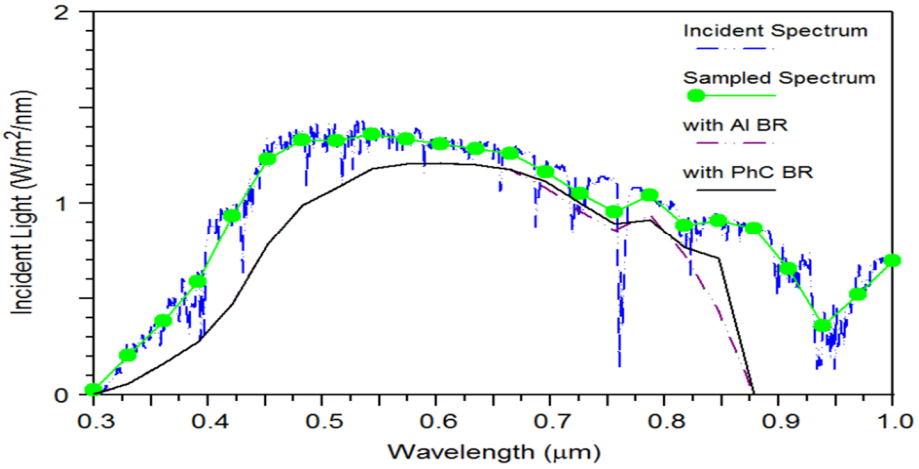

Figure 3.6: Absorption spectrum comparison for the two structures

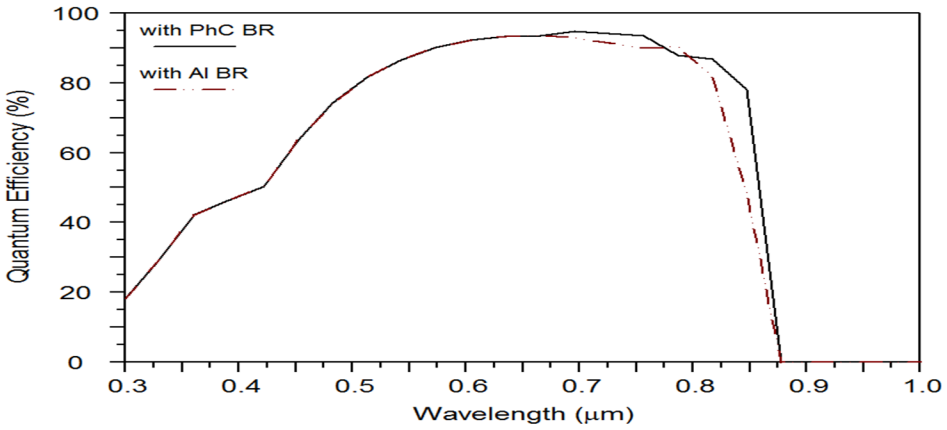

Figure 3.7: Quantum efficiency comparison for the two structures

The analysis of the effects of dark recombination has been taken into account through the Auger and SRH recombination effects, as per Equation (3.3) and (3.4). These results have also indicated the superiority of PhC LTS based design. However, the results for both the structures have shown more resistance to the Auger than SRH recombination. Results listed in Table 3.2 provide

the values for combined effect of dark recombination and are in contention according to the theory. The SRH dark recombination dominance in GaAs solar cells is due to the effect of defect levels that are created unintentionally due to high doping, although there is little contribution from the Auger recombination due to the much smaller intrinsic carrier concentration. SRH recombination dominates in the space charge region as here both the carriers are almost similar and because of high absorption of GaAs devices, carrier densities in the junction region are high [13]. Higher efficiency in case of PhC LTS predict that the proposed structure is more robust to these effects and could provide higher output even in practical conditions.

The comparison analysis of the two structures has also been done for surface and interface recombination. The study has been undertaken as surfaces and interfaces typically contain a large number of recombination centers because of the abrupt termination of the semiconductor crystal, which leaves a large number of electrically active states. The surface and interface recombination velocity in GaAs, however is considerably reduced by the use of AlGaAs double hetero-structures that confined minority carriers in the GaAs quantum well [127]**,** still these phenomena notably affects the final values, as demonstrated by the simulation results and thus it is desirable to study the performance of the device under these effects. In order to justify this effect, the values of 40 m/s for recombination velocities for GaAs and AlGaAs [123, 124]**,** have been considered. The simulation results in this case, too, demonstrate the better performance for PhC BR based cell, indicating that the proposed LTS indeed has a potential to provide better results, surpassing all the major effects that GaAs material cell usually has.

Simulation studies has also been done for the incomplete ionization effect for the two structures. Here too, the results have shown that the effect if present degrades the performance of the device. While neglecting incomplete ionization is usually a fair assumption for devices with relatively low doping ($\sim 10^{16}$ cm^{-3}), it becomes questionable for the devices with higher dopant concentrations [128]. The results have shown that the impact ionization also plays a role in the functioning of the cell, still the PhC LTS based cell performs fairly well than the Al BR. At last, all the effects together have been considered. The results show that, again, the performance of the PhC BR is much better as compared to the Al BR (Figure 3.5).

The BR in TFSC is basically required to have very low absorption. We have used GaAs rods in the SiO_2 background; the reason for this is that the combination provides the much larger band-

gap for the wavelength range of interest as can be seen from Figure 3.2. Also, during fabrication the design would provide better stability, due to same lattice of the GaAs rods and upper layer materials. Although, from the transmission graph it is also clear that there is some absorption in the structure, (as R+T < 1) but keeping above mentioned factors in mind, we choose to go with the proposed design. Thus still a lot of research is required to find the combination for PhC design for solar cells which could provide enough band-gap without much absorption.

Table 3.2: Results of various designed structures considering different effects

Parameters Compared	**Structure under ideal conditions**		**Structure with bulk spontaneous recombination**		**Structure with combined effect of both Auger+SRH recombination**		**Structure with interface recombination**		**Structure having effect of incomplete ionization**		**Structure having the effect of Auger+SRH+ Bulk spontaneous+ Interface recombination**	
	With PhC BR	With Al BR	With PhC BR	With Al BR	With PhC BR	With Al BR	With PhC BR	With Al BR	With PhC BR	With Al BR	With PhC BR	With Al BR
Voc (V)	1.106	1.103	1.106	1.1034	1.072	1.0715	0.9987	0.9981	1.029	1.0285	0.9984	0.9977
Jsc (A/m^2)	-277.15	-264.14	-277.16	-264.18	-277.08	-264.02	-277.03	-264.11	-277.09	-264.09	-276.92	-263.90
Fill Factor (%)	89.33	89.34	89.34	89.32	88.58	88.60	87.05	86.92	88.84	88.83	86.94	86.84
Optimal Bias Voltage (Vm, V)	1.017	1.012	1.017	1.012	0.984	0.983	0.903	0.902	0.944	0.943	0.902	0.900
Optimal Bias Current (Jm, A/m^2)	-273.10	-260.24	-273.11	-260.23	-272.13	-259.33	-271.13	-258.35	-272.79	-259.97	-270.92	-258.15
Collection Effi. (%)	99.719	99.583	99.732	99.583	99.672	99.554	96.866	96.693	99.691	99.561	96.789	96.653
Cell Effi. (%)	30.428	28.929	30.430	28.926	29.252	27.843	26.758	25.454	28.141	26.801	26.701	25.401

The optimized structure has PhC dimensions in nm range, due to which the fabrication of the structure over large area is certainly a challenging task. Also, the lattice mismatch between the

background PhC material and the layers required to be deposited over that also need to be considered. Thus, as discussed in section 2.7, conventional lithography techniques could not be used. Here, one of the viable approach could be to fabricate PhC structure and the above structure over that, separately and then go for wafer bonding. For the fabrication of PhC structure, as proposed in our design, the stack and draw approach, as used for the PhC fiber fabrication, seems more realistic. The procedure relies on manual assembly of glass capillaries and rods into an appropriate preform stack whose structure corresponds approximately to the desired PhC structure. By tuning process parameters such as temperature, preform feed rate etc, the size of the rods and their regularity can be controlled. The GaAs/AlGaAs layer structures could be fabricated using either MBE or MOCVD process, followed by popular epitaxial lift off method [129], [130]. After that suitable wafer bonding technique such as Low Pressure – Plasma Assisted Bonding can be used. Then, the contacts could be deposited and patterned to allow ARC deposition and to reduce reflections through the front surface. This might be the one method by which the fabrication of the proposed structure could be done, although the author feels that lot more research is required to be done in this area.

3.5. Conclusion

The chapter presented optical and electrical numerical and simulation study of the broadband low loss light trapping structure for GaAs thin film solar cell using PhC BR and its comparison with the metallic (Al) BR. The structure has been optimized and it has been found that the PhC as a BR has the realistic potential to improve the performance of the cell. The single PhC structure for both specular and non-specular reflections has been used, thus reduces the design complexities, without compromising with efficiency. The effect of radiative and non-radiative recombination on the structures have also been analyzed, and found that even in non-ideal situations the performance of the PhC design is much better as compared to the Al BRs. Thus, one could conclude that the proposed PhC LTS has a realistic potential to improve the efficiency of GaAs thin film cells, which is basically due to their omni-directional reflectivity, and that too without having the losses of metallic reflector, which made more photons to contribute to the electrical current generation and improving the overall efficiency of the solar cell.

Chapter 4

Photonic Crystal Diffraction Grating Based Efficient Back Light Trapping Structure for GaAs Thin Film Solar Cell

4.1. Introduction

The last chapter deals with the study and analysis of the PhC LTS as a single back reflector (BR), working as a PBG structure. Although, the proposed design has provided the appreciable enhancement in the performance of the GaAs thin film cell, the main issue is the complexity associated in the practical realization of the design through the present facilities available. The chapter, however, provided the possible method for the design and fabrication of the structure but the method is still required to be verified before it could be established. Also, as the PhC LTS there works as a PBG design, the structure is highly fabrication tolerance dependent. The study and analysis of the design set the initial founding stone for the subject and demonstrated that the PhC LTS indeed have the capability to enhance the efficiency of GaAs TFSC. Thus, there is a need to explore and engineer the design which could be more practically feasible, fabrication tolerant and at the same time maintain our hypothesis that PhC LTS would enhance the efficiency of thin film GaAs cells.

This chapter proposes a more practical GaAs TFSC with PhC LTS and demonstrates a design optimization using PhC structure as diffraction grating and Diffraction Bragg Grating (DBR) as low loss dielectric BR to enhance the optical efficiency for cells with very thin GaAs active layers. The design has been optimized for the 500 nm thick active layer in a generalized manner, which is also applicable for other thicknesses of active layers. Incident waves have been

considered to be normal to the 2D PhC LTS and in general out of the plane of periodicity of the structure at an angle to the normal direction of incidence. Thus, the 2D PhCs are basically act as diffracting grating structures due to the periodic arrangement of the holes or rods in a background [58]. The structure, through proper optimization, has demonstrated a significantly enhanced absorption in the high wavelength range, leading to a notable enhancement in the efficiency, as clearly established by the simulation results.

The structure proposed has taken its inheritance from the basic design demonstrated by Feng et al. [61], having various key modifications, like incorporation of 2D PhC structure design, demonstration of the design effectiveness for GaAs thin film material, including others (discussed in next section). The performance evaluation of the two different material combinations for the back LTS (2D PhC + DBR) has also been demonstrated, having either GaAs rods in SiO_2 background with Si/SiO_2 alternate layers for DBR structure or GaAs rods in Indium Tin Oxide (ITO) background with Si/ITO alternate layers for DBR structure. The former structure has higher dielectric contrast and provided better optical performance but less electrical conductivity whereas the latter structure would provide better electrical conductivity but less efficient optical light trapping.

The structure's performance has also been compared with the Lambertian light trapping efficiencies limits for TFSC as suggested by Yablonovitch and Cody [131, 24], who first derived analytical solutions for light path enhancement possible in bulk PV cells considering ideal Lambertian light-scatterers. Lambertian limit will provide the information about how much the light trapping could enhance the efficiency of an active material and thus could provide the maximum value of the efficiency that could be achieved using an ideal loss less light trapping scheme. Thus the comparison of the results of the proposed scheme with that of the Lambertian limits would demonstrates the fact that how much the proposed structure could be close to an ideal one. The study of the structure has shown the proposed structure results, although are short of the Lambertian limits, but still these periodic LTS have the ability to effectively increase the efficiency of the TFSC.

The optimized structures have been simulated for various thicknesses of active layer and in order to demonstrate the effectiveness of the proposed PhC LTS design, the role of each part of the LTS has been studied and analyzed. Analysis of the optimized structures have shown that the

contribution from the diffraction grating is most significant for thinner cells for their efficiency improvement. It has been shown that the impact of ARC, although constant in performance enhancement, increasingly becomes dominant with increasing active layer thickness and ultimately overtakes the total contribution of the back LTS (PhC grating and DBR) for absorption layer thicknesses larger than 750 nm. In all, about 17% and 12% efficiency enhancement can be achieved by using the LTS in 100 and 500 nm thick GaAs solar cells respectively and a relative efficiency improvement as high as 230% for a cell with 100nm active layer thickness has been achieved, with LTS as compared to the reference bare cell without LTS.

4.2. Proposed Cell Structure

A schematic diagram of the presented LTS is shown in Figure 4.1. The sunlight is assumed to be incident from top of the figure perpendicular to the plane of PhC periodicity. The structure consists of an ARC of ITO at the top followed by an $Al_{0.8}Ga_{0.2}As$ window layer of about 20 nm (high band gap material layer used to reduce surface recombination), layer of active GaAs material, and a back reflector that consists of a diffraction grating of 2D PhC (having combination of GaAs rods in either SiO_2 background or ITO background) with a DBR. The DBR stack consists of four pairs of either Si/SiO_2 or Si/ITO with thickness of quarter-wavelength. It is required that the back LTS should have negligible absorption, but the large refractive index contrast is also required among materials in order to fulfill the large reflective requirement, so it is required to have a tradeoff between the two and thus the structure has been designed to have very limited absorption in the wavelength range of interest, having high index contrast. There is a buffer layer between the diffraction grating and the DBR, which is assumed to be either SiO_2 or ITO with thickness equivalent to DBR layer thickness of same material. The wavelength dependent material parameters have been considered for GaAs and AlGaAs [94], for Si and SiO_2 [132] and for ITO [126]. The rest of the structural parameters will be optimized in the following section. One interesting feature of the structure is that due to the existence of back trapping assembly instead of back contacts, front contacts might be a better option.

The proposed design, inherited from [60], has several key improvements. The study is based upon the altogether different active material (GaAs), and modified as per the requirement of the active layer (like using the AlGaAs window layer) to take the structure as close to practical structure as possible. The hexagonal PhC lattice structure has been used as it provides better

diffraction than square lattice [58]. The study of the proposed design is basically concentrated on the thin films (from 100 nm to 1500 nm) of active layer as against the thick films in [60]. Also, in [60] the authors only provided the absorption values in the active layer, but did not quote them in terms of efficiency, without considering the shadow effects or the collection efficiency losses into account, whereas the present work considered all these real world effects into account, to take the studies as close to practical values as possible.

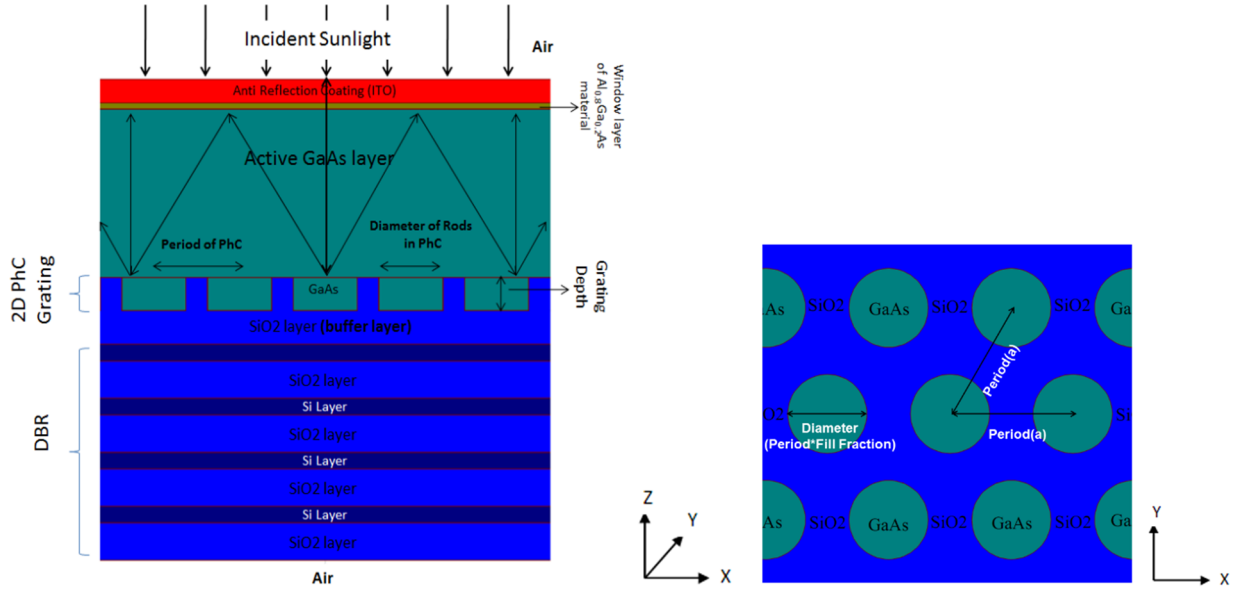

(a) (b)

Figure 4.1: (a) Schematic Diagram of the thin film GaAs solar cell using light trapping Structure; (b) Designed 2D PhCs structure.

4.3. Cell Efficiency Calculation Methodology

The 3D simulation and structural analysis of the proposed structure has been done through the FDTD method [133] (kindly refer to section 2.6 for detailed discussion about FDTD). Periodic Boundary Conditions (PBC) have been used for both x and y PhC periodic directions, taking into account only single period of the structure whereas PML boundary conditions have been considered for z dimension, considering layer of air at the top and bottom of the device. The various important parameters used during the simulation of the structure includes mesh size (or grid size) which is taken as 25 nm in x and y direction (direction of PhC structure periodicity) and 1 nm in z direction, time step size is taken as 1.875×10^{-3} fs, PML width is taken as 500 nm.

As the motive of the study is to demonstrate the optical effect of PhC LTS and mechanism behind the light trapping in these structures rather than transport properties of the cell, the

simulation neglected the details of the charge carrier collection and internal quantum efficiency has been set equal to one, i.e. we have considered that each absorbed photon contributes to the generation of electron-hole pair. Rather, we have tried to incorporate the electrical losses by incorporating the loss in collection efficiency and through shadowing effects.

To calculate the solar cell efficiency, the total optical absorption spectrum, $A(\lambda)$ of the entire device has been calculated, which is the sum of the absorption spectra within each layer, $A_i(\lambda)$ as $A(\lambda) = \sum_i A_i(\lambda)$ Absorption in the active GaAs layer has only been considered as useful absorption and taken into effect for efficiency calculations. Given these spectra, the number of absorbed photons at a wavelength λ within each layer is therefore given as:

$$n_i(\lambda) = \frac{S(\lambda)A_i(\lambda)}{E(\lambda)} = \frac{\lambda}{hc} S(\lambda)A_i(\lambda) \tag{4.1}$$

where, $S(\lambda)$ is a specific incident spectrum, (which is AM1.5G here) and $E(\lambda)$ is the energy of the incident photon, equivalent to hc/λ, where h is Planck's constant and c is the velocity of light in free space. The combined number of electron-hole pairs generated at a wavelength λ and collected by the electrodes is given as [13]:

$$n_{e-h}(\lambda) = \sum_i \eta_s \eta_i n_i(\lambda) = \frac{\lambda}{hc} \sum_i \eta_s \eta_i S(\lambda) A_i(\lambda) \tag{4.2}$$

where, η_s represents the shadowing effects and η_i is included to take collection efficiencies into account. Here, we have considered 90% collection efficiencies based on the measurements from previous GaAs solar cells results as per [34], whereas we have considered 6.6% shadowing effect. Thus, the total number of electron-hole pairs collected by the electrodes is therefore:

$$N_{e-h} = \int_\lambda n_{e-h}(\lambda) d\lambda \tag{4.3}$$

The above integral is taken over from 300 to 1000 nm computed at an interval of 1 nm. Lower value of the wavelength has been decided as the photon flux below this value is small in the standard AM1.5 solar spectrum [48], whereas the upper limit has been decided considering the band gap of the GaAs material at room temperature, i.e. about 1.432 eV [134]. Above the band gap, absorption is considered to be zero. However, limiting of the wavelength integration range affect the final results as compared to the full AM1.5 solar spectrum, which has slightly more number of photons in the range, but at the same time considerably reduces the computational time when optimizing the structures, without much affecting the efficiency.

Using the above equation, J_{sc} could be calculated as $J_{sc} = qN_{e\text{-}h}$ (in A/m^2), where q represents the electronic charge and V_{oc} is obtained from $V_{oc} = (kT/q)ln(J_{sc}/J_{s0} + 1)$ (in V), where k is the Boltzmann's constant, T = 300 K, and J_{s0} is the reverse bias saturation current. Using these calculated values of J_{sc} and V_{oc}, the solar cell efficiency, η is given as:

$$\eta = \frac{\Gamma_f V_{oc} J_{sc}}{P_{in}} \tag{4.4}$$

where Γ_f is the fill factor of the cell, calculated as $\Gamma_f = V_m.J_m/V_{oc}.J_{sc}$ and $P_{in} = \int S(\lambda)d\lambda$ (W/m^2), represents the total incident power, whereas V_m and J_m represent the voltage and current density at the maximum power point.

The chapter also deals with the comparison of the proposed structure results with that of the Lambertian limits for GaAs solar cells. These limits for light trapping were first derived considering the three main assumptions [131, 24], as follows:

1. The device has Lambertian scattering structure either at the front or at the back.
2. The active material is considered to have weak absorption for solar spectrum range, both for the single pass as well as for enhanced efficiency case. This condition is given by,

   $$4n^2\alpha t << 1 \tag{4.5}$$

   where n is the refractive index of the active material, α is the absorption coefficient and t is the thickness of the active layer.
3. The active layer thickness, t, is much larger than the wavelength inside it, λ/n.

Based on these assumptions, it has become possible to calculate the absorption is terms of $\alpha(\lambda)t_{eff}$, where t_{eff} is the effective path length for the photon inside the active layer. Now, as per Yablonovitch hypothesis [24], the maximum enhancement that could be achieved in case of planar cell surrounded by an isotropic medium is given as $4n^2/sin^2\gamma$ where $sin\gamma$ is 1 for the isotropic case [24]. Thus, here the absorption in Lambertian case, A_{LLY} can be calculated as:

$$A_{LLY}(\lambda) = 1 - e^{-4n^2\alpha(\lambda)t} \tag{4.6}$$

The Lambertian limits for GaAs solar cell have been calculated for different active layer thicknesses under ideal conditions, considering 100% collection efficiency.

4.4. Structural Optimization

In this section, a comprehensive study of the proposed design and its usefulness for efficiency enhancement of GaAs TFSC application has been presented. Step by step optimization of each layer has been done. GaAs active layer of 500 nm thickness has been considered having 20 nm $Al_{0.8}Ga_{0.2}As$ window layer at the top of active layer, having higher band gap than GaAs layer in order to reduce surface recombination. The optimization process used is inherited from the work presented in the work of [61], [86] etc. The same procedure could have also been applicable to other active layer thicknesses. The various elements of the proposed structure have been optimized as shown in the succeeding section.

4.4.1. Anti-Reflection Coating (ARC)

In the proposed design, just a single planar layer ARC has been taken, especially for simplicity in design (both for simulation and proposed fabrication flow), and to be more focussed towards the role of PhC back LTS, although it can easily be extended to multilayer ARC cases [135]. It is evident that the single-layer ARC structure has zero reflection at its center wavelength. Therefore, choosing an appropriate center wavelength λ_c will be crucial to obtain relatively low reflectivity in a certain wavelength range of interest and to achieve the maximum cell efficiency. On the basis of this, the thickness of the ARC equal to quarter of central wavelength, given as $t_{ARC} = \lambda_c/4n_1$, where n_1 is the Refractive Index (RI) of ARC material (for more details kindly refer to section 3.3) [13]. Now considering RI of air and layer beneath ARC ($Al_{0.8}Ga_{0.2}As$ in our case), ITO has been taken as ARC, which also acts as Transparent Conducting Oxide (TCO). The optimization results are shown in Figure 4.2.

Initially before the start of optimization study, thickness of ARC has been set to the value of 65 nm (corresponds to central wavelength at 500 nm), the grating period of the PhC structure taken to be 600 nm and the grating depth set to be 100 nm. The center wavelength for the DBR is considered as 750 nm. Later, we will show through results that these parameters are very close to their optimal values. From the simulation, it is found that the structure would provide optimal efficiency for 70 nm ARC thickness, which corresponds to central wavelength value of 526 nm as per material parameters used for ITO [126]. It proves to be a good validation for our simulations. It has also been shown that as compared to the structure without ARC, more than 30% relative increase of cell efficiency can be achieved by using this optimized ARC.

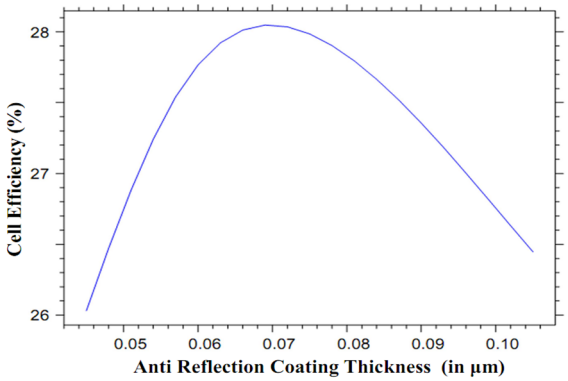

Figure 4.2: Anti-Reflection coating thickness Vs. Cell Efficiency graph

4.4.2. Photonic Crystal (PhC) Diffraction Grating

The diffraction grating plays a very vital role in the LTS, by diffracting the unabsorbed photons at oblique angles based on different diffraction orders. The work considered a 2D PhCs having hexagonal lattice as shown in Figure 4.1(b), having GaAs rods in SiO_2 background. The hexagonal lattice arrangement is used as this would provide better performance than square lattice arrangement [58]. The combination of the materials for PhC LTS is so chosen that the RI contrast of the two materials is large enough to provide sufficient diffraction of light within the absorption layer. For optimization of the diffraction grating performance, one has to optimize its period or lattice constant, radius of rods and grating depth. Radius of the rods are optimized in terms of Fill Fraction (*ff*) for PhC LTS, as $R/a = ff/2$. From the structure, it is obvious that the diffraction grating plays a very important part in the LTS as DBR in itself could enhance the path length by a factor of 2 at the maximum, due to lack of light bending mechanism in DBR, whereas diffraction grating could bend the light to the angles more than the critical angle at GaAs-ARC-air interface, and thus could trap them efficiently.

The detailed analysis of the PhCs diffraction grating has been done as per the description provided in [60]. The optimization results for PhC period is shown in Figure 4.3. As described in the previous chapter, for sufficient diffraction from the PhC LTS, it is necessary for its period to be larger than the wavelength of light in the active layer, i.e. $a > \lambda/n(\lambda)$. This condition is satisfied for $a > 250$ nm, as per material parameters used. As per [60], for a particular active layer thickness in a solar cell structure using PhC grating, there are several diffraction resonances from the diffraction grating whose peaks overlap and leads to overall absorption enhancement as also discussed in chapter 3. The diffracted resonant mode wavelength is given through Equation (3.13). In our case, it is required that these diffraction resonances should exhibit peaks to allow

absorption of wavelengths near the band edge. The solution of Equation (3.13) suggest that the values of period larger than ~ 250 nm is required for diffraction resonances to occur in our case. Simulation results have shown these resonances are most effective for *a* equal to 650 nm.

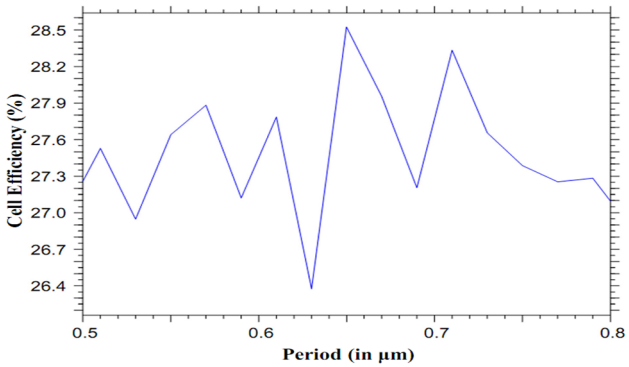

Figure 4.3: Period Vs. Cell Efficiency graph

The optimization study of the radius of the PhC structure rods has been taken next, keeping all other parameters constant. The radius of rods in PhC LTS should assume a value that maximizes the diffraction. Maximum diffraction is expected from the PhC when the Fourier components of the dielectric function of the 2D PhC is a maximum. The Fourier component of an array of rods in dielectric background is known to be [58]:

$$\varepsilon(G) = f(\varepsilon_{GaAs} - \varepsilon_{SiO_2})\frac{2J_1(GR)}{GR} \tag{4.7}$$

where $f = \pi R^2/((\quad)*a^2)$ is the fill ratio for the hexagonal lattice structure. Using effective dielectric constant values of 3.45 and 2.25 for GaAs and SiO_2 respectively, the first Fourier component (G_1) is maximized for R/a = 0.35. Thus initially the *ff* (= $2R/a$) value has been set to the value of 0.7. *ff* values were then optimized and found that optimal value found at 0.65 as shown in Figure 4.4, which is very near to the calculated value, thus validating the simulations.

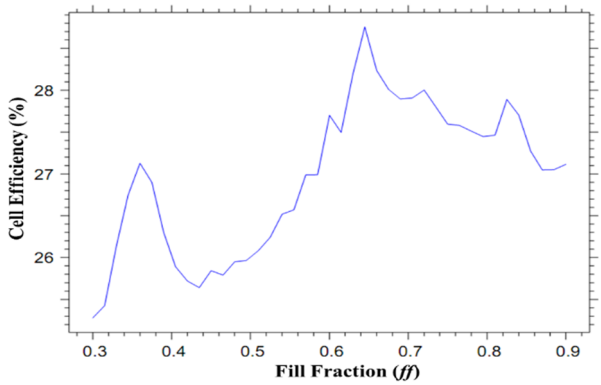

Figure 4.4: Fill Fraction (where Fill Fraction*Period = Diameter of the rod) Vs. Cell Efficiency graph

The optimization study of the grating depth has been taken up next. The depth of the grating should be such that the specularly reflected beam from PhC should be minimized. The sum of the reflection coefficient from GaAs and ITO should become zero for the specific value of grating depth [60]. Using this initial approximation, the value of grating depth has been set to the value of about 100 nm. Then, the value of grating depth was optimized, keeping all other parameters constant. The simulation results provide the optimum values of thickness of grating depth as 97.5 nm as shown in Figure 4.5, which is very close to the calculated values.

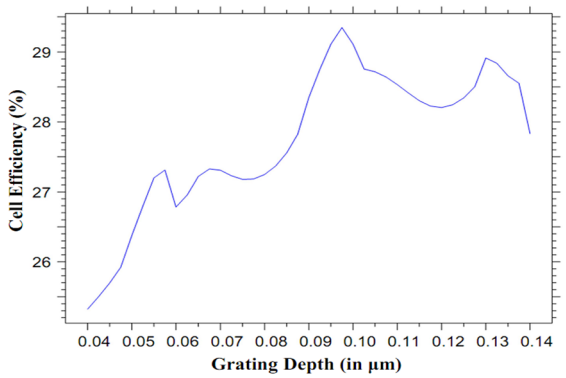

Figure 4.5: Grating depth Vs. Cell Efficiency graph

Although there is another peak is observed near the 130 nm but there the efficiency starts to drop quickly, and thus is expected to be fabrication sensitive, so the 97.5 nm should be a better choice for grating depth.

4.4.3. Distributed Bragg Reflector (DBR)

DBR also plays an important part in the LTS as it provides the baseline reflections by reflecting the light transmitted through the diffraction grating [61], however it could by itself only enhance the optical path length up to twice at the most [61]. The designed DBR, consisting of 8 alternating Si and SiO_2 layers, followed by 2D PhC LTS represents an economical method for making an omni-directional reflector that is much simpler than fabrication of 3D PhCs. Although more number of layer can theoretically provide better baseline reflections, this will also increase the overall thickness of the device, which we want to keep as thin as possible. Therefore we stick ourselves to only 4 pairs of above mentioned materials to study the effect of combination of PhC LTS with DBR at the back.

The thickness of the DBR layers should also be equal to the quarter wavelength of the central wavelength in the material, i.e. $\lambda_c/(4n)$, where n is the refractive index of the respective material.

The thickness of the DBR layers is taken as quarter wavelength thick in order to provide maximum specular reflections through the DBR for those photons which are not diffracted by the PhC grating [13], [61]. The combination of the two materials is so chosen to provide wide band reflections because of high refractive index contrast and low absorption. In other words, DBR is nothing but a Bragg stack or 1D PhC structure. Although GaAs has a high refractive index, it also has considerable absorption as compared to Si, which is not desirable for the DBR. The optimization results have been demonstrated in Figure 4.6 and Figure 4.7 for Si and SiO_2 thickness respectively, provided Si thickness of 50 nm and SiO_2 thickness of 122.5 nm, corresponding to the central wavelength at about 770 nm, as per material parameters used.

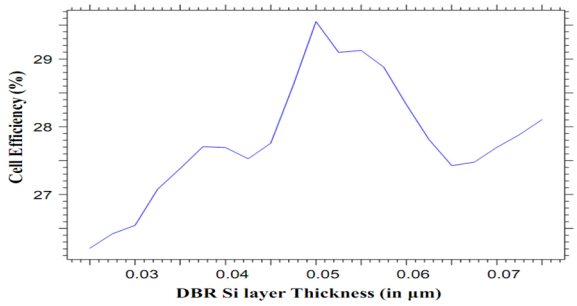

Figure 4.6: Grating depth Vs. Cell Efficiency graph

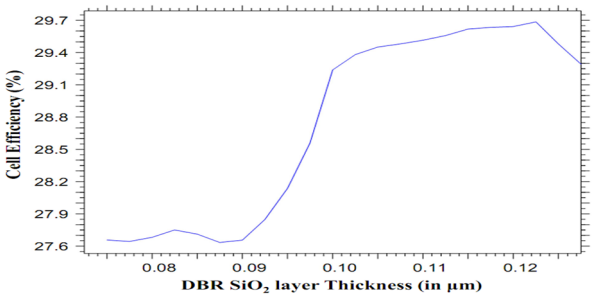

Figure 4.7: DBR SiO2 layer thickness Vs. Cell Efficiency graph

This completes the design optimization for 500 nm thick GaAs solar cell having ITO as ARC, 2D PhC as diffraction grating and DBR for baseline reflections, both together forming a back LTS. The optimized parameters are summarized in Table 4.1, and 3D figure of the optimized structure is shown in Figure 4.8.

Table 4.1: Summary of the optimized parameters for 500nm thick GaAs active layer

S.No.	Parameters	Values
1.	Thickness of Anti-Reflection Coating (ITO)	70 nm
2.	Period	650 nm
3.	Fill factor	0.645
4.	Grating Depth	97.5 nm
5.	Thickness of DBR Si layer	50 nm
6.	Thickness of DBR SiO_2 layer	122.5 nm

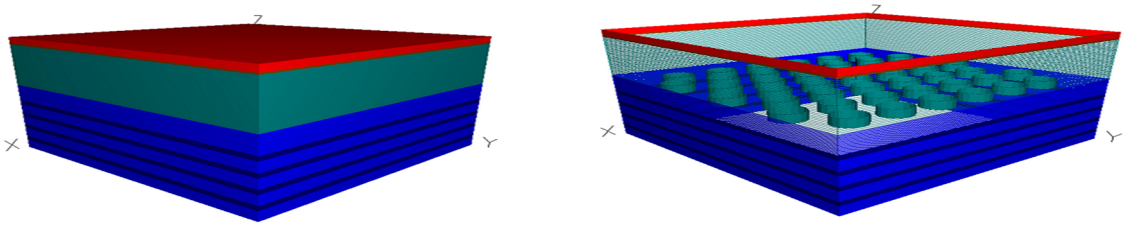

(a) (b)

Figure 4.8: Schematic diagram of the proposed thin film GaAs based solar cell having PhC based diffraction grating and Distributed back reflector

4.5. Performance Analysis of the Proposed Configuration

The section demonstrates the following issues, which include the absorption enhancement ratio for the proposed structure compared to the reference cell consisting of ARC and DBR, the proposed LTS based GaAs cell performance variation with incident light and the fabrication tolerance that the proposed structure could provide, during proposed device fabrication.

4.5.1. Analysis with Incident Angle Variation

Incident light angle is the angle described by the incident light with reference to the normal direction of the surface of the cell in the plane of the paper [61]. Figure 4.9 shows incident angle vs. the cell efficiency graph for 500 nm active layer GaAs cell. As expected, as the incident angle of sunlight increases, the efficiency decreases. It is interesting to note that with a small titled incident angle, the efficiency drops a little and then again increases. This little increase can be attributed to two reasons: One, the zeroth order reflections path length might be slightly increased due to the tilted incidence; other, the tilted incidence results in break of symmetry of the first-order reflections, creating a situation similar to that in a blazed grating [61, 135].

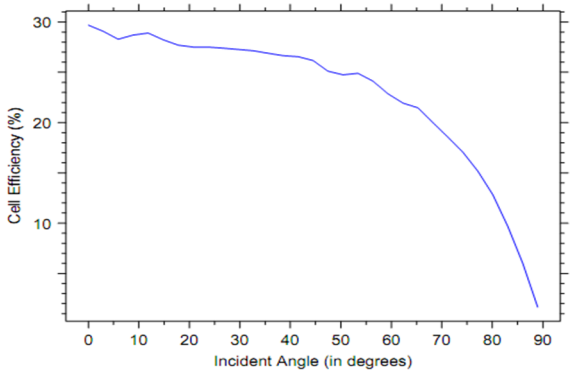

Figure 4.9: Incident angle Vs. Cell Efficiency graph for 500 nm active layer cell.

Nevertheless, reflections from the front surface quickly led these effects to wash out. It can be noted from the figure that the structure is able to perform almost equivalent to the normal

incidence up to about 60^{o} or so, retaining nearly 80% of the normal incidence efficiency and thus shows significant performance enhancement as compared to metallic and other LTS.

4.5.2. Absorption Enhancement in the Structure

The absorption enhancement ratio is found out by dividing the absorption in the PhC diffraction grating based optimized solar cell over the reference cell without the photonic crystal, having ARC and DBR only. The result has been shown in Figure 4.10 for 500 nm active layer GaAs cell, which indicates that PhC diffraction grating enhances the performance of the solar cell mainly near its band edge, where improvement in path length has the paramount requirement, and hence increases the efficiency. The PhC generates modes of diffraction at these wavelengths, effectively increasing the path length of incident photons.

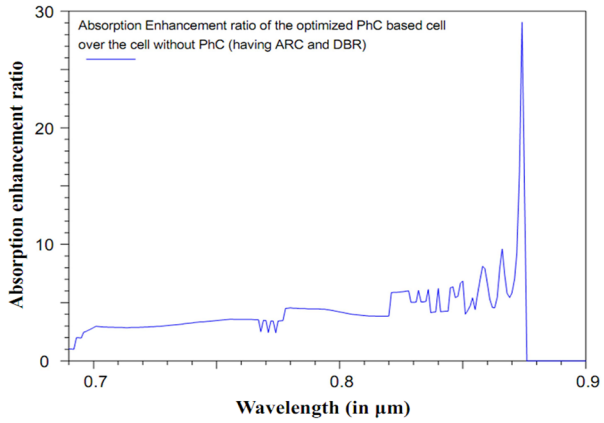

Figure 4.10: Absorption enhancement ratio for the 2DPhC based solar cell as compared to the reference cell having ARC and DBR only for 500 nm active layer cell.

4.5.3. Analysis for Fabrication Tolerances

It is also necessary to check how the efficiency output of the device varies with the variation in the optimal parameters for the proposed structure, as the final parameters after fabrication may be slightly different from the desired values [136]. In order to test the structure, for this very phenomenon, a two dimensional contour plot for the efficiency has been derived around the optimal set of parameters for 500nm thin GaAs active layer, obtained by varying the value of *a* and *ff* for 2D PhC structure, as shown in Figure 4.11. From the figure, it is clear that the efficiency for the proposed structure reduced only by 1% even for the 10% variations in the lattice structure. Thus, one can interpret that the proposed structure exhibits good tolerance with regards to a variation of the parameters of the proposed PhC structure and thus provide good fabrication tolerances and thus could be realized using available fabrication techniques.

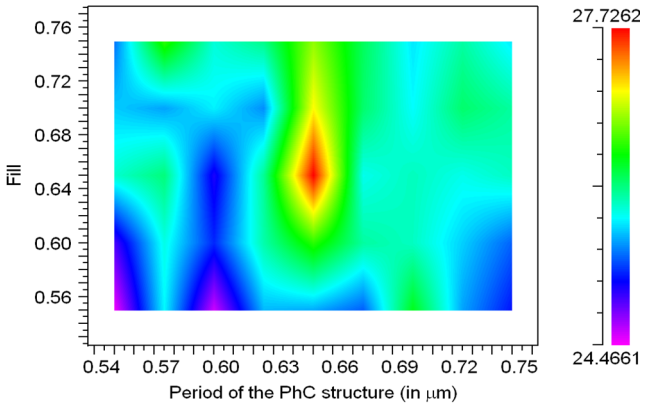

Figure 4.11: Contour Map for efficiency having Period of the PhC structure on x-axis and fill factor of the PhC structure on the y- axis for 500 nm GaAs active layer, to check fabrication tolerances for the structure

Accurate fabrication of such a nm period PhC structures, as also used here, on large areas is certainly difficult to achieve through conventional photolithography. Thus usually either holographic or e-beam, or other similar lithography technique is preferred to design such structures precisely. A periodic intensity pattern can be produced by interference between two or more coherent light beams in holographic lithography, whereas in e-beam lithography (for details kindly refer to section 2.7), high intensity electron beams are used to create patterns. These modern day lithography techniques, indeed make it possible to practically achieve high symmetry structures having period even smaller than 100nm over large area. The pattern could be transferred to the small area and a sample could be synthesized and the same process could be repeated over a large area to get area patterned cells.

4.6. Alternate PhC and DBR Structure for Back Light Trapping

In the earlier sections, it has been shown that the optimized back light structure that includes 2D PhC diffraction grating and DBR consisting of combinations of GaAs rods in SiO_2 background and alternate layers of Si and SiO_2, respectively. The material combinations are so chosen, so that both the diffraction grating and DBR should be of dielectric materials having high index contrast together with low absorption, free from all the problems arising due to metal-dielectric interface [53], and to provide economical method for 2D PhC and DBR fabrication. But, for such a structure, collection of charge carriers could be a problem. Thus, for such a back LTS, a thin ITO layer on top of the DBR, followed by interdigitated contacts to collect electrons on the side is necessary, which results in a complex device structure. In order to overcome this problem, SiO_2 could be replaced by another oxide, ITO [60]. Although ITO offers low dielectric contrast

and has higher absorption than SiO_2, such a structure would be more conductive and can be used directly as back contact, an important advantage for solar cells. The 2D diffraction grating structure for both the material combinations has been shown in Figure 4.12.

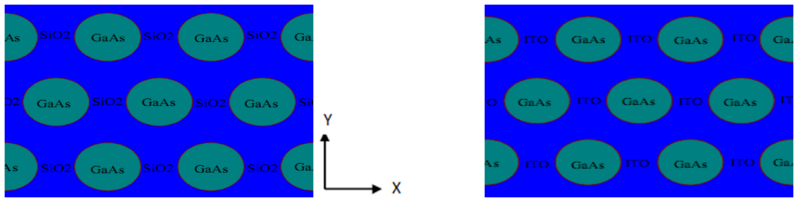

(a) (b)

Figure 4.12: Schematic Diagram of 2D hexagonal lattice PhC diffraction grating (a) having GaAs rods in SiO_2 background; (b) having GaAs rods in ITO background

In order to calculate the performance of the two diffraction grating structures, two separate PhC structures have been designed, using optimized values as calculated above, considering GaAs substrate below the PhC structure and buffer layer. The absorption is calculated as (1-R-T), considering R+T+A=1. The results for the two structures are shown in Figure 4.13 (a) and (b) respectively. From the figures, it could easily be observed that the 2D PhC diffraction grating having GaAs rods in SiO_2 has better optical performance than the ITO based structure, which is mainly due to the better index contrast and less absorption in the SiO_2 structure. It has also be observed that in the SiO_2 based structure the absorption becomes zero at the band edge of GaAs, whereas in ITO based structure even after band edge of GaAs, the structure is still absorbing which clearly indicates the absorption in the structure due to ITO layer.

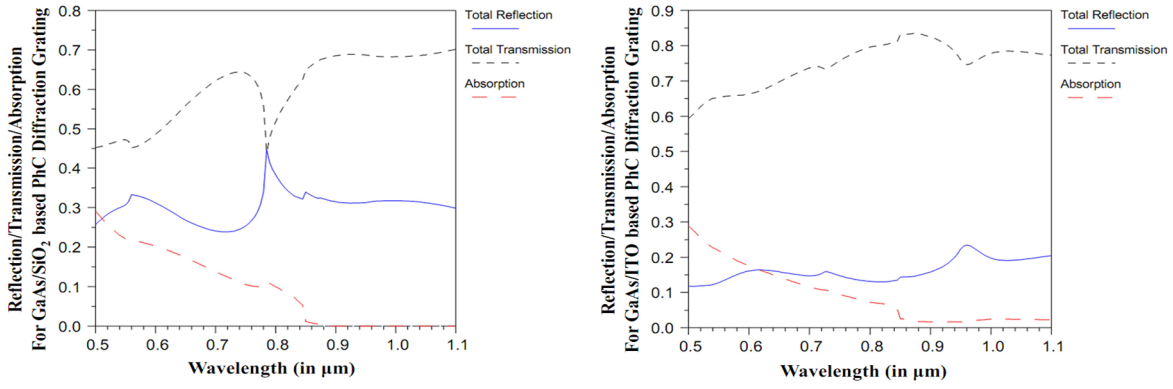

(a) (b)

Figure 4.13: Absorption, Transmission and Reflection Graph for the 2D PhC diffraction grating having (a) GaAs rods in SiO_2 background, (b) GaAs rods in ITO background.

Next, the same process has been repeated to analyze the performance of two material combination structures for DBR consisting of alternate layers of Si/SiO_2 and Si/ITO respectively.

Again, the two separate DBR structures have been designed, and analysis has been done, distinctly. The results have been shown in Figure 4.14. Again the optical performance of the SiO_2 structure is better than the ITO based structure, due to the better index contrast for the SiO_2-Si alternate layers, providing large stop band in the wavelength range of interest.

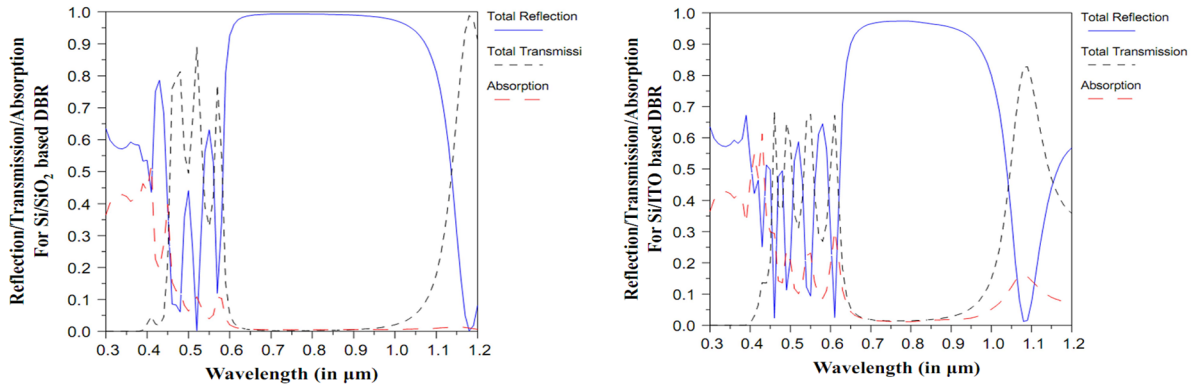

(a) (b)

Figure 4.14: Absorption, Transmission and Reflection Graph for the 1D PhC back reflector or DBR having (a) alternate Si and SiO_2 layers, (b) alternate Si and ITO layers.

Both the results shown above indicate that SiO_2 based structures outperforms the ITO based structures on optical performance grounds, but still ITO based structure can provide better electrical conductivity than the SiO_2 based structures and could be used directly as back contacts, and thus provide ease of fabrication. The author has also designed and simulated the entire solar cell structure for ITO based elements, and found that for 500 nm thick active region about 26% efficiency has been achieved with proposed LTS as against the 27.5% efficiency that has been achieved in case of SiO_2 based structures and thus could be handy for the practical LTS based devices from fabrication point of view, without much affecting the efficiency.

4.7. Performance Analysis of the Proposed Configuration with the Thickness Variation of the Absorption Layer

The section deals with the establishment and demonstration of the fact that the PhC LTS affects the efficiency of the thinner cells more as compared to the thicker cells. In Table 4.2, summary of the absolute achievable cell efficiency for different active GaAs layer thicknesses has been listed, including the Lambertian limit efficiencies. It has been shown that the maximum achievable cell efficiency for the proposed structure having 100 and 500 nm thick active layer cells is about 24.9% and 27.7%, respectively, which are more than thrice for 100 nm cell and

almost reaching twice for 500 nm thick cell. The results listed in Table 4.2, clearly show that the effect of light trapping is more prominent for thinner cells as compared to the cells having thicker active layers.

Table 4.2: Cell efficiency calculations summary for the optimal structures having different active layer thicknesses

Active layer thickness (nm)	Cell Efficiency (%) without ARC and without Back LTS (η_{bare})	Cell Efficiency (%) with ARC and without Back LTS (η_{ARC})	Cell Efficiency (%) with ARC and DBR without PhC LTS (η_{DBR})	Cell Efficiency (%) with ARC and with complete Back LTS (η_{LTS})	Lambertian Limit efficiency (%) (η_{LLY})
100	7.52881	9.82392	13.112	24.9716	26.011
250	12.4267	16.4622	19.7768	25.8822	27.7568
500	15.5072	20.5386	22.8439	27.7262	28.45
750	16.9282	22.3135	23.8721	27.9201	29.5096
1000	17.6352	23.2647	24.4906	28.4824	29.766
1500	18.4429	24.2248	24.8738	28.9031	30.384

Now, to distinguish the roles of ARC and back LTS (PhC grating plus DBR), the cell thickness vs. cell efficiency graph has been plotted for three cases: 1) for bare case, i.e. cell without light-trapping structure, 2) with AR coating only, and 3) with AR coating and back LTS together, as shown in Figure 4.15. The figure indicates that for the cells having active layer thickness less than 1000 nm, back LTS plays very effective role and its influence percentage is more than that of ARC. Although, when the active layer thickness exceeds 1000 nm, the back LTS contribution decreases quickly, whereas the ARC contribution percentage remains more or less constant.

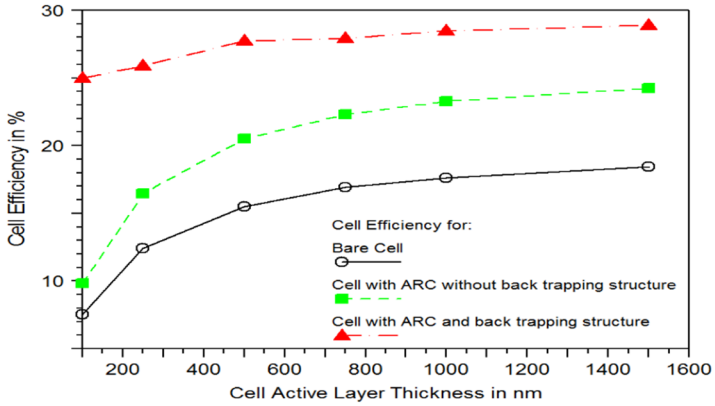

Figure 4.15: Total cell efficiency versus the active layer thickness graph for various GaAs cell configuration

The reason for this is that, for the cell having thinner active layer thickness (like for 100 nm thin active layer), the back LTS enhances absorption for the wide wavelength range from 480 nm till the band edge of GaAs, in which the majority of solar spectrum is focused [137, 62].

Nevertheless, for the thicker active layer structure, smaller efficiency enhancement is achieved as less amount of photons having wavelength within the band gap of GaAs reached the back LTS, as with the increase in the active layer thickness most of the incident photons get absorbed in single pass due to the higher absorption coefficient and thickness product and thus the need and effect of LTS ceases [63, 59]. Also, the enhancement occurs for thicker cells in the region which overlapped with the one of the major dip regions of solar spectrum at around 825–875 nm [61].

It can also be observed that, although the effect of back LTS structure ceases for the thicker cells but the effect of ARC in the efficiency improvement remains almost constant, because the ARC coating basically performs the task of reduction in reflections of the incident light from the top and to provide the efficient coupling of the incident spectrum to the inner absorption layer, and thus the effect of ARC remains valid throughout the spectrum range. It is noteworthy that, although this fact is valid for the case of planar ARC, but the effect might become thickness dependent for other complex designs of ARC as shown in [44, 62].

In order to find the effect of each element of LTS, the cell efficiencies for the structures having different active layer thicknesses have been calculated for various light trapping combinations including for bare cell without LTS, ARC only without back LTS, having ARC with DBR structure, ARC with PhC Grating and DBR structure and Lambertian limit efficiencies. Figure 4.16 shows the effect of each element in the efficiency enhancement for the GaAs cell for six different cell thicknesses. From the figure it is clear that the contribution from the grating is more than the DBR for all thickness cases, especially for thinner cells, thus proves that the DBR alone can’t enhance the efficiency for the proposed cells to this much level. From the figure, it can also be observed that for the thinner cells, the back structure can enhance absolute efficiency up to 15% (in case of 100 nm cell), whereas this value becomes only 3.5% for thicker cell (in case of 1500 nm cell). The figure also demonstrates the fact that how so ever the proposed structure has increased the efficiency of the GaAs thin film cells, but still these efficiencies are under the Lambertian Limit values. Although, from this considerable enhancement one can easily predict that these PhC based LTS, if properly designed and optimized, has the potential to take the TFSC performance towards the Lambertian limits.

Table 4.3 summarizes the detailed contribution from each part of the LTS in terms of percentage contribution. Methodology of calculation has been derived using the previous studies conducted

by Feng et al. in [61]. Total efficiency increase provided in Table 4.3 has been calculated taking the efficiency for the structure having back PhC LTS with DBR assisted by ARC at top, η_{LTS} given in column 4 of Table 4.2 and then that efficiency is compared with the bare cell efficiency, η_{bare} provided in column 2 of Table 4.2. Mathematically, it has been derived as:

$$\text{Total Efficiency Increase (in \%)} = \frac{(\eta_{LTS} - \eta_{bare})}{\eta_{bare}} \times 100\% \tag{4.8}$$

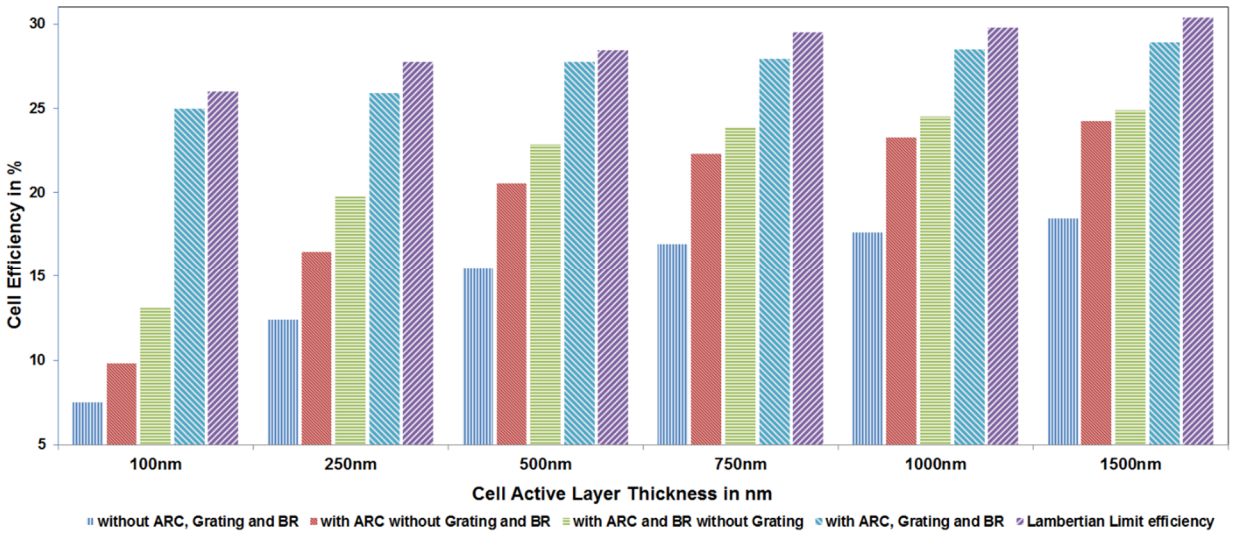

Figure 4.16: Graphical representation of impact of each element of the LTS in cell efficiency

Now, the third column in Table 4.3, provides the % efficiency enhancement contribution due to ARC alone, excluding back LTS. Here we have taken the efficiency calculations for the structure having only ARC at top, without back LTS as shown in column 3 of Table 4.2. Then this efficiency for structure having only ARC, η_{ARC} is compared with the bare cell efficiency, η_{bare}. Mathematically, it has been derived as:

$$\text{Efficiency Contribution by ARC (in \%)} = \frac{(\eta_{ARC} - \eta_{bare})}{\eta_{bare}} \times 100\% \tag{4.9}$$

Next, the fourth column in Table 4.3 provides the information about the contribution of the back LTS in the efficiency enhancement. In order to calculate the contribution of the back trapping structure, we have taken the value of η_{LTS} and deducted the value of η_{ARC} from it and then compared the results with η_{bare}. Mathematically, it has been derived as:

$$\text{Efficiency Contribution by Back Trapping Structure (\%)} = \frac{(\eta_{LTS} - \eta_{ARC})}{\eta_{bare}} \times 100\% \tag{4.10}$$

The fifth and sixth columns of Table 4.3 demonstrate the effects of DBR and 2D PhC structures alone, respectively in the proposed structure efficiency enhancement. To find these structures efficiency values, we have initially found the efficiency of the structure having ARC at the top and DBR at the back without PhC LTS, η_{DBR}. Then, from the resultant efficiency, we have reduced the efficiency η_{ARC} and then compared the result with η_{bare}. We have also added another column in Table 4.2, which will provide this value of η_{DBR} at various active layer thicknesses. Mathematically, it has been derived as:

$$\text{Efficiency Contribution by DBR in back LTS (\%)} = \frac{(\eta_{DBR} - \eta_{ARC})}{\eta_{bare}} \times 100\% \qquad (4.11)$$

Next, in order to calculate the effectiveness of the PhC LTS in the back trapping scheme, we have taken efficiency of the final proposed structure, η_{LTS}, achieved after introducing PhC structure in the above described structure having only DBR as back light reflector and deduct the value of η_{ARC} from the final efficiency value and then compared the result with that of the η_{bare}. Mathematically, it has been derived as:

$$\text{Efficiency Contribution by PhC structure in back LTS (\%)} = \frac{(\eta_{LTS} - \eta_{DBR})}{\eta_{bare}} \times 100\% \qquad (4.12)$$

Table 4.3: Contribution in efficiency from each part of the LTS for various active layer thicknesses

Active layer thickness (nm)	Total efficiency increase (%)	% Efficiency Contribution by ARC	% Efficiency Contribution by Back LTS	% Efficiency Contribution by DBR	% Efficiency Contribution by Grating
100	231.68	30.48	201.20	43.67	157.52
250	108.28	32.47	75.80	26.67	49.13
500	78.80	32.45	46.35	14.87	31.48
750	64.93	31.81	33.12	9.21	23.91
1000	61.51	31.92	29.59	6.95	22.64
1500	56.72	31.35	25.37	3.52	21.85

Using the above calculations, it has been predicted that the efficiency of an optimal LTS for 100 nm thick active layer cell, have been enhanced to 230%, including contribution of 30% from ARC, 43% from DBR and more than 150% from PhC diffraction grating, whereas for 1000 nm cell this enhancement reduced to 61%, which includes contribution of almost 32% from ARC and only about 29% from back LTS, as can be seen from Table 4.3. It could also be observed that the decrease in the efficiency enhancement for the thicker cells is mainly due to the decrease

in the contribution from the back LTS and in that too due to the decrease in contribution from the diffraction grating. From Table 4.3, it has again become validated that the contribution from ARC remains almost constant, irrespective of the thickness of the active layer in the cell.

4.8. Conclusion

In conclusion, it has been shown that, by combining a 2D PhC diffraction grating and DBR, efficiency enhancement in the performance of the solar cells take place and that too without losses associated with textured metallic reflectors. The dielectric PhC structure provides loss-less diffraction of photons, increasing the photon path length within the absorber layer. The role of each element of the LTS has been studied for its contribution in efficiency improvement. It has also been shown that the enhancement is more profound for the thinner cells, which is basically due to the contribution from the back trapping structure and that too mainly from diffraction grating, providing almost thrice the efficiency for a 100 nm active layer cell. The contribution of LTS decreases with increasing thickness of active layer whereas the contribution from ARC almost remains constant even with increasing thickness of active layer. The structures performance has also been compared with that of the Lambertian limits and it has been shown that although the proposed structure results are away from these limiting values, but still these periodic LTS shows potential to take the efficiency enhancement in GaAs thin film cells towards these limiting values.

Chapter 5

Light Trapping in Thin Film GaAs Solar Cells using 2D Photonic Crystal Structures at Front Surface

5.1. Introduction

The last two chapters presented the designs for thin film GaAs solar cells with PhC LTS incorporated as a back reflector. The primary objective of PhC LTS in those cases were to improve the absorption of low energy, high wavelength photons either through effective reflection or diffraction phenomena or through the combination of both, as the actual thickness of active GaAs layer by itself does not allow these high wavelength photons to be absorbed in single pass. Thus a large fraction of available spectrum that otherwise could be lost due to incomplete absorption, has been utilized for useful absorption through PhC LTS and that too without encountering losses associated with metallic back reflector, as successfully demonstrated by the previous chapters results [138, 139]. However, the incomplete absorption occurs, not only due to the absorption depth limitations in TFSC, but practically there are also major losses due to reflections from the top surface as well as electrical losses, like interface and non-radiative recombination, including others.

Reflections from the top surface in a solar cell proves to be one of the key factors in the reduction in efficiency [13]. It has also been established in the previous chapter that although the PhC LTS at the back shares the major contribution for efficiency enhancement of thinner cells, its contribution ceases with the increase in thickness of active GaAs layer, as the structure at the back basically functions to improve the absorption of low energy photons, especially near its

band edge. However, the contribution from ARC at the top remains almost constant in absorption enhancement irrespective of the thickness of active layer. Thus not only the BR design as a part of LTS but also the design of ARC at the top is one of the key factors in designing the high efficiency thin film GaAs cells.

As already discussed in previous chapters, ARC will provide help in index matching for the incident light and thus maximize absorption. However, to design an ARC which could provide incident light coupling through minimizing reflections over the entire solar spectrum range and also reducing outward movement of photons from the top surface is really difficult to design. Usually a planar single layer ARC is used at the top, but as mentioned in the previous chapter, it works around a central wavelength to obtain relatively low reflectivity in a certain wavelength range of interest.

With this motivation, the chapter deals with the optical optimization and analysis of the performance of the LTS consisting of PhC structure at the top (having hexagonal structure with air holes in the extending from top Indium Tin Oxide (ITO) layer followed by the AlGaAs window layer), followed by the hetero-junction structure of GaAs active layer having window layer of AlGaAs at immediate above and bottom of the GaAs active layer. Single layer planar back reflector (BR) of Al is placed at the bottom of the structure. The purpose of the work is to study and demonstrate the effectiveness of PhC structure placed at the top to enhance the efficiency of the GaAs TFSC.

The PhC structure proposed here has been designed to contribute in the improvement of the efficiency almost throughout the solar spectrum, assisted by the Al BR. The PhC structure at the top, helps in index matching and thus assists in the coupling of the incident light to the absorbing layer. The structure, hence, helps in the reduction of the reflections from the top and at the same time also helps in increasing the optical path length for high wavelength photons through diffraction and thus contributes for the improvement in absorption almost throughout the solar spectrum. Moreover, the PhC LTS also increases the escape angle for the outward moving photons, thus also helps in the angular performance enhancement of the device.

The Maxwell equations are used to analyze the effect of the PhC structure [54] and to solve these equations, to calculate absorption in the active layer, RCWA numerical method is used in the chapter, since it directly exploits the periodical nature of the device [62, 61, 36]. The optical

performance of the structure has been analyzed through calculating absorption in the active layer and reflectance from the top surface together with external (or internal) quantum efficiency and I-V curve measurements [120, 137, 140]. The chapter also reports the angular performance of the device with reference to the incident angle and also shows the absorption enhancement in the device as compared to the planar reference structure. As also discussed in the previous chapters, the AM1.5 solar spectrum has been considered to be incident normal to the 2D PhC [58].

The chapter presents the optimization study for 50 nm thin GaAs active layer in a generalized manner and follows the same process for the optimization of the other thicknesses. The proposed structure then has been simulated for various active layer thicknesses ranging from 50nm to 5000nm. Then we have analyzed the contribution of every part of the proposed LTS in the efficiency enhancement and the performance of the structure is then compared with that of the Lambertian efficiency as well as that of the planar reference structure having single planar ITO ARC at the top and planar Al BR.

As already discussed in the previous chapter that the initial analytical solution for ideal Lambertian light trapping was given by Yablonovitch and Cody [24, 131], which was later modified by Green [141] that could be applicable for any active material. Using the same analytical solutions, Figure 5.1 shows the comparison of efficiency for GaAs active material for Lambertian light trapping and a bare cell (consisting only a slab of active material layer of particular thickness, without any kind of light trapping structure (LTS) for ideal case) cases.

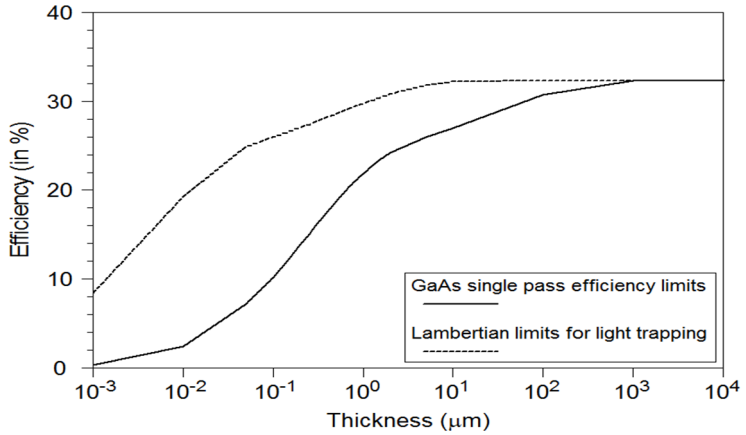

Figure 5.1: Cell Efficiency versus active layer thickness graph for GaAs based solar cell using AM1.5 solar spectrum [10]. Ideal case has been considered without assuming any kind of loss.

The results presented in the figure are just the extension of Lambertian light trapping values presented in the last chapter, however here they are presented in graphical manner and also

compared with single pass efficiency values. Thus, a design of low loss near to ideal LTS can prove to be a boon for the development of high efficiency thin film GaAs cell, through which it might achieve the efficiency near to S-Q limit [20]. The basic material parameters such as refractive index of GaAs, used in the figure are taken from [132].

It has been observed that the overall relative cell-efficiency enhancement that can be achieved with proposed LTS is about 127% for a 50nm-thick cell as compared to the single pass efficiency (with losses), where the maximum contribution in performance enhancement (about 98%) is from the PhC structure and the remaining is from the BR. The results are also compared with that of the planar reference cells and Lambertian limits, which show about 23% relative efficiency enhancement for 50nm thin cell with proposed PhC LTS as compared to the planar cell.

With the increase in the thickness of the active layer, the contribution from the BR becomes almost negligible whereas the contribution from the PhC LTS becomes almost constant. This is basically due to the case as PhC LTS here also helps in the reduction of reflections through impedance matching thus the importance of the PhC almost remains valid for the entire wavelength range, and not only for the higher wavelength photons absorption. However, still the achieved efficiency are short of the Lambertian limits and thus a lot more is required to be done to achieve the limiting efficiency.

5.2. Proposed Structure Design

The proposed design uses the same heterojunction of GaAs/AlGaAs as shown in previous chapters, but with inclusion of PhC LTS at the top. The proposed PhC LTS based thin film GaAs solar cell has been shown schematically in Figure 5.2. To facilitate comparison, a commonly used planar reference cell without PhC LTS has been shown in Figure 5.3. The sunlight is assumed to be incident from top of the structure, perpendicular to the plane of PhC periodicity, as shown by black arrows at the top in Figure 5.2 and 5.3 [48]. The medium surrounding the device is considered to be air. The device consists of 2D PhC LTS at the top having hexagonal lattice arrangement. The PhC structure consists of air holes in the ITO background followed by $Al_{0.8}Ga_{0.2}As$ window layer. Active layer of GaAs is placed below this window layer. $Al_{0.3}Ga_{0.7}As$ back window layer is placed below the active layer followed by the single planar metallic back reflector of Al.

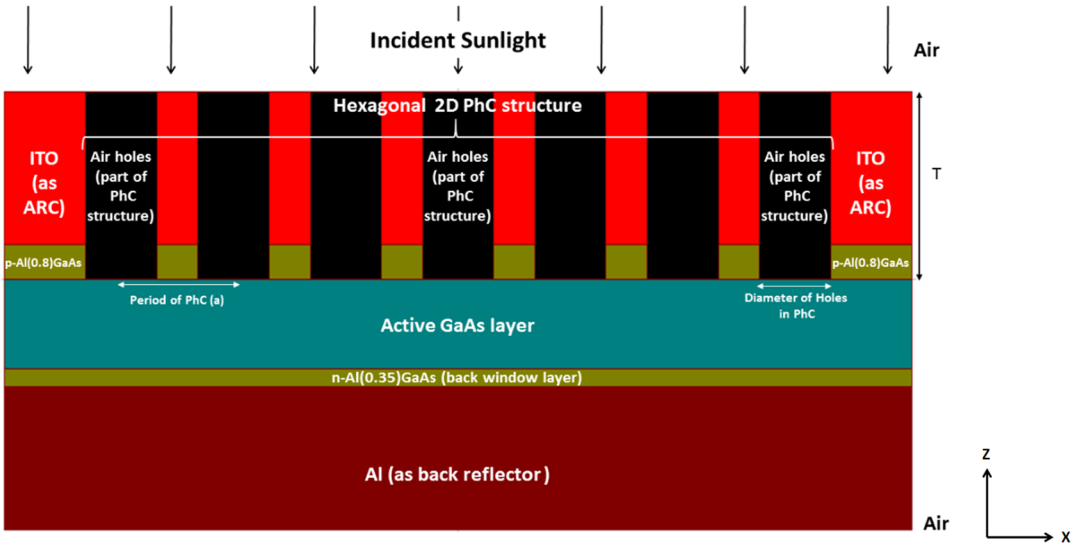

Figure 5.2: Schematic diagram of the proposed thin film GaAs cell (x-z direction, side view) with PhC LTS at the top assisted by Al BR

The planar reference structure shown for comparison in Figure 5.3 does not contains the PhC LTS, instead it only has a single planar ARC of ITO of same thickness as that used for PhC structure, to have fair comparison of the proposed PhC based device with common planar device. In this work, the wavelength dependent material parameters are considered for GaAs and AlGaAs [94], Al [142] and ITO [126].

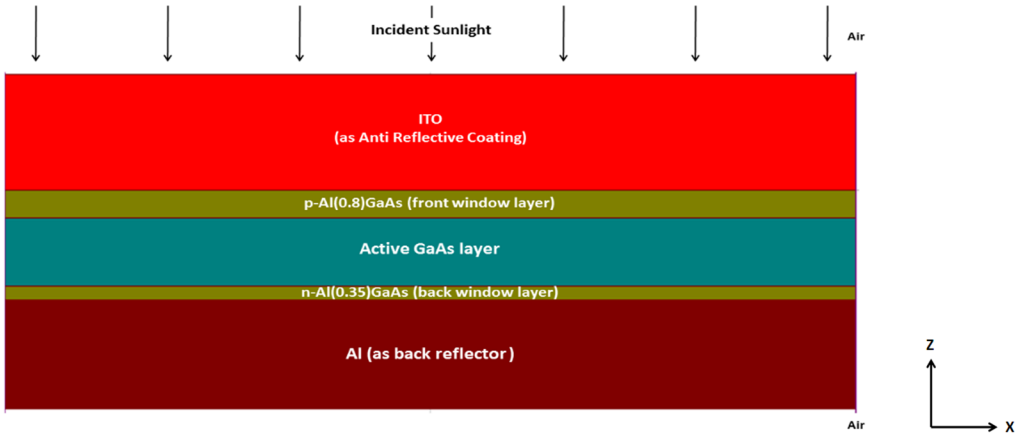

Figure 5.3: Schematic diagram of the proposed thin film GaAs cell (x-z direction, side view) without PhC LTS, having planar ITO layer at the top assisted by Al BR

The single planar Al BR is considered to be as close as possible to being an ideal metallic reflector, neglecting semiconductor-metal interface patterns since the field localization in the interface would limit the optical gains that the LTS would otherwise provide [63, 143]. Here, we have considered just a single planar BR as our main aim is to study the effectiveness of the PhC LTS at the top where BR has only been used to assist the PhC structure. ITO has been used at the

top (for detailed discussion, kindly refer to chapter 3 and 4), as it could effectively provide good impedance matching for minimizing reflections from the top [138, 126]. Moreover, ITO, which is a popular transparent conducting oxide (TCO), also fulfills the requirement that the PhC structure should have minimum absorption together with large refractive index contrast, in order to provide large diffraction. Thus, the structure has been designed to have very limited absorption in the wavelength range of interest, with high index contrast and good conductivity.

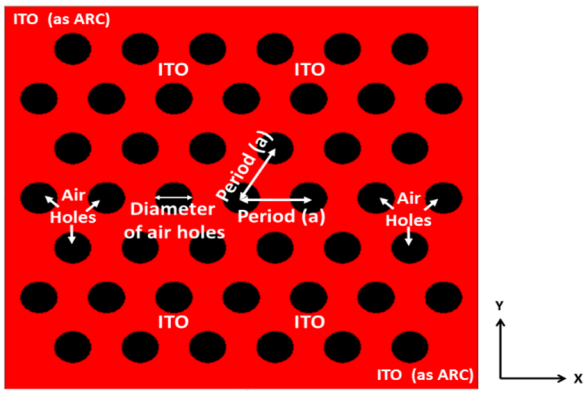

Figure 5.4: Schematic diagram of the proposed structure having PhC structure (y-z direction)

The top view of 2D PhC structure configuration has been shown in Figure 5.4, having etching depth, *T*, extending from the top ITO layer uptill the beneath $Al_{0.8}Ga_{0.2}As$ layer, which is directly in contact with the active GaAs layer. Instead of square arrangement of holes, hexagonal structure has been used throughout this work, as it provides better diffraction as compared to the square assembly, as shown in the previous studies [58].

5.3. Theoretical Numerical Approach and Efficiency Calculations

Considering the sun light as a plane-wave incident on the top surface of the cell, absorption, reflection and transmission has been calculated by RCWA method [144, 105, 145]. RCWA represents the electromagnetic fields as a sum over coupled waves. A periodic permittivity function is represented using Fourier harmonics (discussed in detail in section 2.6). We have used commercially available RSoft's DiffractMod software, based on RCWA algorithm to perform the 3D simulation analysis and determine the absorption and reflection spectra for the proposed device and then calculated the related parameters based on these results [106].

Here, the number of harmonics, M plays an important part in determining the accuracy of the result, as discussed in section 2.6. Thus, a convergence study to find the value of M has been performed, where several simulations have been done with different harmonics to see how the

simulation results change. The result of the convergence study has been shown in Figure 5.5. As the figure shows that the results become almost stable when M become 5, thus for the simulation analysis M has been considered to be equal to 5, as it takes less computational time and that too without compromising with accuracy.

In order to solve the simulation equations, the structure has been considered as a multilayer periodic structure which is decomposed into stacks of layers having a vertically homogenous region [62]. The algorithm considers the structure to have horizontally PBC. The multilayer structure has been designed in the vertical direction, i.e. in z direction having periodic structure in x-y direction. The simulation studies has been done considering only a single period of the structure in x-y dimensions.

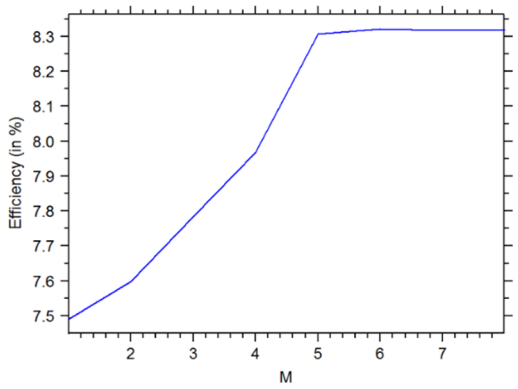

Figure 5.5: Convergence study graph between no. of harmonics and cell efficiency, where M represents the no. of harmonics. In the work, we have used M to be equal to 5.

To calculate the solar cell efficiency, we have calculated the total optical absorption spectrum, $A(\lambda)$ of the entire device through RCWA method, which is the sum of the absorption spectra within each layer, $A_i(\lambda)$ as $A(\lambda) = \sum_i A_i(\lambda)$. Here, we have considered absorption in the active GaAs layer as the only useful absorption, in order to consider only the useful charge carriers, in the similar manner as considered for previous chapter studies. Following the above formulation, the procedure followed to calculate the efficiency of the proposed and reference devices as well as Lambertian limits for GaAs thin film cell is the same as described in detail in section 4.3, and hence not repeated here.

Here, we have taken the Lambertian limits calculated through Equation (4.6) as references for upper efficiency limits to compare the efficiency results of the proposed structures. The absorption spectrum has been compared for the efficiency provided by the Lambertian limits as

well as provided by the proposed PhC LTS based structure and the planar reference structure. We have also calculated the absorption enhancement factor, *F*, which is defined as in [62] as,

$$F(\lambda)=\frac{A(\lambda)}{A_s(\lambda)}=\frac{A(\lambda)}{1-e^{-\alpha(\lambda)t}} \tag{5.1}$$

This enhancement factor has been calculated with reference to the single pass efficiency (considering losses).

5.4. Structural Optimization

The section demonstrates the details of the optimization study of the proposed structure. In order to keep the practical issues in mind, where various parameters affect each other while designing an opto-electronics device, contour maps have been derived to show the optimization of these photonic structures. Initially, the optimization of the 50nm thin active layer cell has been done in a generalized manner, and the same process has been used for the optimization of the other thickness cells. The optimization of the structure includes the optimization of the period or lattice constant of the PhC structure together with its radius or diameter of the circular air holes, *D*, (which in turn also defines the fill factor ratio for background material) and the etching depth or the thickness of these PhC structures, (which includes the optimization of the thickness of front ITO background layer thickness and beneath $Al_{0.8}Ga_{0.2}As$ window layer.

During simulation studies, the active material layer thickness has been kept fixed at a particular value (here 50nm for demonstration purpose). As per the result shown in Figure 5.5, number of harmonics, *M*, for the study has been set to 5. The non-patterned back window layer of $Al_{0.35}Ga_{0.65}As$ has been set to 10nm as per the studies performed earlier, as thicker window layer might degrade the performance of the device [146, 147]. The thickness of the Al BR has been fixed to 80nm which is almost equal to the quarter wavelength thickness for considering central wavelength around wavelength 500nm to maximize reflections from BR [58].

First, a contour map for the cell efficiency has been calculated by varying simultaneously the values of *a* and *D* for optimizing the PhC structure, as shown in Figure 5.6. On the basis of the measured contour plot, the optimal PhC pattern structure has been identified and then it has been analyzed in detail. The figure shows that the optimal value of period has been found out to be 500nm and the value of *D* has been found out to be about 275nm, thus providing the ratio of *D/a*

to be around 0.55. This ratio ultimately defines the filling ratio for the optimal patterning of the PhC design. This value of ***a*** is supposed to maximize the coupling of the incident light from the PhC to the absorption layer, and thus produces a dense distribution of absorption peaks for the desired wavelength range. Here, the PhC structure is not only required to assists in the reduction of reflections from the top through better impedance management but also have to maximize diffraction of photons to the absorption layer, having minimizing absorption of useful photons in the front LTS and diffraction in air.

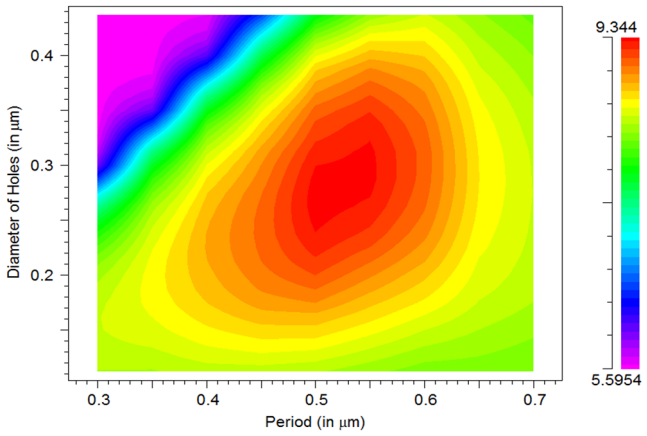

Figure 5.6: Contour map representing the optimization of diameter of the air holes with reference to lattice constant (a) of the PhC structure for the proposed 50nm PhC LTS based cell configuration.

As mentioned in previous chapters, in order to perform this diffraction function, PhC structure period is required to be larger than the wavelength of light in the active layer at the particular wavelength (kindly refer to section 3.3 and 4.4.2 for details). The diffraction exhibit peaks in the absorption for incident wavelengths for values of period larger than ~ 350 nm as clearly shown in the Figure 5.6.

It has been previously shown [62] that when the period is very small (in our case more than 200nm but less than 350nm), only low wavelength photons could couple to the active layer, whereas patterned PhC layer appeared as uniform for high wavelength ones where refractive index of the PhC layer is marked by the effective refractive index of the patterned layer. Although, at this PhC pattern reflections from the top and diffraction in the air has been minimized, but the light trapping is limited only to low wavelength regime where solar flux is weak. However, it does not mean that we could go for very high periods, as increasing the value of *a*, might improve the light trapping of high wavelength photons but also at the same time increases diffraction in air. Thus, there is an optimal value of the period which could not only

reduce the reflections from the top and the diffraction in air, but also improves the light trapping of the high wavelength photons. Simulation results have shown the PhC structures provide most effective guiding and diffraction resonances for the value of *a* equal to 500nm.

As mentioned earlier, in the case when the incident photons wavelength becomes higher than the period of patterned structure, then, instead of behaving as a diffraction grating the structure behaves as a uniform layer, whose effective index is a weighted average of the refractive index of PhC structure. This behaviour can be quantified by recalling the expression for the effective index of an arrangement of air holes in the ITO background, could be given as [58, 62]:

$$\varepsilon_{eff}(f) = \frac{1}{2}\left[f.\varepsilon_{ITO} + (1-f).\varepsilon_{Air} + \frac{1}{f/\varepsilon_{ITO} + (1-f)/\varepsilon_{Air}} \right] \tag{5.2}$$

The same equation can be used for PhC structure in the p-AlGaAs layer beneath. Here, $f = \pi R^2/((\sqrt{3}/2)*a^2)$ is the fill ratio for the hexagonal lattice structure. This provides an information for the effective index matching of the absorption layer with that of the incident medium (air in our case). Using the effective data values of parameters used in the above equation, value of *R* has been calculated. The optimization results for *D* has been shown in Figure 5.6, showing the optimized value to be about 275nm, almost validates our simulation results.

Through Figure 5.6 one can also observe that the cell efficiency is varied only by 1%, even if the period and diameter of holes of PhC structure are 10% away from the optimal values. Thus, it could also be inferred that this structure exhibits good fabrication tolerance with regards to a variation of the proposed configuration. Thus, it is quite realistic to fabricate the proposed device using available nano-lithography techniques like nano-imprint or e-beam lithography or any other similar technique, and has the ability to provide optimal results as the simulation studies predict good tolerance for the configuration.

Next, the optimization of the PhC depth in the ITO and p-AlGaAs has been done with reference to the ratio *D/a* as shown in Figure 5.7 and Figure 5.8, respectively. The depth of the PhC LTS should be such that the coupling of light to the active layer should be maximized and specularly reflected beam from PhC into the air should be minimized. The sum of the reflection coefficient from ITO, p-AlGaAs and air should become zero for the specific value of PhC depth [60]. Also, it is required that the proposed PhC should guide as much incident light as possible to the absorbing layer with negligible absorption in the patterned layer. From Figure 5.7, this optimal

value of the PhC structure thickness with ITO background is found out to be around 85nm, whereas the optimal thickness of the etched PhC pattern in p-AlGaAs window layer has been found out to be 40nm. However, as suggested in [147], the thick window layers might adversely effect the electrical performance of the cell, thus instead of using 40nm thickness of p-AlGaAs layer, the author has limited this thickness to 20nm.

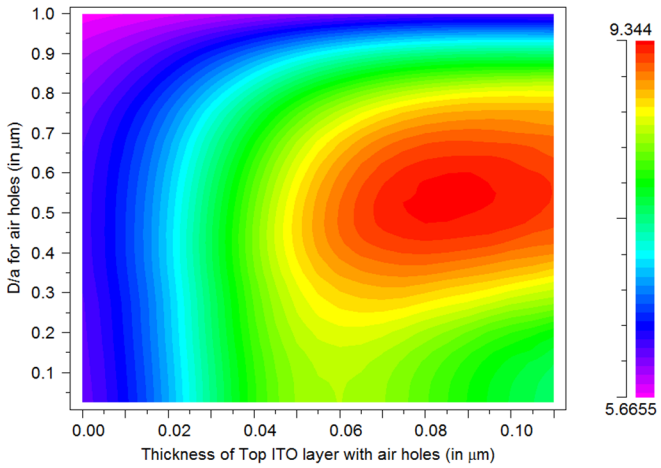

Figure 5.7: Contour plot for cell efficiency optimization as a function of thickness of top ITO layer having PhC LTS and *D/a* ratio for the proposed 50nm PhC LTS based cell configuration.

Thus, the total etching depth becomes 105 nm from the top (85 nm in ITO layer and 20nm in p-AlGaAs layer). From Figure 5.7 and 5.8, one can also find out that there is good tolerance for efficiency around the optimized etching and *D/a* parameters and there is only about 1% decrease in final cell efficiency, for around 10% variation in the optimal values.

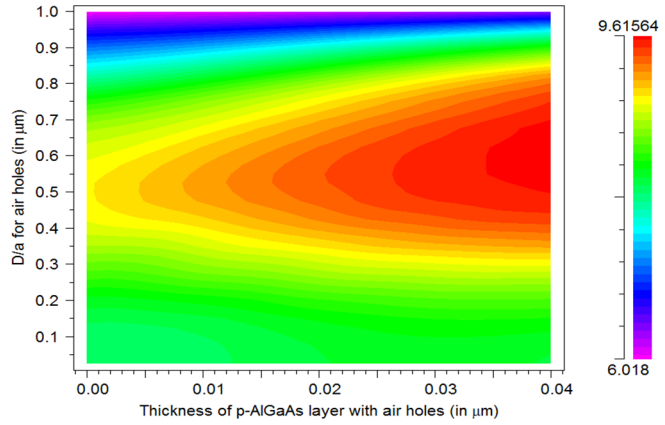

Figure 5.8: Contour plot for cell efficiency optimization as a function of thickness of p-Al(0.8)GaAs layer having PhC LTS and D/a ratio for the proposed 50nm PhC LTS based cell configuration. Here, instead of using 40nm optimal value, we have limit the value of p-AlGaAs to 20nm for electrical reasons [147].

Here, optimizing an appropriate etching thickness for the PhC structure plays an important part in the cell efficiency enhancement. Appropriate etching thickness perturbs the slab guided modes

and the PhC grating makes them accessible from an incident radiation [63]. As mentioned earlier, the condition is similar to the diffraction grating, which deflects the normally incident light to the oblique direction and thus increases the path length for that wavelength photons. The diffracted waves propagate at nearly grazing angle within the material, with a large propagation path, thus improves absorption within the active layer within the wide spectral range. Thus, the role of the PhC LTS is to couple the incident radiation field to the guided slab modes, without significantly varying the modes themselves. Increase in this etching thickness might substantially increase the absorption in the PhC structure, and thus decreases the light coupling and ultimately efficiency [63]. The optimized parameters for 50nm thin GaAs active layer PhC LTS based cell having 2D PhC design used at the top are summarized in Table 5.1, and 3D figure of the optimized structure is shown in Figure 5.9.

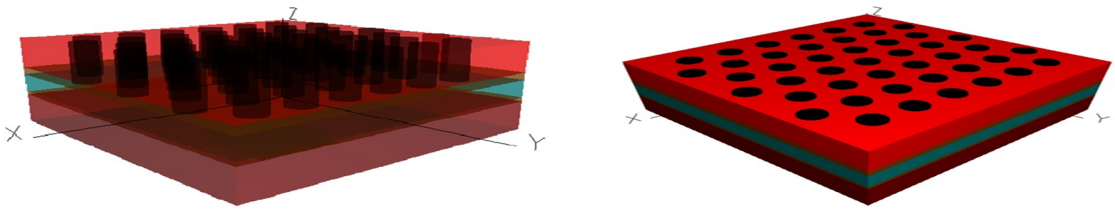

(a) (b)

Figure 5.9: 3D view of the final proposed PhC LTS based thin film GaAs cell with pattern (a) inside view; (b) outside view

Table 5.1: Summary of the optimized parameters for the 50 nm thick GaAs active layer

S. No.	Parameters	Values (nm)
1.	Thickness of anti-reflection coating (ITO having PhC structure etched)	85
2.	Thickness of p-Al(0.8)GaAs window layer (having PhC structure etched)	20
3.	Thickness of n-Al(0.35)GaAs back window layer	10
4.	Thickness of back reflecting layer of Aluminum	80
5.	Period of the PhC structure at the top (a)	500
6.	Diameter of the air holes etched as the part of PhC structure (D)	275
7.	*D/a* (ratio)	0.55
8.	Thickness of the PhC structure etched from the top (etched in top ITO and p-AlGaAs)	105

5.5. Performance Analysis of the Proposed Structure

The section deals with the discussion and analysis of the performance of the proposed 50nm active layer thin film GaAs solar cell with PhC LTS in terms of the calculated absorption and reflection spectra, spectral distribution as per AM1.5 solar cell spectra [48], absorption

enhancement as per Equation (5.1) and angular performance with variation in incident light angle. The results are compared with that of the Lambertian limit [24, 141], ideal and practical single pass efficiency. For better understanding of the performance enhancement in the proposed PhC LTS based design, the results are also compared with a reference planar cell as shown in Figure 5.3. At last, to clarify the absorption in the structure in the entire incident spectrum, we have used the electric field intensity diagrams for various incident wavelengths.

5.5.1. Absorption and Reflection Spectra

The absorption and reflection spectra for the proposed 50nm active layer thickness PhC LTS based cell has been calculated and are compared for different configurations. The calculated absorption graph is shown in Figure 5.10, where absorption is normalized to a maximum value of unity, the case when the entire incident light gets absorbed in the active layer. One can observe from the figure that the absorption starts to dip exponentially after 400nm and drops below almost 50% after 450nm for the ideal single pass case. The condition become even worse when losses have been included, including reflections from the top, collection efficiency losses and shadowing effects in the calculations for single pass case.

Now, consider the case of reference cell having planar LTS. From the figure, one can observe that after 450nm, the absorption in the reference cell has been enhanced as after this wavelength the effect of LTS has become significant. Also, due to the ARC at the top, reflections have also been reduced. Next, in the case of the proposed PhC LTS based cell, which is shown by dark blue line patterned by open circles in the figure, one can observe that the enhancement in the absorption is achieved for almost the entire incident wavelength range as PhC LTS in our design. This has been achieved through the patterned structure as it provides better impedance matching and perturbed many quasi guided modes as compared to the planar reference cell. For patterned structure, the line shape of the resonance broadens for increasing energy, according to the fact that a higher intrinsic absorption produce slower and broader features in the absorption spectra [62, 36]. Here, the absorption enhancement ceases beyond around 670nm as beyond this range, the effect of BR becomes dominant and both the PhC LTS based cell and the reference cell have the same Al BR of equal thickness. From the figure, one can also observe that we could achieve higher efficiency practically with the proposed structure, albeit still under the Lambertian limit efficiency values.

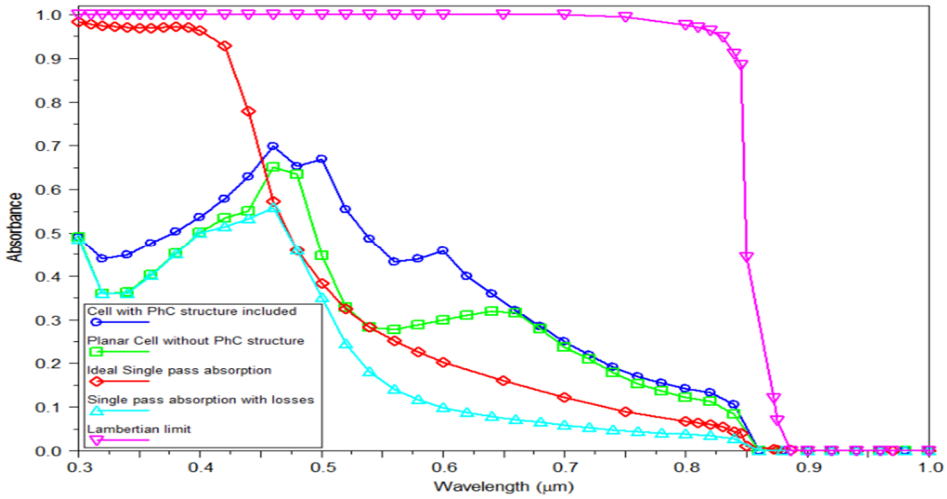

Figure 5.10: Calculated absorption spectra for the proposed 50nm GaAs active layer cell having 2D PhC LTS.

Calculated reflectance spectra for the proposed 50nm active layer GaAs cell has been shown in Figure 5.11, in comparison to the reference cell. Here, the reflectance from the structure includes all the diffraction orders, and as can be observed from the figure, the reflectance is always less in the PhC LTS based cell. This happens since the PhC structure provides both the better impedance matching condition (as the PhC LTS provides the intermediate effective refractive index) and light trapping. At high wavelengths, the reflection contribution is basically due to incomplete absorption in the active layer, which is nearly complementary to absorbance spectrum. At low wavelengths, there is a residual reflection, but it is evident that the intermediate patterns provide a spectral band of low reflectance, which is broader than that of the reference cell. In the patterned cell there is still diffraction in air due to large number of allowed modes [62]. This diffraction in air could be reduced with small lattice constant value, but as mentioned earlier the period of the PhC structure cannot be reduced to the very small value as this adversely affects the trapping of high wavelength photons.

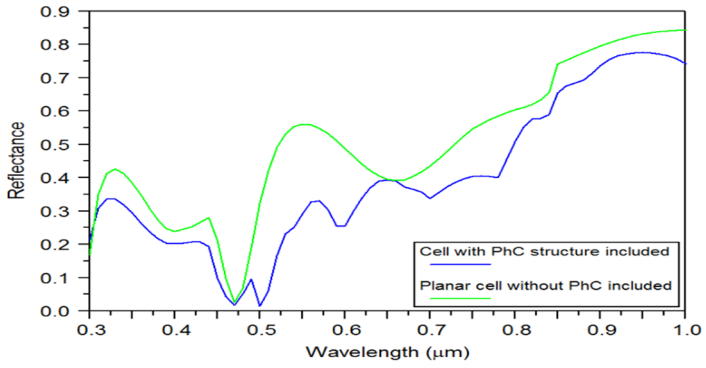

Figure 5.11: Calculated reflection spectra for the proposed 50 nm active layer cell with PhC patterning and its comparison with the non-patterned planar solar cell structure.

5.5.2. Analysis for Spectral Distribution

The smoothened spectral distribution graph for the proposed PhC LTS cell with 50nm GaAs active layer has been shown in Figure 5.12. As shown in the previous results, this figure also shows the performance enhancement for the patterned structure as compared to the reference cell and single pass values. Here, we have reported the spectral distribution for both Lambertian limits as predicted in [131] and [141], for comparison. Again, one can predict from the figure that this proposed periodic patterning could enhance the efficiency considerable, although not up to the Lambertian limits.

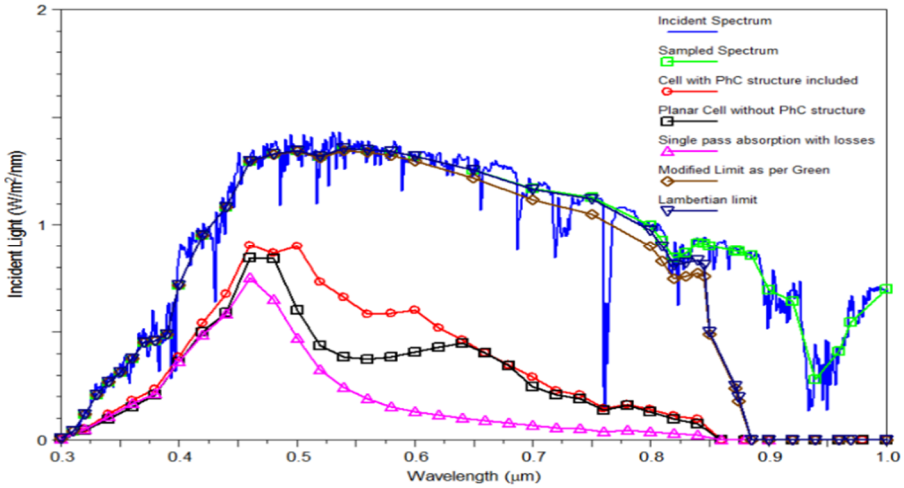

Figure 5.12: Calculated spectral distribution graph for the considered solar spectrum [50] for the proposed 50nm active layer cell with PhC LTS and its comparison with the reference cell having same active layer thickness.

5.5.3. Absorption Enhancement in the Structure

Figure 5.13 demonstrated the absorption enhancement factor, *F*, calculated as per Equation (5.1). The graph clearly shows that there is enhancement in the absorption in the active layer of the GaAs cell due to the proposed PhC LTS and that too within the entire incident spectrum range.

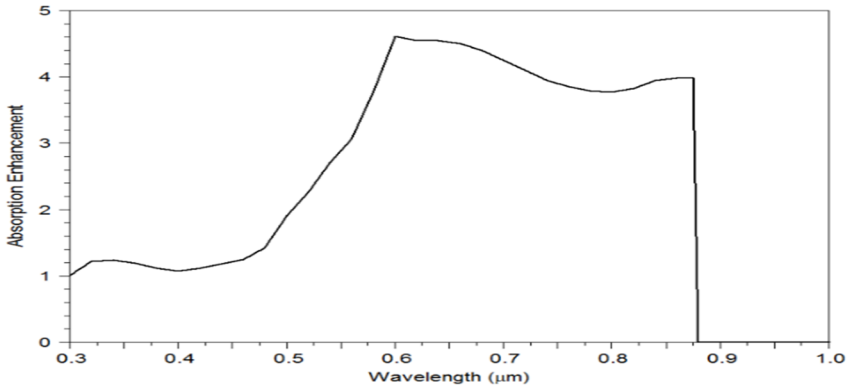

Figure 5.13: Calculated absorption enhancement graph for 50 nm active layer PhC LTS based cell.

The enhancement becomes pronounced beyond 450nm for the reason as beyond this value, the LTS effect becomes dominant and is mainly responsible for guiding, coupling and deflecting photons for absorption in the active layer.

5.5.4. Analysis with Incident Angle Variation

The evaluation of the proposed structure has also been done with respect to the incident light angle, and the calculated values over the angular range of incidence as shown in Figure 5.14, have predicted improved performance of the device as compared to the reference planar cell. It is evident from the figure that angular performance of the proposed LTS provides much better results as compared to the planar cell almost for the entire incident angle range. The result can be attributed to the better diffraction capability and coupling efficiency of the PhC LTS which helps in guiding the light to the active layer for large range of angle of incidence. It can be noted from the figure that our designed structure is able to perform almost equivalent to the normal incidence up to about 75° or so, retaining nearly 80% of the normal incidence efficiency and thus shows significant performance enhancement. Thus, we could say that the efficiency enhancement of the considered PhC LTS is rather robust with respect to variations of the orientation and of the incidence angle. This is an important result, as through this one could predict the proposed structure would yield the same efficiency enhancement for direct and diffuse light, without any need of solar tracking.

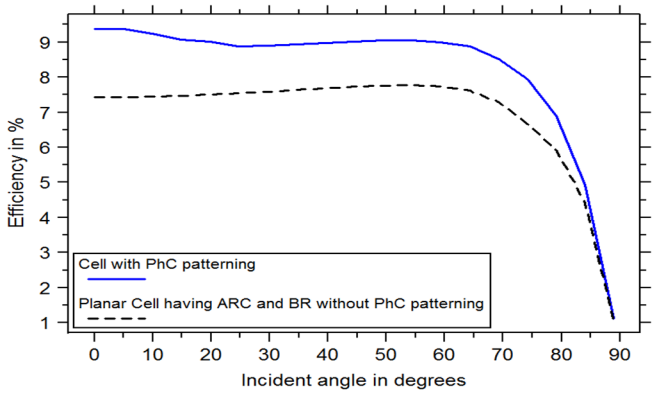

Figure 5.14: Incident angle Vs. Cell Efficiency graph for proposed 50nm active layer based GaAs cell structure with and without PhC patterning

5.5.5. Analysis for Electric Field Intensity at Different Wavelengths of Interest

To have better understanding of the absorption mechanism associate at different incident light wavelength, Figure 5.15 demonstrates electric field intensities at eight different wavelength for

TE polarization ranging from 350nm (high energy photons) to 850nm (low energy photons), as the proposed PhC LTS has effect in the absorption throughout the spectrum. The above mentioned phenomenon can be clarified using the electric field intensities shown in Figure 5.15.

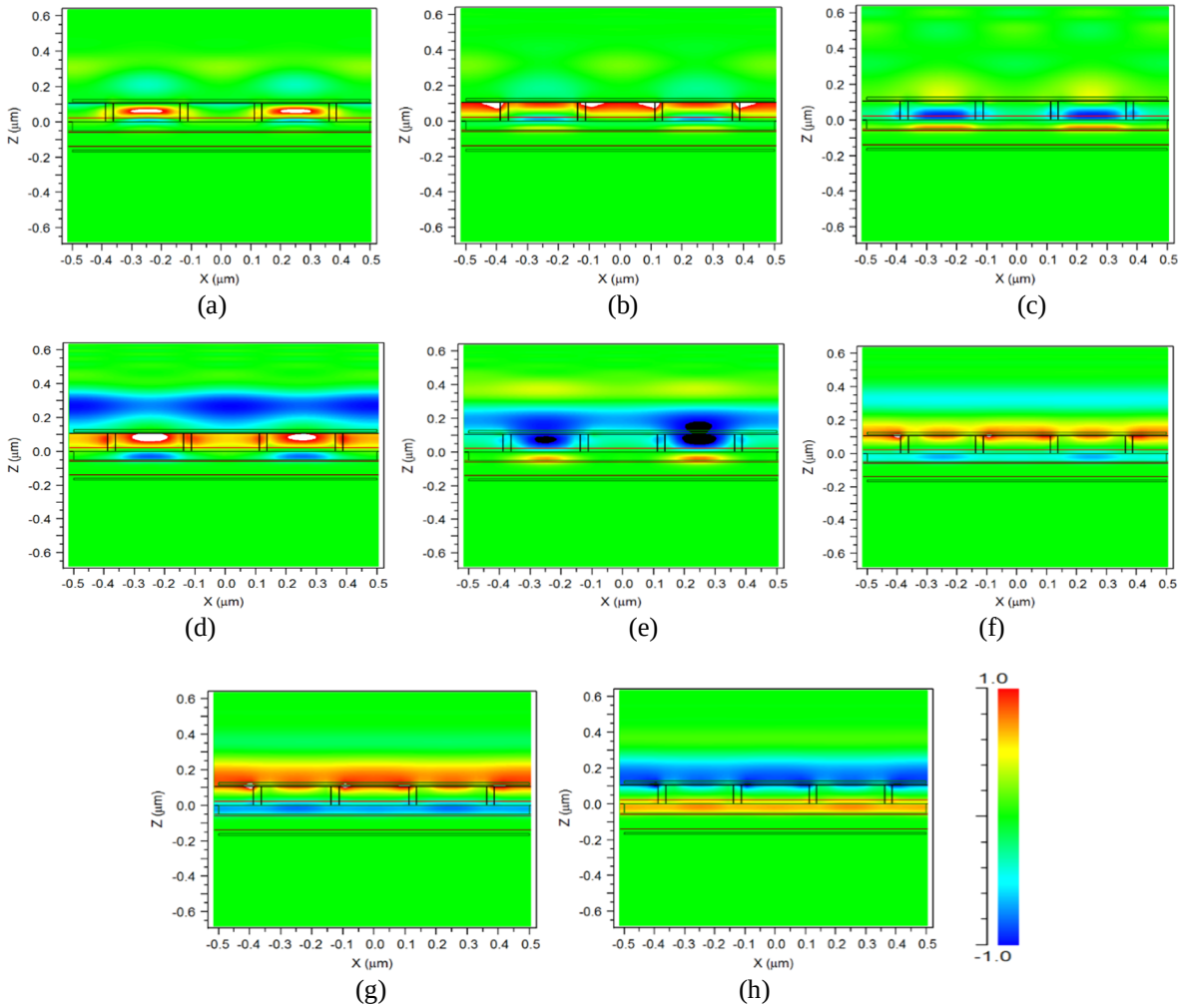

Figure 5.15: Electric field intensities for the proposed 50nm active layer PhC LTS based GaAs cell for TE polarization, calculated at the following wavelengths: (a) 350nm, (b) 450nm, (c) 500nm, (d) 550nm, (e) 600nm, (f) 700nm, (g) 800nm, and (h) 850nm. Vertical stack after figure (h) shows the color reference used to predict intensity.

Figure 5.15 (a) shows the electric field intensity at 350nm. The intensity diagram shows that for high energy incident photons there are considerable reflections from the top surface and also instead of strong coupling of the light from the top surface to the active layer, most of the light remained in the PhC LTS itself, with only small portion of incident light is coupled to the bottom layer. This is the main reason for small value of absorption in the proposed cell around 350nm, as was shown in Figure 5.10. Figure 5.15 (b), shows the electric field intensity at 450nm, indicates that although there are still reflections from the top and resonances in the PhC structure

itself, but less than the case at 350nm and thus, here the coupling of light also get enhanced. Now, Figure 5.15 (c), depicts the case around 500nm, which is as per Figure 5.10, is among the main spectrum areas of enhancement in absorption as compared to the reference cells. One can easily observed from the figure that here the coupling of the incident light from the incident medium to the active layer becomes stronger having very small concentration of light in PhC itself and reduction in reflections.

Figure 5.15(d) and (e) show the electric field intensities at 550nm and 600nm. Here, too although the coupling of light to the active layer is strong and the absorption is better as compared to the reference cells, the reflections are high (which could be accounted due to diffraction in air) and also there is strong resonance in PhC LTS itself. Subsequent figures shows intensity diagrams at 700, 800, 850 and 875nm, respectively and show that as the wavelength increases, the coupling reduces and the reflections from the front surface becomes dominant, and also the resonances in the PhC structures fade away. Thus, on the basis of the above intensity diagrams, one could conclude that although the proposed structure have enhanced the performance of the ultra-thin film GaAs cell, but in order to enhance the efficiency even further to take these values toward S-Q limits using Lambertian predictions, one has to reduce the reflections from the top even further, improve diffraction of light from the top towards active layer and convert the resonances in the PhC structures instead of losses to useful light, by coupling more and more of this light towards useful active medium.

5.6. Performance of the LTS with Variation in Thickness of the Absorption Layer

The section presents the performance analysis of the proposed PhC LTS based GaAs cell by varying the active layer thicknesses and compares the results with various other cell configurations including the reference cell, by using the same optimization procedure as depicted in the previous section. Here, the section also demonstrates the effect of each element of the LTS in the performance enhancement of the cell and how the contribution varies with the active layer thickness and thus determines that the LTS affects the efficiency of the thinner cells more as compared to the thicker cells, in the same way as demonstrated in the previous chapter.

The efficiency chart for various cell configurations for different active layer thicknesses has been depicted in Figure 5.16. The proposed structure efficiency has been calculated first without PhC

LTS having Al BR and then with PhC LTS and BR, in order to analyze the effect of each element in the efficiency enhancement of the proposed PhC LTS cell.

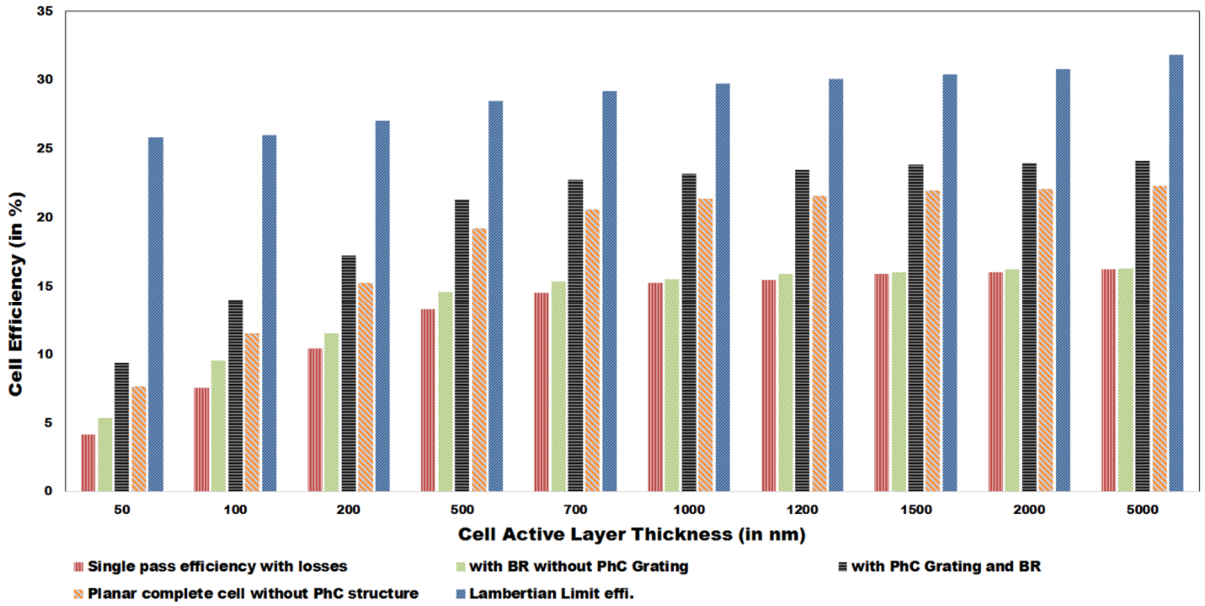

Figure 5.16: Illustration of efficiency for proposed PhC LTS based cell for various GaAs active layer thicknesses and their comparison with various cell configuration.

In Table 5.2, summary of the absolute achievable cell efficiency for different active GaAs layer thicknesses has been listed. Observation of these results clearly indicates that PhC LTS is the main reason for enhancement in efficiency and the contribution of the LTS in the efficiency enhancement of thinner cell is more as compared to the thicker cells.

Table 5.2: Summary of the cell efficiency for the optimal structures with different active layer thicknesses

Active layer thickness (in nm)	**Single pass efficiency with losses (device without ARC and BR) (%) (η_{bare})**	**Cell Efficiency (%) with BR without PhC structure (η_{BR})**	**Cell Efficiency (%) with PhC LTS and BR (η_{LTS})**
50	4.133	5.334	9.383
100	7.529	9.52	14.004
200	10.428	11.53	17.241
500	13.305	14.59	21.315
700	14.523	15.37	22.733
1000	15.275	15.532	23.205
1200	15.475	15.93	23.468
1500	15.91	16.021	23.846
2000	16.024	16.24	23.972
5000	16.271	16.29	24.150

It has been shown that the maximum achievable cell efficiency for the proposed structure having 50 nm and 500 nm thick active layer cells is about 9.38% and 21.32%, respectively, which are more than twice for 50 nm cell and almost 1.5 times for 500 nm thick active layer cell, as compared to the practical single pass efficiency. Now, to distinguish the roles of PhC LTS at the top and Al BR, the line graph has been shown in Figure 5.17, which shows the percentage contribution of PhC LTS and BR in the efficiency enhancement for various GaAs based active layer thicknesses. Methodology of calculation for percentage contribution of different light trapping component has been derived using the previous studies [61] as also discussed in previous chapter. Total efficiency percentage increase has been calculated taking the efficiency for the structure having PhC LTS assisted by Al BR, η_{LTS} and then that efficiency is compared with the bare cell efficiency, η_{bare}. Mathematically, it has been derived as:

$$\text{Total Efficiency Increase (\%)} = \frac{(\eta_{LTS} - \eta_{bare})}{\eta_{bare}} \times 100\% \tag{5.3}$$

The percentage efficiency enhancement contribution due to BR alone, excluding PhC LTS has been calculated next. Here we have taken the efficiency calculations for the structure having only BR, without PhC LTS at top. Then this efficiency for structure having only BR, η_{BR} is compared with the bare cell efficiency, η_{bare}. Mathematically, it has been derived as:

$$\text{Efficiency Contribution by BR (\%)} = \frac{(\eta_{BR} - \eta_{bare})}{\eta_{bare}} \times 100\% \tag{5.4}$$

In order to calculate the contribution of the PhC structure, we have taken the value of η_{LTS} and deduct the value of η_{BR} from it and then compared the results with η_{bare}. Mathematically, it has been derived as:

$$\text{Efficiency Contribution by PhC LTS at the top (\%)} = \frac{(\eta_{LTS} - \eta_{BR})}{\eta_{bare}} \times 100\% \tag{5.5}$$

The close analysis of the results clearly indicates that the percentage contribution of the proposed PhC LTS in the efficiency enhancement of the cell reduces as the active cell area thickness increases, and then almost become stable thereafter (when the active layer thickness becomes more than 500nm), whereas the BR intially has contribution in efficiency improvement, but as the active layer thickness increases, its contribution almost becomes negligible.

Table 5.3 summarizes the exact percentage contibution in the efficiency enhancement of the GaAs cell having various active layer thicknesses due to proposed LTS. From the table, one can

find that when the active layer is as thin as 50nm, total efficiency enhancement in the cell due to proposed LTS is about 127% as compared to the practical bare cell efficiency, and in that enhancement the major contribution is due to the PhC LTS which is about 98% as comapred to the 29% contribution by Al BR. As the cell's active layer thickness increases, the effectiveness of the proposed LTS decreases, as it can be seen from the table that the total increase in efficiency due to LTS becomes almost 50% as the active layer thickness becomes more than 1 μm. Also, it has also been demonstated that for thicker cells, the contribution of the BR decreases rapidly and almost becomes insignificant, whereas the PhC LTS contribution remains more or less constant.

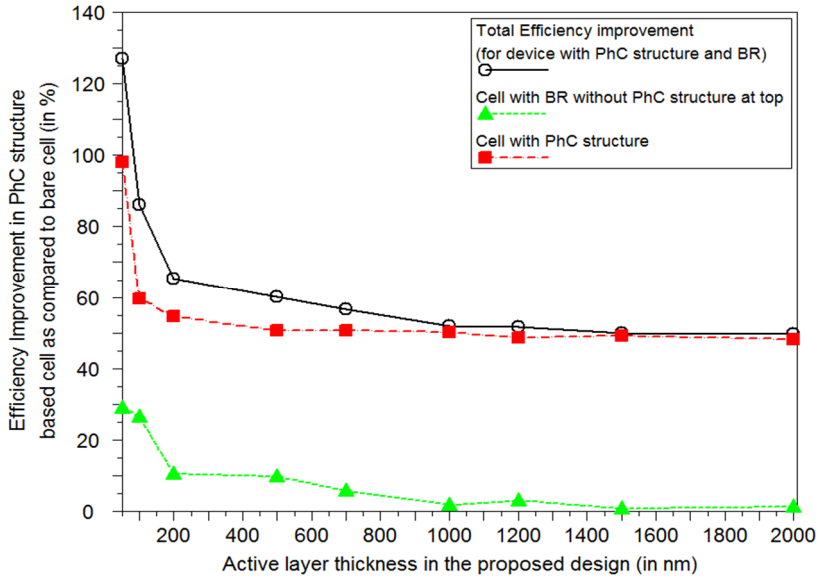

Figure 5.17: Efficiency enhancement graph (in terms of %) for various active layer thicknesses for the proposed PhC LTS based cell as compared to the bare cell (taking losses into account).

The reason for this is that, for the cell having thinner active layer thickness (i.e. less than 1000 nm), the LTS enhances absorption for the wide wavelength range in which the majority of solar spectrum is focused, for which absorption coefficient of the GaAs active material do not allow the cell to absorb the entire solar spectrum. However, for the thicker cells, smaller efficiency enhancement has been achieved as the active layer thickness of the cell in itself is sufficient to absorb most of the spectrum photons in single pass. Also, for thicker cells enhancement happens to be overlapped with the one of the major dip regions of solar spectrum at around 825–875 nm. Although, the contribution from the PhC LTS reduces with the increase in the active layer thickness, it does not become negligible, as happened in the case of the design proposed in

chapter 4 and as the results shown in Table 5.2 and 5.3, is still responsible for efficiency enhancement in the thicker cells.

Table 5.3: Percentage contribution from each part of LTS in cell efficiency enhancement for different active layer thicknesses

Active layer thickness (in nm)	% increase by PhC structure	% increase by BR	Total efficiency increase (%) as compared to bare cell
50	97.998	29.062	127.060
100	59.554	26.444	85.999
200	54.766	10.568	65.334
500	50.545	9.658	60.203
700	50.695	5.832	56.528
1000	50.232	1.682	51.915
1200	48.708	2.940	51.648
1500	49.180	0.698	49.877
2000	48.250	1.348	49.597
5000	48.307	0.117	48.424

The main reason for this is that, here PhC LTS is placed at the top of the active layer, and thus, performs not only the task of diffracting the high wavelength photons to improve their path length, but also performs the task of effective ARC. Therefore, for thicker cells, PhC LTS performs the task of effective ARC whereas for thinner cells, it performs both the function of diffraction as well as ARC. Due to this effect of the PhC LTS, the BR effect in the cell efficiency enhancement is somewhat less as compared to the previous results [138, 139, 61] and becomes almost negligible for thicker active layers.

We have also compared the efficiency of the proposed PhC LTS based cell with that of the reference planar cell and the Lambertian limit efficiency [141]. The results have been summarized in Table 5.4. The analysis of the results predicts that it is possible to enhance the efficiency of the GaAs cell having 50nm thin active layer to about 26% as compared to the planar reference cell. Percentage enhancement has been calculated taking the efficiency for the PhC LTS based design, η_{LTS} and then that efficiency is compared with the reference planar cell efficiency having same active layer thickness, η_{Planar}. Mathematically enhancement in PhC LTS based cell as compared to reference cell has been derived as:

$$\text{Enhancement in PhC LTS based cell (\%)} = \frac{(\eta_{LTS} - \eta_{Planar})}{\eta_{Planar}} \times 100\% \quad (5.6)$$

This improvement in efficiency in proposed PhC LTS based cell as compared to reference cell, proves the effectiveness of the proposed design and shows the structures better light trapping ability, especially for the thinner cells. As the thickness increases, this efficiency enhancement shrinks and instead of becoming insignificant, becomes constant to about 8%. The reason behind this is basically the better light management of the proposed PhC LTS as an ARC, provides better results than the reference cells even for the thicker cells.

Table 5.4: Cell efficiency comparison of PhC structure based device with planar ARC and BR based device and Lambertian limit for different active layer thicknesses

Active layer thickness (nm)	**Single pass efficiency with losses (η_{bare}) (%)**	**Proposed Cell with PhC structure at top and BR (η_{LTS}) (%)**	**Planar complete cell without PhC structure (η_{Planar}) (%)**	**Improvement in Efficiency by PhC design as compared to planar structure (%)**	**Lambertian Limit efficiency (%)**
50	4.133	9.383	7.432	26.3	25.855
100	7.529	14.004	11.50	21.8	26.011
200	10.428	17.241	15.26	13.0	27.05
500	13.305	21.315	19.23	10.8	28.45
700	14.523	22.733	20.58	10.5	29.177
1000	15.275	23.205	21.36	8.6	29.766
1200	15.475	23.468	21.593	8.7	30.051
1500	15.91	23.846	21.96	8.6	30.384
2000	16.024	23.972	22.11	8.4	30.786
5000	16.271	24.150	22.29	8.3	31.82

5.7. Conclusion

The chapter has presented an optical design optimization for the GaAs cell having 2D PhC LTS at the top assisted by the Al BR at the bottom. It has been shown that by combining the 2D PhC structure with BR, the efficiency of the thin film GaAs cell has been enhanced considerably. For demonstration purpose, the work presented the optimization procedure for the 50nm thin active layer cell, which is equally applicable to other active layer thickness cells. The results are then compared with the Lambertian limits for light trapping as well as those for the single pass and reference planar cell efficiency. Then the analysis of the performance of the proposed structure

has been done, which demonstrated the improved performance for the PhC LTS based cell, in terms of absorption, reflection and variation of incident angle. It is interesting to note that the designed structure retains almost 80% of the normal incidence efficiency even for high angle of incidence and thus provides significant angular performance improvement. This improvement in efficiency is basically accounted to the better index matching, trapping of low energy photons and diffraction of incident light to the active layer provided due to the proposed PhC LTS, and thus provides better coupling for useful absorption. Also, it has been shown that the device provides good fabrication tolerances, which is a quality, allowing the device to be practically realized. Also, the work has presented the analysis of effectiveness of the proposed LTS for various active layer thicknesses and the role of each LTS component in the efficiency enhancement of the cell has been predicted. It has also been shown that the enhancement is more profound for the thinner cells, which is basically due to the contribution from the PhC LTS, providing more than twice the efficiency for a 50nm active layer cell. The contribution of LTS, particularly from BR decreases with increasing thickness of active layer whereas the contribution from PhC LTS almost remains constant for thicker active layer cells, basically due to the ARC function of the PhC LTS. At last the efficiency of the proposed LTS cell has been compared with those of reference planar cell and Lambertian limits. It has been found out that, although the efficiency values achieved are under the Lambertian limits for proposed structure, the results have provided noticeable enhancement than the reference cell, thus could pave the way for future high efficiency TFSC.

Chapter 6

P-I-N InGaN/GaN Solar Cell using Photonic Crystal Light Trapping Structures at Top

6.1. Introduction

The last three chapters have dealt with the simulation and analysis of the PhC LTS effects for the thin film GaAs solar cells, considering PhC structures as a back as well as a front LTS. The results have clearly predicted that the PhC LTS based cells outperform the commonly used planar structures. Moreover, these chapters have set the background for the basic process and methodology involved in calculating various figures of merits including efficiency for PhC LTS based solar cells that can be used for other material combinations as well.

However, as one of the key motive of the Ph.D. work is to experimentally verify the simulation results, it is also desirable to design, grow and fabricate the proposed structures. As mentioned in the initial chapters, due to the limitations encountered with the growth and design of GaAs based structure in the Indian labs during the research work, after discussions with many scientific experts within the reach, it has been decided to explore and study the effects of PhC LTS for InGaN/GaN based solar cell structure, due to the materials uniqueness (will be discussed in succeeding sections) having number of qualities similar to that of GaAs and also since some Indian labs including CSIR-CEERI, Pilani are currently working for the growth and fabrication of InGaN/GaN based devices and have the requisite facilities. As the growth technologies used for the InGaN/GaN material systems are almost similar as used for the GaAs based devices, we decided to move forward towards the design, simulation and fabrication studies for InGaN/GaN based solar cell devices having PhC LTS, which further fulfill the requirement to demonstrate the effectiveness for the PhC LTS for solar cells and also would prove that the effect of PhC LTS

for solar cells are usually not material specific. The work described under this title, has been done under this motivation and predicts the enhancement in the performance of the p-i-n InGaN/GaN solar cell with PhC LTS at the top through simulations. In the next chapter, we will discuss about the design, fabrication and experimental analysis of the PhC LTS based InGaN/GaN solar cell.

As discussed in section 2.5, the main problem with the $In_xGa_{1-x}N$ alloys is its epitaxial growth over GaN/sapphire substrate, due to their lattice mismatch. Thus, there is a limit to the thickness of high-quality $In_xGa_{1-x}N$ epitaxial layers that could be grown on GaN/sapphire substrate, which is only few nanometers, particularly for high Indium containing layers [100]. Therefore, it is still a challenge to achieve $In_xGa_{1-x}N$ absorption layers with low band gap (< 2.0 eV) and large thickness at the same time. Thus, critical thickness, Indium concentration and threading dislocations (TDs) limit the conversion efficiency of $In_xGa_{1-x}N$ alloy based solar cells [101].

This motivated us to explore and analyze the working of a solar cell having p-i-n $In_xGa_{1-x}N$/GaN heterojunction structure having i-$In_xGa_{1-x}N$ as the absorption layer, as this will help in better carrier collection with small active layer thickness. Also, the heterojunction structure in solar cells could help in improving the material quality of $In_xGa_{1-x}N$ alloys with relatively high Indium content by growing thin intrinsic layer. However, because of the practical issues discussed earlier, the studies are contented for the nm $In_xGa_{1-x}N$ alloy thin layers and the analysis has been performed by varying Indium concentration from 10% to 20% in steps of 5%. However, thinning down the active $In_xGa_{1-x}N$ layer up to few nm will ultimately hamper its efficiency, no matter how good the absorption coefficient of the $In_xGa_{1-x}N$ material.

Importance of light trapping phenomenon and need of its study for GaAs thin film solar cells has already been discussed in detail in the previous three chapters including analytical derivation of Lambertian light trapping limits for GaAs thin film cells [24, 131, 141] Now, on the basis of these analytical solutions, here we have also predicted the Lambertian efficiencies for $In_xGa_{1-x}N$ active material solar cells and compare them with bare cell efficiencies as shown in Figure 6.1. The figure shows the comparison of efficiencies for the two structures for a particular thickness of the active material for ideal case (i.e. without any loss) for $In_{0.1}Ga_{0.9}N$, $In_{0.15}Ga_{0.85}N$ and $In_{0.2}Ga_{0.8}N$ alloys, which are used for our study.

Similarly as predicted for GaAs solar cells, it could easily be analyzed from the figure that, an optimized LTS in a thinner $In_xGa_{1-x}N$ cell could provide the same efficiency that could otherwise be achieved with a much thicker cell. As already discussed, the incorporation of the PhC LTS indeed has provided some exciting results [138, 60, 61], but most of these research studies are concentrated on Silicon, Amorphous Si or GaAs materials, thus there is also a need to explore whether these findings are equally applicable for $In_xGa_{1-x}N$ based cells or not.

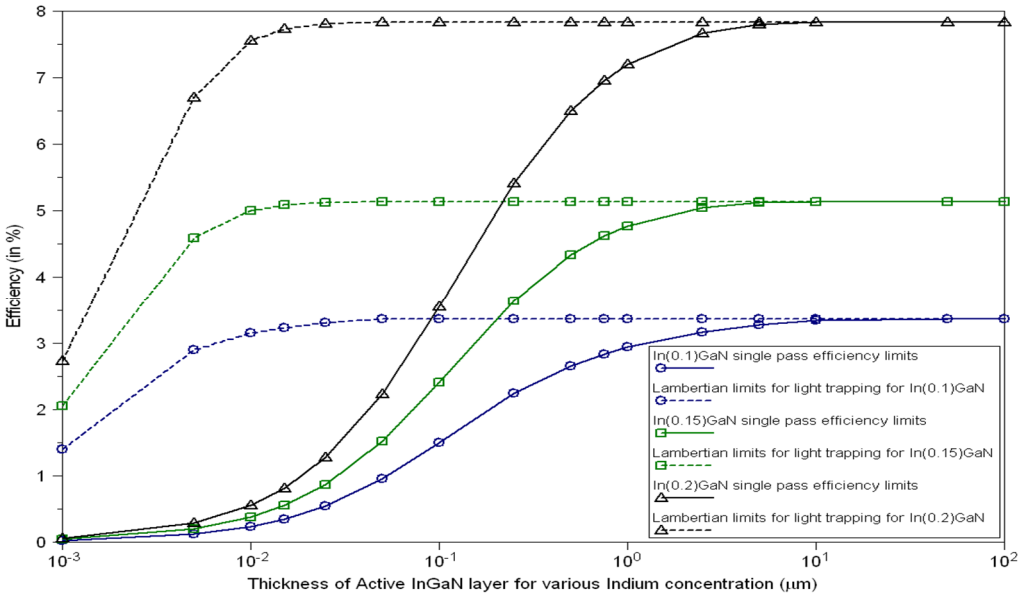

Figure 6.1: Cell Efficiency versus active layer thickness graph for InGaN based solar cell for Indium concentration having 10%, 15% and 20% using AM1.5 solar spectrum [50]. Ideal case is assumed without consideration of any kind of loss.

The chapter, following the same procedure as followed for GaAs thin film cell with adaptations and structural modifications especially required for $In_xGa_{1-x}N$/GaN materials based devices, demonstrates the optical optimizations and analyzes the performance of the LTS consisting of 2D-PhC structure at the top, followed by the hetero-junction structure of i-$In_xGa_{1-x}N$ active layer having layer of GaN immediately above and below of the i-$In_xGa_{1-x}N$ layer. The structure has also been modified by increasing the etching depth of the PhC structure. The two different structures have been compared and analyzed to demonstrate the effectiveness of the PhC structure based LTS. Single layer planar BR of Al is placed at the bottom of the structures. Here, as the PhC structure placed at the top not only helps in the efficient coupling of the incident light to the absorbing layer but also helps in increasing the optical path length for high wavelength photons through diffraction and thus contributes for the improvement in absorption almost throughout the solar spectrum, as already demonstrated in chapter 5.

During the study, different i-$In_xGa_{1-x}N$ layer having Indium content varying from 10% to 20% in steps of 5% with varying thickness has been applied as the active layers. The parameters of the proposed design are taken in such a manner so as to keep them as close to practical values as possible. Here, we have presented the design optimization for the 15 nm thin i-$In_xGa_{1-x}N$ active layer having 10% Indium concentration in a generalized manner, which is also applicable for other thicknesses and Indium concentration of active layers. The study has been performed for two structures: having un-patterned as well as patterned active layer. Although, the structure is not analyzed electrically in this work, optically it demonstrates a significantly enhanced absorption in the desired wavelength range, leading to a notable enhancement in the efficiency.

To calculate absorption in the active layer, RCWA numerical method is used. Also, the performance of the proposed device has been compared with the cell having common planar geometry with ARC and BR having same active layer thickness and also with Lambertian limits. The results show that the appreciable enhancement in the efficiency has taken place in the proposed structures, however the final efficiencies are still under the Lambertian limits.

6.2. Proposed Structure Configuration

Figure 6.2(a) demonstrates the proposed $In_xGa_{1-x}N$/GaN heterojunction cell having PhC LTS at the top extending from the top Indium Tin Oxide (ITO) layer up to p-GaN layer (the structure is almost similar to the structure proposed in chapter 5, with specific adaptations for $In_xGa_{1-x}N$/GaN material system having major modifications in etching depth). Here, we have not used PhC patterning in the active i-$In_xGa_{1-x}N$ layer. The device has 2D PhC LTS at the top having hexagonal symmetry with circular air holes as shown in Figure 6.2(b) [58].

The PhC structure consists of air holes in the ITO background followed by p-GaN window layer. The thickness of the i-$In_xGa_{1-x}N$ layer is kept fixed and taken according to the value of x in $In_xGa_{1-x}N$ alloy, in order to keep the epitaxial nature of the grown layer [100]. Figure 6.2(c) shows the schematic diagram for the proposed PhC LTS based $In_xGa_{1-x}N$/GaN heterojunction cell design having etching depth extended inside the active i-$In_xGa_{1-x}N$ layer. The PhC structure used here is the same as has been used for the structure shown in Figure 6.2(a).

The proposed work consists of only a single planar BR, as the main aim is to study the effectiveness of the PhC LTS at the top and BR has only been used to assist the PhC structure. The single planar Al BR is considered to be as close as possible to be an ideal metallic reflector,

neglecting plasmonic effects at semiconductor-metal interface [63, 143]. ITO has been used at the top to provide good impedance matching for minimizing reflections and absorptions at the top with better conductivity for contacts [138, 126]. The commonly used planar $In_xGa_{1-x}N$/GaN heterojunction cell with planar ITO ARC at the top assisted by the planar Aluminum (Al) BR at the bottom having same thickness as used in its patterned counterparts is used as a reference cell to show the effectiveness of the periodic photonic patterning in the efficiency enhancement.

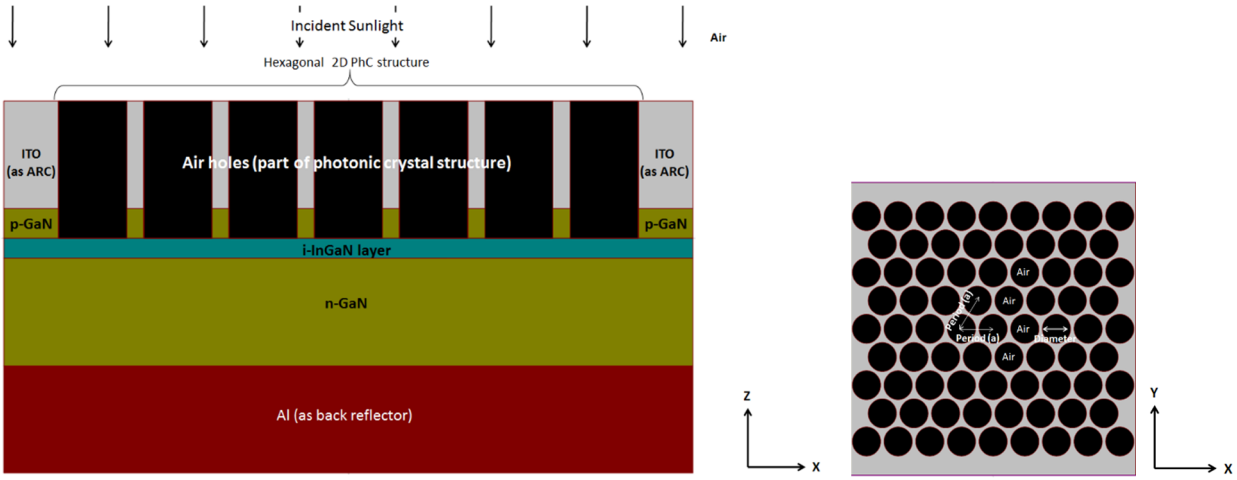

(a) (b)

Figure 6.2: (a) Schematic diagram of the proposed thin film p-i-n InGaN/GaN with PhC LTS at the top (from x-z direction, side view) etched up to p-GaN layer assisted by Al Back reflector without InGaN active layer etched (b) PhC LTS from top view

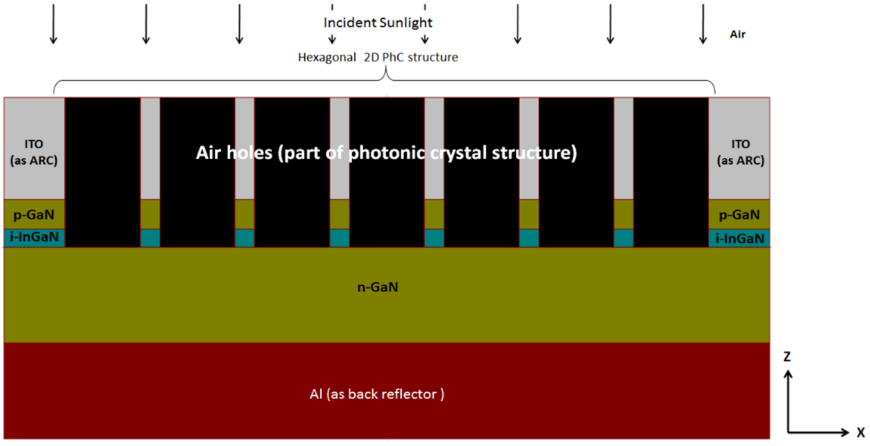

Figure 6.2: (c) Schematic diagram of the proposed thin film p-i-n InGaN/GaN with PhC LTS at the top (from x-z direction, side view) etched up to InGaN active layer assisted by Al Back reflector

6.3. Numerical Approach and Efficiency Calculations

The RCWA method [145] has been used for the calculation of reflections, absorption and transmission through the structures, as described in detail in the chapters 2 and 5. Commercially

available RSoft's DiffractMod software, based on RCWA algorithm has been used to perform the simulation analysis and determine the absorption spectra for the proposed device and then calculated the related parameters based on these results [106, 148].

In order to demonstrate the optical effect of PhC LTS and mechanism behind the light trapping in these structures, the details of the charge carrier collection has been neglected and the internal quantum efficiency has been taken as one. A general expression for the wavelength dependent absorption coefficient for $In_xGa_{1-x}N$ used in the simulation is given in [149], [150] as:

$$\alpha(cm^{-1}) = 1.0x10^5.[C.(E_{ph} - E_g) + D.(E_{ph} - E_g)^2]^{1/2} \quad (6.1)$$

where E_{ph} is the photon energy, C and D are composition dependent parameters, taken from [149], [151] for $In_xGa_{1-x}N$ alloys. E_g is the composition dependent energy band-gap of $In_xGa_{1-x}N$ which is calculated as follows:

$$E_{gInGaN} = xE_{gInN} + (1-x)E_{gGaN} - b.x.(1-x) \quad (6.2)$$

where x is the Indium content, E_{gInN} = 0.7 eV, E_{gGaN} = 3.42 eV and b is the bowing parameter considered as 1.43 [152], [153]. The wavelength dependent model of Adachi has been used for the determination of refractive index, n of $In_xGa_{1-x}N$ [152], [154] as follows:

$$n(E) = [A.(E_{ph}/E_g)^{-2}.\{2 - (1+E_{ph}/E_g)^{1/2} - (1-E_{ph}/E_g)^{1/2}\} + B]^{1/2} \quad (6.3)$$

where $A(In_xGa_{1-x}N)=13.55x+9.31(1-x)$ and $B(In_xGa_{1-x}N)=2.05x+3.03(1-x)$ [150].

Now, on the basis of the above calculated values of refractive index and absorption coefficient for $In_xGa_{1-x}N$ alloys, the solar cell efficiencies could be computed. Also, the wavelength dependent material parameters are considered for Al [142] and ITO [126] materials. To calculate the solar cell efficiency, we have calculated the total optical absorption spectrum, $A(\lambda)$ of the entire device, which is the sum of the absorption spectra within each layer, $A_i(\lambda)$ as $A(\lambda) = \sum_i A_i(\lambda)$. Here, we have considered absorption in the active i- $In_xGa_{1-x}N$ layer as the only useful absorption.

Following this, the same optical performance analysis procedure has been followed as described in previous chapters for the analysis of GaAs thin film cells (kindly refer to section 4.3 of chapter 4 and section 5.3 of chapter 5). Lambertian limit efficiencies predicted in Figure 5.1 for various InGaN concentrations are calculated as per the analytic solutions also described in detail in the chapters 4 and 5. For simulation studies, the absorption integral is taken over from 280 to 1000

nm range. Lower value of the wavelength has been decided as the photon flux below this value is very small in the standard AM1.5 solar spectrum [48], whereas the upper limit has been decided beyond the band gap of the $In_xGa_{1-x}N$ material, to cover the major portion of the spectrum, at room temperature. The absorption is considered to be ceased above the band gap.

6.4. Structural Optimization

This section demonstrates the structural optimization of the proposed structure to derive the optimized parameters for the LTS. As mentioned earlier, the optimization procedure is inherited from previous chapters, with material and structural specific modifications. First the design has been optimized for the design having PhC LTS etched from the top ITO layer up to p-GaN layer followed by optimization for the structure having PhC patterned active $In_xGa_{1-x}N$ layer. Prior to optimization, i-$In_xGa_{1-x}N$ active layer thickness has been fixed to the value as per the Indium concentration, in order to preserve its epitaxial nature [100]. For i-$In_{0.1}Ga_{0.9}N$ alloy case, it has been fixed at 15 nm. All the parameters are kept as close to the practical values as possible. The optimization includes the optimization of the PhC structure period, diameter and etching depth. The Al BR thickness is taken to be close to the quarter wavelength thickness in order to improve reflections from the back, keeping the band gap value of $In_xGa_{1-x}N$ alloy in view [142].

The results for the optimization of the period of the two proposed devices PhC LTS have been shown in Figure 6.3 (a) and (b) respectively. The figures show that the optimal value of period has been found out to be 340 nm for non-patterned active layer structure and 175 nm for patterned active layer structure. This value of period is supposed to maximize the coupling of the incident light to the absorption layer, and thus produces a dense distribution of absorption peaks for the desired wavelength range.

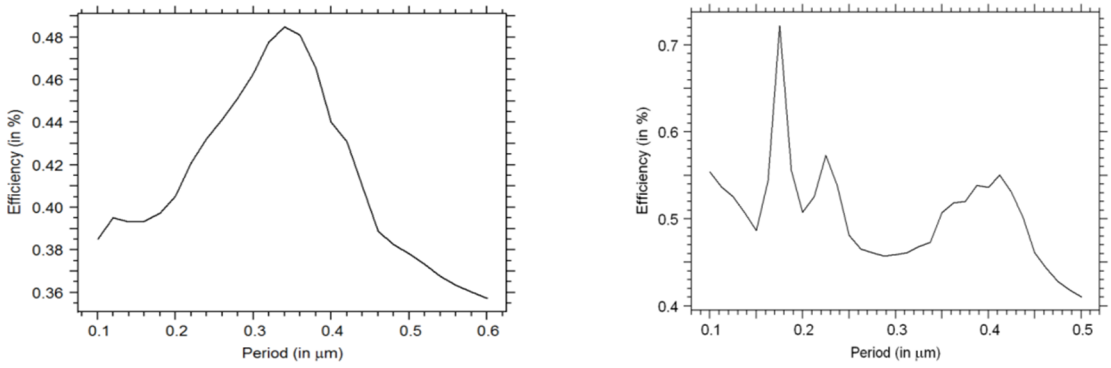

Figure 6.3: Period for PhC structure (a) without patterned i-$In_{0.1}GaN$ layer, (b) with pattern i- $In_{0.1}GaN$ layer

The optimization of the period in patterned $In_xGa_{1-x}N$ layer device provides more peaks and dips due to increase in the depth of PhC structure up to active layer, since oscillations in the absorption layer become stronger [63] as compared to LTS without active layer patterning. Here, as the PhC structure for light trapping is placed at the top, it should not only assist in the trapping of the higher wavelength photons but also helps to maximize diffraction of photons to the absorption layer, minimizing absorption of photons in the front LTS and diffraction in air.

Now, in order to perform this diffraction function, as mentioned earlier, PhC structure period is required to be larger than the wavelength of light in the active layer. As per the $In_xGa_{1-x}N$/GaN material parameters used, this condition is satisfied for value of period, *a* equal to around 100nm. However, there are several such diffraction resonances created within the entire solar spectrum which overlap and lead to overall efficiency improvement [60] (kindly refer to section 5.3 for details).

As discussed in section 5.4, in the case when the incident photons wavelength becomes higher than the period of the PhC patterned structure, instead of behaving as a diffraction grating the structure behaves as a uniform layer, whose effective index is a weighted average of the refractive index of PhC structure, mathematically given by Equation (5.4). The equation can be used for PhC structure in the p-GaN layer and $In_xGa_{1-x}N$ layers beneath and provides an information for the effective index matching of the absorption layer with that of the incident medium.

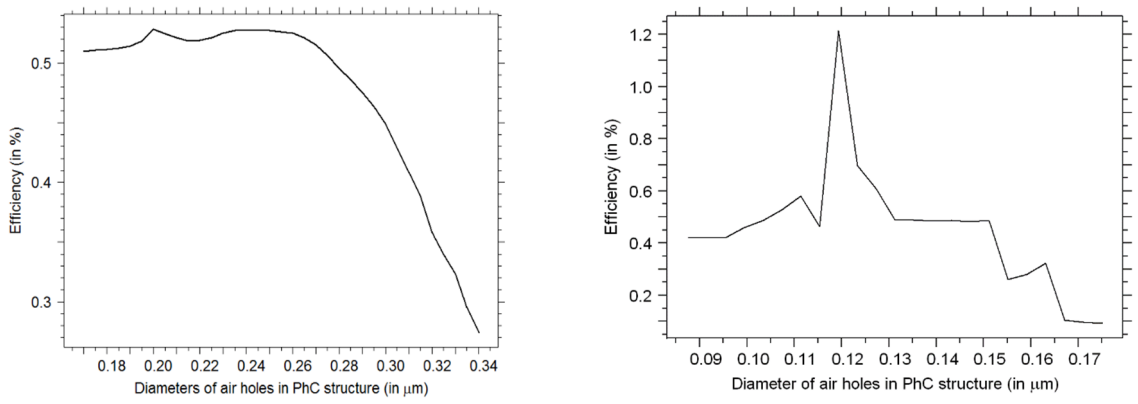

(a) (b)

Figure 6.4: Diameter of air holes in PhC LTS vs. efficiency graph for structure (a) without PhC patterned i- $In_{0.1}GaN$ layer having periodic pattern etched up to p-GaN layer, (b) with pattern i- $In_{0.1}GaN$

Using the effective data values of parameters used in equation (6.4), value of air holes radius could be calculated. The optimization results for the holes diameter has been shown in Figure

6.4(a) and (b) for un-pattrerned and patterned active layer structure respectively, showing the optimized value of diameter of air holes to be about 230nm and 120nm.

The optimization results for the PhC depth in the ITO and p-GaN has been shown in Figure 6.5(a) and (b), respectively. The etching depth of the PhC structure in the active layer patterned device is kept fixed for the entire active layer, which is 15 nm in demonstrated case of $In_{0.1}Ga_{0.9}N$ alloy. It is required that the depth of the PhC LTS should be such that the coupling of light to the active layer is maximized and specularly reflected beam from PhC into the air is minimized. Also, it is required that the proposed PhC should guide as much incident light as possible to the absorbing layer with negligible absorption. From Figure 6.5(a), this optimal value of the PhC structure thickness with ITO background is found out to be around 85 nm, whereas the optimal thickness of the etched PhC pattern in p-GaN window layer has been found out to be 25 nm. Thus the total etching depth for the PhC structure in $In_{0.1}Ga_{0.9}N$ alloy based structure for un-patterned active layer structure has become 110 nm whereas in case of patterned PhC structure this value increases to 125 nm including the thickness of active layer.

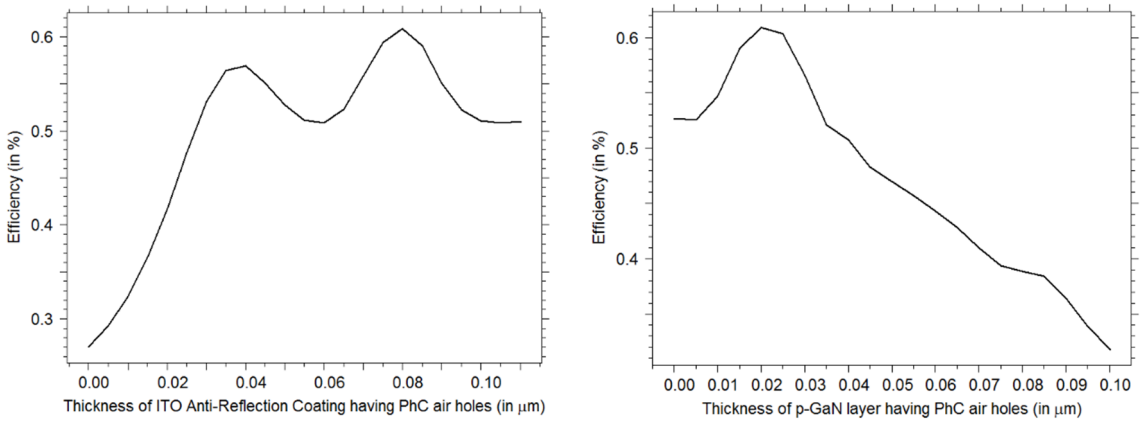

(a) (b)

Figure 6.5: Thickness vs efficiency graph for (a) ITO ARC layer having PhC LTS with air holes, (b) p-GaN layer having PhC LTS with air holes

In case of non-patterned active layer case, appropriate etching thickness, perturbs the slab guided modes and the PhC grating makes them accessible from an incident radiation [63]. The condition is similar to the diffraction grating, which deflects the normally incident light to the oblique direction and thus increases the path length for that wavelength photons. The diffracted waves propagate at nearly grazing angle within the material, with a large propagation path, thus improves absorption within the active layer for the wide spectral range. Thus, the role of the PhC

LTS is to couple the incident radiation field to the guided slab modes, without significantly varying the modes themselves. Increase in this etching thickness might substantially increase the absorption in the PhC LTS, and thus decreases the light coupling and ultimately efficiency [63].

However, in case of patterned active layer, the case is different and more complicated than the un-patterned case [63]. Here, the patterned layer is used to absorb the incident light, instead of just coupling it to the absorbtion layer. Here, the fraction of absorbed energy in the patterned layer shows strong oscillations with pronounced peaks and dips, as clearly evident from Figure 6.4(b) and 6.5(b). These oscillations point to an alternation of modes concentrated in the patterned active layer. In patterned active layer structure, it is possible to use the resonances that take place inside the PhC structure to enhance absorption, which otherwise are considered as loss, if not coupled to underlying active layer as in case of un-patterned active layer. Thus, the configuration, theoretically should provide better results as compared to unpatterned structure, which is also validated through our results presented in succeeding sections. The optimization of n-GaN layer has been shown in Figure 6.6, which provides the optimal value of the layer around 80 nm equally applicable to both patterned and un-patterned active layer designs.

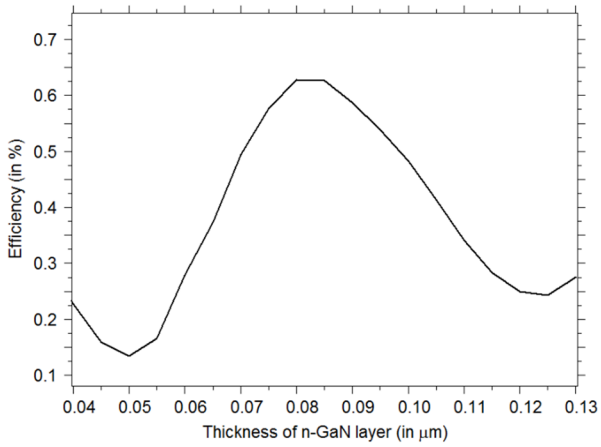

Figure 6.6: Thickness vs efficiency graph for n-GaN layer below active i- $In_{0.1}GaN$ layer,

This completes our design optimization for $In_{0.1}Ga_{0.9}N$/GaN PhC LTS based cell having 2D PhC design used at the top with un-patterned and periodically patterned $In_{0.1}Ga_{0.9}N$ layer. The optimized parameters are summarized in Table 6.1 and 3D schematic of the optimized structure is shown in Figure 6.7. The same optimization process has also been followed for other $In_xGa_{1-x}N$ alloy based active layer in the proposed solar cell structure.

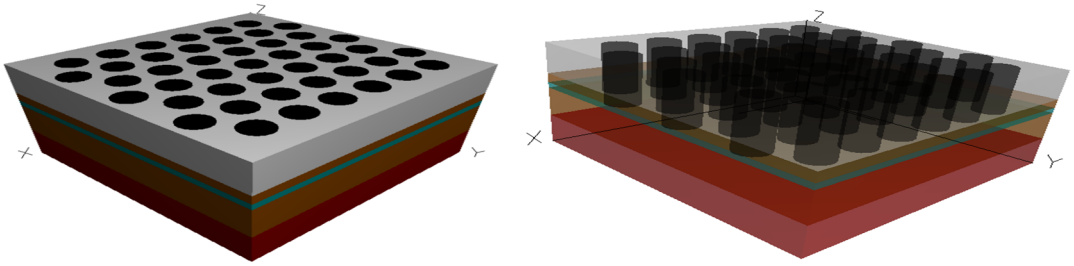

(a) (b)

Figure 6.7: 3D view of the final proposed PhC LTS based thin film p-i-n $In_xGa_{1-x}N$ /GaN cell with pattern (a) outside view; (b) inside view

Table 6.1: Optimized parameter values used for the efficiency calculations for the proposed structure having p-i-n InxGa1−xN absorbing layer with PhC for various Indium concentration without active layer patterning

Layer type	**Doping (cm^{-3})**	**Thickness (in nm) in z direction**					
		In(0.2)GaN		In(0.15)GaN		In(0.1)GaN	
		Un-patterned active layer	Patterned active layer	Un-patterned active layer	Pattern-ed active layer	Un-patterned active layer	Patterned active layer
Chromium/Gold (Cr/Au) for p-type contact	--	100/20	100/20	100/20	100/20	100/20	100/20
Indium Tin Oxide (ITO) as Anti Reflection Coating with PhC patterning	--	90	90	90	90	85	85
p-GaN having PhC patterning	$5*10^{+17}$	25	25	25	25	25	25
i-$In_xGa_{1-x}N$	10^{16} (naturally n-type)	5	5	10	10	15	15
n-GaN	$5*10^{+18}$	100	100	90	90	80	80
Aluminium (Al) which serves as both back reflector	--	60	60	55	55	50	50
Chromium/Gold (Cr/Au) for n-type contact	--	100/20	100/20	100/20	100/20	100/20	100/20
Period or lattice constant of the hexagonal lattice PhC structure having air holes	--	400	240	390	220	340	175
Radius of the air holes	--	180	95	150	88	115	60
Height of the air holes required to be etched	--	115	120	115	125	110	125
Sapphire substr. (c-plane)	--	250 um					

6.5. Performance Analysis of the Proposed Configuration

The section discusses the performance of the proposed structures with $In_{0.1}Ga_{0.9}N$ active layer with reference to the planar reference structure. The performance has been demonstrated and discussed in terms of the J-V curve, spectral distribution as per AM1.5 solar cell spectra, quantum efficiency and angular performance with variation in incident light angle.

6.5.1. J-V Curve Analysis

The J-V curve for both the proposed structure has been shown in Figure 6.8. It is clear from the graph that, the proposed structure having PhC LTS extended up to the active layer, outperformed the reference structure as well as the structure having PhC LTS without active layer patterning. The structure with patterned active layer provides 1.2214% efficiency as per our calculations, which is way ahead of the efficiency for the proposed structure without un-patterned active layer having PhC at the top layer (0.628%) and planar reference efficiency (0.405%).

The reason for the increase in the efficiency is basically the increase in the light trapping in the proposed structures. Among the two proposed structures, the structure having periodically patterned active layer performs better than the un-patterned one, as in the patterned active layer, the increase in light matter interaction takes place, which allows the light resonances in the PhC structure for useful absorption instead of losing that light due to coupling to the incident medium through diffraction as in case of un-patterned active layer. Also the patterned active layer structure would provide better index matching due to PhC incorporation in the active layer. Thus, the patterned active layer structure would allow the absorption of high wavelength photons in a better way as compared to the un-patterned active layer structure. The case will become clearer through the spectral distribution and quantum efficiency graph that follows.

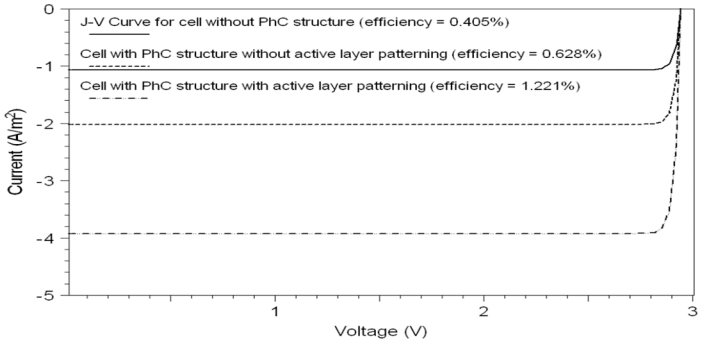

Figure 6.8: Solar Cell J-V curve comparison between the PhC patterned and non-patterned proposed solar cell having p-i-n $In_{0.1}Ga_{0.9}N$ /GaN structure with and without active layer patterning

6.5.2. Analysis for Spectral Distribution

The spectral distribution curve for the two proposed structures and the planar reference cell has been shown in Figure 6.9. Here, one could observe that the reason for the comparatively low efficiency, for all the structures, is the low band gap of $In_{0.1}Ga_{0.9}N$ layer, due to which, the major portion of the solar spectrum is lost without absorption. In order to increase this absorption limit, one has to increase the Indium content in the $In_xGa_{1-x}N$ layer, keeping the epitaxial nature of the structure. However, here our basic motive is to show the effectiveness of the PhC LTS, so we limit ourselves on the study of the effect of PhC LTS on $In_{0.1}Ga_{0.9}N$ layer based solar cell. From, the figure, it is clear that the absorption of the spectrum is better in case of patterned active layer structure. As compared to the reference cell, the proposed structure having PhC at the top without active layer pattern, provides enhancement throughout the spectrum, as here PhC LTS is placed at the top.

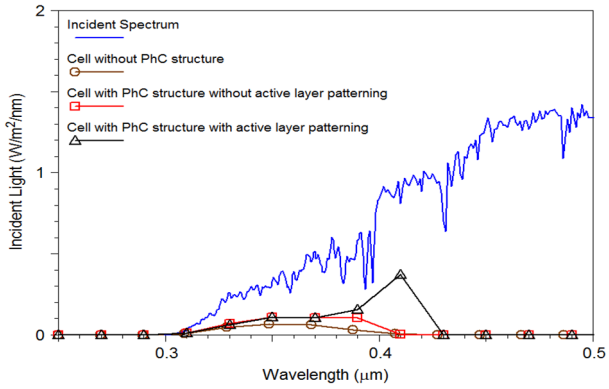

Figure 6.9: Calculated spectral distribution graph for the incident solar spectrum [50] for the proposed i-$In_{0.1}Ga_{0.9}N$ active layer cell with PhC LTS and its comparison with the reference cell having same active layer thickness.

6.5.3. Quantum Efficiency Analysis

The quantum efficiency graph for the three structures has been shown in Figure 6.10. The figure describes the behavior of the structures at different incident wavelength photons. It is clear from the figure that the structure with PhC LTS provides better quantum efficiency throughout the absorption spectrum as compared to the planar reference structure. Between the two PhC pattern structures, the structure with active layer pattern provides better efficiency on account of increase in light matter interaction which would provide better diffraction of high wavelength photons and thus ultimately increase the optical path length of these photons and allow them to be absorbed in the active layer as their optical path length then become more the absorption depth required to absorb these photons.

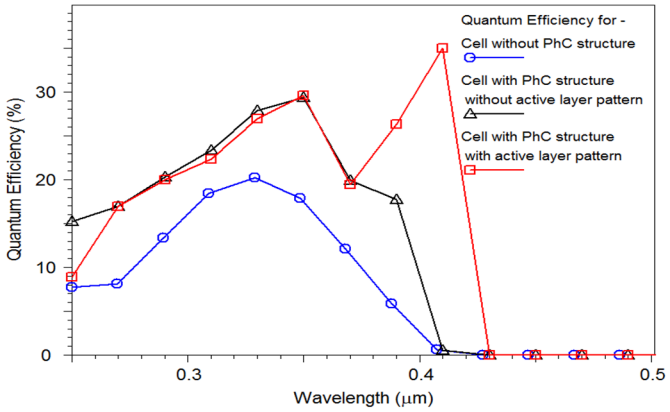

Figure 6.10: Calculated quantum efficiency graph for the incident solar spectrum [50] for the proposed i- $In_{0.1}Ga_{0.9}N$ active layer cell with PhC LTS and its comparison with the reference cell having same active layer thickness.

6.5.4. Analysis with Incident Angle Variation

The performance of the proposed structures with respect to the variation in incident angle has also been studied, as shown in Figure 6.11. The results here too predict and demonstrate the better performance for the structure having active layer patterned as compared to the un-patterned active layer structure. Although the studies predict the better performance throughout the incident light angle for the structure having active layer patterning, it also shows that with increase incident angle its performance degrades early as compared to the structure without active layer patterned, which is able to perform almost equivalent to the normal incidence up to about 75° or so, retaining nearly 80% of the normal incidence efficiency.

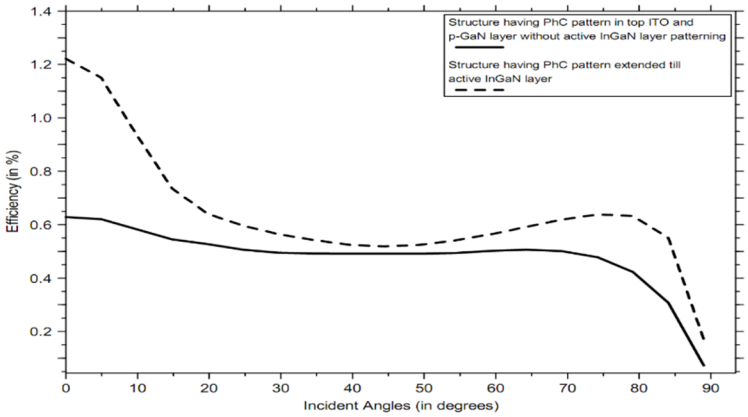

Figure 6.11: Incident angle Vs. Cell Efficiency graph for proposed i-$In_{0.1}GaN$ active layer based p-i-n $In_{0.1}GaN$ /GaN cell structure with and without PhC patterned active layer

The reason for this might be the early breaking of the symmetry for the structure having active layer patterning with the change in the incident angle, which might increase the reflections from the top. Thus, in order to reduce this degradation, one has to look for the structure which would provide better symmetry for all the directions as compared to the presented structure.

6.6. Performance Analysis of the Proposed Structure for Different Indium Concentration in $In_xGa_{1-x}N$ in the active layer

The section analyzes and lists the efficiency of the various solar cell configurations used in the chapter, with varying Indium content. Table 6.2 enlists the values of efficiency achieved as per our calculations, for the proposed structures and compares them with the reference planar cell values. From the table, we can see that the basic reason for increase in the efficiency of the proposed cell is the increase in the short circuit current in the proposed structures, which is basically due to the increase in the absorption of incident photons.

Table 6.2: Results obtained for the proposed p-GaN/i-$In_xGa_{1-x}N$/n-GaN based structure with PhC patterning on top

Structure Type	Various Indium content	Shado -wing effect	Collection efficiency	Voc (in V)	Jsc (in A/m^2)	Vm (in V)	Jm (in A/m^2)	Fill factor (%)	Effi. (%)
Proposed cell with PhC patterning in the top ITO, p-GaN and active $In_xGa_{1-x}N$ layers	In(0.2)GaN	6%	90%	2.55	10.638	2.43	10.526	94.379	2.8441
	In(0.15)GaN	6%	90%	2.75	7.049	2.63	6.98	94.715	2.04
	In(0.1)GaN	6%	90%	2.95	3.9228	2.8284	3.8873	95	1.2214
Proposed cell with PhC patterning in the top ITO and p-GaN layers	In(0.2)GaN	6%	90%	2.55	8.477	2.43	8.387	94.379	2.2661
	In(0.15)GaN	6%	90%	2.75	4.519	2.63	4.41	94.715	1.34
	In(0.1)GaN	6%	90%	2.95	1.9388	2.8284	1.9212	95	0.6283
Proposed cell without PhC patterning	In(0.2)GaN	6%	90%	2.55	2.224	2.43	2.20	94.379	0.5945
	In(0.15)GaN	6%	90%	2.75	2.368	2.63	2.345	94.715	0.685
	In(0.1)GaN	6%	90%	2.95	1.3018	2.8284	1.29	95	0.4053

Although, with increasing Indium concentration in $In_xGa_{1-x}N$ layer, V_{oc} decreases on account of decreasing band gap of $In_xGa_{1-x}N$ alloy, but the loss is compensated by the increase in the value of J_{sc}, which is basically due to the more number of photons now available from the solar spectrum for the higher Indium content to contribute to electron-hole pair generation. However, in the case of planar reference cell it is not true, as could be seen from the table where although

the J_{sc} value increases for the 15% Indium content but reduces for 20% Indium content. This happens basically due to reduction in thickness of the active layer considered, with increasing Indium content, to keep the epitaxial behavior of the practical structure. However, for patterned proposed cells, the case is slightly different. In PhC LTS based cells, with the increase in Indium concentration, band gap of $In_xGa_{1-x}N$ alloy increases, thus more solar spectrum becomes available for absorption and here PhC LTS plays a vital role to improve the absorption of those photons which otherwise cannot be absorbed due to all the mentioned reasons described in the previous sections.

The results listed in Table 6.3 (graphically shown in Figure 6.12), compare proposed cell values with that of the Lambertian limits and ideal bare cell efficiency considering $In_xGa_{1-x}N$ layer of same thickness and Indium concentration. From the table, it is clear that the light trapping in the cell improves its performance as compared to devices without LTS. Between the two proposed PhC LTS designs, the LTS with the active layer patterning provides better performance as compared to the unpatterned active layer LTS. The similar trend follows for different Indium content cells with PhC LTS. However, the table also predicts that the efficiency values for the proposed cells are still under the Lambertian limits.

Table 6.3: List of the comparison of proposed InGaN/GaN based solar cell structure efficiency with that of the Lambertian Limit and single pass efficiency for various Indium concentration used.

Indium Content in InGaN (%)	**Thickness of InGaN active layer used in the proposed structure (in nm)**	**Lambertian Limit Efficiency (%) for same thickness and Indium concentration**	**Efficiency with PhC patterning in active InGaN layer (%)**	**Efficiency with PhC patterning at top with unpatterned active layer (%)**	**Efficiency without PhC patterning (%)**	**Single pass Efficiency (ideal, without considering losses) (%)**
10	15	3.2316	1.2214	0.6283	0.4053	0.3465
15	10	5.0089	2.04	1.34	0.685	0.3794
20	5	6.7049	2.8441	2.2661	0.5945	0.2861

On the basis of the above analysis, we could say that the proposed structures have the ability to improve the efficiency of the $In_xGa_{1-x}N$/GaN heterojunction cell although further improvement is possible to approach Lambertian limits. On the basis of the optical analysis of the presented LTS, the main strategies that can be proposed for the future design of more efficient thin film cells with a photonic pattern include design to reduce reflection losses from the top, increase in the trapping of high wavelength photons and reducing diffraction in air.

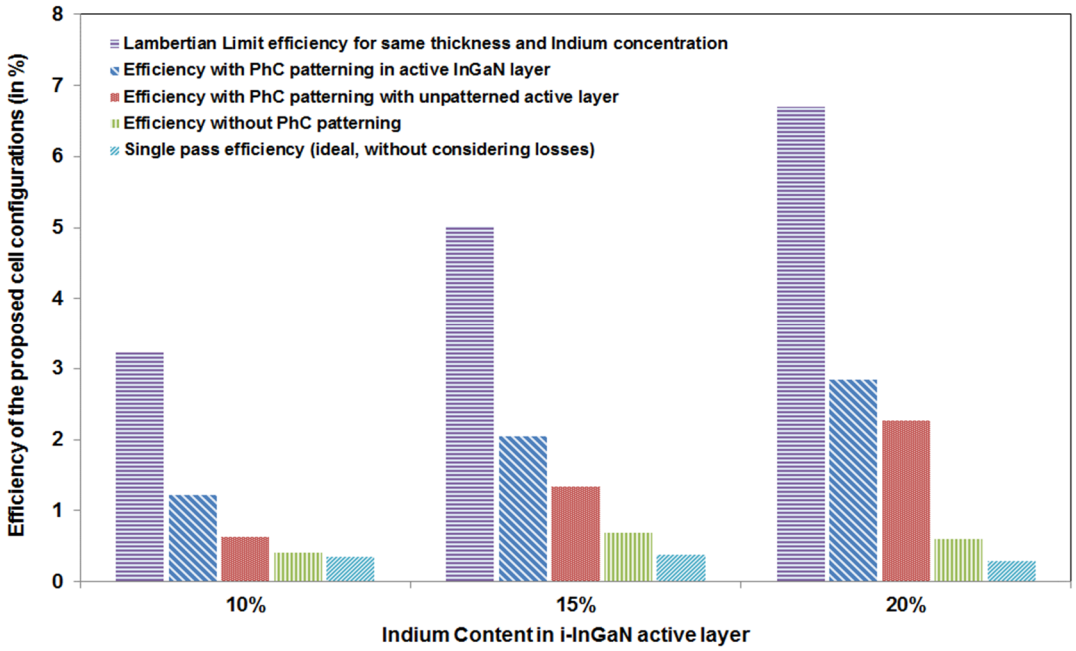

Figure 6.12: Graphical representation for the efficiency enhancement in the p-i-n $In_xGa_{1-x}N$/GaN solar cell due to PhC structure with varying Indium composition and its comparison with Lambertian limits

6.7. Conclusion

The chapter presented the design and optical optimization of the PhC LTS in $In_xGa_{1-x}N$/GaN heterojunction solar cell assisted by the Al BR. The work has presented two designs for the PhC LTS, where etching depth for the periodic structure is kept to the top of the active layer whereas in another etching depth is increases to inside the active $In_xGa_{1-x}N$ layer. The chapter presented the optimization procedure for the $In_{0.1}Ga_{0.9}N$ active layer based cell in a generalized manner, which is equally applicable to other Indium content and thickness cells. It has been shown that the PhC LTS based cell provides better efficiency as compared to the planar reference cell and between the two proposed structures, the device with active layer patterned performs better as compared to un-patterned active layer structure. The results are compared with the Lambertian limits as well as those for the single pass and reference planar cell efficiency. It has been found out that the efficiency values achieved for proposed structure are higher than that of the reference cell. The studies are also carried out for other Indium concentrations show similar trend.

Chapter 7

Design and Fabrication of p-i-n Superlattice based InGaN/GaN Solar Cells using Photonic Crystal Light Trapping Structure

7.1. Introduction

The previous chapter explored and presented the design and optical simulation analysis of the effects of top PhC LTS for p-i-n $In_xGa_{1-x}N$/GaN solar cells. The chapter theoretically demonstrated the enhancement in the performance of the $In_xGa_{1-x}N$/GaN based cell having PhC structure at the top. This chapter takes a step further and demonstrates the experimental analysis through design and fabrication of the PhC LTS for slightly modified design with $In_xGa_{1-x}N$/GaN superlattice active layer.

$In_xGa_{1-x}N$/GaN superlattice structure as the absorption layer instead of thick $In_xGa_{1-x}N$ layer, would help in improving the material quality of $In_xGa_{1-x}N$ alloys with high Indium content and would exhibit better device performances compared with those of devices with an $In_xGa_{1-x}N$ single layer as the active layer [155, 156], as presented in last chapter. Although optical simulations predict better performance for the single layer structure, electrically due to its inherited disadvantages, superlattice structure are expected to provide better performance in practice.

Although superlattice structure provides better performance than the single layer structure, the efficiency of these $In_xGa_{1-x}N$/GaN based solar cells are still very low as compared to other material cells and well under few percent. Here, we are presenting experimental analysis of the effect of PhC LTS on $In_xGa_{1-x}N$/GaN superlattice active layer based solar cells, as to the best of

our knowledge, till date no literature has provided details of the experimental analysis for such kind of a structure.

Here, the chapter proposes a p-i-n solar cell device having $In_{0.18}Ga_{0.82}N$/GaN superlattice structure as active layer accompanied by the PhC LTS at the top. The absorption layers were divided into ultra-thin intrinsic $In_{0.18}Ga_{0.82}N$/GaN (well/barrier) superlattice layers. The small thickness of the active $In_xGa_{1-x}N$ layer will ultimately hamper its efficiency, no matter how good the absorption coefficient of the $In_xGa_{1-x}N$ material. Thus, in order to improve the performance of this cell, hexagonal PhC LTS has been incorporated at the top of the cell with air holes in the Indium Tin Oxide (ITO) and p-GaN layer. As already demonstrated through simulations, the PhC structure at the top, not only helps in reducing the reflections from the top, especially for high energy photons but also helps in increasing the optical path length for high wavelength photons through diffraction [60, 61]. In the subsequent sections, we will discuss the design; simulation and fabrication methodologies adopted and then analyze the results for the proposed structure. The results have shown that although the resultant efficiencies are low, still the PhC LTS incorporated at the top significantly improved the performance of the device.

7.2. Proposed Structure Architecture

The schematic diagram of the proposed p-i-n $In_{0.18}Ga_{0.82}N$/GaN superlattice structure based solar cell having PhC LTS at the top has been shown in Figure 7.1. The sunlight is assumed to be incident from top of the structure, perpendicular to the plane of PhC periodicity. The structure consists of anti-reflection coating (ARC) of ITO as a top layer, followed by p-GaN layer. The superlattice structure is sand-witched between the p and the n type GaN layer.

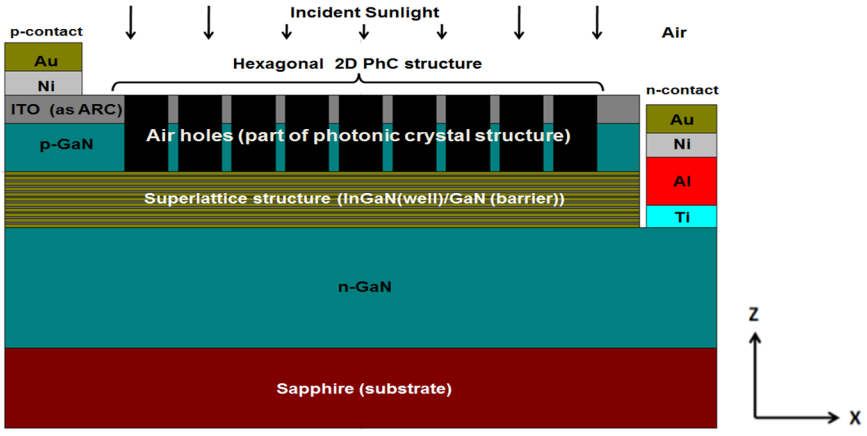

Figure 7.1: Schematic diagram of the proposed InGaN/GaN superlattice structure based solar cell with PhC patterning (not on scale).

The two dimensional (2D) PhC structure has been designed to have hexagonal pattern having air holes in high dielectric background. The proposed PhC structure depth extends from the top ITO layer till p-GaN layer above the superlattice structure. The schematic diagram of the proposed PhC and superlattice structure is shown in Figure 7.2(a) and (b), respectively. The proposed structure is considered to be grown on c-plane sapphire (0001) substrate. 2D PhC structure having hexagonal structure with circular air holes is shown in Figure 7.2(a). The absorbing superlattice structure consists of intrinsic $In_xGa_{1-x}N$/GaN pair having respective thickness of 2 nm and 7 nm. Total 10 pairs of i- $In_xGa_{1-x}N$/GaN have been used to provide total superlattice layer thickness of about 90 nm, as shown in Figure 7.2 (b). Here, we are proposing the front contacts for the design as shown in Figure 7.1; since these contacts are less complicated from the fabrication point of view. For p-type ohmic contact we have used Ni/Au whereas for n-type contacts Ti/Al/Ni/Au has been used. The other details of the structure are listed in Table 7.1.

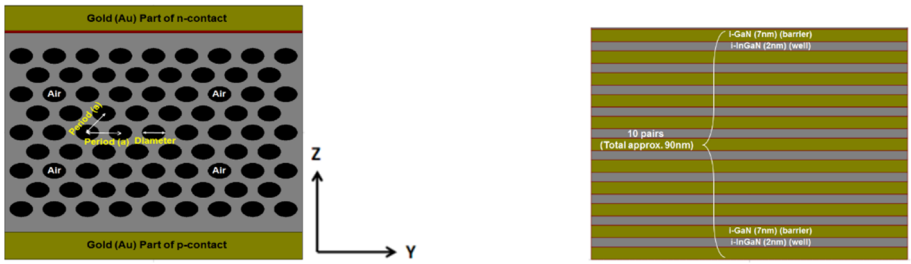

(a) (b)

Figure 7.2: (a) Schematic diagram of the proposed structure with PhC structure (top view) (b) Superlattice structure of the proposed solar cell (used in both planar and PhC patterned structures), with 10 pairs of InGaN (2nm)/GaN(7nm).

7.3. Numerical Methodology Adopted

Following the same trend from the past few chapters, to numerically analyze the design, Rigorous Coupled Wave Analysis (RCWA) method [144, 145] has been used for the calculation of reflections, absorption and transmission through the structure. Commercially available RSoft's DiffractMod software, based on RCWA algorithm has been utilized to perform the 3D simulation analysis for the proposed device [106]. Quantum well effects are incorporated into the design using RSoft's LaserMOD tool. The electrical losses have been incorporated through averaged loss in collection efficiency and through shadowing effects.

The same general expressions, as described in the chapter 6, have been used for the calculation of wavelength dependent absorption coefficient, α, composition dependent energy band-gap, E_g and refractive index for $In_xGa_{1-x}N$ during simulation studies (equation (6.1) to (6.3)). On the

basis of the above equations, the values of refractive index and absorption coefficient for $In_{0.18}Ga_{0.82}N$ alloys have been calculated. The wavelength dependent material parameters are considered for ITO [126] and sapphire [157]. Using the above calculated values, the final cell efficiency has been derived through calculating the total optical absorption spectrum of the entire device through RCWA method, which is the sum of the absorption spectra within each layer. We have considered absorption in the active superlattice layer as the only useful absorption. We have considered 85% collection efficiency whereas shadowing effects are considered to be 10% in order to take the results close to practicalities as possible.

Following these assumptions, the same optical simulation process, as described in previous chapters has been utilized for the theoretical analysis of the presented structure. The simulation analysis is taken over the spectrum range from 280 to 1000 nm in steps of 1 nm. As mentioned in the previous chapter, the photon flux below 280 nm is almost negligible in the standard AM1.5 solar spectrum [48] to effect the final efficiency, whereas the upper limit (1000 nm) has been decided beyond the band gap of the $In_xGa_{1-x}N$ material, to cover the major portion of the spectrum, at room temperature. The absorption is considered to be ceased above the band gap. On the basis of the above mentioned numerical procedure, the optimization of each and every parameter related to the proposed design has been done keeping superlattice layer thickness and sapphire substrate thickness fixed (for detailed optimization procedure kindly refer to chapter 6 and is not discussed here as the main focus of the work is the experimental analysis of the proposed design and to check the validity of the theoretical findings). The optimized parameters are listed in Table 7.1 and the 3D schematic diagram of the proposed structure is shown in Figure 7.3 (a) and (b).

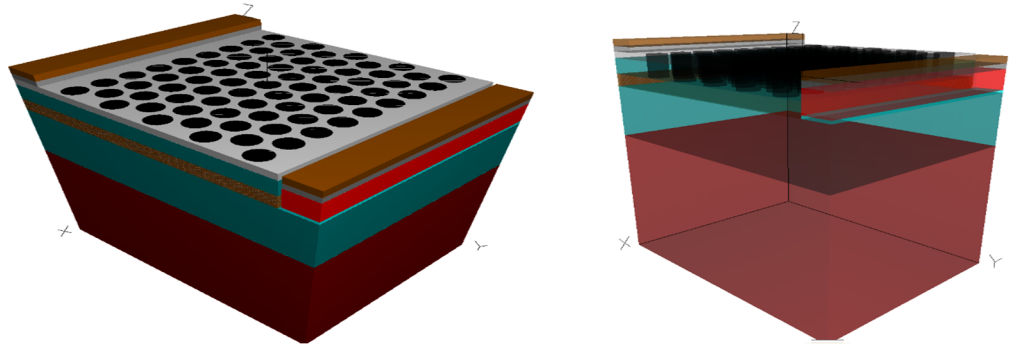

(a) (b)

Figure 7.3: 3D view of the final proposed PhC based superlattice structure with PhC LTS (a) outside view; (b) inside view

Table 7.1: Optimized parameter values used for the efficiency calculations for the proposed structure having $In_xGa_{1-x}N/GaN$ superlattice absorbing layer with PhC patterning at the top layer

S.No.	Layer type		Doping (cm^{-3})	Thickness (in nm) in z direction
1.	Nickel/Gold (Ni/Au) for p-type contact		----	40/50
2.	Indium Tin Oxide (ITO) as Anti Reflection Coating at top		----	80 (having PhC patterning)
3.	p-GaN layer below ITO (Mg doped)		$5*10^{+17}$	120 (having PhC patterning)
4.	Superlattice structure with 10 pairs having total thickness of approx. 90nm	i-$In_{0.18}Ga_{0.82}N$	10^{16}(naturally n-type)	2
		i-GaN	10^{+16} cm^{-3}	7
5.	n-GaN (Si doped)		$5*10^{+18}$	4×10^{3}
6.	Sapphire (c-plane-0001)		----	500×10^{3}
7.	Titanium/Aluminum/Nickel/Gold (Ti/Al/Ni/Au) for n-type contact		----	20/150/40/50
8.	Period or lattice constant of the hexagonal lattice PhC structure having air holes		----	300
9.	Radius of the air holes		----	110
10.	Height of the air holes required to be etched		----	200

7.4. Experiment

Samples used in the work were grown on c-plane (0001) sapphire substrate using metal organic chemical vapor deposition (MOCVD) system (for details kindly refer to section 2.7). First a GaN nucleation layer was deposited over the sapphire substrate followed by GaN buffer layer and p-i-n structure [99, 155]. The p-i-n structure consist of Si doped n-GaN layer of 4 μm thickness, 10 stacks of superlattice structure with $In_{0.18}Ga_{0.82}N$ well (2 nm) and GaN barrier (7 nm) layers followed by Mg doped p-GaN layer of 120 nm. Immediately after the deposition of p-GaN rapid thermal annealing (RTA) was done in order to activate the acceptor dopants in N_2 environment at 700°C for 1 min. Indium content was found out to be about 18% using x-ray diffraction analysis. The carrier concentrations used for p-GaN and n-GaN layers were around 5×10^{17} and $5 \times 10^{18} cm^{-3}$ respectively. The superlattice structure has been grown at 800°C.

Mesa etching was done on the sample to form n-contact to n-GaN and then, n-contacts (finger configuration) were designed using Ti/Al/Ni/Au (20/150/40/50) by e-beam evaporation process and photolithography process using appropriate masking [158]. Then, ITO of 80 nm was

deposited on the top of the p-GaN using RF sputtering at 400°C at 27 mTorr in N_2 atmosphere followed by RTA at 550°C for 3 min. ITO layer does the function of anti-reflection coating (ARC) and current spreading layer at the top. Finally, ohmic contacts were designed using Ni/Au (40 nm /50 nm), which were deposited on ITO layer using the same process as given for n-contact designing except the metallization process and work as p-contact [159]. The fabricated solar cell device structure was of the size 1×1 mm^2.

Next, the fabrication of the hexagonal 2D PhC LTS on the top ITO and p-GaN layers has been done with e-beam lithography (EBL) process using Raith e-line plus system (for details kindly refer to section 2.7). The diameter of the air hole was 220 nm and period was 300 nm. The sample was etched with RIE using BCl_3, Cl_2 and Ar chemistry to provide the overall PhC LTS depth of 200 nm through top ITO and p-GaN layers.

7.5. Results and Discussions

The absorption and reflectance spectra for the simulated structures have been shown in Figure 7.4 and 7.5 respectively. Figure 7.4 compares the absorption spectra for cell with and without PhC LTS. Maximum absorption of the available photons in the active layer has been considered as unity. Results clearly indicate the superiority of cell with PhC structure, throughout the spectral range of interest.

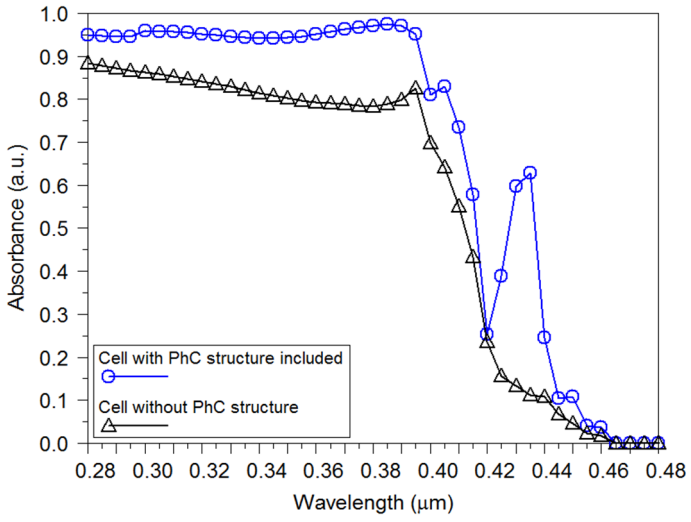

Figure 7.4: Calculated absorption spectra for the proposed cells.

The enhancement in absorption accounts to reduction in reflection from the top of the cell due to proposed PhC LTS for low wavelength photons (between 280 nm to 400 nm), the concept become clearer through Figure 7.5. Absorption drops near the band edge due to limited thickness

of active layer, still, for these high wavelength photons (beyond 410 nm till band gap), there is improvement in absorption due to increase in optical path length of these otherwise unabsorbed photons (sharp peak around 430 nm), as discussed before. Figure 7.5 demonstrates the reflection spectra for the proposed structure with PhC LTS and compares the result with structure without PhC LTS. The figure clearly shows the notable reduction in reflections from the top for the lower wavelength region, in comparison to the design without PhC LTS. However, the reflections from both the structures increase for high wavelength photons near band edge, still the average reflections from the proposed PhC LTS is found out to be less than the reference structure.

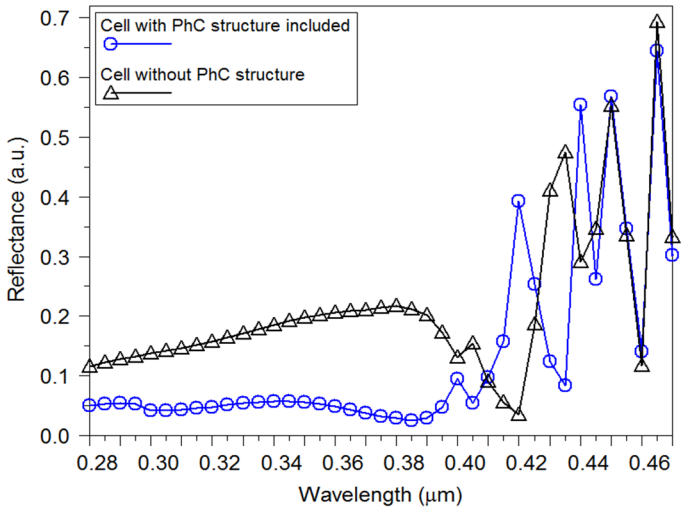

Figure 7.5: Calculated reflection spectra for the proposed structures.

Room temperature photoluminescence (PL) spectra for the grown sample of $In_{0.18}Ga_{0.82}N/GaN$ superlattice solar cell structure is shown in Figure 7.6. The excitation source of 266 nm was used and excitation power was kept at 350 μW, small enough to avoid screening of the internal electric field [160].

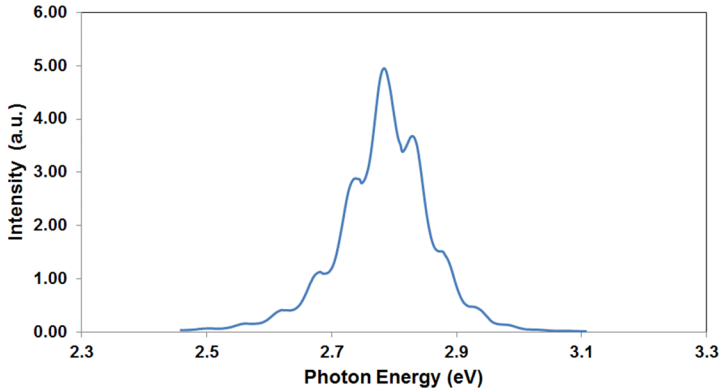

Figure 7.6: Room Temperature Photoluminescence spectra for the proposed $In_{0.18}Ga_{0.82}N/GaN$ superlattice solar cell structure.

The peak for the PL is at 446.2nm (2.78 eV) having full width at half maximum (FWHM) of 20 nm, indicates about 18% presence of Indium in GaN matrix [161]. Fabry Parot interference patterns could easily be observed through local peaks indicating the better surface quality of the final structure. The results thus indicate that the InGaN/GaN solar cells with the superlattice have good crystalline quality [162, 163].

The results from reciprocal space mapping (RSM) measurement is shown in Figure 7.7. Pendellösung fringes are clearly visible from the figure, which would otherwise be absent, if the grown hetero-epitaxial layers results in of poor interface quality and non-uniform thickness [43]. As the structural defects enhanced and the device quality degrades, the observation of Pendellösung fringes in RSM would become ceased. The figure demonstrates that the diffraction peaks of GaN and $In_{0.18}Ga_{0.82}N$ layer peaks are aligned along a vertical line parallel to the Q_y axis, indicating that the $In_{0.18}Ga_{0.82}N$ epitaxial layer is reasonably strained to the GaN substrate which implies no relaxation or misfit dislocations in the $In_xGa_{1-x}N$ layer over the GaN/sapphire substrate system.

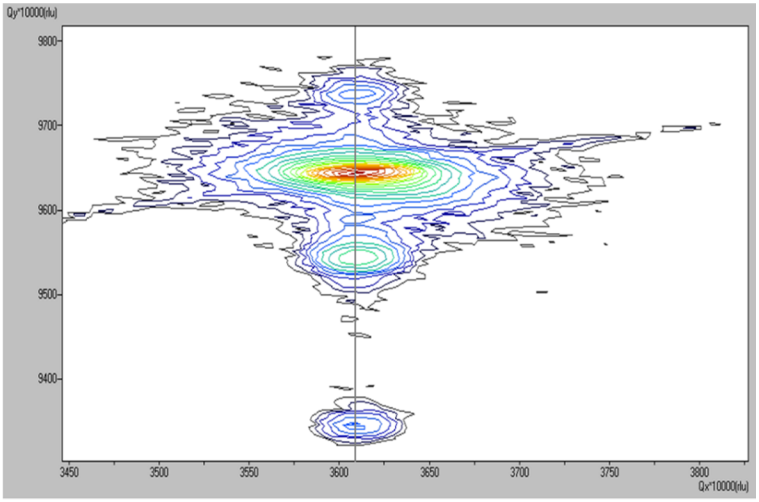

Figure 7.7: Reciprocal space mapping (RSM) of $In_{0.18}Ga_{0.82}N$/GaN superlattice solar cell.

Figure 7.8 (a) shows the scanning electron micrograph (SEM) of the designed PhC LTS on top of the ITO layer. The figure shows the patterning of photoresist by EBLwith desired hexagonal PhC structure having 300 nm period and 220 nm diameter. From the figure, one could find that the desired pattern has been transferered to the prepared sample in a precise manner. Figure 7.8 (b) shows the SEM image of the prepared PhC patterned structure over the grown sample after RIE. The analysis of the figure indicates that the PhC pattern is successfully transferred from the photoresist to the ITO layer beneath. Insets of the Figure 7.8 show the larger picture of the PhC

structure at low resolution to demonstrate the large area development of the patterning on to the prepared sample. Figure 7.9 (a) shows the SEM image of the prepared sample without PhC patterning on the top at 100 μm resolution. From the figure, p and n contacts fingers are visible on the top. For comparison, PhC patterned structure based device is shown in Figure 7.9 (b).

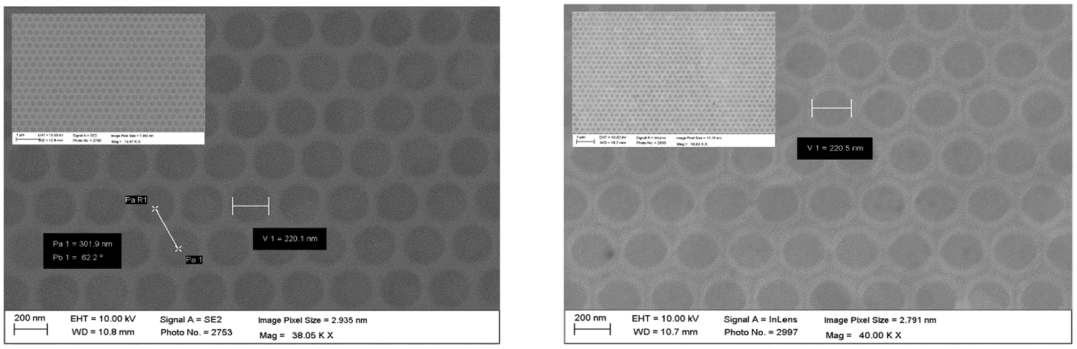

(a) (b)

Figure 7.8: Scanning electron micrographs (SEM) of (a) the designed hexagonal PhC structure on top of ITO after electron beam lithography (EBL); (b) the PhC structure after RIE. Inset in both the graphs provide the larger images of the sample at low resolution from the top

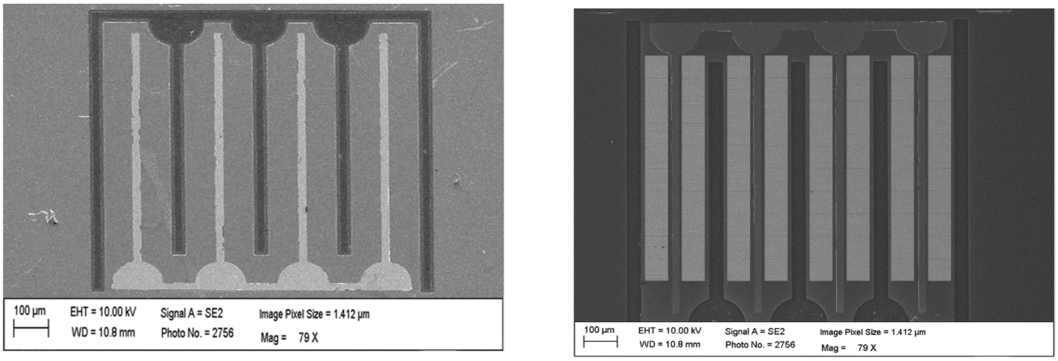

(a) (b)

Figure 7.9: (a) SEM of the planar structure used for comparison having n and p contacts without PhC structure patterning (b) SEM of the final proposed device having PhC structure at the top

Figure 7.10 shows the typical current-voltage and power-voltage curve for the proposed PhC LTS based $In_{0.18}Ga_{0.82}N$/GaN solar cell and its comparison with the structure without PhC LTS. The measurement of solar cell efficiency was performed using an AM1.5 solar simulator light source (1000W/m^2) at standard test conditions. The measurement set was first calibrated using the standard cell. The results clearly indicated better performance of PhC LTS based cell in comparison to planar cell without PhC structure, as predicted in simulation. The results shows better performance for PhC LTS based device throughout the solar spectrum as PhC structures on top not only enhances the absorption of high wavelength photons but also performs the task to reduce reflections from the top and index matching.

The results indicate the improvement of about 59% in efficiency of the device with PhC LTS in comparison to reference planar cell without PhC structure. The proposed device provides better results compared to the reference cell both in term of V_{oc} and J_{sc} which leads to overall efficiency improvement, indicating the fact that PhC LTS indeed has a potential in increasing the efficiency of proposed cell through PhC LTS. The enhancement in efficiency is mainly accounted by the improvement in the value of J_{sc} as clearly observed through the results. The basic phenomenon responsible for this short circuit current enhancement is light trapping provided by the PhC structures, which increases overall optical path length for the photons in the absorption layer and thus allows the more number of charge carriers to be generated inside the active layer.

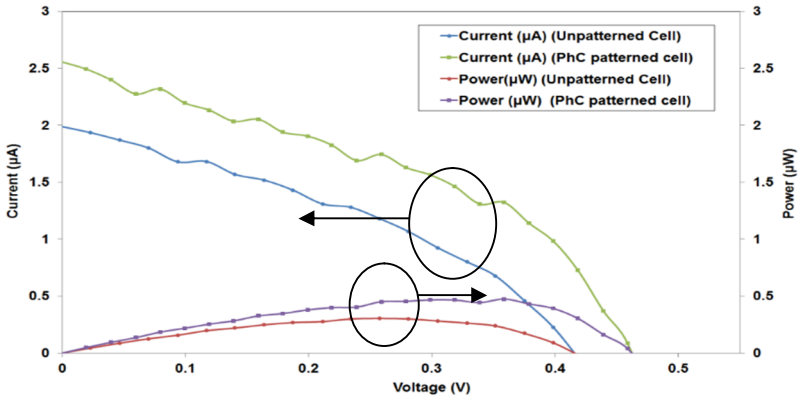

Figure 7.10: Typical Current-Voltage and Power-Voltage curve for the proposed design with and without PhC patterning for experimental device measured under 1 sun AM1.5G standard test conditions

There is also slight increase in the V_{oc} for the patterned structure. The addition of PhC LTS allows the trapping of photons within the active material leading to reabsorption of photons, ultimately increasing the carrier density in the active region. This process leads to an increase in Fermi-level splitting and as a result the densities of charge carrier increase, yielding a higher output voltage on the device (as V_{oc} in a solar cell is determined through quasi Fermi level splitting) [164]. The results are listed in Table 7.2. The snapshot of the final prepared fabricated structure is shown in Figure 7.11 (a) and (b).

From the table one could observe the discrepancy between the theoretical values and the experimental results owing to the structural defects arising from lattice mismatch between the substrate and over grown layers. It has been predicted that $In_xGa_{1-x}N$ /GaN-based solar cell with InGaN absorption layers are sensitive to structural defects [155]. Also, due to hetero-interfaces series resistance in the device could degrade the device fill factor [155]. There could also be

increase in the leakage current that might lead to the reduction in the experimental device parameters [43].

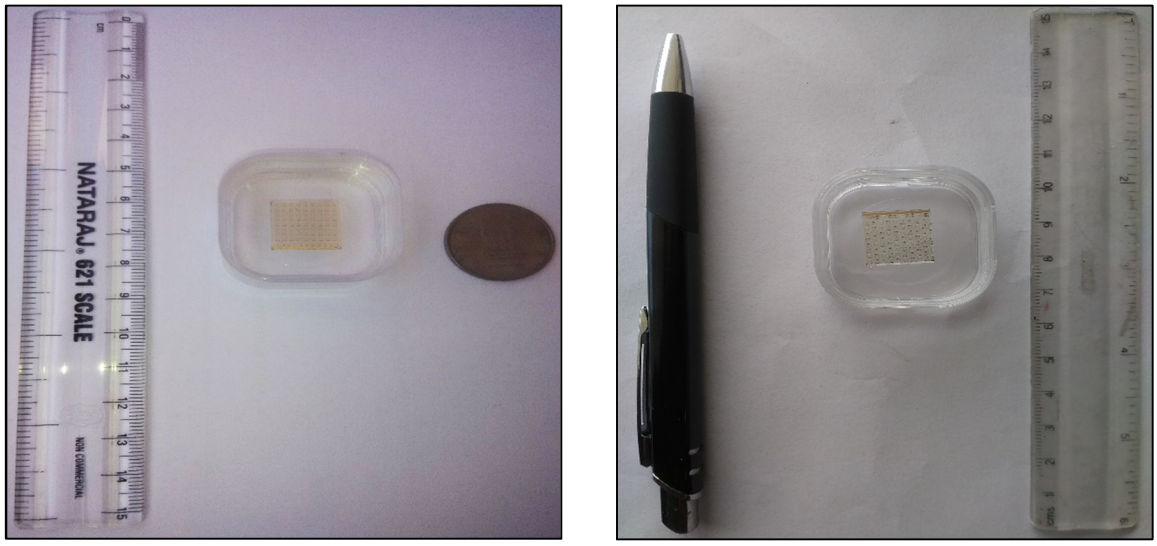

Figure 7.11: Snapshot of the prepared PhC LTS based superlattice InGaN/GaN solar cell; (a) in comparison with a coin, (b) in comparison with a pen.

Theoretically our simulation results have predicted the efficiency improvement of about 157% through PhC LTS and as these studies are mainly focused to derive the optical performance enhancement in the device due to PhC LTS shows comparatively higher results as here the study did not incorporate the effect of recombination losses and structural defects directly [45, 44]. Thus, in order to predict the experimental values more precisely through simulations, prediction of incorporation of structural defect and threading dislocation densities during growth and fabrication and their effect on final devices are required.

Table 7.2: List of the various results obtained for the proposed p-GaN/i-$In_{0.18}Ga_{0.82}N$-i-GaN/n-GaN based structure with PhC patterning on top

Parameters Calculated	**Theoretical Calculations**		**Experimental Calculations**	
	Unpatterned Structure	PhC patterned Structure	Unpatterned Structure	PhC patterned Structure
Voc (V)	0.875	0.903	0.422	0.459
Jsc (A/m^2)	3.355	7.826	3.093	3.997
Fill factor (%)	58.66	62.703	36.37	40.34
Efficiency (%)	0.172	0.443	0.047	0.075
Percent (%) Improvement	157.4%		59.6%	

Although the conversion efficiency is low, the work provides the possible future for $In_xGa_{1-x}N$ alloy systems based solar cell to improve their performance without actually increasing the $In_xGa_{1-x}N$ layer thickness beyond their epitaxial limit. In order to improve the conversion efficiency further, it is required to increase the Indium content and thickness of the active layer without degrading the structural quality of the device, which is still a challenge to achieve.

7.6. Conclusion

In conclusion, we have demonstrated the design, optical simulation, fabrication, characterization and its analysis for the InGaN/GaN superlattice active layer based solar cell having PhC LTS on the top. The PhC structures are designed through EBL. The results demonstrated by solar simulator analysis predict notable performance improvement for the proposed cell design as compared to the reference planar cell. The efficiency improvement of about 59% is shown experimentally for the proposed structure with PhC LTS. The optical simulation results predict even better improvement in performance of the device as compared to experimental results due to non-incorporation of structural defects.

Chapter 8

Conclusion and Future Work

8.1. Contributions of Thesis

In the thesis, an effort has been made to find out a way to improve the absorption in the thin film solar cells (TFSC) especially for GaAs and InGaN/GaN active material based designs using PhC LTS. The work has given us the opportunity to explore the novel and exciting field of PhC LTS based solar cells and the results achieved through the research work carried out in itself have demonstrated the effectiveness of these sub-wavelength photonic structures for the enhancement in the performance of the TFSC. The field has been explored through design, optimization, simulation and experimental analysis, and investigated through various aspects of using PhC LTS to enhance the efficiency of TFSC.

As the main motive of the thesis is to explore and demonstrate the effectiveness of PhC LTS for GaAs and InGaN/GaN alloy based TFSC, the investigator has explored and analyzed the effect of these periodic LTS through numerical modelling, simulation and experimental studies. However, as mentioned during the previous chapters, due to unavailability of required equipment in a particular lab or due to limitation of time and resources related to growth and fabrication of GaAs solar cells in Indian labs, unfortunately it was not possible to practically design and show the experimental analysis of the PhC LTS for GaAs solar cells. However, I was fortunate to achieve the fabrication of PhC LTS based InGaN/GaN TFSC and subsequently demonstrate the effectiveness of the PhC LTS for TFSC experimentally, with the help of scientists at CSIR-CEERI, Pilani and using NRF facility at IIT, Delhi. The author has successfully carried out the fabrication and experimental analysis of the InGaN/GaN superlattice based solar cells, which was indeed a complex task. Although the results achieved through the designed InGaN/GaN solar cell structure with PhC LTS have scope for further improvement, they clearly demonstrate the effectiveness of the PhC LTS for the TFSC and set the guidelines for practical implementation of these devices for future terrestrial applications. The major findings achieved during the Ph.D. duration, through the

design, simulation and experimental analysis of the periodic PhC structure for light trapping for GaAs and InGaN/GaN solar cell have been summarized below:

8.1.1. The work have demonstrated the design, simulation and experimental analysis of PhC LTS for thin film solar cells, using them (a) as a photonic band gap structure at the back, (b) as a diffraction grating at the back assisted by distributes bragg reflector, (c) at front surface of the cell etched above (but not through) active layer, and (d) at front surface etched through inside the active layer.

8.1.2. The effectiveness of the PhC LTS for different designs has been demonstrated and analyzed for GaAs as well as for InGaN/GaN active material cells.

8.1.3. It has been predicted and proved through different designs and results that the PhC LTS have indeed the ability to enhance the efficiency of the TFSC, irrespective of the material system used.

8.1.4. When PhC configuration used as a PBG structure at the back of a heterojunction GaAs thin film cell (chapter 3), the purpose was to design a broadband BR inducing a weak parasitic absorption and that could also serve for light-trapping purposes.

i. The optical and electrical performance of the PBG structure based cell has been investigated and compared with Al back reflector based design.
ii. The results show that the 2D PhC configuration as a PBG structure could have a real potential for enhancing the efficiency of such cells and found that the performance of the PhC solar cells even in worst practical case (i.e. including recombination effects) was better than the Al reflector based cell.

8.1.5. The PhC has also been designed as a diffraction grating at the back of the GaAs solar cell (chapter 4). The LTS has been designed via combination of 2D PhC diffraction grating assisted by Distributed Bragg Reflector (DBR), in order to design virtual 3D non-metallic back reflector for efficiency enhancement.

i. It has been demonstrated that with careful design optimization, the presented LTS can lead to notable cell-efficiency enhancement for the cells with very thin active layer, mainly due to PhC structure contribution.
ii. According to our simulation, the overall cell efficiency can be enhanced 3.5 times for a 100 nm-thick cell with light-trapping structure and this enhancement remains only 1.5 times for 1500 nm-thick cell. It is found that

for thin cells the improvement is mainly contributed by the optimized back trapping structure whereas the contribution from the ARC remains almost constant.

iii. Although the structure having PhC as a diffraction grating has provided less efficiency values than the PhC LTS as a PBG configuration for ideal conditions, the structure designed is more practically feasible.

8.1.6. We have also studied the design using PhC as a LTS placed at the top of a heterojunction GaAs solar cell with a periodic pattern extends from top layer to inside the p-AlGaAs window layer placed just above the active layer of GaAs material (chapter 5).

i. The PhC LTS design at the top is different from the back reflector design, as when placed at the top, LTS not only has to improve the optical path length for high wavelength photons but also has to provide better coupling of incident light to the active layer and also reduce the reflections throughout the entire wavelength range. Thus, the design of efficient PhC LTS at the top is more complicated than designing PhC LTS at the back.

ii. The performance of the proposed structure is compared with Lambertian limits and the planar cell, taken as reference. It has also been analyzed how PhC LTS effect the performance of the design with the thickness of active layer.

iii. It has been found that similar to the PhC LTS at the back, here too considerable increase in efficiency has been achieved, especially for thinner active layers, demonstrating the advantage of PhC based structures for TFSC, however still the efficiencies are under the Lambertian limits.

iv. The results demonstrated that the efficiency achieved with front PhC LTS design is less as compared the previous designs shown in chapter 3 and 4, however this design is most applicable from the fabrication point of view and the same design is realized with the InGaN/GaN structure to show the effect of PhC LTS on the thin film cells, due to the constraint, already discussed in the growth and fabrication of GaAs structure in India.

8.1.7. The report also discusses the design based on p-i-n InGaN/GaN solar cell using PhC LTS at the top assisted by the planar metallic (Al) BR (chapter 6). Two different designs has been studied, in one the PhC structure etching depth extending from the top ARC up to the p-GaN layer placed above the active layer,

whereas in other design the PhC LTS etching depth has been extended up to the $In_xGa_{1-x}N$ absorbing layer, starting from the top ITO layer.

i. The work presents the theoretical optical simulation studies and optimization of the required parameters of the structure, which helps to investigate and demonstrate the effectiveness of the LTS in the efficiency enhancement of the structure for InGaN/GaN solar cell.

ii. The work also demonstrates the Lambertian light trapping limits for the practical Indium concentrations (10% to 20%) in $In_xGa_{1-x}N$ active layer cell. The work also presents the comparison between the proposed designs and also compares their results with that of a planar reference cell.

iii. The studies are carried out for various Indium concentrations. The results indicate considerable enhancement in the efficiency due to the PhC LTS, mainly because of better coupling, low reflectance and diffraction capability of the proposed LTS, although it is still under the Lambertian limits.

iv. Although the design seems to provide good efficiency results theoretically, the problem of structural defects and threading dislocation might not allow the device to provide same efficiency as predicted through simulation due to growth of single layer $In_xGa_{1-x}N$ over the lattice mismatch substrate. Thus, one also have to think about the structures which could allow to provide better results optically as well as electrically without degrading the epitaxial nature of the device like superlattice structure.

8.1.8. The chapter 7 presents the design, simulation and fabrication and its analysis for the InGaN/GaN superlattice structure based solar cell having PhC LTS etched from the top surface above active layer.

i. Although, optically the proposed superlattice structure has smaller output than the structure proposed in chapter 6 due to extremely thin active layer, practically (electrically) the superlattice structure would provide better results.

ii. The $In_{0.18}Ga_{0.82}N$/GaN structure was grown through metal organic chemical vapor deposition. Superlattice structure has been considered for absorption. PhC LTS has been prepared precisely using e-beam lithography.

iii. Both simulation and experimental results have demonstrated that the PhC LTS leads to the considerable enhancement in the efficiency of the proposed

design. The experimental device studies exhibit the enhancement of about 59% in efficiency as compared to superlattice structure without PhC LTS.

iv. The experimental results confirm the better performance for the PhC based solar cell devices and are in well contention with the theoretical studies and demonstrate, which could be arguably considered as, one of the most important finding of the thesis.

Table 8.1 summarizes the results obtained for various designs presented in chapter 4 and 5 together considering GaAs active material. Analysis of the results for both the designs predict notable improvement in the output of the cell as compared to single pass efficiency and planar reference cell, especially due to the PhC LTS effects. Out of the two designs, the results for the structure having PhC LTS at the back assisted by DBR (structure proposed in chapter 4) provide higher output. The reason for this is that when PhC LTS is placed at the back, they have to be designed to reflect only the higher wavelength spectrum photons, thus the structure is designed to support only few diffraction modes, as compared to the PhC LTS design placed at the top. PhC LTS at the top (chapter 5), as discussed previously, has to work throughout the solar spectrum and thus has to support large number of modes efficienctly, which ultimately increases the complexity in the working of the structure and effects the overall output adversely. However, between the two design, it is more practically feasible to design and fabricate the PhC structure at the top (design proposed in chapter 5), as the proposed PhC structure in that case would be fabricated over the complete heterojunction structure of GaAs and thus there is a very limited possibility of PhC structure fabrication process to effect the epitaxial nature of the GaAs structure.

The comparison of the above mentioned two structures with PhC as a PBG structure (chapter 3) provides better results for efficiency for PBG structure based design for 1500 nm thick active material for ideal case. The ideal case efficiency results for PBG based design is almost equivalent to the Lambertian limit values. However, for the case considering recombination effects, the result reduces by almost 12% as compared to the ideal case values. Also, there is a genuine bottleneck in the practical realization of such a PhC PBG structure, as for such a design a conventional lithography processes cannot be used to design the structure (as discussed in chapter 3). Thus, we could conclude that out of the three proposed cell designs having GaAs active material, design having PhC LTS at the back would provide the best results theoretically, however practically the design having PhC LTS at the top is most feasible from growth and fabrication point of view.

Table 8.1: Cell efficiency comparison of PhC structure based device and Lambertian limit for different cell thicknesses for GaAs active material

Active layer thickness (in nm)	**Single pass efficiency with losses (device without LTS) (%)**	**Planar complete cell efficiency without PhC structure (%)**	**Proposed Cell efficiency with PhC structure at top and planar BR (%)** ***(chapter 5)***	**Efficiency of cell with planar ARC and with Back PhC LTS (%)** ***(chapter 4)***	**Lambertian Limit efficiency (%)**
100	7.529	11.50	14.004	24.9716	26.011
250	10.428	15.26	17.841	25.8822	27.05
500	13.305	19.23	21.315	27.7262	28.45
750	14.523	20.58	22.783	27.9201	29.177
1000	15.275	21.36	23.205	28.4824	29.766
1500	15.91	21.96	23.846	28.9031	30.384

The thesis also presents the two different designs for InGaN/GaN solar cells with PhC LTS as discussed before, having PhC LTS at the top for both with variation in active layer design. The closeness to practical realization possibility, as mentioned above, is the basic reason to incorporate PhC LTS at the top, in contrast to using PhC LTS at the back or as a PBG structure. The thesis has discussed about the PhC LTS effect for p-i-n InGaN/GaN structure having single planar active layer (chapter 6) as well as for InGaN/GaN superlattice structure based design (chapter 7). Out of the two structures, theoretically through optical simulation, planar layer structure provided better results, however practically superlattice based design would outperform the single layer structure. On inclusion of electrical effects in simulations, the results reduced to very low values as demonstrated for superlattice based structure in section 7.5, indicating the structural sensitivity for InGaN based solar cells. Still, the experimental values found out for the proposed design in chapter 7, clearly suggest that the PhC LTS indeed has a capability to boost the output for a thin film cell and can pave a possible way for future high efficiency thin film solar cells.

8.2. Future Work and Concluding Remarks

The various proposed PhC LTS presented and analyzed in the thesis have contributed to the efficiency enhancement to the designed solar cells, but still these efficiencies are more or less under the Lambertian values. Thus, there is still room for improvement to achieve the ultimate aim of Lambertian limits [141] and thus the S-Q values [20]. On the basis of the analysis of the presented LTS, as mentioned earlier, there are three main strategies that can be proposed for the future design of more efficient thin film cells with a photonic pattern:

- Reflection losses have to be reduced over the largest possible incident wavelength range,
- Light trapping has to be tailored to increase absorption at high wavelength photons.
- Losses in the structure should be reduced and that light should be coupled to the active layer to convert into useful absorption.

The proposed structures in the thesis have predicted reduction in reflections from the top either through using planar ARC or using PhC LTS, however there are still reflections from the top and thus in order to reduce these reflections even further, the front surface could be improved towards a multilevel pattern, which would provide a smoother variation of effective refractive index from air to the active material. Also, combination of periodic patterns could also be proposed for both front as well as at back, which might provide the better trapping throughout the incident spectrum as compared to single pattern through the wavelength range of interest. Researchers have also suggested that periodic pattern alone may not be able to reach the Lambertian limits. Indeed, the broad range of Fourier components needed for light scattering suggests that addition of some amount of disorder may be useful. Thus it has been suggested that the combination of ordered structures, like proposed in this thesis, together with sub-wavelength random micro-roughness, appears to be especially promising as it would take advantage of optimized diffraction in the optical range as well as Rayleigh scattering with a continuous spectrum of wave-vector components [62].

In the presented work, we have proposed the detailed optical analysis of the proposed LTS structure, but have not considered the electrical transport and the possible presence of defects at the patterned surfaces (except for chapter 3, to be more focused on optical enhancement), giving rise to surface or interface recombination. In the periodic structures like presented PhC structures, surface or interface recombination might have become very crucial. However, the electron transport properties could benefit from the reduced active layer thicknesses as we have used thin films as absorbing layer. Also, one has to take care of the diffusion properties of the GaAs and InGaN/GaN materials, as they have small diffusion lengths, thus increasing the active layer thickness beyond certain value is also not practical to achieve limiting values as with the increase in the active layer thickness, recombination would also increase, thus light trapping plays all the more important role for TFSC based on these materials. Thus, a detailed investigation of actual cell architecture including optical and electrical properties would again be very helpful and this can be the direction for extending the present work towards real cell structures.

As discussed during chapter 2 that EBL is one of the best techniques available for the fabrication of periodic structures in nm range. EBL is widely accepted throughout the world for R&D applications due to its preciseness, however from mass production and industrial point of view, EBL is not recommended as it usually takes long time to pattern a small area. Thus, there is also a need to look towards alternatives which can provide inexpensive, bulk, precise patterning of periodic structures in nm range. Out of many available alternates, one of the viable approach is a Nanosphere lithography. The process promises to have all the major advantages related to top-down (due to the action of patterning the structured layers such as in a conventional lithography technique) and bottom up (due to the self-organization of the colloidal spheres) approach. The process has the advantage both in terms of low cost and small time to transfer the pattern to the desired substrate having capability to manufacture long range ordered arrays of nanostructures which are equidistant and have the same environment. Thus, the process could be helpful to design future low cost PhC based TFSC, which can further extended the acceptability of the devices.

Now, in the end, it is my genuine optimism that the work presented in the thesis would provide some useful insight for the field and help to design new PhC LTS for GaAs as well as InGaN/GaN solar cells in the future which will pave the path for low cost high efficiency devices, greatly reducing the dependence on fossil fuels for our energy needs, which would ultimately help our society and may prove to be of immense benefit for countries like India, having serious energy dependence (almost a crisis) and where sun shines almost for 10 months a year. As the study of PhC LTS based solar cell is relatively new to our country, the work is a sincere effort to highlight the subject as these periodic structures can prove to be a boon for high efficiency TFSC and can immensely support the society like ours.

Bibliography

[1] Ministry of New and Renewable Energy, "Jawaharlal Nehru National Solar Mission: Phase II-Policy Document," New Delhi, 2012.

[2] C. S. Solanki, "Solar PV Energy for Academic Campuses in India," Department of Energy Science and Engineering, Indian Institute of Technology, Bombay, Mumbai, India, June, 2009.

[3] E. Becquerel, "Mémoire sur les effets électriques produits sous l'influence des rayons solaires," *Comptes Rendus*, vol. 9, p. 561–567, 1839.

[4] C. E. Fritts, "On a New Form of Selenium Photocell," *American Journal of Science*, vol. 26, p. 465, 1883.

[5] U.S. Energy Information Administration: Independent Statisctics and Analysis, "Country Analysis Brief: India," June, 2016.

[6] International Energy Agency, "Statistics, IEA Energy Atlas," May 2016.

[7] International Energy Agency: World Energy Outlook Special Report, "India Energy Outlook," Paris, France, 2015.

[8] Ministry of Power, "Power Sector at a Glance ALL INDIA," Sept. 2016. [Online]. Available: http://powermin.nic.in/en/content/power-sector-glance-all-india.

[9] UN Climate Change Conference Paris 2015, "Sustainable Development Goals," United Nations, Nov. 2015. [Online]. Available: http://www.un.org/sustainable development/cop21/.

[10] Government of India, "India's Intended Nationally Determined Contribution: Working towards climate justice," United Nations Framework Convention on Climate Change, Paris, France, 2015.

[11] Ministry of New and Renewable Energy, "Jawaharlal Nehru National Solar Mission: Towards Building SOLAR INDIA," Goverment of India, New Delhi, India, 2008.

[12] National Center for Photovoltaic Research and Education (NCPRE), "Why Solar for beginners," June 2013. [Online]. Available: http://www.ncpre.iitb.ac.in.

[13] J. Nelson, The Physics of Solar Cell, London: Imperial College Press, 2008.

[14] Wikipedia, "The timeline of solar cells," Apr. 2016. [Online]. Available:

https://en.wikipedia.org/wiki/Timeline_of_solar_cells. [Accessed Aug. 2016].

[15] W. Adams and R. Day, "The Action of Light on Selenium," *Proceedings of the Royal Society, London,* vol. A25, p. 113, 1877.

[16] W. Hallwachs, "Über die Strahlung des Lichtbogens," *Annalen der Physik,* vol. 318, pp. 38-64, 1904.

[17] J. Czochralski, "Ein neues Verfahren zur Messung der Kristallisationsgeschwindigkeit der Metalle," *Zeitschrift für Physikalische Chemie,* vol. 92, p. 219–221, 1918.

[18] D. M. Chapin, C. S. Fuller and G. L. Pearson, "A New Silicon p-n Junction Photocell for Converting Solar Radiation into Electrical Power," *Journal of Applied Physics,* vol. 25, no. 5, p. 676–677, April, 1954.

[19] D. M. Chapin, C. S. Fuller and G. L. Pearson, "Solar energy converting apparatus". USA Patent 2780765 A, Feb. 1957.

[20] W. Shockley and H. J. Queisser, "Detailed balance limit of p-n junction solar cells," *Journal of Applied Physics,* vol. 32, no. 510, p. 510, 1961.

[21] Z. I. Alferov, V. M. Andreev, M. B. Kagan and I. I. T. V. G. Protasov, "Solar-energy converters based on p–n AlxGa1-xAs–GaAs heterojunctions," *Fiz. Tekh. Poluprovodn. (Sov. Phys. Semicond.),* vol. 4, no. 2047, 1971.

[22] D. Carlson and C. Wronski, "Amorphous Silicon Solar Cells," *Applied Physics Letters,* vol. 28, pp. 671-673, 1976.

[23] M. o. N. a. R. Energy, "Introduction," [Online]. Available: http://mnre.gov.in/mission-and-vision-2/mission-and-vision/. [Accessed Sept. 2016].

[24] E. Yablonovitch and G. D. Cody, "Intensity Enhancement in Textured Optical Sheets for Solar Cells," *IEEE Transactions on Electron Devices,* vol. 29, no. 2, pp. 300-305, 1982.

[25] School of Photovoltaic and Renewable Energy, University of New South Wales Engineering, "Research Highlights," [Online]. Available: https://www.engineering.unsw.edu.au/energy-engineering/research/research-highlights. [Accessed Sept. 2016].

[26] B. O'Regan and M. Grätzel, "A low-cost, high-efficiency solar cell based on dye-sensitized colloidal TiO2 films," *Nature,* vol. 353, no. 6346, p. 737, 1991.

[27] J. Gee, "Optically enhanced absorption in thin silicon layers using photonic crystals," in *Twenty-Ninth IEEE Photovoltaic Specialists Conference,* New Orleans, Louisiana, USA, 2002.

[28] C. Honsberg, O. Jani, A. Doolittle, E. Trybus, E. Namkoong, I. Ferguson, D. Nicol and A. Payne, "InGaN– A new solar cell material," in *Proceedings of the 19th European Photovoltaic Science and Engineering Conference*, Paris, France, June 7-11, 2004.

[29] University of Delaware, "UD-led team sets solar cell record, joins DuPont on $100 million project," July 2007. [Online]. Available: http://www1.udel.edu/PR/UDaily /2008/jul/solar072307.html. [Accessed Aug. 2016].

[30] National Renewable Energy Laboratory, "NREL Solar Cell Sets World Efficiency Record at 40.8 Percent," August 2008. [Online]. Available: http://www.nrel.gov/news /press/2008/625. [Accessed Sept 2016].

[31] Alta Devices, "About the company," July 2016. [Online]. Available: http://www.altadevices.com/about/.

[32] Australia Renewable Energy Agency, "ARENA supports another solar world record," May 2016. [Online]. Available: http://arena.gov.au/news/arena-supports-another-solar-world-record/. [Accessed Sept. 2016].

[33] J.M. Pearce, N. Podraza, R.W. Collins, M.M. Al-Jassim, K.M. Jones, J. Deng, C.R. Wronski,"Optimization of open circuit voltage in amorphous silicon solar cells with mixed-phase (amorphous+nanocrystalline)," *Journal of Applied Physics,* vol. 101, no. 11, p. 114301, 2007.

[34] M. A. Green, K. Emery, Y. Hishikawa, W. Warta and E. D. Dunlop, "Solar cell efficiency table (vesion 48)," *Progress in Photovoltaics,* vol. 24, no. 7, pp. 905-913, 2016.

[35] Admin, August 6 2012. [Online]. Available: http://altadevices-blog.com..

[36] Z. Yu, A. Raman and S. Fan, "Fundamental limit of nanophotonic light trapping in solar cells," *Proceedings of the National Academy of Sciences of the United States of America,* vol. 107, no. 41, p. 17491–17496, Oct. 2010.

[37] Wikipedia, "Thin film solar cell," 2016 2016. [Online]. Available: https://en.wikipedia.org/wiki/Thin-film_solar_cell. [Accessed Sept. 2016].

[38] Ossila - enabling innovative electronics, "Perovskites and Perovskite Solar Cells: An Introduction," 2015. [Online]. Available: https://www.ossila.com/pages/perovskites-and-perovskite-solar-cells-an-introduction. [Accessed Sept. 2016].

[39] M. Liu, ,. M. B. Johnston and H. J. Snaith, "Efficient planar heterojunction perovskite solar cells by vapour deposition," *Nature Letters,* vol. 501, no. 12509, pp. 395-398, 2013.

[40] V. Y. Davydov, A. A. Klochikhin, R. P. Seisyan, V. V. Emtsev, S. V. Ivanov, F. Bechstedt, J. Furthmuller, H. Harima, A. V. Mudryi, J. Aderhold, O. Semchinova and J. Graul, "Absorption and Emission of Hexagonal InN Evidence of Narrow Fundamental Band Gap," *Physica Status Solidi B,* vol. 229, no. 3, pp. R1-R3, 2002.

[41] J. Wu, W. Walukiewicz, K. M. Yu, J. W. Ager III, E. E. Haller, H. Lu, W. J. Schaff and Y. a. N. Y. Saito, "Unusual properties of the fundamental band gap of InN," *Applied Physics Letters,* vol. 80, no. 21, pp. 3967-3969 , 2002.

[42] X. Cai, S. Zeng and B. Zhang, "Fabrication and characterization of InGaN p-i-n homojunction solar cell," *Applied Physics Letters,* vol. 95, 2009.

[43] X. Zheng, R. Horng, D. S. Wuu, M. Chu, W. Liao, M. Wu, R. Lin and Y. Lu, "High-quality InGaN/GaN heterojunctions and their photovoltaic effects," *Applied Physics Letters,* vol. 93, p. 261108, December 2008.

[44] T. F. Gundogdu, M. Gökkavas and E. Ozbay, "Absorption enhancement in InGaN-based photonic crystal-implemented solar cells," *Journal of Nanophotonics,* vol. 6, pp. 061603-1-9, 2012.

[45] O. Jani, I. Ferguson, C. Honsberg and S. Kurtz, "Design and characterization of GaN/InGaN solar cells," *Applied Physics Letters,* vol. 91, no. 13, pp. 132 117-1–132 117-3, 2007.

[46] F.A. Lindholm, J.G. Fossum and E.L., Burgess, "Application of the superposition principle to solar-cell analysis," *IEEE Transactions on Electron Devices,* vol. 26, pp. 165-171, 1979.

[47] PVEducation.org, "Solar Energy Operations," [Online]. Available: http://pveducation.org/pvcdrom/solar-cell-operation/iv-curve. [Accessed Sept. 2016].

[48] National Renewable Energy Laboratory, "Reference Solar Spectral Irradiance: Air Mass 1.5 (G-173-03, ASTM)," 2004. [Online]. Available: http://rredc.nrel.gov/solar/spectra/am1.5/. [Accessed Sept. 2016].

[49] PVEducation.org, "Standard Solar Spectra," May 2007. [Online]. Available: http://www.pveducation.org/pvcdrom/appendices/standard-solar-spectra. [Accessed Oct. 2016].

[50] Wikipedia, "Air mass (solar energy)," May 2011. [Online]. Available: https://en.wikipedia.org/wiki/Air_mass_(solar_energy).

[51] A. Naqvi, F.-J. Haug, K. Soderstrom, C. Battaglia, V. Paeder, T. Scharf, H. P. Herzig and

C. Ballif, "Angular behavior of the absorption limit in thin film silicon solar cells," *Progress in Photovoltaics: Research and Applications,* vol. 22, no. 11, pp. 1147-1158, 2014.

[52] B. Yan, J. M. Owens, C. Jiang and S. Guha, "High-Efficiency Amorphous Silicon Alloy Based Solar Cells and Modules," *MRS Symposium Proceedings,* vol. A23.3, p. 862, 2005.

[53] J. Springer, A. Poruba, L. Mullerova, M. Vanecek, O. Rech and K. B., "Absorption loss at nanorough silver back reflector of thin-film silicon solar cells," *Journal of Applied Physics,* vol. 95, pp. 1427-1429, 2004.

[54] J. D. Joannopoulos, Photonic crystals - Molding the flow of Light, New Jersey: Princeton University Press, 1995.

[55] J. W. S. Rayleigh, "On the remarkable phenomenon of crystalline reflexion described by Prof. Stokes," *Philosophical Magazine,* vol. 26, p. 256–265, 1888.

[56] E. Yablonovitch, "Inhibited spontaneous emission in solid state physics and electronics," *Physical Review Letters,* vol. 58, p. 2059–2062, 1987.

[57] S. John, "Strong localization of photons in certain disordered dielectric superlattices," *Physical Review Letters,* vol. 58, pp. 2486-2489, 1987.

[58] R. Biswas, C. G. Ding, I. Puscasu, M. Pralle, M. McNeal, J. Daly, A. Greenwald and E. Johnson, "Theory of subwavelength hole arrays coupled with photonic crystals for extraordinary thermal emission," *Physical Review B,* vol. 74, no. 045107, pp. 1-6, July 2006.

[59] P. Bermel, C. Luo, L. Zeng, L. C. Kimerling and J. D. Joannopoulos, "Improving thin-film crystalline silicon solar cell efficiencies with photonic crystals," *Optics Express,* vol. 15, no. 25, pp. 16986-17000, Dec 2007.

[60] D. Zhou and B. R., "Photonic Crystals Enhanced Light Trapping in Thin film solar cells," *Journal of Applied Physics,* vol. 103, p. 093102 , 2008.

[61] N. N. Feng, J. Michel, L. Zeng, J. Liu, H. C.Y., K. L.C. and D. X., "Design of Highly Efficient Light-Trapping Structures for Thin-Film Crystalline Silicon Solar Cells," *IEEE Transactions on Electron Devices,* vol. 54, no. 8, pp. 1926-1933, August 2007.

[62] A. Bozzola, M. Liscidini and L. C. Andreani, "Photonic light-trapping versus Lambertian limits in thin film silicon solar cells with 1D and 2D periodic patterns," *Optics Express,* vol. 20, no. S2, pp. 224-243, 2012.

[63] S. Zanotto, M. Liscidini and L. C. Andreani, "Light trapping regimes in thin-film silicon solar cells with a photonic pattern," *Optics Express,* vol. 18, no. 5, pp. 4260-4274, 2010.

[64] Wikipedia, "Photonic crystal," [Online]. Available: https://en.wikipedia.org/wiki /Photonic_crystal. [Accessed Sept. 2016].

[65] V. P. Bykov, "Spontaneous emission from a medium with a band spectrum," *Soviet Journal of Quantum Electronics,* vol. 4, no. 7, pp. 861-871, 1975.

[66] K. M. Ho, C. T. Chan and C. M. Soukoulis, "Existence of a photonic gap in periodic dielectric structures," *Physical Review Letters ,* vol. 65, no. 25, p. 3152, 1990.

[67] E. Yablonovitch, T. Gmitter and K. Leung, "Photonic band structure: The face-centered-cubic case employing nonspherical atoms," *Physical Review Letters,* vol. 67, no. 17, p. 2295, 1991.

[68] J. Wijnhoven and W. Vos, "Prepration of Photonic Crystals made of Air Spheres in Titania," *Science,* vol. 281, pp. 802-804, 1994.

[69] U. Grüning, V. Lehmann and C. M. Engelhardt, "Two□dimensional infrared photonic band gap structure based on porous silicon," *Applied Physical Letters ,* vol. 66, p. 3254, 1995.

[70] T. F. Krauss, R. M. S. De La Rue and S. Brand, "Two-dimensional photonic-bandgap structures operating at near-infrared wavelengths," *Nature ,* vol. 383, pp. 699 - 702, 1996.

[71] R. Cregan, B. Mangan, J. Knight, T. Birks, P. S. J. Russell, P. Roberts and D. Allan, "Single-mode photonic band gap guidance of light in air," *Science,* vol. 285, no. 5433, pp. 1537-1539, 1999.

[72] A. Blanco, E. Chomski, S. Grabtchak, M. Ibisate, S. John, S. W. Leonard, C. Lopez, F. Meseguer, H. Miguez, J. Mondia, G. A. Ozin, O. Toader and H. van Driel, "Large-scale synthesis of a silicon photonic crystal with a complete three-dimensional bandgap near 1.5 micrometres," *Nature,* vol. 405, pp. 437-440, 2000.

[73] J. M. Dudley, G. Genty and S. Coen, "Supercontinuum generation in photonic crystal fiber," *Reviews of Modern Physics,* vol. 78, no. 1135 , 2006.

[74] J. W. Galusha, L. R. Richey, J. S. Gardner, J. N. Cha and M. H. Bartl, "Discovery of a diamond-based photonic crystal structure in beetle scales," *Physical Review E,* vol. 77, no. 050904(R), 2008.

[75] T. Baba, "Slow light i Photonic Crystals," *Nature,* vol. 2, no. 8, pp. 465-473, 2008.

[76] J. N. Munday, "The effect of photonic bandgap materials on the Shockley-Queisser limit," *Journal of Applied Physics,* vol. 112, p. 064501, 2012.

[77] P. Kuang, A. Deinega, M. Li Hsieh, S. John and S. Yu Lin, "Light trapping and near-unity solar absorption in a three-dimensional photonic-crystal," *Optics Letters,* vol. 38, no. 20, pp. 4200-4203, 2013.

[78] Y. Nam, Y. X. Yeng, A. Lenert, P. Bermel, I. Celanovic, M. Soljačić and E. Wang, "Solar thermophotovoltaic energy conversion systems with two-dimensional tantalum photonic crystal absorbers and emitters," *Solar Energy Materials & Solar Cells,* vol. 122, pp. 287-296, 2014.

[79] A. Al-Rashid and S. John, "Optical Biosensing of Multiple Disease Markers in a Photonic-Band-Gap Lab-on-a-Chip: A Conceptual Paradigm," *Phyical Review Applied,* vol. 3, no. 034001, pp. 1-19, 2015.

[80] K. Sakoda, Optical Properties of Photonic Crystals, Berlin, Germany: Springer-Verlag, 2001.

[81] C. Kittel, Quantum theory of solids, Wiley, 1963.

[82] J. Krˇc, G. Cernivec, A. Campa, J. Malmstr¨om, M. Edoff, F. Smole and M. Topiˇc, "Optical and electrical modeling of Cu(In,Ga)Se2 solar cells," *Optical and Quantum Electronics ,* vol. 38, no. 12, pp. 1115-1123, 2006.

[83] S. Eyderman and S. John, "Light-trapping and recycling for extraordinary power conversion in ultra-thin gallium-arsenide solar cells," *Scientific Reports,* vol. 6, no. 28303, pp. 1-7, June, 2016.

[84] H. Ding, L. Lalouat, B. Gonzalez-Acevedo, R. Orobtchouk, C. Seassal and E. Drouard, "Design rules for net absorption enhancement in pseudo-disordered photonic crystal for thin film solar cells," *Optics Express,* vol. 24, no. 6, pp. A650-A666, 2016.

[85] X. Sheng, L. Z. Broderick and L. C. Kimerling, "Photonic crystal structures for light trapping in thin-film Si solar cells: Modeling, process and optimizations," *Optics Communication,* vol. 314, pp. 41-47, 2014.

[86] X. Wang, M. Khan, J. L. Gray, M. A. Alam and M. S. Lundstrom, "Design of GaAs Solar Cells Operating Close to the Shockley–Queisser Limit," *IEEE Journal of Photovoltaics,* vol. 3, no. 2, pp. 737-744, 2013.

[87] A. Chutinan, N. Kherani and S. Zukotynski, "High-efficiency photonic crystal solar cell

architecture," *Optic Express,* vol. 17, no. 11, p. 8871–8878, 2009.

[88] G. Demesy and S. John, "Solar energy trapping with modulated silicon nanowire photonic crystals," *Journal of Applied Physics,* vol. 112, p. 074326 , 2012.

[89] S. Mallick, M. Agrawal and P. Peumans, "Optimal light trapping in ultra-thin photonic crystal crystalline silicon solar cells," *Optics Express,* vol. 18, no. 6, p. 5691, 2010.

[90] S. Eyderman, A. Deinega and S. John, "Near perfect solar absorption in ultra-thin-film GaAs photonic crystals," *Journal of Materials Chemistry A,* vol. 2, no. 3, pp. 761-769, 2014.

[91] J. G. Mutitu, S. Shi, C. Chen, T. Creazzo, A. Barnett, C. Honsber and D. W. Prather, "Thin film silicon solar cell design based on photonic crystal and diffractive grating structures," *Optics Express,* vol. 16, no. 19, p. 15238, Sept. 2008.

[92] M. Florescu, H. Lee, I. Puscasu, M. Pralle, L. Florescu and D. Z. J. P. D. Ting, "Improving solar cell efficiency using photonic band-gap materials," *Solar Energy Materials and Solar Cells,* vol. 91, pp. 1599-1610, 2007.

[93] G. J. Bauhuis, P. Mulder, E. J. Haverkamp, J. C. C. M. Huijben and J. J. Schermer, "26.1% thin-film GaAs solar cell using epitaxial lift-off," *Solar Energy Materials and Solar Cells,* vol. 93, p. 1488–1491, 2009.

[94] D. E. Aspnes, S. M. Kelso, R. A. Logan and R. Bhat, "Optical properties of AlxGa1−xAs," *Journal of Applied Physics,* vol. 60, pp. 754-767, 1986.

[95] C.-Y. Cho, J.-B. Lee, S.-J. Lee, S.-H. Han, T.-Y. Park, J. W. Kim, Y. C. Kim and S.-J. Park, "Improvement of light output power of InGaN/GaN light-emitting diode by lateral epitaxial overgrowth using pyramidal-shaped SiO2," *Optics Express,* vol. 18, no. 2, pp. 1462-1468, 2010.

[96] J. W. Shon, J. Ohta, K. Ueno, A. Kobayashi and H. Fujioka, "Fabrication of full-color InGaN-based light-emitting diodes on amorphous substrates by pulsed sputtering," *Scientific Reports,* vol. 4, no. 5325, 2014.

[97] R. Dahal, B. Pantha, J. Li, J. Y. Lin and H. X. Jiang, "InGaN/GaN multiple quantum well solar cells with long operating wavelengths," *Applied Physics Letters* , vol. 94, no. 6, p. 063505, 2009.

[98] R. H. Horng, S. T. Lin, Y. L. Tsai, M. T. Chu, W. Y. Liao, M. H. Wu, R. M. Lin and Y. C. Lu, "Improved conversion efficiency of GaN/InGaN thin-film solar cells," *IEEE Electron*

Device Letters, vol. 30, no. 7, pp. 724-726, 2009.

[99] C. C. Yang, J. K. Sheu, X. W. Liang, M. S. Huang, M. L. Lee, K. H. Chang, S. J. Tu, F. W. Huang and W. C. Lai, "Enhancement of the conversion efficiency of GaN-based photovoltaic devices with AlGaN/InGaN absorption layers," *Applied Physics Letters,* vol. 97, no. 2, p. 021113, 2010.

[100] A. V. Lobanova, A. L. Kolesnikova, A. E. Romanov, S. Y. Karpov, M. E. Rudinsky and E. V. Yakovlev, "Mechanism of stress relaxation in (0001) InGaN/GaN via formation of V-shaped dislocation half-loops," *Applied Physics Letters,* vol. 103, no. 15, p. 152106, 2013.

[101] N. G. Weimann, L. F. Eastman, D. Doppalapudi, H. M. Ng and T. D. Moustakas, "Scattering of electrons at threading dislocations in GaN," *Journal of Applied Physics,* vol. 83, no. 7, pp. 3656-3659, 1998.

[102] K. Yee, "Numerical solution of initial boundary value problems involving Maxwell's equations in isotropic media," *IEEE Transactions on Antennas and Propagation,* vol. 14, no. 3, p. 302–307, 1966.

[103] A. Taflove, "Application of the finite-difference time-domain method to sinusoidal steady state electromagnetic penetration problems," *IEEE Transactions on Electromagnetic Compatibility,* vol. 22, no. 3, p. 191–202, 1980.

[104] RSoft, "FullWave (v2015.06) User Guide," Synopsys, Inc. (Optical Solutions Group) , New York (USA), 2015.

[105] M. G. Moharam and T. K. Gaylord, "Rigorous coupled-wave analysis of dielectric surface-relief gratings," *Journal of the Optical Society of America,* vol. 72, no. 10, pp. 1385-1392, 1982.

[106] R. D. Group, "DiffractMod v2015.06 User Guide," Synopsys, Inc., Optical Solutions Group , New York, USA, 2015.

[107] M. Moharam and T. K. Gaylord, "Rigorous coupled-wave analysis of planar-grating diffraction," *Journal of Optical Society of America,* vol. 71, no. 7, pp. 811-818, 1981.

[108] K. Han and C.-H. Chang, "Numerical Modeling of Sub-Wavelength Anti-Reflective Structures for Solar Module Applications," *Nanomaterials,* vol. 4, pp. 87-128, 2014.

[109] R. D. Group, "BandSOLVE v2013.12 User Guide," Synopsys, New York, USA, 2015.

[110] Australian National University, "Materials Technology: MOCVD reactor," Nov. 2002. [Online]. Available: http://www.anu.edu.au/CSEM/machines/MOCVD.html. [Accessed

Oct. 2016].

[111] R. Pelzel, "A Comparison of MOVPE and MBE Growth Technologies for III-V Epitaxial Structures," in *CS MANTECH Conference*, New Orleans, Louisiana, USA, May, 2013.

[112] L. Maissel, "Applications of Sputtering to the Deposition of Films,"," in *Handbook of Thin Film Technology*, New York, McGraw-Hill, 1970.

[113] G. Monaco, "Coating Technology: Evaporation Vs Sputtering," Satisloh , Italy , 2016.

[114] D. Depla, S. Mahieu and J. Greene, "Sputter deposition processes," 2010. [Online]. Available: https://biblio.ugent.be/publication/1095343/file/1095356. [Accessed Oct. 2016].

[115] D. Smith, Thin-Film Deposition: Principles Practice, New York: McGraw-Hill, 1995.

[116] CNR-IFN Trento, "RF-Sputtering principles," 1999. [Online]. Available: http://www.tn.ifn.cnr.it/facilities/rf-sputtering-facility/rf-sputtering-principles. [Accessed Oct. 2016].

[117] Z. Cui, Nanofabrication: Principles, Capabilities and Limits, Springer, 2008.

[118] G. R. Suñé, "Electron Beam Lithography for Nanofabrication (Ph.D. Thesis)," University of Barcelona, Barcelona, 2008.

[119] B. Berčič, "Introduction to Electron Beam Lithography," Sept 2006. [Online]. Available: http://www-f7.ijs.si/uploads/images/SPIN%20-%20OFF%20TEHNOLOGIJE/Electron_ Beam_Lithography.pdf. [Accessed Oct. 2016].

[120] C. Honsberg and A. M. Barnett, "Light Trapping in Thin Film GaAs Solar Cells," in *Photovoltaic Specialists Conference, 1991*, 1991.

[121] M. Grupen and K.Hess, "A Self-Consistent Calculation of the Modulation Response for Quantum Well Laser Diodes," *Applied Physics Letters*, vol. 65, no. 19, pp. 2454-2456, 1993.

[122] C. Honsberg and S.Bowden, August 2014. [Online]. Available: http://pveducation.org /pvcdrom.

[123] O. Madelung, Semiconductors – Basic Data, 2nd Edition ed., Berlin: Springer-Verlag, 1996.

[124] J. Piprek, Semiconductor Optoelectronic Devices, London: Academic Press, 2003.

[125] R. Aguinaldo, "Modeling Solutions and Simulations for Advanced III-V Photovoltaics Based on Nanostructures," Rochester, NY, 2008.

[126] T. A. F. König, P. A. Ledin, J. Kerszulis, M. A. Mahmoud, M. A. El-Sayed, J. R. Reynolds and V. V. Tsukruk, "Electrically tunable plasmonic behavior of nanocube–polymer nanomaterials induced by a redox-active electrochromic polymer," *ACS Nano*, vol. 8, no. 6, p. 6182–6192, May 2014.

[127] P. A. Folkes, B. Connelly and F. Towner, "Minority Carrier Lifetime and Interfacial Recombination Velocity in GaAs/AlGaAs Double Heterostructures," Adelphi, 2012.

[128] G. Xiao, J. Lee, J. Liou and A. Ortiz-Conde, "Incomplete ionization in a semiconductor and its implications to device modeling," *Microelectronics Reliability*, vol. 39, pp. 1299-1303, 1999.

[129] J. J. Schermer, P. Mulder, G. J. Bauhuis, M. M. A. J. Voncken, J. v. Deelen and E. a. L. P. K. Haverkamp, "Epitaxial Lift-Off for large area thin film III/V devices," *Physica Status Solidi (a)*, vol. 202, no. 4, pp. 501-508, March 2005.

[130] R. R. LaPierre, A. C. E. Chia, S. J. Gibson, C. M. Haapamaki, J. Boulanger, R. Yee, P. Kuyanov, J. Zhang, N. Tajik, N. Jewell and K.M.A. Rehman, "III–V nanowire photovoltaics:Review of design for high efficiency," *Physica Status Solidi RRL*, vol. 7, no. 10, pp. 815-830, April 2013.

[131] E. Yablonovitch, "Statistical ray optics," *Journal of Optical Society of America*, vol. 72, no. 7, pp. 899-907, July 1982.

[132] E. D. Palik, Handbook of Optical constant of solids, 3 ed., Boston: Academic Press, 1998.

[133] J. Berenger, "A perfectly matched layer for the absorption of electromagnetic waves," *Journal of Computational Physics*, vol. 114, no. 2, pp. 185-200, 1994.

[134] J. S. Blakemore, "Semiconducting and other major properties of gallium arsenide," *Journal of Applied Physics*, vol. 53, pp. R123-R181, 1982.

[135] N. N. Feng, G. R. Zhou and W. Huang, "Space mapping technique for design optimization of antireflection coatings for photonic devices," *Journal of Lightwave Technology*, vol. 21, no. 1, pp. 281-285, Jan. 2003.

[136] Y. Park, E. Drouard, O. El Daif, X. Letartre, P. Viktorovitch, A. Fave, A. Kaminski, M. Lemiti and C. Seassal, "Absorption enhancement using photonic crystals for silicon thin film solar cells," *Optics Express*, vol. 17, no. 16, pp. 14312-14321, 2009.

[137] L. Zeng, Y. Yi, C. Hong, J. Liu, N. Feng, X. Duan, L. C. Kimerling and B. A. Alamariu, "Efficiency enhancement in Si solar cells by textured photonic crystal back reflector,"

Applied Physical Letters, vol. 89, no. 11, pp. 111-113, Sep. 2006.

[138] N. Gupta and V. Janyani, "Design and Optimization of Photonic Crystal Diffraction Grating based Efficient Light Trapping Structure for GaAs Thin Film Solar Cell," *Journal of Nanoelectronics and Optoelectronics,* vol. 11, no. 4, pp. 407-415, 2016.

[139] N. D. Gupta and V. Janyani, "Optical and Electrical Simulation Studies of Light Trapping in GaAs Thin Film Solar Cells Using 2D Photonic-Crystal," *Journal of Nanoelectronics and Optoelectronics,* vol. 11, no. 3, pp. 368-376, 2016.

[140] W. Yang, Z. Liu, Y. Xie, J. Cai, S. Liu, H. Gong and Z. Wu, "Improvement of GaN light-emitting diodes with surface-treated Al-doped ZnO transparent Ohmic contacts by holographic photonic crystal," *Applied Physics A,* vol. 107, pp. 809-812, March 2012.

[141] M. A. Green, "Lambertian Light Trapping in Textured Solar Cells and Light-Emitting Diodes: Analytical Solutions," *Progress in Photovoltaics: Research and Applications,* vol. 10, pp. 235-241, 2002.

[142] A. D. Rakić, D. A. B., J. M. Elazar and M. L. Majewski, "Optical properties of metallic films for vertical-cavity optoelectronic devices," *Applied Optics,* vol. 37, no. 22, pp. 5271-5283, 1998.

[143] M. Kroll, S. Fahr, C. Helgert, C. Rockstuhl, F. Lederer and T. Pertsch, "Employing dielectric diffractive structures in solar cells–a numerical study," *Physica Status Solidi (A),* vol. 205, no. 12, pp. 2777-2795, Oct. 2008.

[144] R. Petit, Electromagnetic Theory of Gratings, Berlin: Springer-Verlag, 1980, p. 174.

[145] E. Popov and M. Neviere, "Maxwell equations in Fourier space: fast-converging formulation for diffraction by arbitrary shaped, periodic, anisotropic media," *Journal of the Optical Society of America A,* vol. 18, no. 11, pp. 2886-2894, 2001.

[146] N. de Angelis, J. C. Bourgoin, T. Takamoto and A. Khan, "Solar cell degradation by electron irradiation. Comparison between Si, GaAs and GaInP cells," *Solar Energy Materials & Solar Cells ,* vol. 66, pp. 495-500, 2001.

[147] Y. Mir, A. Amine, M. Bouabdellaoui, K. Zazi and M. Zazoui, "The window layers effect on the hardness improvement of space solar cells exposed to the 1 MeV electron irradiations," *Optical and Quantum Electronics,* vol. 45, no. 11, pp. 1189-1197, 2013.

[148] S. Kazuaki, Y. Atsushi, T. Tatsuya, H. Akio, S. Masakazu, K. Masanori, N. Yoshiaki, F. Pastorelli and W. Kentaro, "Antireflection Film, Solar Battery Cell, Method for

Manufacturing Antireflection film and Method for Manufacturing Solar Battery Cell". Japan Patent JP2011119740 (A), 16 06 2011.

[149] G. Brown, J. Ager, W. Walukiewicz and J. Wua, "Finite Element Simulations of compositionally graded InGaN solar cells," *Solar Energy Materials & Solar Cells,* vol. 94, pp. 478-483, 2010.

[150] M. Nawaz and A. Ahmad, "A TCAD-based modeling of GaN/InGaN/Si solar cells," *Semiconductor Science Technologies,* vol. 27, p. 035019, 2012.

[151] J. F. Muth, J. H. Lee, I. K. Shmagin, R. M. Kolbas, H. C. Casey Jr., B. P. Keller, U. K. Mishra and S. P. DenBaars, "Absorption coefficient, energy gap, exciton binding energy, and recombination lifetime of GaN obtained from transmission measurements," *Applied Physics Letters,* vol. 71, p. 2573, 1997.

[152] J. Wu and W. Walukiewicz, "Band gaps of InN and group-III nitride alloys," *Superlattices Microstruct.,* vol. 34, pp. 63-75, 2003.

[153] M. Anani, H. Abid, Z. Chama, C. Mathieu, A. Sayede and B. Khelifa, "InxGa1-xN refractive index calculations," *Microelectronics Journal,* vol. 38, pp. 262-266, 2007.

[154] N. Ravindra, P. Ganapathy and J. Choi, "Energy gap–refractive index relations in semiconductors – An overview," *Infrared Physics & Technology,* vol. 50, pp. 21-29, 2007.

[155] J. Sheu, C. Yang, S. Tu, K. Chang, M. Lee, W. Lai and L. Peng, "Demonstration of GaN-Based Solar Cells With GaN/InGaN Superlattice Absorption Layers," *IEEE Electron Device Letters,* vol. 30, no. 3, pp. 225-227, March 2009.

[156] S. J. Chang, Y. K. Su, Y. C. Lin, R. W. Chuang, C. S. Chang, J. K. Sheu, T. C. Wen, S. C. Shei, C. W. Kuo and D. H. Fang, "MOCVD growth of InGaN/GaN blue light emitting diodes on patterned sapphire substrates," *Physics Status Solidi (c),* vol. 0, no. 7, p. 2253–2256, Oct. 2003.

[157] M. J. Dodge, "Refractive Index" in Handbook of Laser Science and Technology, Volume IV, Optical Materials: Part 2 ed., Boca Raton: CRC Press, 1986.

[158] L. Chen, J. Ho, C. Jong, C. Chiu, K. Shih, F. Chen, J. Kai and L. Chang, "Oxidized Ni/Pt and Ni/Au ohmic contacts to p-type GaN," *Applied Physics Letters* , vol. 76, no. 25, p. 3703, 2000.

[159] S. Ruvimov, Z. Liliental-Weber, J. Washburn, K. J. Duxstad, E. E. Haller, Z.-F. Fan, S. N. Mohammad, W. Kim, A. E. Botchkarev and H. Morkoc, "Microstructure of Ti/Al and

Ti/Al/Ni/Au Ohmic contacts for n-GaN," *Applied Physics Letters,* vol. 69, no. 11, p. 1556, 1996.

[160] Ž. Gačević, A. Das, J. Teubert, Y. Kotsar, P. K. Kandaswamy, T. Kehagias, T. Koukoula, P. Komninou and E. Monroy, "Internal quantum efficiency of III-nitride quantum dot superlattices grown by plasma-assisted molecular-beam epitaxy," *Journal of Applied Physics,* vol. 109, no. 103501, May 2011.

[161] G. S. Rodríguez, A. Montero, B. Peláez, M. López, Y. Moreno, M. López, G. Puente and O. d. M. Pereira, "Photoluminescence Spectroscopy as a Tool for Quality Control of GaN Thin Film to Be Used in Solar Cell Devices," *Materials Sciences and Applications,* vol. 5, pp. 267-270, April 2014.

[162] C. L. Tsai, Z. F. Xu, Y. S. Lee and G. Fan, "Realization of InGaN solar cells with InGaN/GaN superlattice absorption layers by metalorganic vapor phase epitaxy (MOVPE)," in *IEEE 4th International Nanoelectronics Conference (INEC)*, Tao-Yuan, Taiwn, 2011.

[163] Y. Qi, H. Liang, W. Tang, Z. Lu and K. M. Lau, "Dual wavelength InGaN/GaN multi-quantum well LEDs grown by metalorganic vapor phase epitaxy," *Journal of Crystal Growth,* vol. 272, pp. 333-340, 2004.

[164] Y. Xu and J. N. Munday, "Designing photonic materials for effective bandgap modification and optical concetration in photovoltaics," *IEEE Journal of Photovoltaics,* vol. 4, pp. 233-236, 2014.

Publications

International Journal Papers

1. **N.D. Gupta** and V. Janyani, **"Lambertian and Photonic Light Trapping Analysis with Thickness for GaAs Solar Cells based on 2D Periodic Pattern",** *In IET-Optoelectronics*, Accepted, May, 2017.
2. **N.D. Gupta** and V. Janyani**, "Analysis of Light Trapping in thin film GaAs solar cells using 2D Photonic Crystal Structures at front surface",** *In IEEE Journal of Quantum Electronics*, vol. 53, issue 2, pp. 4800109, Apr., 2017.
3. **N.D. Gupta**, V. Janyani and Manish Mathews, "**Light Trapping in p-i-n Superlattice based InGaN/GaN Solar Cells using Photonic Crystal**", *In Optical and Quantum Electronics*, Springer, vol. 48, issue 11, pp. 1-17, Nov. 2016.
4. **N.D. Gupta** and V. Janyani, "**Simulation and analysis of the absorption enhancement in p-i-n InGaN/GaN solar cell using photonic crystal light trapping structures**", *In Optical Engineering*, SPIE, vol. 55, issue 10, pp. 107102, Sept. 2016.
5. **N.D. Gupta** and V. Janyani, "**Design and Optimization of Efficient Photonic Crystals Diffraction Grating based Light Trapping Structure for GaAs Thin Film Solar Cell**", *In Journal of Nano-electronics and Optoelectronics*, ASP, vol. 11, issue 4, 2016.
6. **N.D. Gupta** and V. Janyani, "**Optical and electrical simulation studies of GaAs thin film Solar cell using 2D Photonic Crystals**", *In Journal of Nano-electronics and Optoelectronics*, ASP, vol. 11, issue 3, 2016.
7. **N.D. Gupta** and V. Janyani, "**Dense wavelength division demultiplexing using photonic crystal waveguides based on cavity resonance**", *In Optik-International Journal of Light and electron Optics*, Vol. 125, Issue 19, p.5833-5836, Oct. 2014.
8. D. Bhatia and **N. D. Gupta**, "**Design of Different Demultiplexers for Wavelength Division Multiplexing Systems Based On Photonic Crystal Waveguide**", *In International Journal of Innovative Research in Computer and Communication Engineering*, Vol. 2, Issue 2, p.3001-3014, February 2014

9. **N.D. Gupta** and V. Janyani, **"Analysis of Effectiveness of Photonic Crystals Diffraction Grating and Distributed Bragg Reflector based Back Light Trapping Structure for GaAs Thin Film Solar Cell",** *In IETE Journal of Research*, Mar., 2017 (Under Revision).
10. **N.D. Gupta,** V. Janyani, M. Mathews, Monika and R. Singh**, "Design and Fabrication of InGaN/GaN Superlattice based Solar Cell using Photonic Crystal Structure at the Front Surface",** *In Optics and Laser Technology***,** Elsevier, May, 2017 (Under Revision).
11. M. Radhouene, M. Najjar, **N.D. Gupta** and V. Janyani**, "Design and Simulation Twelve Channels Optical Demultiplexer Based on Two Dimensional Photonic Crystal Resonant Filters",** *Telecommunication Systems*, Springer, Dec., 2016 (Under Review).

International Conference Papers

1. **N.D. Gupta** and V. Janyani, "**Efficiency Enhancement in Thin Film GaAs Solar Cell using Photonic Crystals as Reflection and Diffraction Gratings for Light Trapping**", *In Springer Proceedings of Physics*, ICRTMD-2015, Amity University, Noida, Dec., 2015 **(Best Paper Award)**.
2. **N.D. Gupta** and V. Janyani, "**Absorption enhancement in p-i-n superlattice based InGaN/GaN solar cell using Photonic Crystals**", *In Conference on Advanced Material Processing-2015*, MNIT, Jaipur, Dec. 2015.
3. **N. D. Gupta**, V. Janyani, G. Singh, and H. Tsuda, "**Design and Analysis of Low Loss Highly Efficient Light Trapping Structure for GaAs Thin Film Solar Cells using Photonic Crystals as Diffraction Grating**," *In Frontiers in Optics 2015,* OSA Technical Digest (online) (Optical Society of America, 2015), paper FTu3C.4, San Jose, CA USA
4. **N. D. Gupta** and V. Janyani, "**Design and Simulation of Light Trapping in Thin Film GaAs Solar Cell using Photonic Crystals as back reflector**," *In 12th International Conference on Fiber Optics and Photonics*, OSA Technical Digest (online) (Optical Society of America, 2014).
5. **N.D. Gupta** and V. Janyani, "**Study and possible modifications of various designs for Photonic Crystals based thin film solar cells**", *In IONS-Asia 6*, IIT-Kaharagpur, 10-12 Dec., 2014.

6. **N.D. Gupta** and V. Janyani, "**Efficiency Enhancement in the thin film GaAs solar cell using Photonic Crystal as a back reflector**", *In IEEE Conference Proceedings*, WRAP'13, IIT, New Delhi ,India, Dec.17-18, 2013.
7. A. Jakhar, M. Mathew, A. Chauhan, K. Singh, V. Janyani and **N. D. Gupta**, "**A Top-Down Approach for Fabrication of Nanorods on GaN based LEDs using Self Assemble Ni**", *In International Conference on Optical & Wireless Technologies* (OWT-2017), MNIT, Jaipur (India), March, 2017.
8. M. Radhouene, N. Monia, **N. D. Gupta** and V. Janyani, "**Optimization of Three Channels Optical Demultiplexer Based On Photonic Crystal Ring Resonator**", *In IEEE Conference on Recent Advances in Lightwave Technology*, Bengaluru (India), 21-23 Sept. 2016.

National Conference Papers

1. A. Jakhar, **N. D. Gupta**, V. Janyani, "**Study of Light Trapping in Solar cells based on Perovskite materials**", *In OSA YSC on Photonic Technologies*, MNIT, Jaipur, India, p.32-34, April, 2016
2. **N.D. Gupta** and V. Janyani, "**Photonic Light Trapping in p-i-n InGaN/GaN Solar Cell with 2D periodic pattern**", *In IETE Zonal Seminar (North)*, MNIT, Jaipur (Raj.), 5th March, 2016.

Brief CV

Nikhil Deep Gupta received his B.E. degree from Rajasthan University, Jaipur, India in 2009 in Electronics and Communication Engineering with Honors. He received his M.Tech. from Maulana Azad National Institute of Technology (MANIT), Bhopal, India in 2011 with a Gold Medal. After that, he had worked as Junior Research Fellow at Malaviya National Institute of Technology (MNIT), Jaipur, India in a Defense Research and Development Organization (DRDO), India sponsored project. Since Jan. 2013, he has been pursuing Ph.D. at Malaviya National Institute of Technology (MNIT), Jaipur, India. His areas of interest are thin film solar cells and their applications, solar PV systems and its applications, opto-electronics, optical communication, photonic crystals and photonic crystal based devices. He is currently graduate student member of Optical Society of America (OSA), Society of Photo - Optical Instrumentation Engineers (SPIE) and International Association of Engineers (IAENG).